ABSTRACT

MANKE, JONATHAN PETER. Assessment of Superposition as a Design Framework for the Combined Effects of Soil Improvement and Foundation Remediation. (Under the direction of Dr. Debra Laefer.)

The problem of pile foundation reuse provides an ideal opportunity to evaluate the validity of superposition as a design paradigm for ground intervention and ground reinforcement (GIGR) techniques when used in combination with in situ foundations. Grouted, helical piers, a relatively new technology, are proposed as a capacity improvement option for existing pile foundations. The relationship between these geotechnical elements was evaluated through the axial and lateral testing of small-scale, cast-in-place foundations in uniform, dry sand. These tests showed that the implementation of ground modification techniques caused an increase in the axial and lateral load-deflection performance of the foundation, with superposition as the most probable design methodology.

ASSESSMENT OF SUPERPOSITION AS A DESIGN FRAMEWORK FOR THE COMBINED EFFECTS OF SOIL IMPROVEMENT AND FOUNDATION REMEDIATION

by

JONATHAN PETER MANKE

A thesis submitted to the Graduate Faculty of
North Carolina State University
in partial fulfillment of the
requirements for the Degree of
Master of Science

CIVIL ENGINEERING

Raleigh
2004

APPROVED BY:

Roy Borden, Ph.D. Committee Member	Shammir Rahman, Ph.D. Committee Member

Debra Laefer, Ph.D.
Chair of Advisory Committee

DEDICATION

I dedicate this thesis to my parents, who raised me in love and taught me to believe that I am capable of anything. To my mother, whose smile and laughter will forever live in my heart, and my father, a man whom I strive to emulate in all aspects of life, as a father, husband and person.

BIOGRAPHY

Jonathan Peter Manke was born October 13th, 1978 to David and Sharon Manke in Des Moines, Iowa. He is the youngest of three brothers and resided in Green Bay, Wisconsin from 1979 – 1997, until graduating with honors from West DePere High School. He participated in both basketball and track throughout high school, finishing as the state discus champion. He then attended the University of Wisconsin-Milwaukee on a Track and Field Scholarship where he studied structural engineering and achieved athletic and academic success throughout. In May of 2002 he graduated with a Bachelor's of Science Degree in Civil Engineering. After spending a month in Europe, he accepted a graduate position at North Carolina State University and began pursuit of a Master's of Science Degree in Geotechnical Engineering in January, 2003 under the direction Dr. Debra Laefer.

A reminder of all the monotonous and frustrating but necessary activities performed to complete the research presented here.

ACKNOWLEDGMENTS

The author is truly grateful for the support of family, friends and faculty, whose emotional council and companionship made the completion of this research possible.

The author would like to express special thanks to Dr. Debra Laefer and Dr. Roy Borden, for their patience and wisdom throughout the author's graduate experience, and to Dr. M S Rahman for sitting on my committee with such short notice.

Additional appreciation is expressed to Russell Lindsey of Russell Lindsey Excavating and Stanley Rupiper of Precision Pier USA, Inc. for their technical contributions and Jim Foster of Global Pak for his generous donation, all of which expedited the lab portion of this research.

Special thanks go to Jerry Atkinson for his technical experience and consult throughout the lab portion of this research, and to various undergraduate lab assistants whose mere presence made the lab experience more bearable.

Finally, the author is truly indebted to the close friends who tolerated the hours of complaining and provided companionship through this difficult endeavor.

TABLE OF CONTENTS

LIST OF TABLES

LIST OF FIGURES

1 INTRODUCTION

1.1 Background

As the design life of many mid-twentieth century buildings are reaching their end, urban redevelopment is increasingly becoming an issue in the U.S. Compounding the problems of urban redevelopment is an escalating demand to replace existing buildings with larger and heavier structures. While the U.S. is in the early stages of urban redevelopment, European countries have dealt with multiple generations of urban reconstruction. A major problem associated with such urban reconstruction is ground congestion from utilities, transportation tunnels, archeological remains, and old pile foundations (Chapman et al., 2002). This congestion, especially from old foundations, complicates new foundation installation, thereby decreasing constructability and increasing construction costs.

When dealing with existing foundations, three options exist: avoidance, removal, and reuse. The most common European solution has been avoidance, where existing foundation elements are left in place, and new foundation elements are installed at locations unoccupied by the abandoned foundations. Often times, however, the existing foundation elements are in premium locations to support the new structure, resulting in inefficient locations for the new foundation elements. These poor locations require the implementation of load transfer structures and excessively large new foundation elements. Europeans have found that after several cycles of avoidance based redevelopment, sufficient ground space for new foundation installation no longer exists. While avoidance is the most economical short-term solution, its long-term repercussions make it a poor alternative, and, because foundation removal can be extremely expensive (Chow et al., 2002) and dangerous to adjacent structures, the most theoretically appealing long-term solution is foundation reuse.

The main challenges to reusing existing foundations are physical assessment and capacity enhancement. Physical assessment is necessary to determine the condition and functionality of the existing piles. In-situ pile assessment has been extensively studied (Chapman et al., 2001, Zhang et al., 1985, Schaap et al., 1985) and, thus, will not be discussed here. Capacity enhancement of the existing foundation is often needed to accommodate the larger loads of the new structures. This can be achieved by either strengthening the soil conditions or providing additional foundation elements. Most literature on in-situ capacity enhancement discusses methods for improvement of new foundation elements, which requires the installation of various technologies during pile construction (Brusey, 2000, Littlechild et al., 2000), with little focus on in-situ capacity enhancement of existing foundations. Both soil improvement and additional structural elements can be accomplished by the implementation of ground improvement and ground reinforcement (GIGR) technologies.

While GIGR technologies offer tremendous potential to reuse existing foundations, the absence of widely adopted design procedures for these innovations hampers the design community from significantly contributing economical and verifiable installation approaches. Design standardization of GIGR technologies has been hindered by the fact that the technology is largely "contractor-driven", patented, and proprietary, and is further complicated by the growing trend to use many of these techniques in conjunction with each other, thus increasing the complexity of performance prediction. When existing geotechnical installations (e.g. foundations and retaining walls) are also included, and these features possess unknown loading capacity, the scenarios approach a near impossibility for sufficiently conservative designs at a reasonable cost, when new, higher loads are proposed.

Therefore, a design approach is needed to accurately and reliably predict the performance of GIGR technologies, when integrated with existing geotechnical installations.

1.2 Research Objectives

Consequently, the problem of foundation reuse, specifically pile foundations, provides an ideal opportunity to pioneer a new design framework to consider the performance of GIGR techniques, specifically grouted helical piers, when used in combination with each other and with in-situ foundations. This thesis presents an experimental study of such a program. The objective of this research is to consider superposition as a new design paradigm for composite foundations and propose using grouted, helical piers to investigate deep foundation rehabilitation as the initial test case.

1.3 Organization of Thesis

Chapter 2 contains background of design and construction issues related to the research presented here. Chapter 3 presents the scope of the experimental work and the selected methodology, while Chapter 4 presents the experimental results. Chapter 5 is a comparative analysis and discussion of the results while Chapter 6 is a discussion of the appropriate design method to be used for composite foundations. Chapter 7 offers a summary of the testing and various conclusions drawn from this experimentation.

2 BACKGROUND

2.1 Introduction

Relevant areas to this research include methods of pile foundation enhancement, grouted helical pier manufacturing and installation practices, various design procedures and methodologies, physical modeling, and previous pile group model testing. Section 2.2 discusses pile foundation enhancement through soil and structural improvement, while section 2.3 presents a specific improvement option: grouted, helical piers. Section 2.4 illustrates various design procedures and methodologies that could define the relationship between the grouted pier and existing foundation. As physical modeling is proposed to evaluate which methodology is appropriate for a composite foundation, section 2.5 illustrates issues related to physical modeling and section 2.6 presents related model testing.

2.2 Enhancement options

An existing foundation's capacity can be enhanced through various ground improvement or ground reinforcement (GIGR) technologies that result in structural improvement, soil improvement, or some combination of the two, with the main objective being to increasing the shaft resistance, end-bearing, or both. Many GIGR technologies exist to achieve these improvements (Schaefer, 1997). In this thesis the term GIGR will cover both categories and those technologies that use a combination of the two approaches, such as grouted, helical piers.

2.2.1 Structural Improvement

Structural improvement can be accomplished by 1) lengthening or widening the pile to increase the pile's surface area and, thus, its shaft resistance, 2) expanding the shaft's cross-sectional area to augment end-bearing resistance, or 3) adding structural members to

the pile group (Shvets et al., 1996). Since changing the geometry of an in-situ pile is untenable, the addition of structural members is the most desirable option.

The location of new structural elements can be either inside or outside the perimeter of the exiting pile cap. If added inside, the pile cap must either be removed or have holes drilled through it to accommodate the installation of new elements. Both of these options can prove difficult and time consuming (Shvets et al., 1996), and may not be possible due to access considerations and possible endangerment of surrounding structures. Alternatively, the introduction of additional elements outside the perimeter of the existing pile cap poses an easier installation and a lower risk to surrounding buildings, and attaching the new elements to the existing pile cap, either by local connections of each element or by a global expansion of the entire pile cap, is often most desirable (Shvets et al., 1996). Unfortunately, through such intervention, pile cap expansion can become complex, as it is difficult to extend the reinforcement into the new area (Martin et al., 2000). The local connections, while the easier of the two, can become complicated if large moments are present at the connection point.

2.2.2 Soil Improvement

Soil improvement can increase a pile's end bearing capacity or shaft resistance through changes to the soil characteristics and is typically achieved through various grouting techniques (Welsh et al., 1991, Warner, 2004). Enhancement of the end bearing resistance requires improvement of the soil below the pile base (Van der Stoel, 2003, Breitsprecher et al., 2003), but can be difficult to implement and complicated to verify the soil improvement, especially if the pile depths are unknown. Consequently, increasing the shaft resistance by improving the soil density, and subsequently the lateral stress, around the pile shaft to is a

more straight forward approach, as the soil around the shaft is more accessible than the pile toe. In such a case, the shaft resistance of a pile (f_s) can be determined by a friction model:

$$f_s = K_{o*} \sigma'_{z*} \tan \varphi_f \quad \textbf{(Equation 2.1)}$$

where: K_o = the coefficient of lateral earth pressure, σ'_z = the vertical effective stress, and φ_f = the soil-foundation interface friction angle (Coduto, 2001). The vertical effective stress is directly related to the soil unit weight, and the soil-foundation interface friction angle is directly related to the contact area between the pile and the soil.

2.2.3 Combination of Structural and Soil Improvement

Some methods, such as the incorporation of jet grouted columns, grouted helical piers, or additional driven piles, can offer both soil and structural improvement (Durgunoglu et al., 2003, Warner, 2003). These methods can densify the existing soil conditions, while creating an additional structural element for the existing foundation. As grouted, helical piers were selected as the improvement method for the presented experimental program, only further details on this technique are provided.

2.3 Existing grouted, helical pier methods

Helical piers and grouting have each been implemented for many years, however, using helical piers in conjunction with grouting is a relatively new application of the technology. The following sections define and illustrate existing helical pier, grouting, and grouted, helical pier technologies.

2.3.1 Helical piers

Helical piers are more commonly known as helical anchors, (Figure 2.1), and while the names refer to the same physical product, the difference is in their application (Perko et al., 2000). Where resistance to tensile forces is primarily needed, the term helical anchor is

typically used, and when compression forces dominate, as in foundations, the term helical pier is employed (Perko et al., 2000). A helical pier typically consists of two or more helices attached to a solid steel shaft.

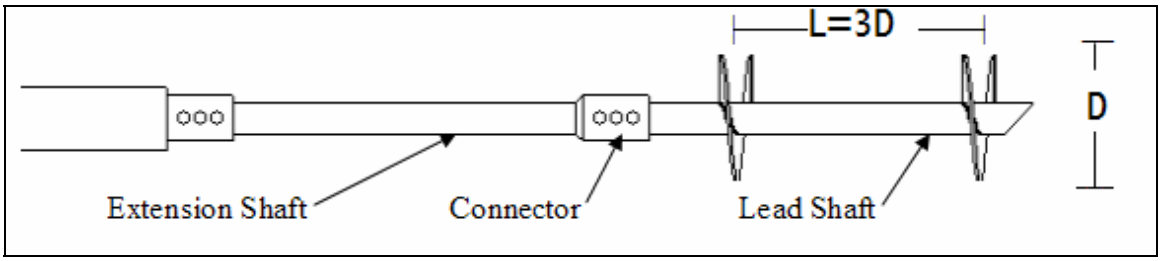

Figure 2.1 Schematic of helical pier (Rogers, 2002)

Helical elements have a wide range of applications, including foundations, retaining walls and anchors, and the design method for the determination of helical pier capacity is widely accepted to be the bearing capacity of the helices on their respective soil (Perko et al., 2000, Rogers, 2002) [Eq. 2.2]:

$$q_u = cN_c + q' N_q \qquad \textbf{(Equation 2.2)}$$

where: q_u = ultimate bearing capacity, c = cohesion, q' = overburden pressure, N_c , N_q = bearing capacity factors.

2.3.2 Grouting

Grouting has found a number of successful applications and is continuing to be implemented in new ways (Fang, 1991, Warner, 2004). Despite the wide range of applications in which grouting can be utilized, the unpredictability of treatment effectiveness has limited the appeal of grouting as a quantifiable ground improvement option (El-Kelesh et al., 2003, Warner, 2004). The difficulty of creating a viable design method to determine the affect of grouting is due to the high variability, anisotropic behavior and permeability of soil profiles. For these reasons, a quantifiable evaluation of grout-based soil improvement has not been well established, and, while various experiments have been performed to determine

a verifiable relationship between grouting techniques and soil improvement (Warner, 2003, Lees et al., 2003), none have included the effect of ground reinforcement techniques in the proximity of existing foundations.

2.3.3 Grouted, helical piers

Helical piers offer the ability to deliver grout (either pressurized or non-pressurized) into the soil system if the solid shaft is replaced by a hollow shaft. Current grouted, helical pier technologies involve the "helical pulldown micropile" (Vickars et al., 2000) and the "micropier". The selected application for this research is the micropier and the installation and application for it is presented in the following sections. Micropier and grouted, helical pier are both used interchangeably throughout the remainder of this paper.

2.3.3.1 Installation

The micropier is similar to the typical helical pier as previously described (Figure 2.1). All micropiers, however, implement a hollow shaft, approximately 4″ in diameter, and two helices (typical diameters ranging from 8″-18″) with a pitch of 3″. The helices are spaced at a distance of approximately three helix diameters from each other, with the top helix either passing through the same path as the lead helix, or offset by $1^{1}/_{2}$″ so that it carves a distinct, second path. The hollow shaft allows for the installation of grout, which is delivered to the ground through holes placed a few inches below the bottom helix. Located in front and slightly above the holes are displacement fins that push the soil away from the shaft, allowing for the grout to flow freely into the surrounding soil.

Figure 2.2 shows the installation method for a grouted, helical pier. The pier assembly (Figure 2.2a) is rotated with minimal axial force such that the helices pull the pier into the ground (Figure 2.2b). A path is carved into the soil by the advancing helices, which

is subsequently filled by a gravity fed, neat grout mix (Figure 2.2c). Simultaneous installation and grouting is achieved through the use of a grout swivel. Additional extensions can be added to the lead section (Figure 2.2d) to reach the desired depths (Figure 2.2e), where the pier is then detached from the installation equipment resulting in a reinforced, foundation element. An excavated, full-scale micropier can be seen in Figures 2.3 and 2.4.

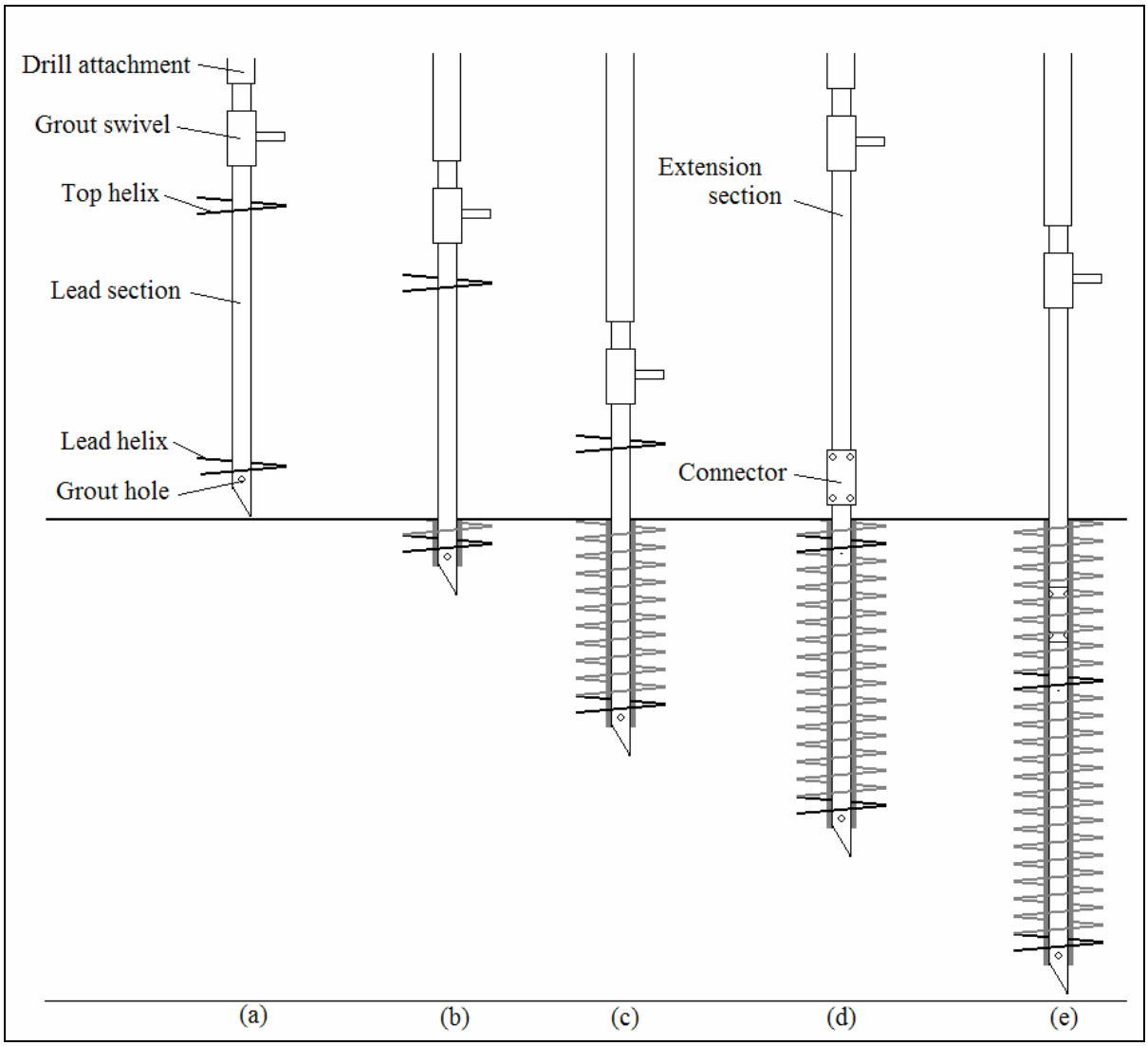

Figure 2.2 Grout installation procedure

Figure 2.3 Closeup of full-scale excavated pier

Figure 2.4 Full-scale excavated pier

If a more uniform profile is desired, the pier is "backed out" then re-advanced until the spiral of grout becomes a continuous element, without the ridges; the general tapered shape remains as it is a function of the lower helix being of a smaller diameter than the upper one. The helical pier can also be removed, filling the space previously occupied by the shaft with grout, leaving a grouted column

A major advantage to the micropier is the ease of installation, as small construction equipment can be used to install these elements on projects with limited available space. As it is a relatively new technology, there has been relatively minimal, published field and laboratory verification studies. (The information in this section was obtained from personal communication with a micropier contractor, Russell Lindsey of Russell Lindsey Excavations, January 4th, 2004).

2.3.3.2 Application

The grouted, helical pier can be used to both add additional foundation elements and potentially improve the soil conditions. In this research, the piers will be installed

between the existing piles and at a sufficient angle such that the piers extend to the base of the piles. As the piers will not be directly attached to the foundation, they will be evaluated only in their ground improvement capacity.

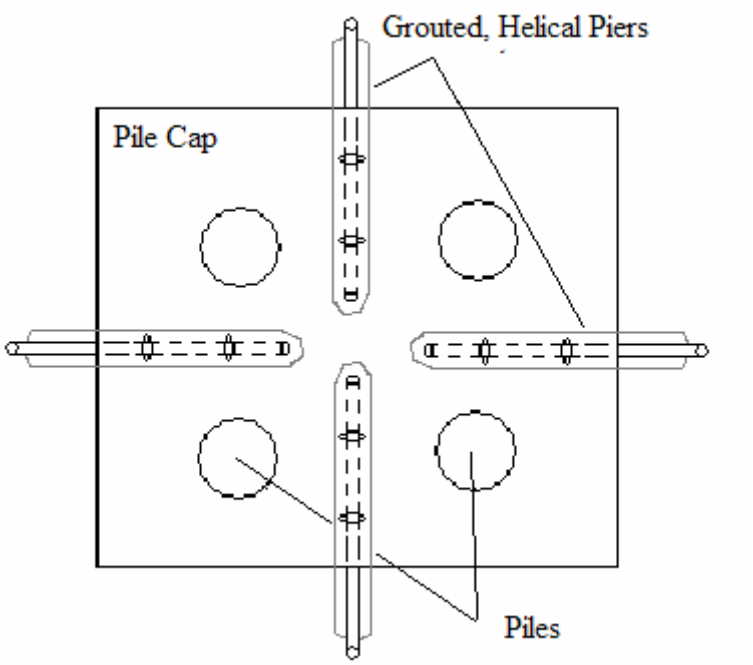

Figure 2.5 Schematic plan view of proposed grouted, helical pier installation

2.4 Design methodologies

Theoretically, several design paradigms are possible to represent the effects of the grouted, helical piers on a composite foundation, including basic superposition, modified superposition, nonlinear superposition, chain theory, and combined effect (Figure 2.6). Each of these methods is described here.

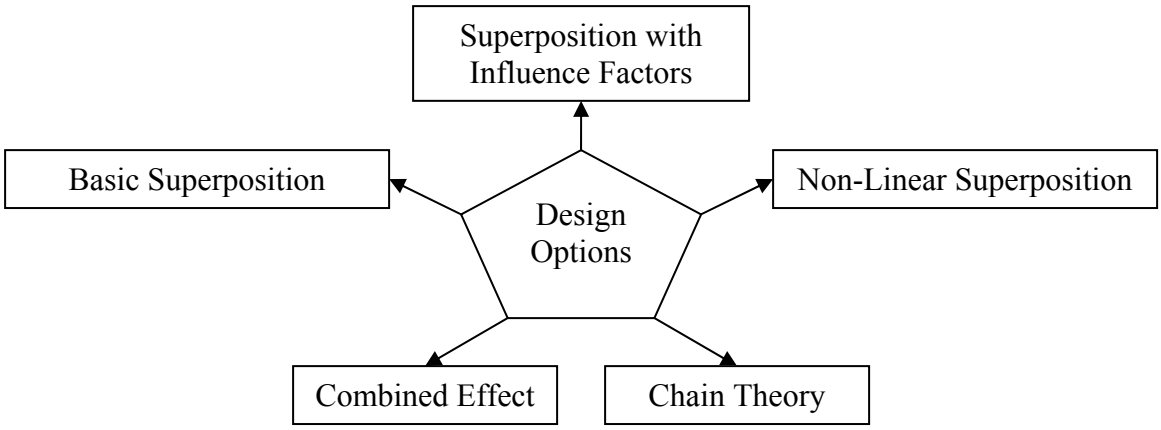

Figure 2.6 Types of design methods

2.4.1 Basic Superposition.

Basic superposition is when the summation of all component performance is equal to the total performance of all elements. Basic superposition is often used both in calculating pile capacity (i.e. the shaft resistance is combined with the end bearing capacity to provide the total available load resistance) and when evaluating the total settlement generated by two separate applied loads (if a load "P" causes a settlement, "x", and a load "Q" causes a settlement, "y", then the total load "P + Q" causes a settlement of "x + y", only if the settlement function is linear), and is illustrated in Figure 2.7.

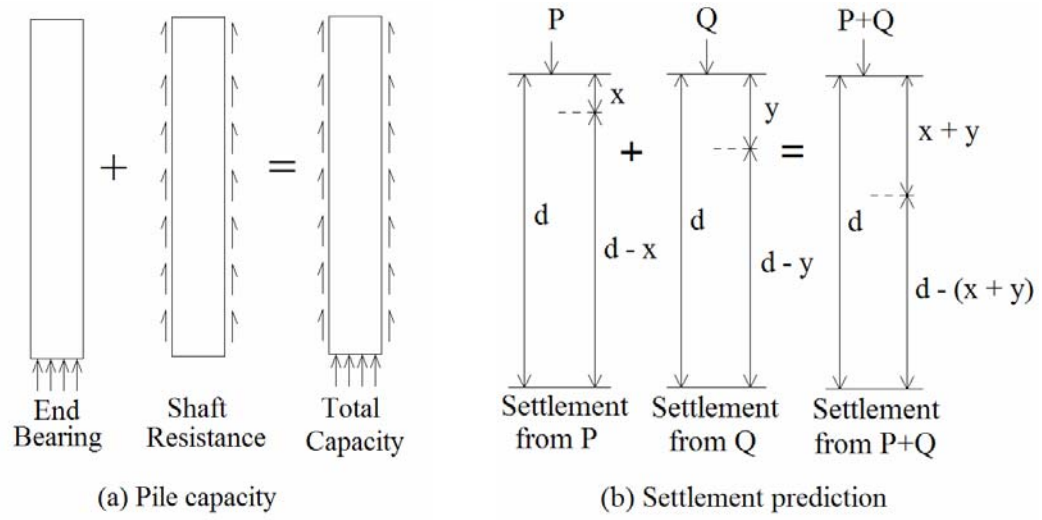

Figure 2.7 Examples of superposition

2.4.2 Modified Superposition.

The process of modified superposition incorporates influence factors to alter the contribution of a component. These influence factors can increase or decrease the component's contribution and can, under certain circumstances, entirely eliminate the effect of a component altogether. The concept of increasing influence factors is illustrated by the previously mentioned research conducted by Akinmusuru (1980). Akinmusuru stated that the total capacity of a piled footing can be determined by the following relationship:

$$Q_t = \alpha \cdot Q_p + \beta \cdot Q_c \qquad \textbf{(Equation 2.3)}$$

where: Q_t = the total capacity of a piled footing, Q_p = the capacity of the piles, Q_c = the capacity of the pile cap, and α and β = influence factors that alter the capacity of the piles and cap contribution. The total capacity is still found through superposition, however, the contributing components are altered by influence factors.

2.4.3 Non-Linear Superposition.

A variation of modified superposition is non-linear superposition, which is used when determining pile group settlement. Standard design practice dictates that while the number of piles does affect the total settlement, pile spacing and pile diameter most strongly influence response, making the contribution of an additional pile non-linear (Poulos et al., 1980). Specifically, the settlement calculations for a pile group (ρ_G) with four symmetrically arranged piles of equal diameter can be performed using equation 2.4.

$$\rho_G = P_1 \cdot \rho_1 \cdot (1 + 2\alpha_1 + \alpha_2) \qquad \textbf{(Equation 2.4)}$$

where P_1 is load in each pile, ρ_1 is the displacement of a single pile under unit load, and α_1 and α_2 are interaction factors for spacing. These interaction factors relate a ratio of pile spacing and diameter to a pile stiffness factor (Poulos et al., 1980). If another pile is added, the equation becomes more complex, as the original interaction factors change, and more interaction factors are needed, to account for the new pile's interaction with the existing piles (Poulos et al., 1980). While the interaction factors are superimposed, they do not change linearly and, thus, a non-linear superposition exists.

2.4.4 Chain theory

An alternative to superposition is the chain theory, where the weakest component in the system controls the design; the capacity at which the first component fails controls the capacity of the entire system. For example, a ground anchor takes the capacity of each component of the system into consideration: the steel, grout, steel/grout interface, and the soil/grout interface. The anchor's capacity is not a sum of the strengths of each component, but the load at which the first of these components fails (Jarred et al., 1997).

2.4.5 Combined Effect

Combined effect is a design method in which the total strength may be a value somewhere between the capacity of the weakest and strongest components. In masonry design, the strength of the mortar is substantially less than that of the brick, however, the final masonry strength is considered to be an intermediate value between the two. To calculate this intermediate strength, a brick assemblage is tested, and the following equation is used to predict its strength (Hilsdorf, 1969):

$$f_p' = \frac{\left[f_{cb}' \cdot \left(f_{tb}' + \alpha \cdot f_j'\right)\right]}{\left[U_u \cdot \left(f_{tb}' + \alpha \cdot f_{cb}'\right)\right]} \qquad \textbf{(Equation 2.5)}$$

where f'_p = the composite strength, f'_{cb} = the compressive strength of a masonry unit, f'_{tb} = the tensile strength of a masonry unit, f'_j = the mortar strength, U_u = the non-uniformity factor, and $\alpha = \frac{j}{4.1 \cdot h}$, j = mortar thickness, h = masonry unit thickness.

The resulting composite strength is a value between the compressive strength of the masonry unit and that of the mortar (Figure 2.8).

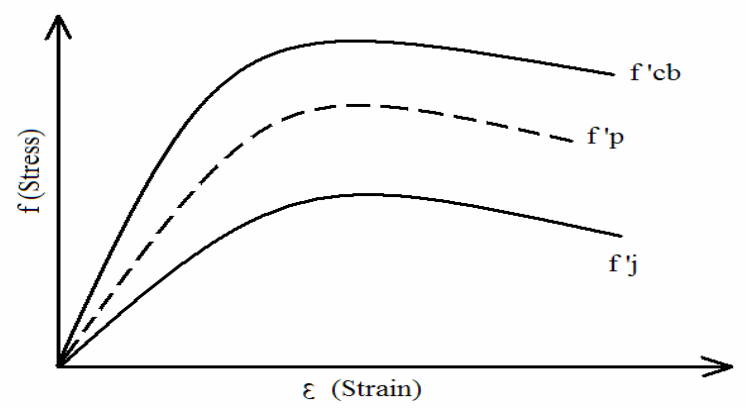

Figure 2.8 Comparison of composite, masonry and mortar strength

Without thorough exploration, the appropriateness of any of these methods for composite GIGR installations remains unknown.

2.5 Physical modeling

Due to the high cost of full and large-scale testing for geotechnical applications, small-scale modeling has become a common experimental practice for determining the behavior of pile groups and is used for the experimentation presented here. Three main types of modeling methods have been developed for small-scale testing: models under normal gravity conditions (1-g modeling), centrifuge modeling and increased stress-gradient method (Altaee et al., 1994). Additionally, when performing small-scale modeling, three issues must be addressed when relating the model to the prototype: geometric-scale ratio, stress-scale ratio, and stress gradient scale ratio (Altaee et al.,

1994). 1-g modeling has become commonly accepted, however, a major concern is the inability to translate the results from the model to the prototype as it does not address the stress and stress-gradient scaling issues (Altaee et al., 1994). While centrifuge testing has been shown to successfully address these issues (Ko et al., 1984), and the increased stress gradient has been tested to show good correlation with centrifuge testing (Zelikson, 1969, and Yan et. al., 1989), both methods are difficult to implement because of the need for specialized equipment. These limitations resulted in 1-g modeling being chosen for the pilot study presented herein. It has long been established that the scaling of material properties based on Buckingham Pi relationships can improve the extrapolation of model tests to the full-scale prototype (Langhaar, 1951). At 1-g, this has been done at as little as a $^{1}/_{10}^{th}$ scale for soil-structure interaction models in dry, cohesionless material (Laefer, 2001). The critical element is a reduction of the strength and stiffness properties of the structural elements to compensate for the loss of strength and stiffness in the model sand because of the low confinement pressures (Laefer, 2001). The 1-g model scaling presented here will implement this material property scaling technique in an attempt to better translate the model results to the prototype.

2.6 Model testing of pile groups

Although the general design procedure for driven piles and drilled shafts can be considered largely well-established, (Chellis, 1961, Tomlinson, 1994, O'Neill et al., 1999), the issue of single pile performance versus group performance remains a topic of interest for many researchers and is the focus of many model-scale tests. Traditionally, pile groups have been categorized as either free-standing, where the pile cap is considered to not make contact with the ground, or piled footings, where the pile cap is in

contact with the ground (Poulos et al., 1980, Long, 1993). These studies have been conducted in both sand and clay, but have largely focused on driven piles (by pushing the piles into the soil) or by backfilling around the piles (Mayne et al., 1994). As the experimental program presented in the following chapters involves small-scale model testing of drilled shaft, piled footings in sand, only previous research concerning axially and laterally loaded foundations in these areas are reviewed in detail.

Because the majority of pile group research, at any scale, has been performed on free-standing pile groups, only two previous studies, Akinmusuru (1980) and Kishida and Meyerhoff (1965), were found to involve small-scale, axially loaded piled footings in sand, and no studies were found concerning laterally loaded piled footings in any soil.

Akinmusuru tested the capacity increase of a pile group foundation when the additional capacity of the pile cap in contact with the ground was considered. The pile groups were tested in sand and modeled using steel tube of various diameters and lengths. Akinmusuru (1980) proposed that the total capacity of a piled footing is more than simply the sum of the capacity of the individual pile cap and piles by two interaction factors, as previously seen in equation 2.3.

Kishida and Meyerhoff presented a study on the evaluation of the bearing capacity of both free standing pile groups and piled footings. The study included both concentric and eccentric loading of small-scale foundations modeled by steel tube, and two failure mechanisms for piled footings were presented, equivalent pier failure (Figure 2.9a) and individual pile failure (Figure 2.9b). The results of their study showed that the bearing capacity of piled footings increased with small eccentricities, but as the eccentricity became large, the capacity dramatically decreased.

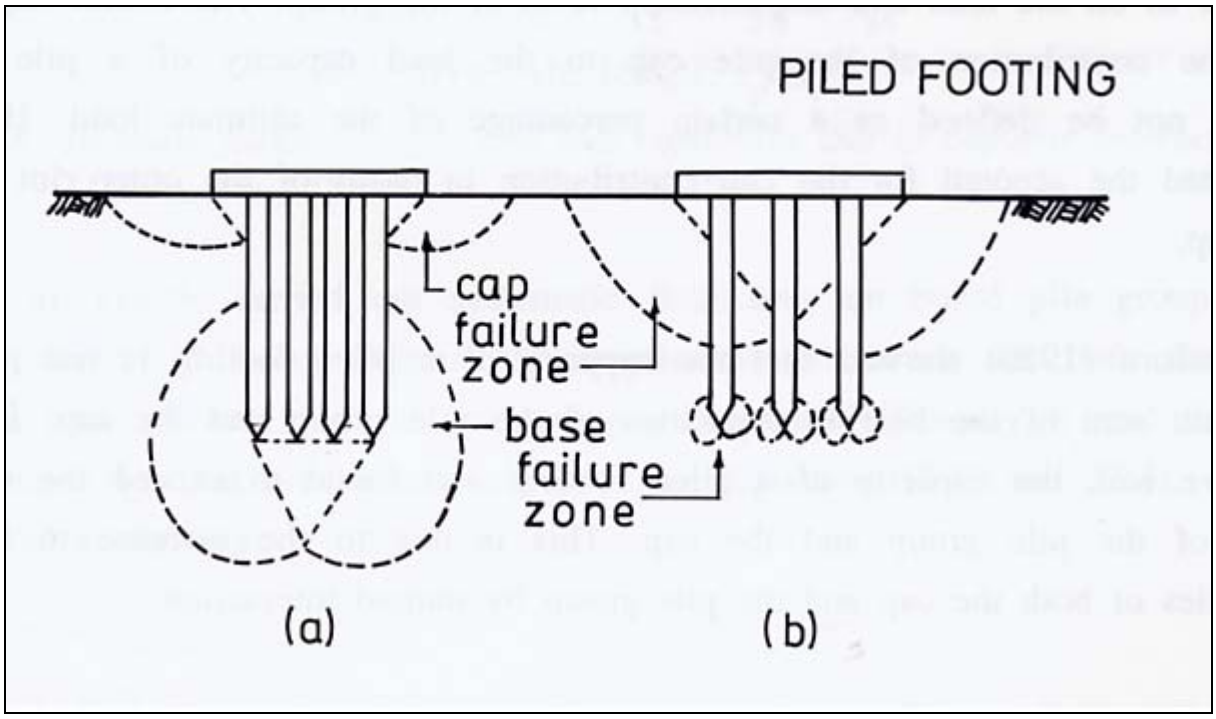

Figure 2.9 Failure mechanism for piled footings (Kishida et al., 1969)

While two studies were found to include small-scale piled footings, only one, by Mayne and associates (1994), was found concerning modeled drilled shafts. Their research, however, was performed on laterally loaded individual drilled shafts in clay, rather than sand. The study evaluated how the lateral load-displacement response was affected by shaft length, diameter, spacing, and surface roughness, as well as eccentricity of the load.

To date, there are no published studies on small-scale experimental programs investigating such pile groups used in conjunction with GIGR techniques. The research presented here was conducted to determine the behavior of piled foundations in the presence of GIGR technologies.

2.7 Summary

The potentially most desirable option for capacity improvement of a deep foundation, without destruction of the superstructure involves the addition of new foundation elements, while leaving the existing pile cap intact. Elements can be both directly connected to the pile group or simply installed in the general vicinity of the existing foundations. Direct connection of these new elements to the pile cap can increase the capacity of the foundation, but complications can arise when these elements are connected to the pile cap or when access restrictions may not allow for direct connection, thus, raising the question as to what capacity enhancement can be observed if the new elements are added but not connected to the cap. Exploration of such matters also helps to clarify the questions of the load transfer mechanism that can be expected in complicated composite GIGR intervention. The use of grouted, helical piers allows the existing pile cap to remain intact as the piers can be installed at an angle to extend into the soil surrounding the existing piles. These additional foundation elements have the potential to both improve the existing soil conditions and offer additional load carrying capabilities and, when combined with the existing foundation elements, create a complex composite foundation. The testing of small-scale models offers an initial evaluation as to the influence of the GIGR technologies on the performance of a pile group.

3 EXPERIMENTAL PROGRAM

3.1 Introduction

The following chapter describes an experimental program to assess the influence of GIGR elements on an existing foundation system as a composite foundation. Section 3.2 describes the components of a composite foundation. Section 3.3 presents the testing program and methodology, while section 3.4 discusses the geometrical and material property scaling. The test setup is presented in section 3.5, the instrumentation for both the axial and lateral tests is illustrated in section 3.6, and the excavation and documentation processes are shown in section 3.7

3.2 Components

A composite foundation is a complex integration of components, consisting of both foundation and GIGR elements. Every component impacts the performance of the foundation system and each in turn is influenced by many technology-specific variables. The specific components of the composite foundation under consideration for this research are the pile cap, cast-in-place piles, helical piers, and low-pressure grouting.

3.2.1 Pile Cap

The pile cap's main function is to transfer the structure's loads through the piles to the soil. Many pile foundation designs consider only the capacity of the piles (as a free-standing pile group), neglecting any bearing capacity from the pile cap (Long, 1993, Poulos et al., 1980). The pile cap, however, is typically in contact with the ground, often resulting in a configuration that has been referred to as a piled footing (Long, 1993). The contact offers additional capacity to the foundation, but, as the pile cap-soil interface is typically large, a large ground movement is needed to mobilize this additional capacity

(Poulos et al., 1980). Despite this phenomenon, the capacity provided by the pile cap is often not considered in the design and is only used towards a higher factor of safety. The pile cap involved with this experimentation, however, will be treated as a piled footing and is considered towards the total foundation capacity.

3.2.2 Piles

Piles transfer structural loads to the soil through both end bearing and side friction. A pile's capacity is directly related to its geometry, as both end bearing and side friction increase with an increased cross-sectional area and surface area (Coduto, 2001). Deep foundations consist of either a single large pile or several piles connected by a pile cap, called a pile group, with an increase in the total number of piles typically resulting in a nonlinear increase of the overall performance of the pile group (Poulos et al., 1980). The details of the piles implemented in this experimentation are described in section 3.4.1.1.

3.2.3 Helical Piers

Helical piers (as described in section 2.3.1) are similar to piles in that their performance is affected by geometry and quantity, however, the installation angle can also have considerable influence, depending on how load is applied to the pier (Rogers, 2002). As helical piers exclusively use the bearing capacity of their helices for axial load, rather than side friction, an increase in the size and number of helices leads to a larger pier capacity (Carville et al., 1995). It should be noted that while larger helix diameters and more helices engage a larger bearing area, a larger number of helices can change the failure mechanism of the pier to cylindrical shear (Figure 3.1).

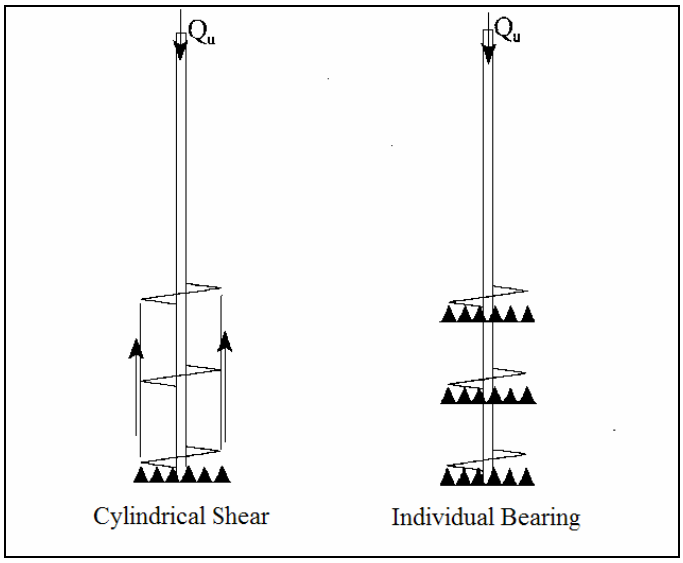

Figure 3.1 Capacity for helical piers (Perko et al., 2000)

The angle of installation is only significant when the loads act eccentrically on the pier as the pier does not perform in its intended manner, and shear or bending can unintentionally become the controlling design factor (Pack, 2000). The helical piers used in this research are described in detail in section 3.4.1.2, and, while installed at an angle, are implemented in such a way that shear and bending do not become the controlling design factor.

3.2.4 Grout

Grout is typically used to alter the in-situ soil conditions, by permeation grouting, compaction grouting, or soil mixing (Fang, 1991). Permeation grouting fills the voids in the soil matrix with a cementitious material, compaction grouting displaces the soil resulting in a denser configuration, and soil mixing is mixing the existing soil with a cementitious material (Warner, 2004). The application of grout can be considered a type of permeation grouting, as the helical piers carve a path in the soil which is consequently filled by unpressurized grout.

The performance of the grout used in this application is based on its injection pressure, mix strength, and bond with the piers and soil. While the injection pressure can significantly affect the radius of influence, the method used in this research involves a low pressure system and the radius of influence is directly related to the helix diameter (section 2.3.3.1). A grout's strength and stiffness is determined by its composition, and is typically greater than the soil in which it is being placed, such that there is a large improvement to the strength and stiffness of the soil being grouted. The grout properties can be changed to meet the specific site needs. Since the grout must bond with the soil and the structural components, the bond strength must be sufficient at each interface for adequate load transfer. The bond strength is different from the grout strength, in so far as there could be a strong grout weakly bonded with various elements in the system (Warner, 2004).

3.3 Methodology

In order to evaluate a composite foundation system involving the four aforementioned components, eight combinations at $^{1}/_{8}^{th}$ scale model testing in a consistent, uniform sand were used to provide an initial assessment of the viability of using superposition as a design approach for composite GIGR foundations, with supplemental work being conducted on individual piling elements.

While each component's performance is affected by its own variables, component interaction in a composite system may generate secondary influences on particular elements. The extent of component interaction is often unknown and causes heightened complexity in system evaluation and subsequent modeling. For this reason, an

experimental testing program of evaluating the influence of each individual component, followed by the evaluation of various combinations was selected.

The experimental program is outlined in Table 3.1, and consists of eight tests used for both axial and lateral loading. These tests are schematically represented in Figure 3.2. As the pile cap is common to all tests, an evaluation of the load-displacement response of only the pile cap needed to be established (Component test 1). Once the cap behavior was evaluated, the individual contributions of the piles, piers, and grout to the load-displacement response of the pile cap could be determined (Component tests 2-4). With each individual component contribution known, various component combinations could then be evaluated and their effects determined (Solution tests 5-8). Additional tests on the axially and laterally loaded Component test 2 were performed to determine the level of repeatability.

Table 3.1 Breakdown of test methodology for both axial and lateral tests

Component	Component Tests				Solution Tests			
	1	2	3	4	5	6	7	8
Cap (C)	x	x	x	x	x	x	x	x
Piles (P)		x			x	x		x
Helical Piers (R)			x		x		x	x
Grout (G)				x		x	x	x

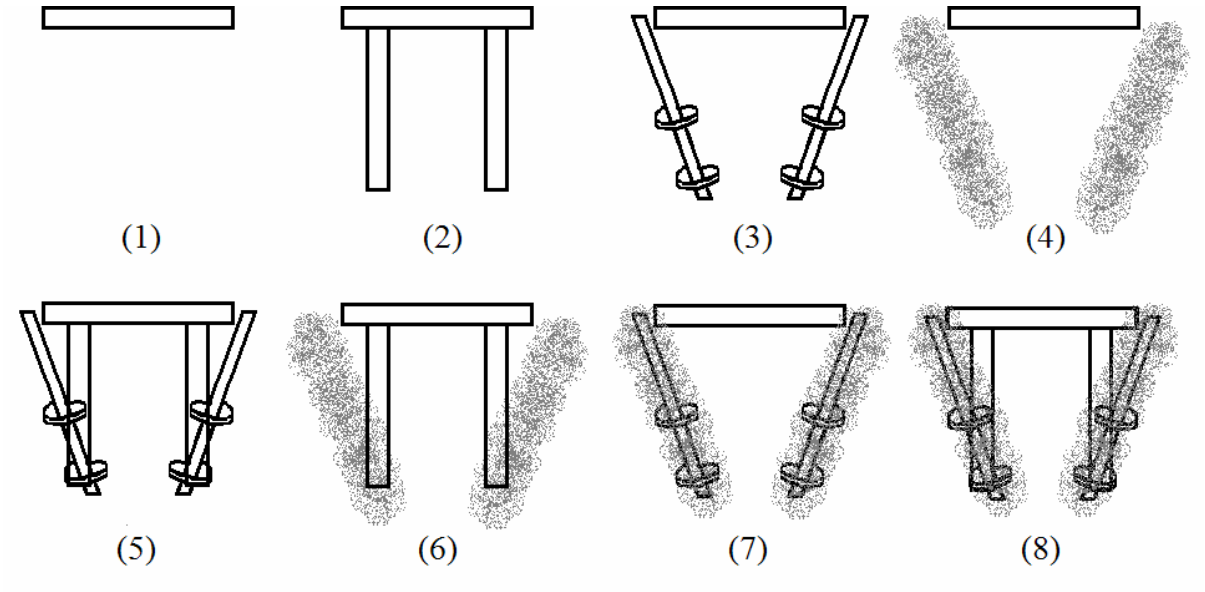

Figure 3.2 Schematic representation of component and combination tests

To further investigate the axial response of the above composite foundations, individual piles were tested axially both before and after being enhanced by GIGR technologies. In order to closely represent the confinement provided by the surrounding piles, the individual piles are cast with the same spacing as the aforementioned foundations, but in a 2x3 pattern, as seen in Figure 3.3. The solid circles represent the top of the piles installed vertically, while the dashed circles and the concentric circles represent the top of the grouted and ungrouted helical piers, respectively, installed at an angle sufficient for the piers to reach the base of the piles.

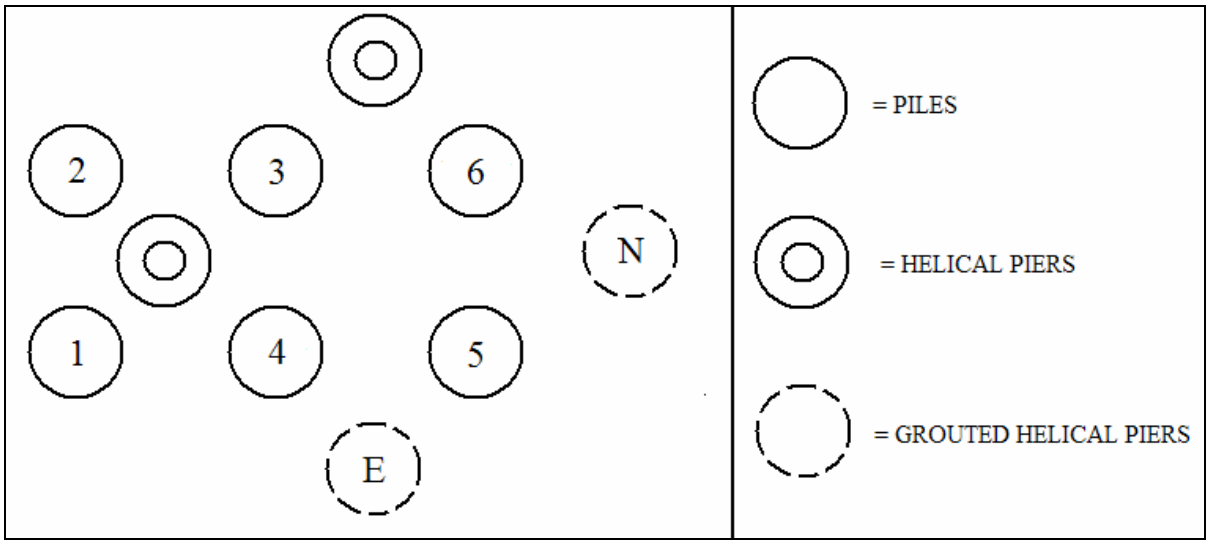

Figure 3.3 Individual piles testing setup

The helical pier in the middle of piles 1, 2, 3 and 4 is not to be installed until after piles 1 and 2 are tested. Thus, piles 1 and 2 are tested prior to any GIGR installations to establish a base-line performance level. Pile 3 is tested with two adjacent ungrouted helical piers, piles 4 and 6 are tested adjacent to one ungrouted and one grouted, helical pier, and pile 5 is tested with two adjacent grouted, helical piers.

The following labeling system was used to more readily reference each of the performed tests. The labeling of each test depended on both test type and component involvement. There were two types of tests, axial (A) and lateral (L), and four components, cap (C), piles (P), piers (R), and grout (G). Thus, LCPRG refers to the laterally tested foundation involving the cap, piles, piers, and grout. In some instances the label may be followed by a number which indicates that it is the *n*th test of that type performed. For example, ACP3 is the third test of the axially loaded cap and pile foundation. For the individual pile tests, each test is referred to as P, then the corresponding number in Figure 3.3, ie. P1. Additional labeling of the piers and piles for each foundation was based on a directional system. For example, the pier on the south

side of the foundation was referred to as S, the pile in the northwest corner of a pile foundation was referred to as NW, and the number in parenthesis after the pile labels was used during testing to indicate which displacement gage was used at each location (Figure 3.4).

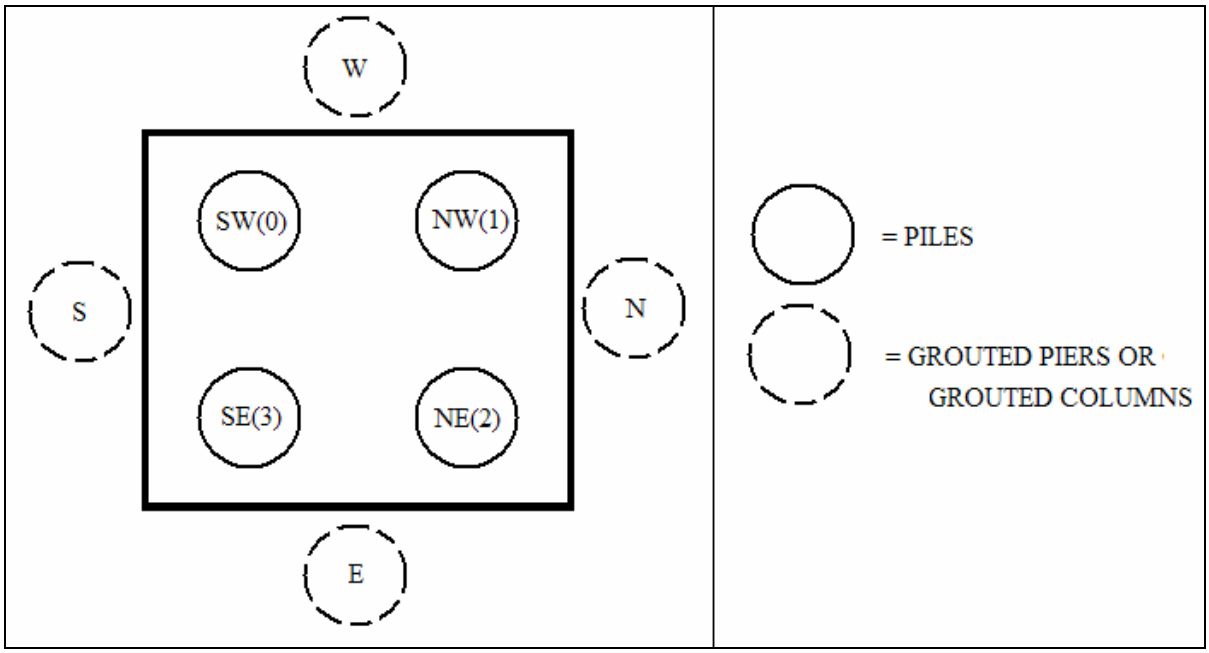

Figure 3.4 Labeling system for piles and piers

3.4 Scaling

This section deals with the two main scaling issues of model testing: geometric scaling and material property scaling.

3.4.1 Geometric scaling

Geometric scaling deals with the dimensional scaling, such as height, length and width. The foundations and helical piers both required physical scaling, as are discussed in the following sections.

3.4.1.1 Pile foundation

The prototype pile foundation was designed based on ADSC standards and specifications (ADSC, 1999). The foundation to be modeled consisted of 4, 18″

diameter, 12′ long, cast-in-place piles in a 2x2 configuration with a center-to-center spacing of 54″. The pile cap was 7.5′ x 7.5′ x 2′ deep. A 10″ diameter reinforcing cage consisting of 6 - #8 longitudinal bars with #4 spiral reinforcing bar at 6″ spacing was placed in each pile, and a 4″ concrete cover was required due to the removal of the casing.

The $^{1}/_{8}^{th}$ scaled model foundation then consisted of 2.25″ diameter, 18″ long, cast-in-place piles in a 2x2 configuration with a center to center spacing of 6.75″. The pile cap was 11.25″ x 11.25″ x 3″ deep. A 1.25″ diameter reinforcing cage was placed in each pile and maintained a 0.5″ concrete cover. The reinforcing bars were represented by $^{1}/_{16}$″ diameter twisted lead wire. The #8 and #4 reinforcing bars had a 1″ and 0.5″ diameter, respectively. At $^{1}/_{8}^{th}$ scale, this became $^{1}/_{8}$″ and $^{1}/_{16}$″ diameters. Each #8 longitudinal reinforcing bar was represented by two $^{1}/_{16}$″ diameter lead wires (twisted to simulate the knurland effect to increase the bond of the wire to the concrete) and the #4 spiral reinforcing bar was represented by a single $^{1}/_{16}$″ lead wire, spaced at 0.75″.

3.4.1.2 Helical piers

The prototype helical piers were taken from technical documents provided by Prescision Pier USA, Inc. The piers consisted of a 4″ diameter, round tube shaft, with two 16″ diameter, 3″ pitch helices spaced at 48″ apart. The base of the shaft was cut at a 45^{o} angle, and the grout hole was located at approximately 5″ from the tip of the pier.

The prototype was scaled down to a 0.5″ outer diameter, 0.37″ inner diameter, 34″ long, round tube shaft, with two 2″ diameter, $^{3}/_{8}$″ pitch helices spaced at 6″ apart. The base of the shaft was cut at a 45^{o} angle, and a $^{1}/_{8}$″ diameter grout hole was located at approximately $^{5}/_{8}$″ from the tip of the pier. Both tube ends were filled with epoxy to

prevent the unintended expulsion of grout and the unwanted introduction of sand into the tube as the pier advanced, and the helices were attached such that the splits were offset 180^{o}. For a more detailed description of the construction of the helical piers, see Appendix B.

3.4.2 Material property scaling

It was felt that full-scale foundations would suffer excessively large displacements before material or bearing capacity failure, leading to the selection of a performance based failure criteria. For this reason, only the material stiffness for the concrete, steel, and grout had to be $^{1}/_{8}^{th}$ their full-scale equivalent and the scaling of the material's strength could be no less than $^{1}/_{8}^{th}$ the full-scale equivalent, as it was not the controlling factor. A material's stiffness is a function of both its geometry and young's modulus and is calculated as AE/L, where A=cross sectional area, E=Young's modulus, and L=element length. If both the geometry and Young's modulus are scaled then the stiffness is scaled, however, if only the geometry or modulus is scaled, then the other can be manipulated such that a scaled stiffness value is achieved.

3.4.2.1 Soil

Dry sand was chosen as the substrata due to the ease and uniformity in which it can be placed. The sand was obtained commercially from a local North Carolina distributor and was marketed as "double washed playground sand". Figure 3.3 shows the grain size distribution curve for this soil. A majority of the sand particles are retained on the 40 and 60 sieves, with a very small percent of fines present. According to the USCS the soil would be considered a poorly graded sand (Das, 1998).

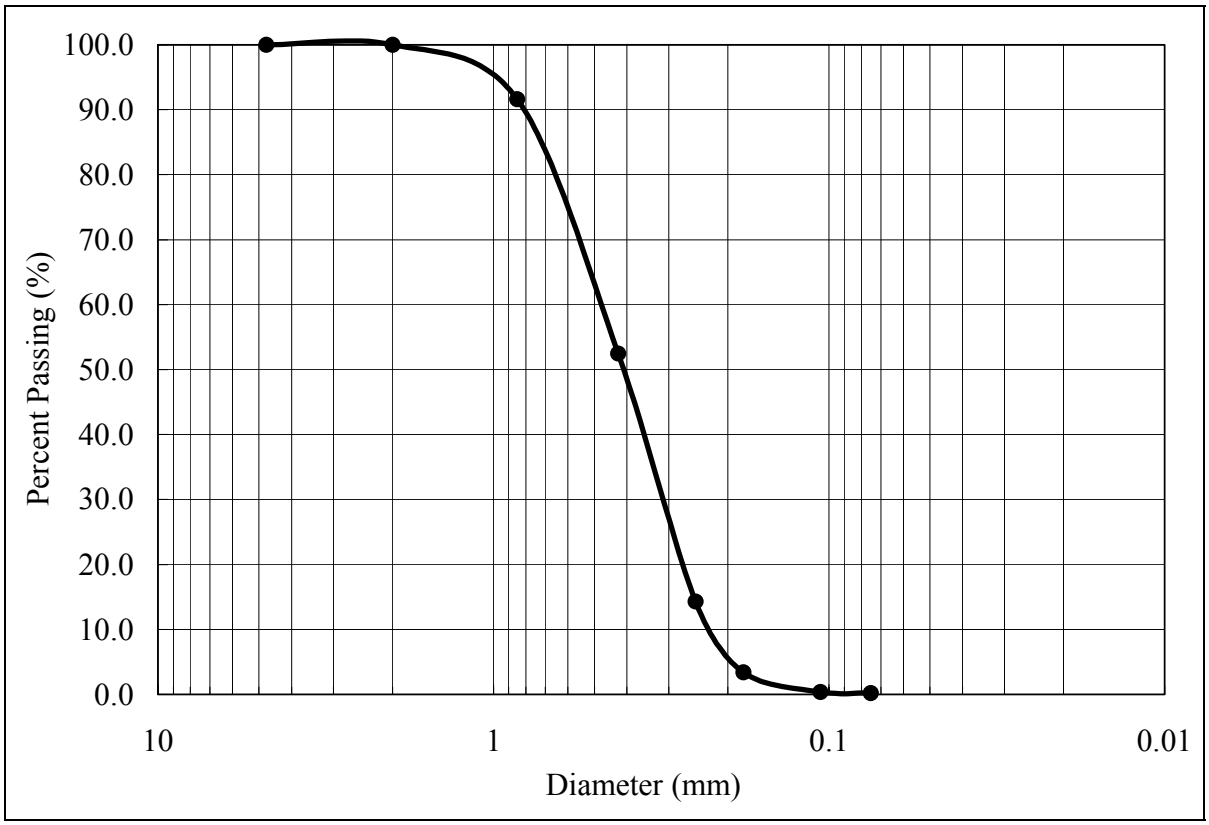

Figure 3.5 Grain-size distribution curve for double washed playground sand

ASTM maximum and minimum density tests (ASTM D 4253 – 00 and ASTM D 4254 – 00, respectively) resulted in a maximum density of 107.61 lbs/ft^3 and minimum density of 90.51 lbs/ft^3. It has been shown that, due to the dilation from a lack of confinement, a sand with a loose relative density behaves as a medium dense configuration (Laefer, 2001). Thus, a loose relative density of 55%, approximately 100.0 lbs/ft^3, was set as the target density.

3.4.2.2 Concrete

Typical concrete strength ranges from 3,000 – 5,000 psi, and the modulus of elasticity is related to the concrete strength by $57{,}000\sqrt{f'c}$ (ACI, 1999), resulting in a range of 3,000,000 to 4,000,000 psi. This led to a $^1/_8{}^{th}$ scale range of 390,000 to 503,000

psi. The concrete mix consisted of Saylor brand Type I/II Portland cement, water and concrete sand, the grains size distribution curve of which can be seen in Figure 3.6.

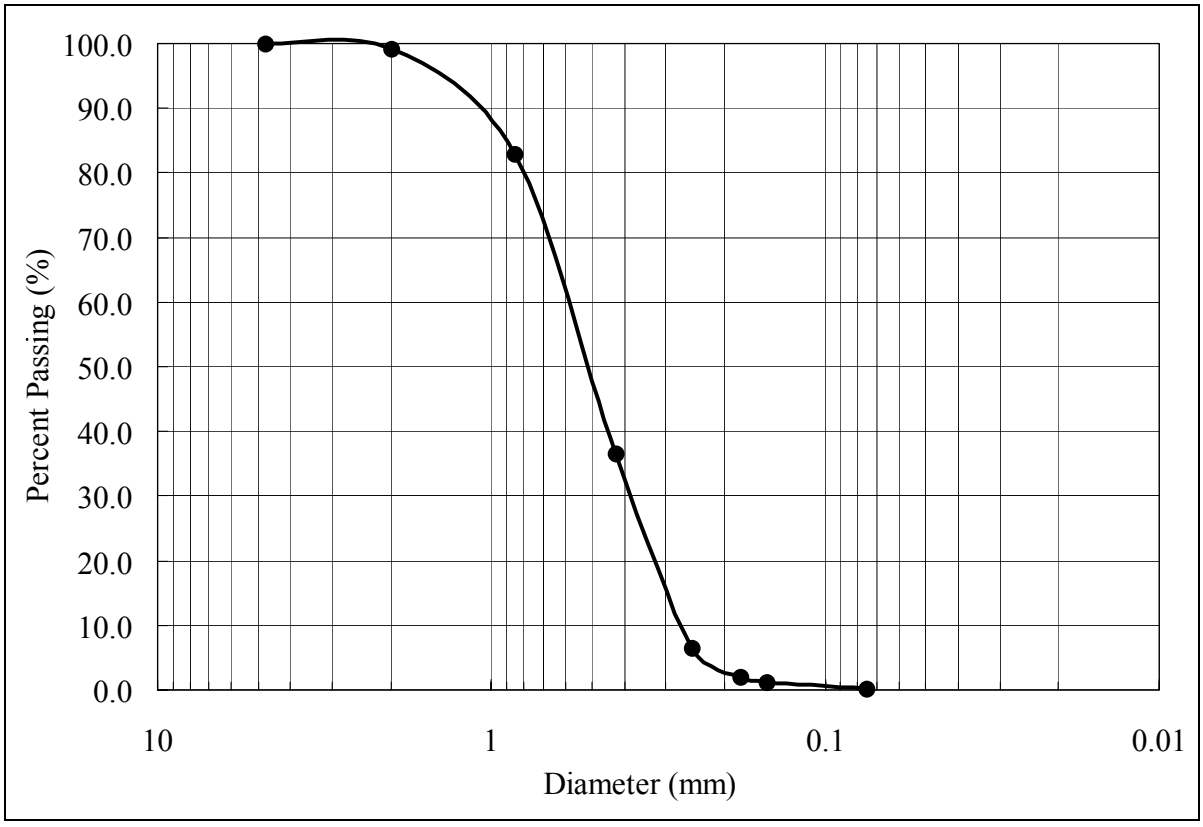

Figure 3.6 Grain-size distribution curve for concrete sand

To scale the modulus of elasticity, "water stoppage" bentonite, obtained from CETCO, was introduced into the concrete mix. Table 3.3 shows the quantities of cement, water, bentonite, sand, and Advaflow (an admixture that reduces segregation and increases workability) used in the final scaled concrete mix, and the resulting strength and modulus of six cylinders cast of this mixture.

Table 3.2 Strength and stiffness of the scaled concrete mix

Label	Cement (grams)	Water (grams)	Bentonite (grams)	Sand (grams)	Advaflow (ml)	Strength* (psi)	Modulus** (psi)
CVM1	1175	1075	100	1850	10	1,503	405,820
CVM2						1,436	363,333
CVM3						1,398	392,788
CVM4						1,641	478,033
CVM5						1,382	425,401
C12						1,482	486,000

*Average = 1,474 psi, Standard Deviation = 94 psi, Coefficient of Variation = 6%
**Average = 425,229 psi, Standard Deviation = 48,459 psi, Coefficient of Variation = 11%

The concrete for each cylinder in Table 3.3 was mixed separately to ensure repeatability, and a grinding machine was used to level the top and bottom surface of each cylinder prior to compression testing. The bentonite was premixed with the water for 30 seconds using a drill driven paint mixer and then prehydrated for 1 hour prior to the introduction of the cement and sand. Additionally, a typical 28-day strength would considerably prolong the testing schedule, so a shorter set time was chosen such that the modulus would still fall into the desired range, but also be reliable. The cylinder tests shown in Table 3.3 were performed at a nine day strength, and yielded consistent stiffness values. As both the geometry and modulus are scaled to their $^{1}/_{8}^{th}$ values, the stiffness of the concrete shows similitude between the model and prototype.

3.4.2.3 Grout

While full-scale concrete has a well-established relationship between strength and elastic modulus, grout mixes do not. To obtain a range for the prototype modulus, a mix was obtained from a grouted, helical pier contractor that uses a 0.44 water to cement ratio from which 10 cylinders were cast and tested at both 10 and 28 day strengths. The modulus results, as seen in Table 3.4, range from 800,000 – 1,000,000 psi, (100,000 –

125,000 psi at a $^{1}/_{8}^{th}$ scale). The top and bottom of the cylinders were ground level prior to constant load rate compression testing.

Table 3.3 Prototype grout mix

Label	Strength (days)	Cement (grams)	Water (grams)	Bentonite (grams)	Sand (grams)	Advaflow (ml)	Strength (psi)	Modulus (psi)
RGM2	28						4,149	962,232
RGM3	28						4,029	776,806
RGM4	10						3,729	895,455
RGM5	28						5,799	1,096,429
RGM6	10						4,605	917,029
RGM7	10						4,442	1,027,189
RGM8	28						5,346	1,013,087
RGM10	10						4,858	1,158,294

*Average = 4,620 psi, Standard Deviation = 694 psi, Cofficient of variation = 15%
**Average = 980,815 psi, Standard Deviation = 120,343 psi, Cofficient of variation = 12%

Similar to the concrete, bentonite was introduced into the grout mix in order to reduce the modulus of elasticity. Table 3.5 shows the quantities of cement, water, bentonite, and Advaflow for each cylinder and the resulting strength and modulus for five cylinders cast of the mixture.

Table 3.4 Scaled grout mixes

Label	Cement (grams)	Water (grams)	Bentonite (grams)	Sand (grams)	Advaflow (ml)	Strength (psi)	Modulus (psi)
FF1						697	117,836
FF2						679	101,933
FF3	1500	1700	200	0	10	679	118,512
FF4						699	88,938
FF6						679	94,121

*Average = 687 psi, Standard Deviation = 10.4 psi, Coefficient of Variation = 1.5%
**Average = 104,268 psi, Standard Deviation = 13,513 psi, Coefficient of Variation = 13%

It was felt that grout installation could be performed without disturbing the concrete after two days of curing. The foundations were tested nine days after casting,

with two days for curing, thus, the grout strength was taken at seven days. Therefore, the cylinders in Table 3.5 show a seven-day strength for the scaled grout mix. As both the geometry and modulus are scaled to their $^{1}/_{8}^{th}$ values, the stiffness of the concrete shows similitude between the model and prototype

3.4.2.4 Steel

One of the drawbacks to model testing using scaled material properties is the difficulty in material modeling. Unlike concrete, whose mixture can be changed to alter the stiffness, a material must be found that has the scaled properties of steel. Section 3.4.1.1 illustrated that geometric scaling was achieved for the steel reinforcing cage by using $^{\mathbf{1}}/_{\mathbf{16}}''$ diameter lead wire. Typically, steel has a modulus of elasticity of 29,000 ksi, leading to a $^{\mathbf{1}}/_{\mathbf{8}}^{th}$ scale modulus of 3,625 ksi. In order to represent the steel reinforcement, $^{\mathbf{1}}/_{\mathbf{16}}''$ lead wire was chosen, which has a Young's modulus approximately $^{\mathbf{1}}/_{\mathbf{12}}^{th}$ that of steel of 2,400 ksi (Buch, 1999). As the geometry is at $^{\mathbf{1}}/_{\mathbf{8}}^{th}$ scale and the Young's modulus is at $^{\mathbf{1}}/_{\mathbf{12}}^{th}$ scale, the steel reinforcing has a $^{\mathbf{1}}/_{\mathbf{12}}^{th}$ scaled stiffness.

Modeling of the helical piers from lead was not feasible because the lead was unable to withstand the high torque applied to the piers during installation. As material stiffness is defined by A*E/L, where A = cross-sectional area of the element, E = modulus of elasticity, and L = the length of the member, the full scale stiffness (A=3.49 in^2, E = 29,000 ksi, L = 144 inch) is calculated as 703 k/in, with the $^{1}/_{8}^{th}$ scale as 88 k/in. Due to the insufficient modulus of the lead, aluminum was selected as a compromise material, with a Young's modulus of 10,000 ksi, it scaled to $^{\mathbf{1}}/_{\mathbf{3}}$ that of steel. The length of the pier is fixed at 18″ due to the foundation geometry, and the cross sectional area is limited due to the rigidity needed for installation, thus, the geometry was predetermined

and could not be altered to modify stiffness. A sufficiently rigid section of 0.0888 in^2 was chosen, resulting in a stiffness for the model helical piers of 49 k/in, resulting in a scaled stiffness of approximately $^1/_{14}^{th}$. Similitude is not as evident for the steel modeling as it is for the concrete and grout material modeling as constructability limited material selection.

3.5 Experimental Setup

The location of this experimentation was an indoor testing pit in the Geotechnical Systems Lab of the Constructed Facilities Laboratory at North Carolina State University. This 12′ x 9′ x 7′ pit (Figure 3.7) provided sufficient space for six foundations to be tested per filling of the pit, with minimal influence from surrounding foundations or the rigid walls and base of the pit (Appendix A). The foundations being tested can be considered either spread footings (for pile caps with no piles) or pile foundations. The layout for each of four rounds can be seen in Figure 3.8.

Figure 3.7 Testing pit

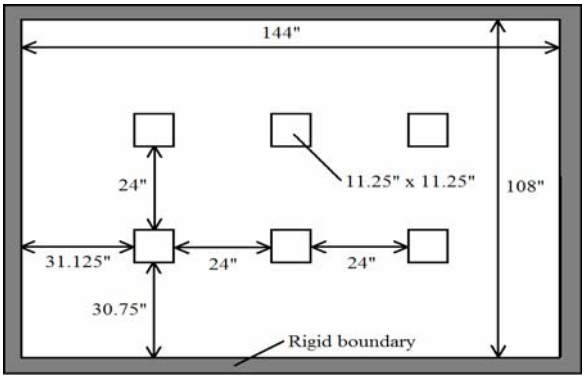

Figure 3.8 Test layout

In order to compare each foundation to those in other rounds it was important to perform the tests in the same soil conditions and to construct the foundations in a consistent manner. The following sections describe the steps followed for the subsurface setup and foundation installation.

3.5.1 Pit preparation

Approximately 60 tons of double washed playground sand with an initial water content of approximately 6% was oven dried to reduce the water content to approximately zero. This promoted consistency in the soil pluviation and subsequent response. Between tests, the sand was stored in 3′ x 3′ x 4′ flexible intermediate bulk containers (FIBCs) and covered in plastic to prevent the reintroduction of moisture. A layer of 4 mil plastic was used as a covering for the pit walls to minimize any soil/wall friction. The pluviation box was placed 3′ above the current sand level, pluviation was initiated, and the box was moved across the pit to minimize mounding. The pit was then progressively filled in 3″ layers using the sand pluviation box (Appendix B), until a 1′ layer was laid.

Upon completion of each 1′ sand layer, a Troxler nuclear density gage was inserted to a depth of 6″ to take density measurements at the center of each 1′ layer. At each of the six foundation locations for each filling of the pit, three density measurements were taken, the averages of which can be found in Appendix G. The trench offset feature on the nuclear density gage was used at each location to account for any density reading interference from the pit walls. Six layers of sand were laid and measured (as previously described), and a finishing box was used to level off any uneven areas at the surface. This apparatus was a small box with pegboard at the bottom that was moved to any location that needed leveling. This sand was also dropped from 3′ until the area was visually level.

3.5.2 Foundation Installation

Once the pit had been prepared, one of two foundation arrangements were installed at each of the six locations consisting of only a pile cap or a pile cap overlaying four cast-in-place piles.

1) Cap only: All six of the 11.25″ x 11.25″ x 3″ cap formworks were placed in their pre-designated location (see Figure 3.8). The forms were leveled in both North/South and East/West directions, and the formwork sides were placed such that they were parallel to the pit walls. Once leveled, any excess sand inside the formwork was removed to ensure a uniform 3″ thick pile cap. Concrete was then poured into the form and troweled to an even surface.

2) Cap and piles: When piles were involved, the same procedure was followed as that for the pile cap placement, except that prior to the casting of the cap the piles were installed. This was achieved with a casing in a manner similar to full-scale cast in place piers. The modeled casing was a 2.25″ diameter piece of PVC, and the auger was a threaded bar with helical shaped washers welded to the shaft and driven by a drill (Figures 3.9 and 3.10). The four PVC casings of a pre-designated length were initially inserted into the sand through a guide (Figure 3.11) to ensure that the piles were installed vertical. The piles were then advanced into the ground by manually pushing on the end of the PVC and inserting the auger until the PVC could no longer be advanced

Figure 3.9 Auger bit

Figure 3.10 Auger bit in drill

Figure 3.11 Casing guide (not installed here)

The sand inside the PVC was then removed using a vacuum, with careful attention paid to ensure that the sand beneath the base of the casing was not disturbed. When the sand was removed, the PVC was again advanced with the auger and the sand was removed until the PVC reached a depth of 18″ below the ground surface. Once the PVC was fully installed, a lead reinforcing cage (Appendix B) was set into each of the PVC casings. The concrete (as described in section 3.4.2.2) was mixed, and a funnel with a 1″ diameter spout was used to tremie the concrete down the center of the cage into the PVC. The concrete mix was sufficiently thick to prevent a free flow from the funnel, so a concrete vibrator was briefly held against the side of the funnel to decrease the viscosity of the concrete causing it to flow into the PVC until the casing was filled to the top. A rod was then placed down the center of the piles to check for any air pockets, and the vibrator was again used to vibrate the rod as it was removed to further reduce the possibility of honeycombing. The PVC was then removed from the sand while vibrating the PVC to ensure concrete flow as the PVC was removed. For the axially loaded tests, a well greased telltale was cast in the center of the reinforcing cage (Appendix B). The remainder of the cap formwork was filled with concrete and leveled

off. As the concrete cured, the telltales were rotated every half hour to break any bond developing between the concrete and the telltale casing.

When installing the individual piles for the PILES testing, the same basic process was followed but with a different casing guide and no telltale installation.

3.5.3 Grout and pier installation

Grouting was performed for two foundation types: those with a grouted helical pier, and those where the helical pier was removed leaving only a grouted column. In both of these foundation arrangements, the concrete was allowed to cure for two days prior to grout installation. The pier installer (as described in Appendix B) was placed such that the pier consistently entered the ground at the middle of the side of the pile cap and at an angle of 79° from horizontal (Figure 3.12), such that the base of the helical pier would reach the base of the cast-in-place piles (Figure 3.13).

Figure 3.12 Installation of helical pier

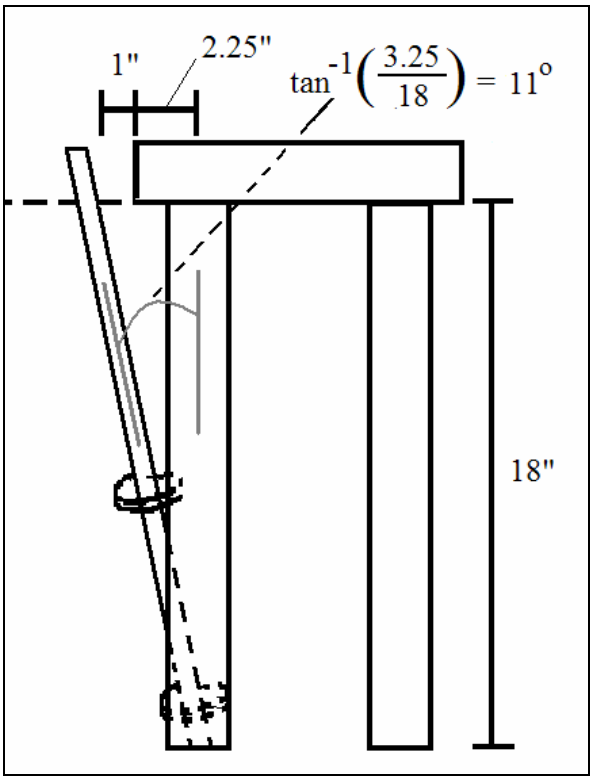

Figure 3.13 Sketch of installation angle

Once the pier installer was in place, the grout (as described in section 3.4.2.3) was mixed and placed into the grout cylinder (as described in Appendix B). The grout was then vibrated with a concrete vibrator to remove any trapped air pockets, and the lid was secured. The exit grout nozzle of the pressurized cylinder was then attached to the helical pier via a grout swivel (Appendix B) and the cylinder was pressurized until the grout flowed into the swivel and out the bottom of the pier.

Once the grout began to exit the base of the pier, the motor was turned on and allowed to pull the pier into the ground. As the pier advanced, the pressure was increased 1 psi per inch until the pier had reached 18″. If the foundation being tested contained a grouted pier, then the pier was detached and left in place. If, however, the foundation being tested only involved a grouted column, the pier was removed. To remove the pier, the motor was reversed and a force was applied to the back of the motor (a weight equivalent to the weight of the motor jig) to help the pier rotate itself from the ground (Appendix B). While the pier was being removed, the grout was still being pumped into the ground to fill any void left by the pier. Several practice grout installations were performed prior to the implementation with respect to the foundations, to determine the appropriate grouting pressures (Appendix C).

3.6 Testing and Instrumentation

As a displacement based failure criteria was chosen, each test was tested to a specified displacement. Typically, full-scale piles require $^1/_4$″ to $^1/_2$″ displacement to fully mobilize the side friction and approximately $^1/_{10}{}^{th}$ the pile diameter to fully mobilize the end bearing (Poulos et al., 1980). At $^1/_8{}^{th}$ scale, these values would be from $^1/_{32}$″ to $^1/_{16}$″ for side friction and would be $^1/_{80}{}^{th}$ the pile diameter. The scaled values were felt to be too small to allow the side shear of the scaled piles to mobilize. Because of the decreased material

strength (due to the decreased stiffness), an initial load test displayed material failure at $^1/_2$″ of displacement. As material failure was not the goal, a $^1/_4$″ displacement was chosen as the failure criteria for both the axial and lateral tests (as described below). The results of the subsequent load-deflection curves were used to establish any systemic failure.

3.6.1 Axial load tests

An overall view of an axial load test setup can be seen in Figure 3.14. The axial load was applied in 50-100 pound increments by a hand-pump driven, 30-ton hydraulic piston jack (Figure 3.15) mounted to a steel reaction beam (Figure 3.16) bolted to the walls of the test pit (Figure 3.17).

Figure 3.14 Axial test setup

Figure 3.15 Hydraulic jack and pump

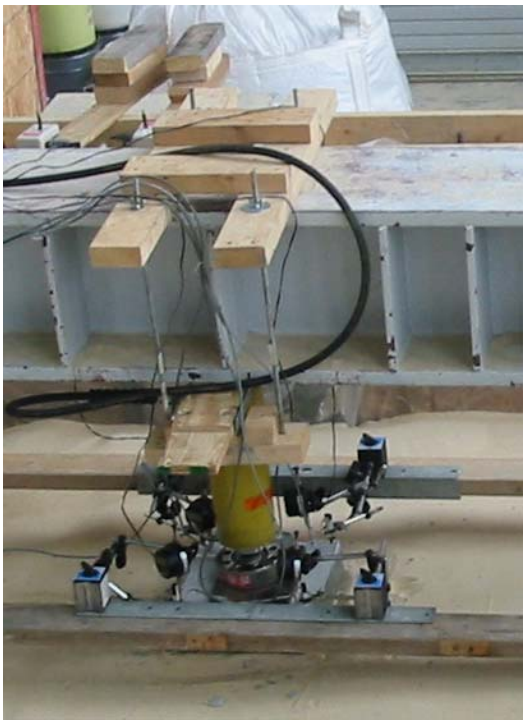

Figure 3.16 Jack mounted to beam

Figure 3.17 Beam bolted to test pit walls

The axial load test instrumentation setup for a cap only test can be seen in Figure 3.18 and for a cap and piles test in Figure 3.19, with the only difference being extra instrumentation for the telltale displacement. A load cell was placed between the jack and a plate on the pile cap to measure the applied load, and an electronic and manual displacement gage was set up on each corner of each foundation (Figure 3.20). The displacement gages were attached to an independent reference frame that was suspended across the pit (Figure 3.14), and was clamped to the pit walls for stability (Figure 3.21). The electronic load and displacement data were collected via a computerized data acquisition system, while the manual gages were hand recorded correlating to the load read from the electronic load cell.

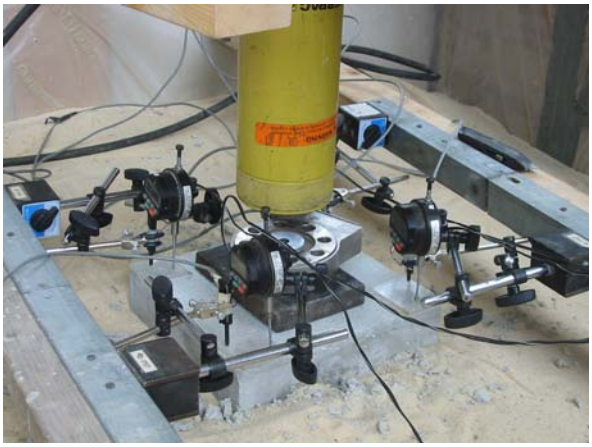

Figure 3.18 Cap test setup

Figure 3.19 Cap and pile test setup

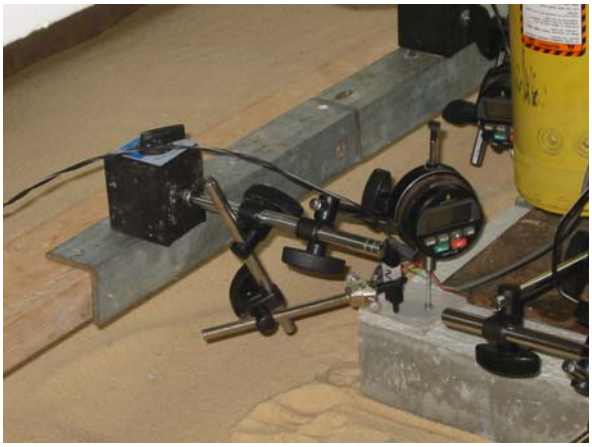

Figure 3.20 Displacement instrumentation

Figure 3.21 Instrumentation stabilization

3.6.2 Lateral load tests

An overall view of the lateral load test setup can be seen in Figures 3.22 and 3.23. The lateral load was applied in 20-40 pound increments by a hand-pump driven, 10-ton hydraulic piston jack (Figure 3.24) that was loaded against the pit wall (Figure 3.25). Approximately 428 lbs of dead weight was placed on top of each laterally loaded foundation to represent a static vertical load applied to the foundation. Each of the two corners on the loaded side was instrumented with both electronic and manual displacement gages (Figures 3.26 and 3.27). The displacement gages for each of the tests were set up on the same independent reference frame as that for the axial load tests.

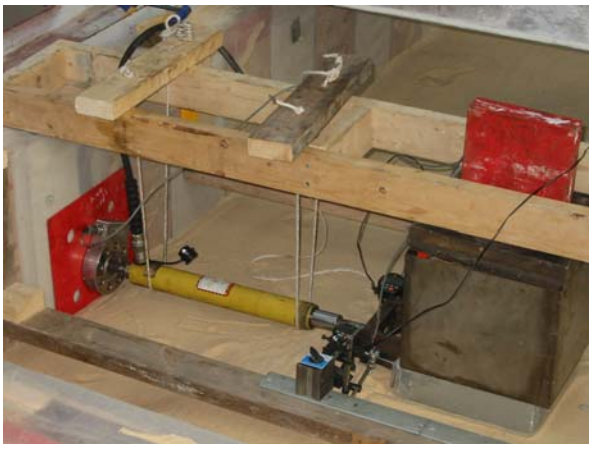

Figure 3.22 Lateral test setup

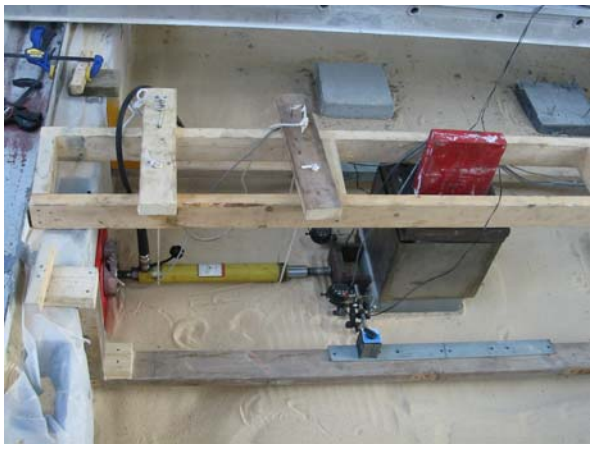

Figure 3.23 Lateral test setup

Figure 3.24 Hydraulic jack and pump

Figure 3.25 Load cell for lateral tests

Figure 3.26 Lateral displacement instrumentation

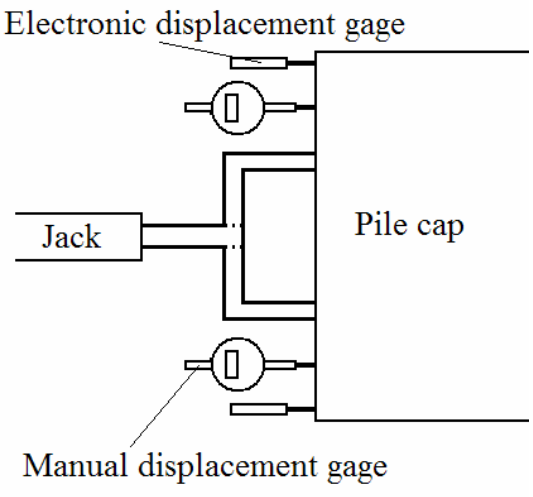

Figure 3.27 Schematic of lateral instrumentation

3.6.3 PILES load test

The test setup for the PILES load test was the same as that of the foundation axial load tests, with exception of the location of the load cell and the displacement gages. The load cell was relocated to between the jack and steel beam. Additionally, the displacement gages measured the displacement of a plate placed across the top of the pile as the surface area of each pile provided insufficient for direct measurement (Figure 3.28).

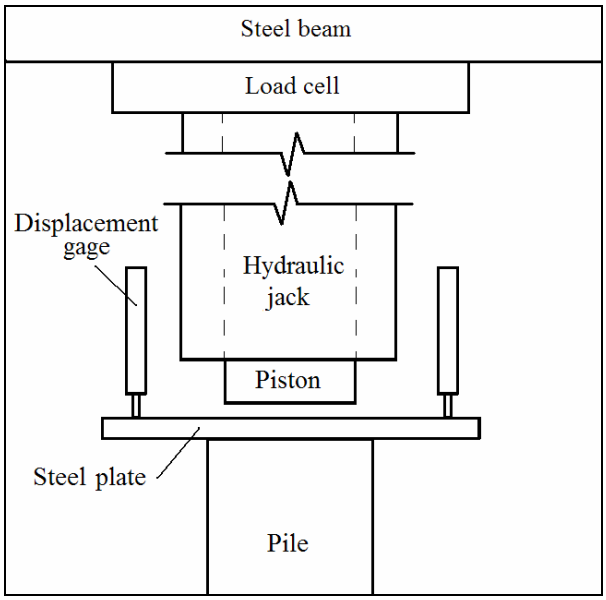

Figure 3.28 Elevation view of axial test setup for PILES test

3.7 Excavation and documentation

Upon completion of all testing, each foundation was carefully excavated. Since sand has a natural angle of repose, a hole adjacent to the foundation was dug such that the sand within the immediate foundation area flowed into the excavation. The new sand that flowed into this area was then removed, allowing for more sand to flow. This excavation method allowed for minimum disturbance of the foundations and piers, however, for some of the grouted piers and grouted columns the soil-grout mix was not

sufficiently rigid and the structure of some of the grouting broke apart as the sand around them was removed. The areas that experienced excavation induced damaged were noted.

Once excavated, each pile group was photographed and measured. The lengths were measured with a measuring tape, and diameters on two perpendicular axes were measured with calipers to an accuracy of $^{1}/_{1000}{}^{th}$ of an inch. Because the piles had fairly consistent diameters, measurements were taken at 2″ intervals. Similarly, each grouted pier and grouted column was photographed and measured. Due to the less consistent diameters of the piers and columns, measurements were taken every inch.

3.8 Summary

The main components for the composite foundations tested here are the pile cap, cast-in-place piles, helical piers and grout. Eight foundations configurations consisting of various combinations of these components are to be tested both axially and laterally to determine the behavior of pile foundations in the presence of grouted, helical piers. These tests are to be performed on small-scale models of drilled shaft foundations in sand, with both geometric and material property scaling. Additional supplemental tests on individual piles are to be performed to further evaluate the influence of the grouted, helical piers on individual piles. The installation, testing and documentation were developed to ensure the comparability of the tests, and these processes were described above.

4 EXPERIMENTAL RESULTS

4.1 Introduction

This chapter is divided into five sections. Sections 4.2, 4.3, and 4.4 provide the results from the axial, lateral and individual pile tests, section 4.5 shows the results from the telltale testing, and section 4.6 shows material property scaling. A picture, schematic representation and load-deflection curve for each test is shown, and a statistical analysis of the pier and pile geometry, for those foundations to which they apply, are provided to indicate the quality of installation.

The displacement used in all load-deflection curves was the average of the deflections at the four corners for the axial load tests, and the two corners on the loaded side for the lateral load test, unless otherwise noted. Each test was run until a minimum average displacement of 0.25″ was reached. Since the manual displacement data set was considerably smaller than the electronic data set, the manually recorded data was used when good correlation occurred between the two sets. Appendix D shows comparisons of the manual and electronically recorded load deflection curves for each test, with 18 of the 22 tests showing good correlation. For the remaining four tests, an average of the manual and electronic displacements was taken. To provide an initial validation of the data, the various cap foundation load deflection curves are shown in reference to the cap only test, and the various cap and pile foundations load deflection curves are shown in reference to the initial cap and piles test. A more detailed comparison of the test results is located in Chapter 5.

For tests in which piles and piers were installed, a statistical analysis, including the average, standard deviation (STDEV) and coefficient of variation (COV), is provided for

the pile and pier diameters to quantitatively show the consistency of the data set. It should be noted that two COV values were taken for each pile's statistical analysis, one including all the diameters and one excluding the top and bottom diameter values. The top diameters, where the pile connects to the cap, and bottom diameters tend to not be as consistent as the intermediate values because of the installation process, ranging from 2.0″-5.0″ for the top diameters and 0.8″-2.1″ for the bottom. When these values are included, the COV values for all the pile diameters are large, implying that the diameters over the length of the pile are not consistent, when in reality, the intermediate diameters are quite consistent, as seen by the always smaller intermediate COV values. A large COV for the intermediate diameters often indicates that there is exposure of the reinforcing cage, with these exposed areas indicated in each table as the values shaded in gray. A pile was considered to be of poor quality if the top diameter was larger than 4″ in diameter and the COV of the intermediate pile diameters was greater than 10. Pictures of each pile foundation can be seen in Appendix E.

When considering the statistical analysis of the pier geometry, it should be noted that most of the grouted columns and grouted helical piers had COV values larger than those seen for the piles. These larger values resulted from the more variable grout installation procedure. Additionally, the COV values only included the pier diameters above the bottom helix, the reason for which being that the grout only extended to the diameter of the helix when the helix passed through the grout. In some instances the installation torque caused the bottom helix to detach from the shaft, preventing further advancement, or would continue to advance to some additional depth but the helix not

passing through the grout. The detached helix resulted in long sections of grouted pier that were approximately equivalent to the shaft diameter.

Similar to the piles table, some of the pier geometry tables have values shaded in gray. These values, however, correspond to sections where the grout disintegrated during excavation and were not measurable. The diameters of these disintegrated areas were assumed to equal that of the adjacent measurable diameter, but were not included in the statistical analysis. Successful grouted installation was considered for piers with a COV smaller than 20% and a grouted length of 14″-16″: pictures can be seen in Appendix F.

4.2 Axial Load tests

4.2.1 Cap Only (AC)

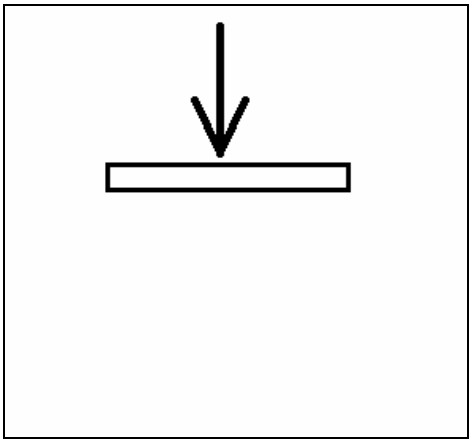

Figure 4.1 Schematic of AC test

Figure 4.2 Picture of AC test

The cap only axial load test was conducted to determine the load-deflection performance of the pile cap, with the resulting load-deflection curve presented in Figure 4.3.

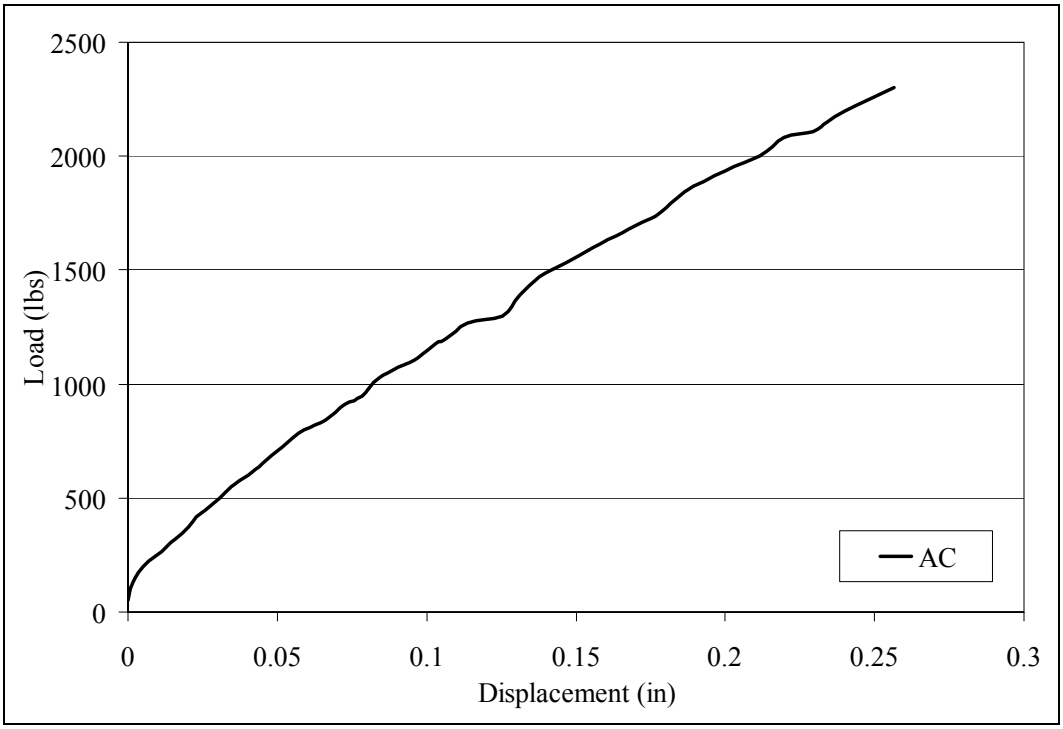

Figure 4.3 Axial load-deflection curve for AC test

4.2.2 Cap and Piles (ACP)

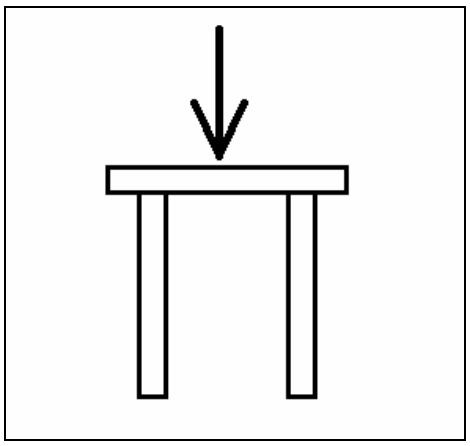

Figure 4.4 Schematic of ACP test

Figure 4.5 Picture of ACP1 test

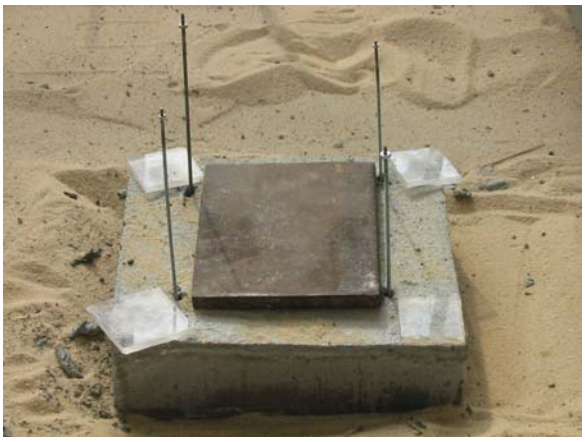

Figure 4.6 Picture of ACP2 test

Figure 4.7 Picture of ACP4 test

The cap and piles axial load test was conducted to determine how the addition of the piles would affect the cap only load-deflection curve. Several of these tests were performed to show the repeatability of the results. Additionally, various methods of telltale installation were evaluated. Figures 4.5-4.7 show pictures of various ACP tests with the main difference being the method of telltale installation.

4.2.2.1 ACP1

A comparison of the initial ACP test load-deflection curve with the cap only test (AC) can be seen in Figure 4.8.

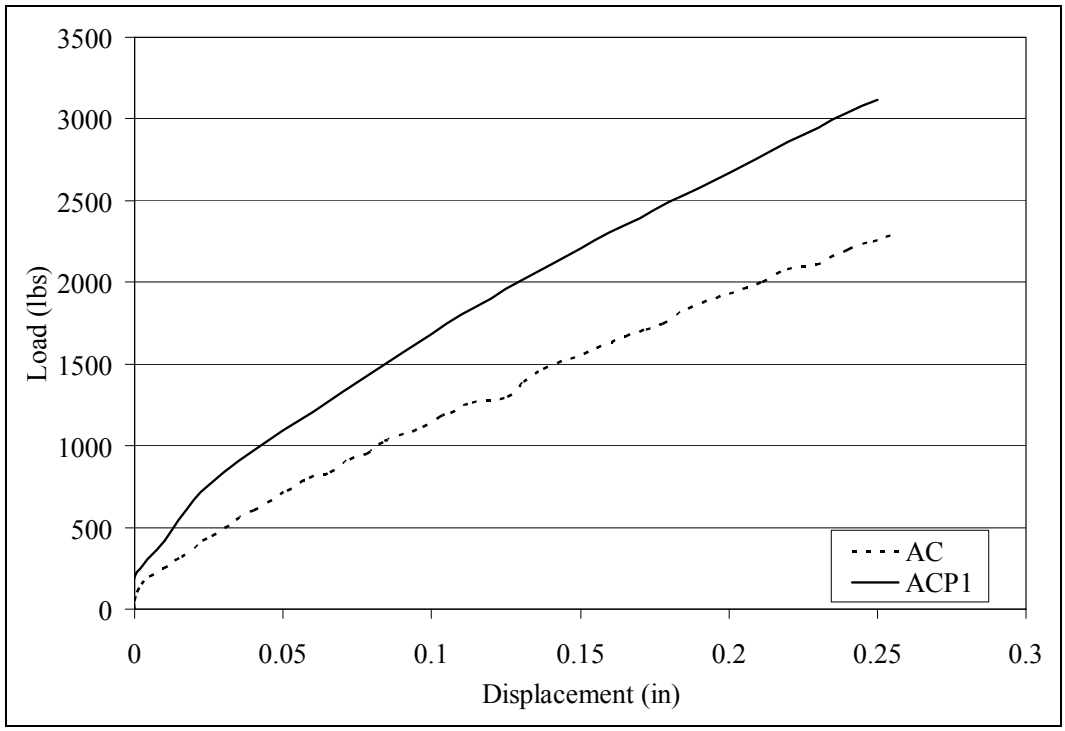

Figure 4.8 Axial load-deflection curve for ACP1 test

Table 4.1 shows the pile geometry for ACP1 with no defects observed upon excavation. All four piles showed similar lengths, measuring between 16.5″ and 17″. Only pile NE(2) had a COV larger than 2.5% over the entire pile length. Considering only the intermediate pile diameters, all COV values were less than 2%. With the top diameters less than 4″ and intermediate pile diameter COV values less than 10%, the piles were considered to be of acceptable quality.

Table 4.1 Pile lengths and diameters at various depths for ACP1

Pile label		SW (0)	NW (1)	NE (2)	SE (3)
Overall length		16.5	16.5	17	16.5
Depth (in)	0	2.186	2.194	2.452	2.204
	2	2.174	2.139	2.155	2.164
	4	2.098	2.121	2.116	2.180
	6	2.061	2.080	2.128	2.147
	8	2.062	2.087	2.087	2.133
	10	2.085	2.078	2.132	2.164
	12	2.084	2.090	2.060	2.126
	14	2.096	2.123	2.077	2.112
	16	2.041	2.129	1.727	2.104
	18	X	X	X	X
Average*		2.098	2.115	2.104	2.148
STDEV*		0.050	0.037	0.184	0.033
COV*		2.377	1.765	8.738	1.537
Average**		2.094	2.102	2.108	2.146
STDEV**		0.038	0.024	0.034	0.024
COV**		1.828	1.165	1.610	1.139

*Statistics include diameters at all depths

**Statistics without the top and bottom pile diameters

4.2.2.2 ACP2

A comparison of the ACP2 and ACP1 load deflection curves can be seen in Figure 4.9.

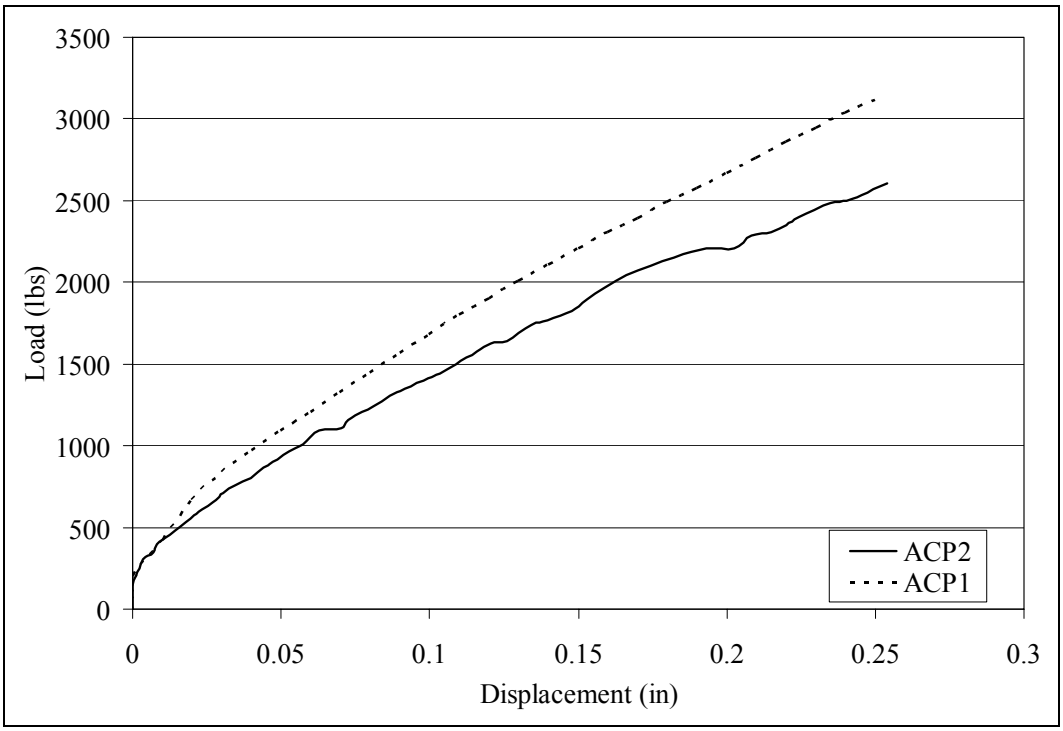

Figure 4.9 Axial load-deflection curve for ACP2 test

Table 4.2 shows the pile geometry for ACP2, with no defects observed upon excavation. All four piles showed similar lengths, measuring between 16″ and 16.5″. All piles had COV values larger than 6% over the entire pile length, with pile SE(3) having a COV of approximately 22%, due primarily to the 3.5″ top diameter. Considering only the intermediate pile diameters, however, all COV values were small, with 3 of the 4 piles having COV values less than 1% and NW(1) at approximately 3%. With the top diameters less than 4″ and intermediate pile diameter COV values less than 10%, the piles were considered to be of acceptable quality.

Table 4.2 Pile length and diameters at various depths for ACP2

Pile label		SW (0)	NW (1)	NE (2)	SE (3)
Overall length		16.5	16.5	16.5	16
	0	2.135	2.411	2.320	3.522
	2	2.084	2.287	2.113	2.142
	4	2.091	2.183	2.123	2.201
	6	2.112	2.158	2.135	2.164
Depth (in)	8	2.077	2.119	2.115	2.140
	10	2.082	2.147	2.127	2.155
	12	2.077	2.121	2.102	2.169
	14	2.110	2.069	2.140	2.173
	16	1.727	1.760	1.687	1.651
	18	X	X	X	X
Average*		2.055	2.139	2.096	2.257
STDEV*		0.125	0.176	0.167	0.504
COV*		6.067	8.219	7.967	22.325
Average**		2.090	2.155	2.122	2.163
STDEV**		0.015	0.069	0.013	0.021
COV**		0.711	3.185	0.618	0.967

*Statistics include diameters at all depths

**Statistics without the top and bottom pile diameters

4.2.2.3 ACP3

A comparison of the ACP3 and ACP1 load deflection curves can be seen in Figure 4.10. It should be noted that while removing a bonded telltale casing, the foundation experienced upward movement. This movement possibly caused the side friction in the piles to be mobilized prior to loading, resulting in an enhanced load-deflection performance.

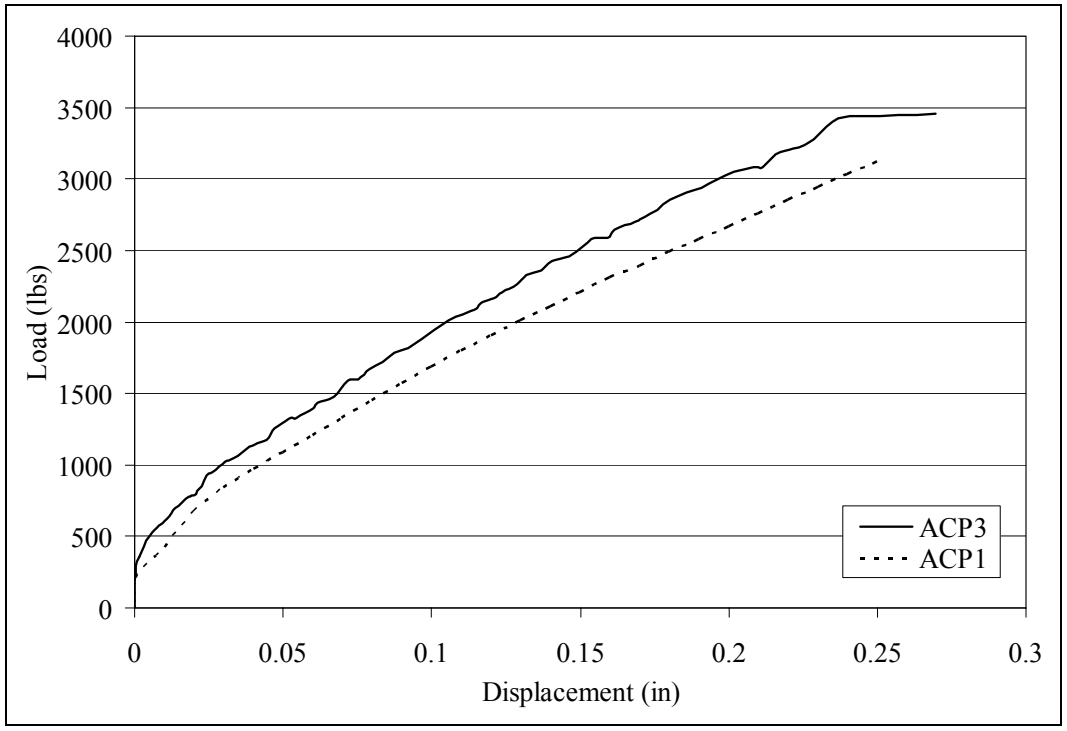

Figure 4.10 Axial load-deflection curve for ACP3 tests

Table 4.3 shows the pile geometry for ACP3 with no defects observed upon excavation. All four piles showed similar lengths, measuring between 18″ and 19.5″. All piles had COV values between 6% and 13% over the entire pile length. Considering only the intermediate pile diameters, however, all COV values were less than 2.5%. With the top diameters less than 4″ and intermediate pile diameter COV values less than 10%, the piles were considered to be of acceptable quality.

Table 4.3 Pile length and diameters at various depths for ACP3

Pile label		SW (0)	NW (1)	NE (2)	SE (3)
Overall length		18	19.5	18.5	18
	0	2.527	2.471	2.198	2.238
	2	2.247	2.264	2.138	2.112
	4	2.229	2.203	2.156	2.137
	6	2.226	2.196	2.256	2.135
Depth (in)	8	2.193	2.153	2.172	2.130
	10	2.196	2.172	2.217	2.130
	12	2.195	2.182	2.197	2.137
	14	2.203	2.167	2.128	2.117
	16	2.275	2.286	2.177	2.148
	18	1.912	1.418	1.603	1.440
Average*		2.220	2.151	2.124	2.072
STDEV*		0.147	0.274	0.187	0.225
COV*		6.638	12.756	8.806	10.862
Average**		2.220	2.203	2.180	2.131
STDEV**		0.029	0.048	0.042	0.012
COV**		1.324	2.158	1.936	0.545

*Statistics include diameters at all depths

**Statistics without the top and bottom pile diameters

4.2.2.4 ACP4

A comparison of the ACP4 and ACP1 load deflection curves can be seen in Figure 4.11.

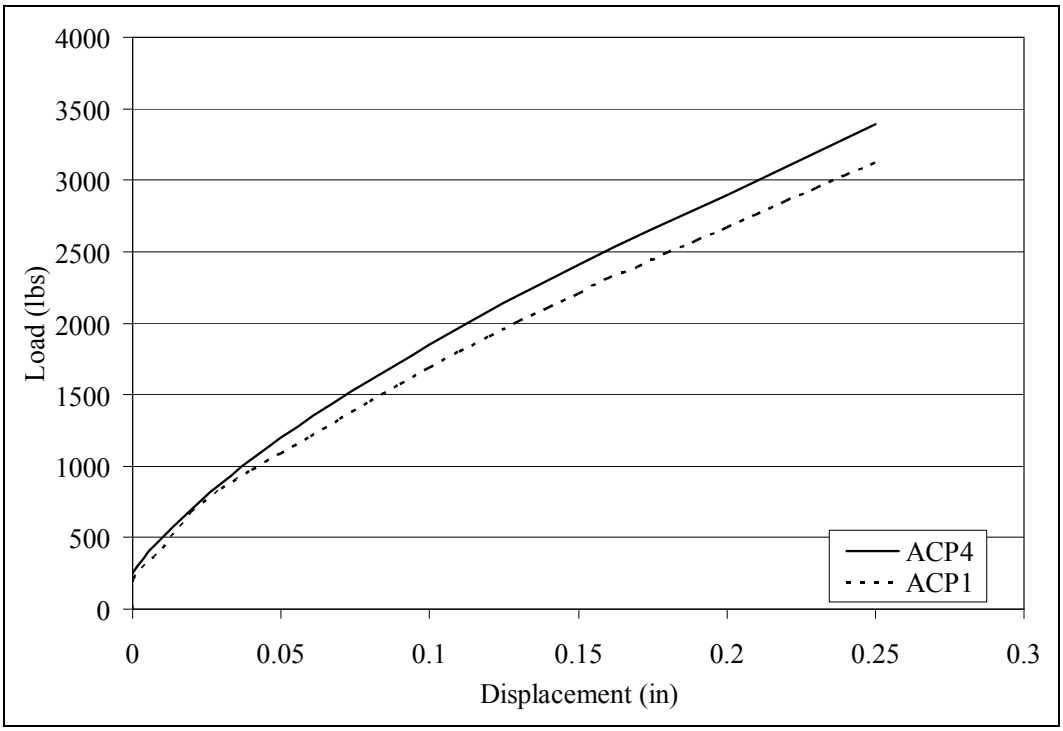

Figure 4.11 Axial load-deflection curve for ACP4 test

Table 4.4 shows the pile geometry for ACP4 with defects observed in NE(2) and SE(3) upon excavation. All four piles showed similar lengths, measuring between 18″ and 18.5″. All piles had COV values between 10% and 52% over the entire pile length. Considering only the intermediate pile diameters, the COV values ranged from 2%-13%. Both NE(2) and SE(3) had top diameters greater than 4″, at 4.929″ and 4.319″, respectively. As the casing for these two piles were removed, large air pockets in the reinforcing cage allowed sand to intrude into the pile. The intrusion of sand caused a depression around the pile at the ground surface that was filled by concrete. This defect caused a large section of the pile to have no concrete (only an exposed reinforcing cage) and the top to have a very

large diameter, in excess of 4″. With the top diameters greater than 4″ and intermediate pile diameter COV values greater than 10%, the piles were considered to be of poor quality.

Table 4.4 Pile length and diameters at various depths for ACP4

Pile label		SW (0)	NW (1)	NE (2)	SE (3)
Overall length		18.5	18	18	18
	0	2.367	2.565	4.929	4.319
	2	2.117	2.065	2.279	2.111
	4	2.111	2.079	1.935	2.038
	6	2.139	2.102	1.666	1.783
Depth (in)	8	2.136	2.111	1.696	2.154
	10	2.124	2.142	1.683	2.179
	12	2.123	2.151	1.851	2.162
	14	2.144	2.109	2.199	2.135
	16	1.709	2.159	2.167	2.167
	18	1.662	1.295	0.692	0.922
Average*		2.063	2.078	2.109	2.197
STDEV*		0.213	0.311	1.088	0.839
COV*		10.328	14.951	51.557	38.202
Average**		2.075	2.115	1.934	2.091
STDEV**		0.148	0.034	0.251	0.132
COV**		7.150	1.591	12.992	6.327

*Statistics include diameters at all depths

**Statistics without the top and bottom pile diameters

4.2.3 Cap and Piers (ACR)

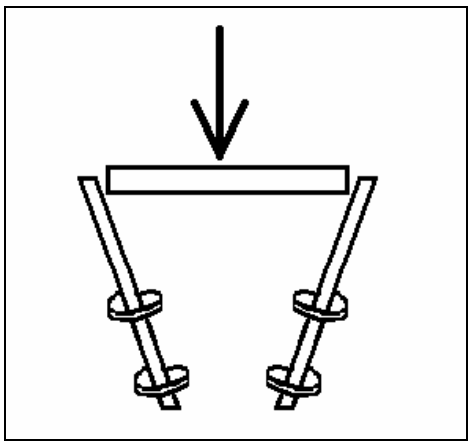

Figure 4.12 Schematic of ACR test

Figure 4.13 Picture of ACR test

The cap and piers test was performed to show the impact of helical piers on the cap only load-displacement curve. A comparison of the ACR and AC load-deflection curves can be seen in Figure 4.14.

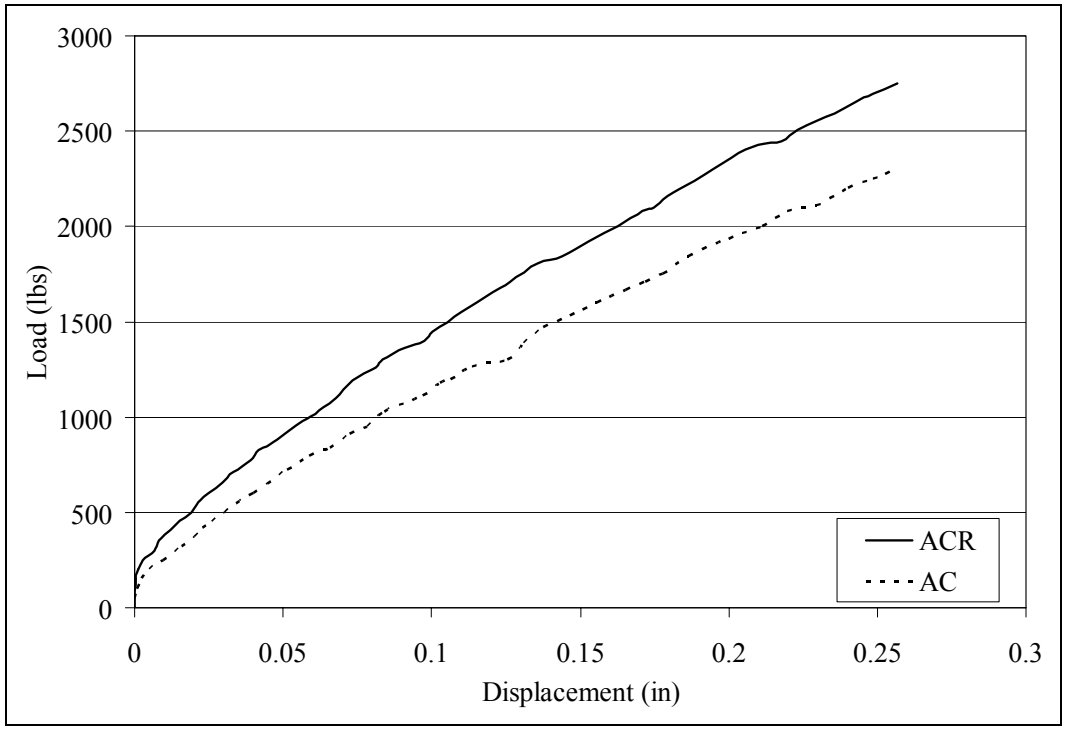

Figure 4.14 Axial load-deflection curve for ACR test

4.2.4 Cap and Grout (ACG)

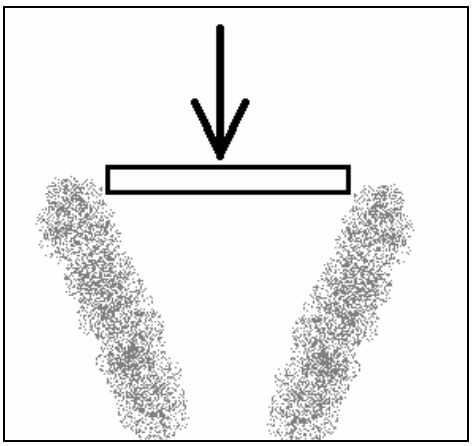

Figure 4.15 Schematic of ACG test

Figure 4.16 Picture of ACG test

The cap and grout test was performed to show how the addition of the grouted columns affected the cap only load-displacement curve. A comparison of the AC and ACG load-deflection curves can be seen in Figure 4.17.

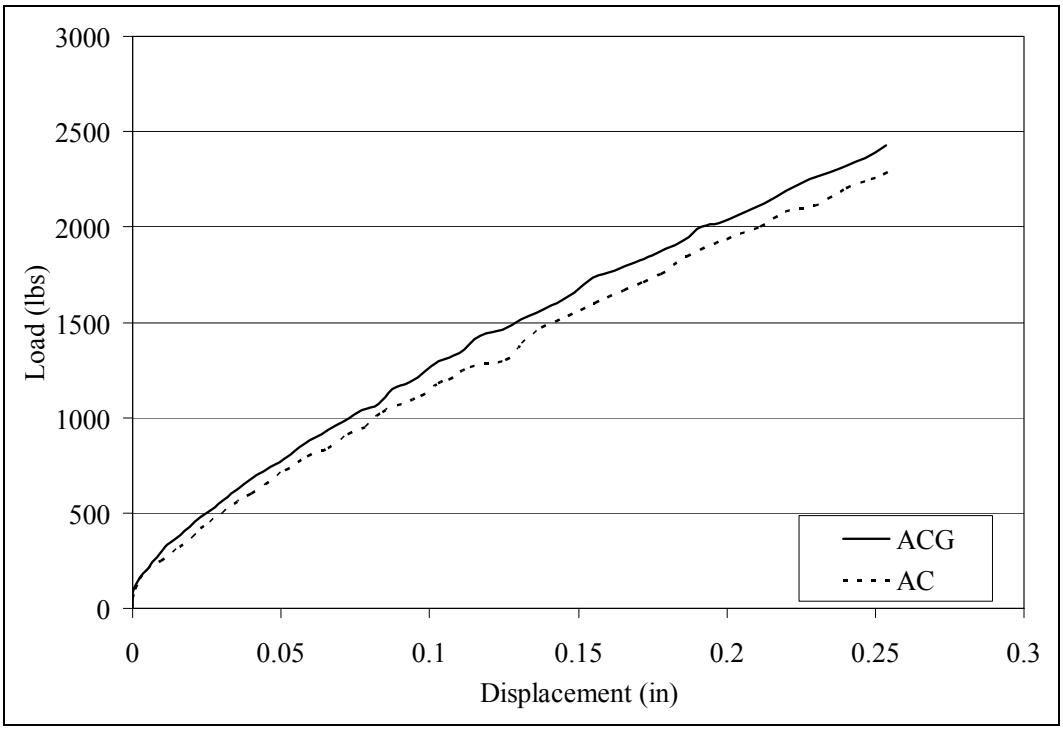

Figure 4.17 Axial load-deflection curve for ACG test

Table 4.5 shows the geometry of the grouted piers for ACG. The overall pier lengths ranged from 13″-18″, while the grouted portion of the piers ranged from 10″-15″. Both pier W and S reached the target 18″ installation depth, however, both also incurred a detached bottom helix that limited the grouted length to 12″ and 15″, respectively. Pier N was installed to 13″ while pier E was installed to 16″, however, both could no longer advance due to detached bottom helices. Their respective grouted lengths were 10″ and 13″. Both pier N and E had sections of grout near the top that fell apart during excavation. The COV values for the 4 piers ranged from 3%-14%, all below the 20% value. While the COV values proved acceptable, the length over which the grout was installed was only considered successful for pier S.

Table 4.5 Pier length and diameters at various depths for ACG

Pier label		W	N	E	S
Overall length		18	13	16	18
	0	1.461	2.029	2.015	1.493
	1	1.943	2.029	2.015	2.503
	2	2.163	2.029	2.015	2.832
	3	2.067	2.029	2.015	2.571
	4	2.108	2.029	2.188	2.257
	5	2.118	2.194	2.148	2.110
	6	2.129	2.175	2.105	2.001
	7	2.120	2.137	2.072	2.064
	8	2.167	2.161	2.110	2.170
Depth (in)	9	2.175	2.137	1.840	2.167
	10	2.135	2.057	1.526	2.098
	11	2.104	0.882	1.842	2.134
	12	2.034	0.790	1.904	2.161
	13	0.811	0.741	1.623	2.056
	14	0.772	X	0.721	2.169
	15	0.727	X	0.692	1.961
	16	0.720	X	0.524	0.803
	17	0.685	X	X	0.733
	18	0.608	X	X	0.747
Average*		2.055	2.127	1.943	2.171
STDEV*		0.189	0.071	0.218	0.292
COV*		9.214	3.353	11.239	13.468

Shaded values are assumed diameters as grout fell apart during excavation.
Horizontal lines in each column separate the above and below helix values
*Above bottom helix.

4.2.5 Cap, Piles, and Piers (ACPR)

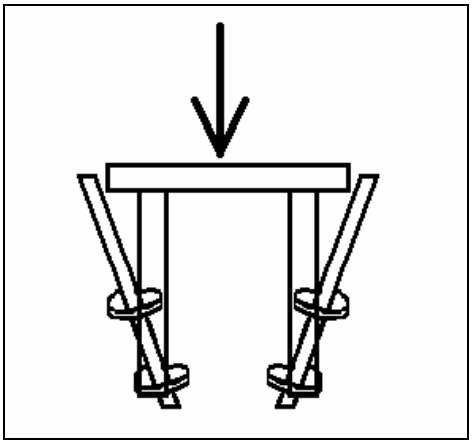

Figure 4.18 Schematic of ACPR test

Figure 4.19 Picture of ACPR test

The cap, piles and piers load test was performed to show how the addition of helical piers affected the cap and piles load-deflection curve. A comparison of the ACP1 and ACPR load-deflection curves can be seen in Figure 4.20.

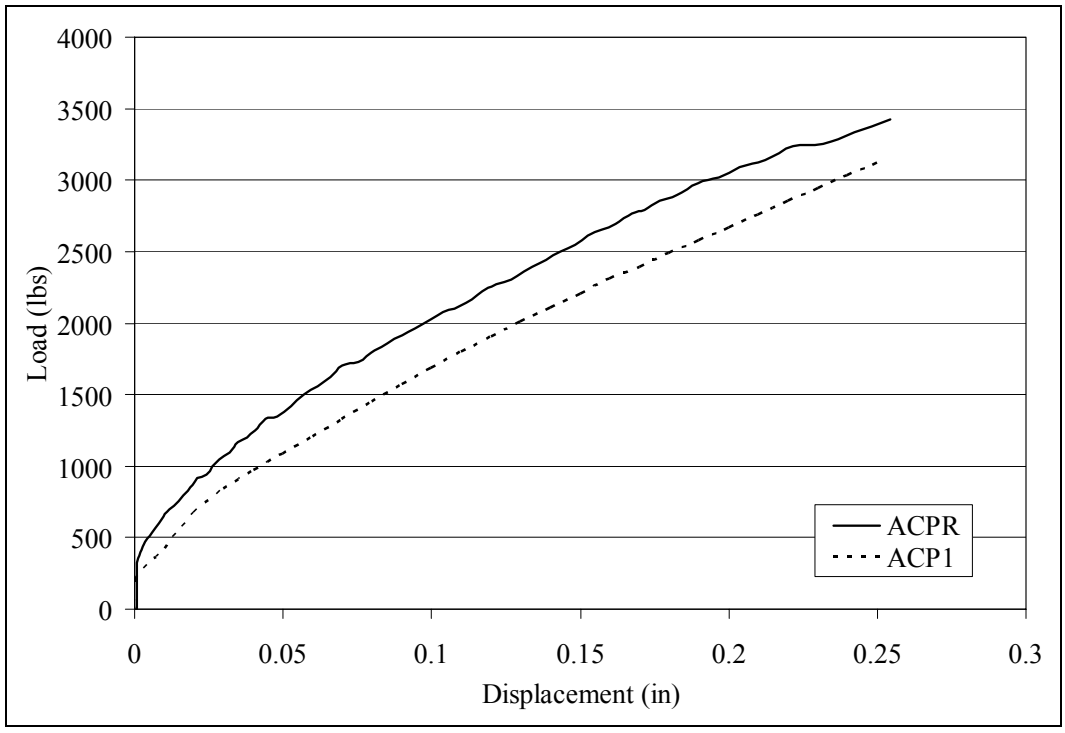

Figure 4.20 Axial load-deflection curve for ACPR test

Table 4.6 shows the pile geometry for ACPR with no defects observed upon excavation. All four piles showed similar lengths, measuring between 17″ and 17.5″. All piles had COV values between 3% and 6% over the entire pile length. Considering only the intermediate pile diameters, all COV values were less than 4%. With the top diameters less than 4″ and intermediate pile diameter COV values less than 10%, the piles were considered to be of acceptable quality.

Table 4.6 Pile length and diameters at various depths for ACPR

Pile label		SW (0)	NW (1)	NE (2)	SE (3)
Overall length		17	17	17	17.5
Depth (in)	0	2.127	2.123	2.183	2.155
	2	2.096	2.106	2.036	2.151
	4	2.004	2.121	2.117	2.144
	6	1.928	2.129	2.131	2.115
	8	1.959	2.125	2.099	2.129
	10	2.095	2.100	2.112	2.110
	12	2.111	2.064	2.127	2.120
	14	2.128	2.112	2.127	2.121
	16	1.953	1.991	2.265	1.714
	18	X	X	X	X
Average*		2.044	2.097	2.133	2.084
STDEV*		0.083	0.044	0.063	0.140
COV*		4.039	2.116	2.936	6.706
Average**		2.046	2.108	2.107	2.127
STDEV**		0.081	0.022	0.033	0.015
COV**		3.955	1.043	1.578	0.716

*Statistics include diameters at all depths

**Statistics without the top and bottom pile diameters

4.2.6 Cap, Piles, and Grout (ACPG)

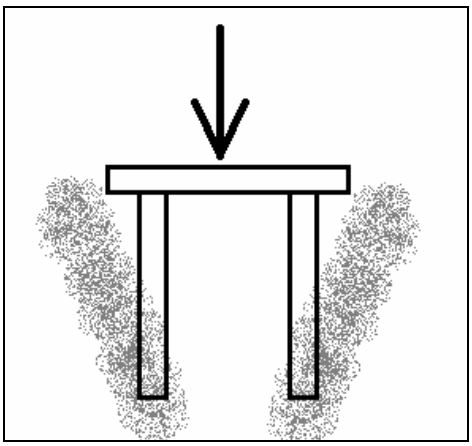

Figure 4.21 Schematic of ACPG test

Figure 4.22 Picture of ACPG test

The cap, piles and grout test was performed to show how the addition of the grouted columns affected the cap and pile load deflection curve. A comparison of the ACP1 and ACPG load-deflection curves can be seen in Figure 4.23.

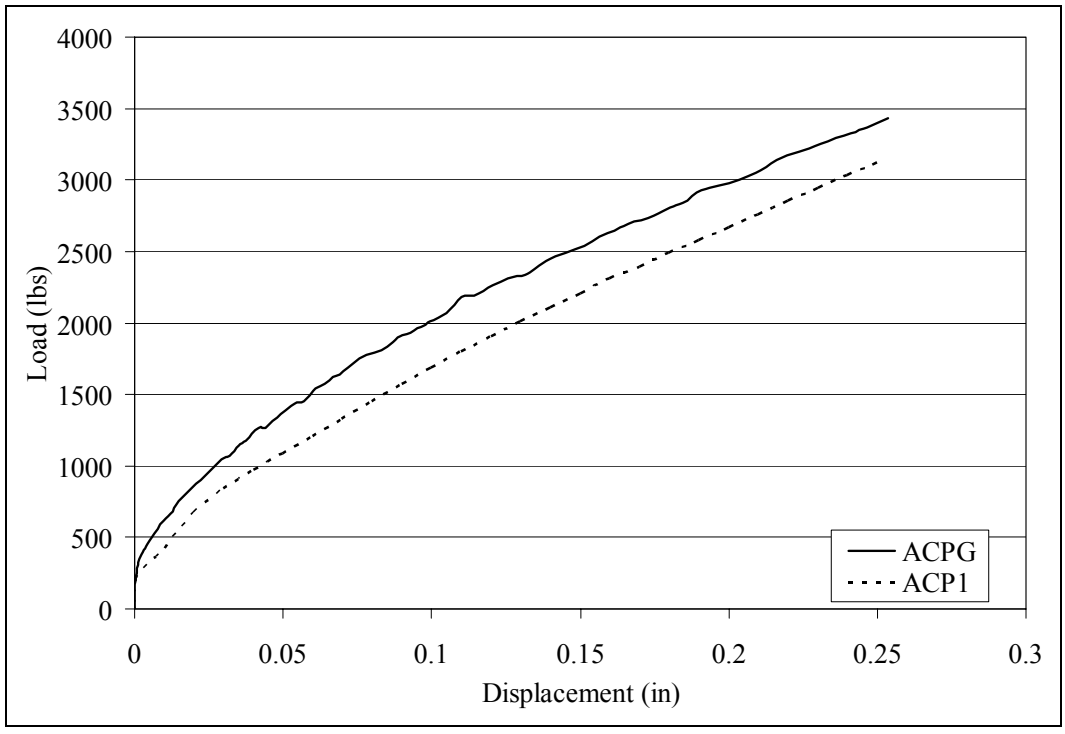

Figure 4.23 Axial load-deflection curve for ACPG test

Table 4.7 shows the pile geometry for ACPG with no defects observed upon excavation. All four piles showed similar lengths, measuring between 18″ and 19.5″. All piles had COV values between 8% and 22% over the entire pile length. Considering only the intermediate pile diameters, however, all COV values were less than 2.5%. With the top diameters less than 4″ and intermediate pile diameter COV values less than 10%, the piles were considered to be of acceptable quality.

Table 4.7 Pile length and diameters at various depths for ACPG

Pile label		SW (0)	NW (1)	NE (2)	SE (3)
Overall length		16.5	17	17.5	17
	0	2.260	2.240	2.283	2.189
	2	2.272	2.185	2.185	2.090
	4	2.194	2.159	2.137	2.115
	6	2.138	2.149	2.134	2.109
Depth (in)	8	2.170	2.149	2.133	2.104
	10	2.115	2.132	2.166	2.100
	12	2.127	2.142	2.136	2.163
	14	2.155	2.151	2.114	2.216
	16	1.377	1.423	1.665	0.780
	18	X	X	X	X
Average*		2.090	2.081	2.106	1.985
STDEV*		0.273	0.249	0.173	0.454
COV*		13.060	11.966	8.205	22.872
Average**		2.167	2.152	2.143	2.128
STDEV**		0.053	0.017	0.024	0.045
COV**		2.452	0.770	1.107	2.131

*Statistics include diameters at all depths

**Statistics without the top and bottom pile diameters

Table 4.8 shows the geometry of the grouted piers for ACPG. All piers reached the target 18″ installation depth, with the grouted portion of the piers at 16″. All the piers had a section of grout near the top that fell apart during excavation. The COV values for the 3 of the 4 piers were from 5%-7%, with the COV for N being nearly 23%. The grouted lengths

and COV values demonstrated successful installation for all piers with the exception of pier N, with a COV greater than 20%.

Table 4.8 Pier length and diameters at various depths for ACPG

Pier label		W	N	E	S
Overall length		18	18	18	18
Depth (in)	0	2.021	2.629	1.859	2.095
	1	2.021	2.629	1.859	2.095
	2	2.445	2.629	1.859	2.251
	3	2.784	2.444	1.859	2.218
	4	2.556	2.195	2.180	2.102
	5	2.295	2.018	2.144	2.078
	6	2.350	1.994	2.193	2.055
	7	2.404	1.974	2.256	2.082
	8	2.445	1.766	2.152	2.031
	9	2.438	1.506	2.115	2.097
	10	2.453	1.389	2.107	2.107
	11	2.659	1.441	2.154	2.112
	12	2.498	1.396	2.216	2.321
	13	2.528	1.520	2.336	2.410
	14	2.614	1.442	2.237	2.292
	15	2.467	1.484	2.301	2.317
	16	2.429	2.396	2.374	2.315
	17	0.887	0.769	0.771	0.799
	18	0.666	0.642	0.585	0.608
Average*		2.461	1.839	2.187	2.180
STDEV*		0.167	0.428	0.125	0.120
COV*		6.803	23.252	5.694	5.521

Shaded values are assumed diameters as grout fell apart during excavation.
Horizontal lines in each column separate the above and below helix values
*Above bottom helix.

4.2.7 Cap, Piers, and Grout (ACRG)

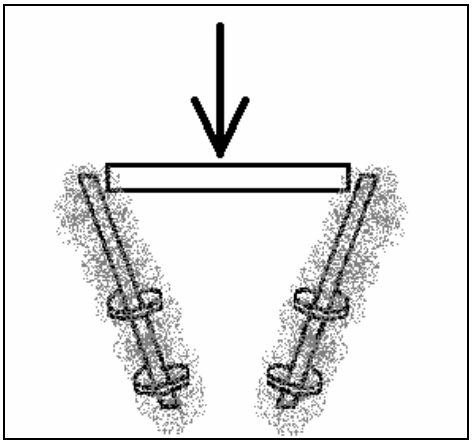

Figure 4.24 Schematic of ACRG test

The cap, piers and grout test was performed to show how the addition of grouted, helical piers affected the cap only load displacement curve. A comparison of the AC and ACRG load-deflection curves can be seen in Figure 4.25.

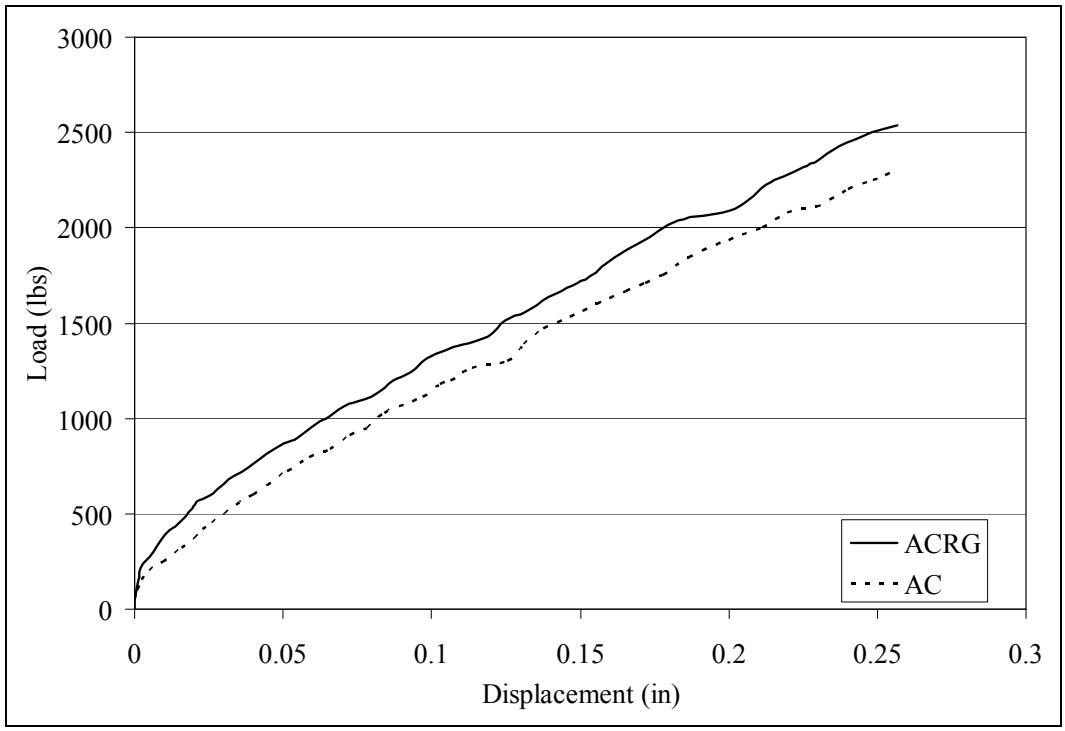

Figure 4.25 Axial load-deflection curve for ACRG test

Table 4.9 shows the geometry of the grouted piers for ACRG. The target 18″ installation depth was reached for all 4 piers, while the grouted portion ranged from 14″-16″. Pier N incurred a detached bottom helix that limited the grouted length to 15″. Both pier W and S had sections of grout near the top that fell apart during excavation. The COV values for the 4 piers ranged from 15%-23%. The grout length was acceptable for all piers, however, only pier W and E were considered successfully installed as both N and S had a COV value greater than 20%.

Table 4.9 Pier length and diameters at various depths for ACRG

Pier label		W	N	E	S
Overall length		18	18	18	18
	0	1.444	2.105	2.210	2.033
	1	1.444	2.133	2.259	2.033
	2	1.444	2.154	2.397	2.033
	3	1.444	2.157	2.206	1.958
	4	1.444	1.997	2.179	2.085
	5	1.444	1.938	2.158	2.057
	6	1.444	1.810	2.142	1.927
	7	1.591	1.815	2.158	2.058
	8	1.615	1.798	2.193	1.948
Depth (in)	9	1.613	1.867	2.120	1.964
	10	1.197	1.261	1.978	1.684
	11	1.166	1.334	1.953	1.570
	12	1.134	1.314	2.039	1.562
	13	1.134	1.266	1.859	1.507
	14	1.198	1.022	1.973	1.381
	15	1.296	0.721	1.838	1.377
	16	1.228	0.704	1.731	1.388
	17	0.734	0.694	0.701	0.744
	18	P	P	P	P
Average*		1.329	1.731	2.082	1.702
STDEV*		0.198	0.386	0.172	0.370
COV*		14.909	22.278	8.268	21.736

Shaded values are assumed diameters as grout fell apart during excavation.
Horizontal lines in each column separate the above and below helix values
*Above bottom helix.

4.2.8 Cap, Piles, Piers, and Grout (ACPRG)

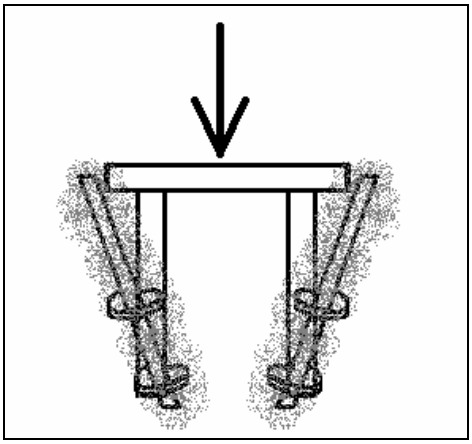

Figure 4.26 Schematic of ACPRG test

Figure 4.27 Picture of ACPRG1 test

The cap, piles, piers and grout test was performed to show how the addition of grouted helical piers affected the cap and piles load deflection curve.

4.2.8.1 ACPRG1

A comparison of the ACP1 and ACPRG1 tests can be seen in Figure 4.28.

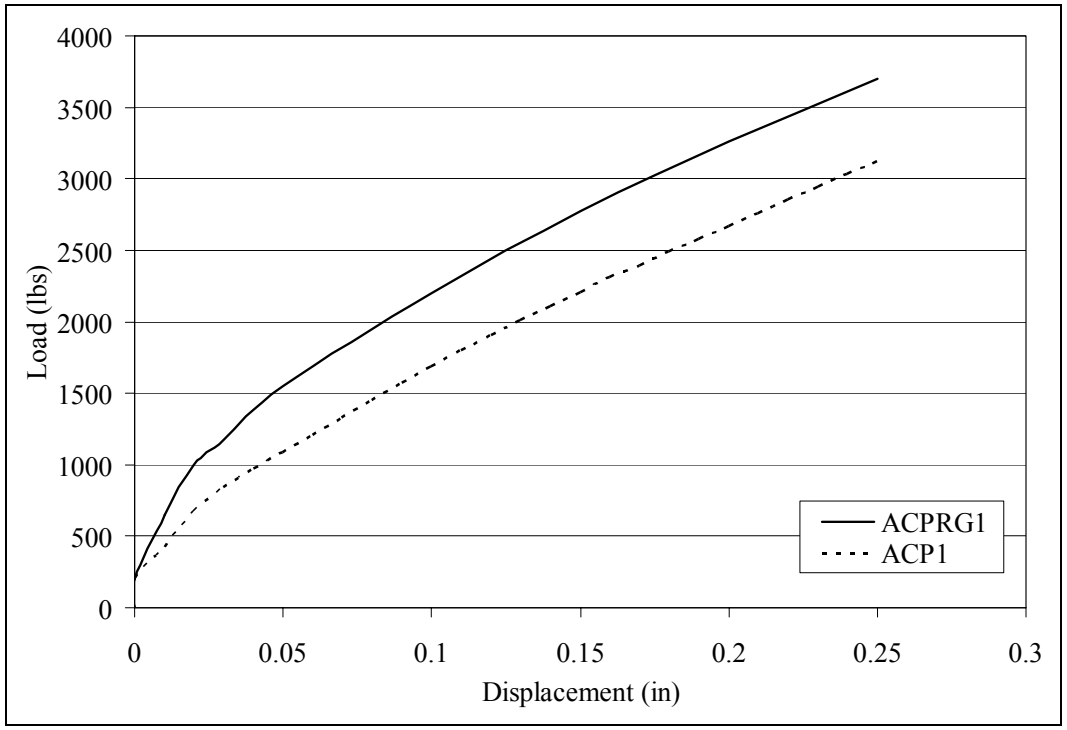

Figure 4.28 Axial load-deflection curve for ACPRG1 test

Table 4.10 shows the pile geometry for ACPRG with cage exposure observed in SW(0) upon excavation. The cage exposure was not considered to significantly alter the individual piles performance. The pile lengths ranged from 16.5″-18″. All piles had COV values between 18% and 25% over the entire pile length. Considering only the intermediate pile diameters, however, all COV values were less than 4.5%. With the top diameters less than 4″ and intermediate pile diameter COV values less than 10%, the piles were considered to be of acceptable quality.

Table 4.10 Pile length and diameters at various depths for ACPRG1

Pile label		SW (0)	NW (1)	NE (2)	SE (3)
Overall length		16.5	17	18	18
Depth (in)	0	3.045	2.264	3.387	3.466
	2	2.017	2.244	2.126	2.165
	4	2.106	2.117	2.083	2.097
	6	1.909	2.157	2.076	2.124
	8	2.074	2.091	2.099	2.120
	10	2.158	2.123	2.118	2.103
	12	2.162	2.106	2.108	2.101
	14	2.141	2.138	2.107	2.100
	16	1.613	0.922	2.124	2.139
	18	X	X	1.098	1.388
Average*		2.136	2.018	2.132	2.180
STDEV*		0.383	0.416	0.543	0.507
COV*		17.917	20.593	25.458	23.262
Average**		2.081	2.139	2.105	2.119
STDEV**		0.092	0.051	0.018	0.024
COV**		4.405	2.375	0.870	1.117

*Statistics include diameters at all depths

**Statistics without the top and bottom pile diameters

Table 4.11 shows the geometry of the grouted piers for ACPRG1. The target 18″ installation depth was reached for 3 of the 4 piers, with pier S being installed to 16″, while the grouted portion ranged from 14″-16″. All piers had sections of grout near the top that fell

apart during excavation. The COV values for the 4 piers ranged from 6%-22%. The grout length was acceptable for all piers, and only pier S had a COV value greater than 20%, causing the remaining 3 to be considered successfully installed.

Table 4.11 Pier length and diameters at various depths for ACPRG1

Pier label		W	N	E	S
Overall length		18	18	18	16
Depth (in)	0	1.989	2.393	1.946	3.078
	1	1.989	2.393	1.946	3.078
	2	1.989	2.393	1.946	2.246
	3	1.989	2.393	1.946	2.146
	4	1.946	2.245	1.946	2.143
	5	1.822	2.106	1.946	2.067
	6	1.860	2.152	1.946	2.162
	7	1.958	2.251	2.106	2.015
	8	1.890	1.992	2.002	1.812
	9	1.942	1.989	2.001	1.681
	10	1.766	2.038	1.962	1.663
	11	1.564	2.231	1.718	1.582
	12	1.468	2.354	2.079	1.541
	13	1.435	2.419	1.603	1.530
	14	1.386	2.312	1.581	1.535
	15	1.461	2.360	1.569	0.756
	16	1.435	2.306	1.530	P
	17	0.756	0.749	0.771	X
	18	P	0.509	P	X
Average*		1.708	2.225	1.827	1.943
STDEV*		0.235	0.147	0.226	0.423
COV*		13.751	6.603	12.383	21.755

Shaded values are assumed diameters as grout fell apart during excavation.
Horizontal lines in each column separate the above and below helix values
*Above bottom helix.

4.2.8.2 ACPRG2

It was felt that some necking had occurred during the installation of ACPRG1, so an additional ACPRG test was performed, ACPRG2. A comparison of the ACP1 and ACPRG2 load-deflection curves can be seen in Figure 4.29.

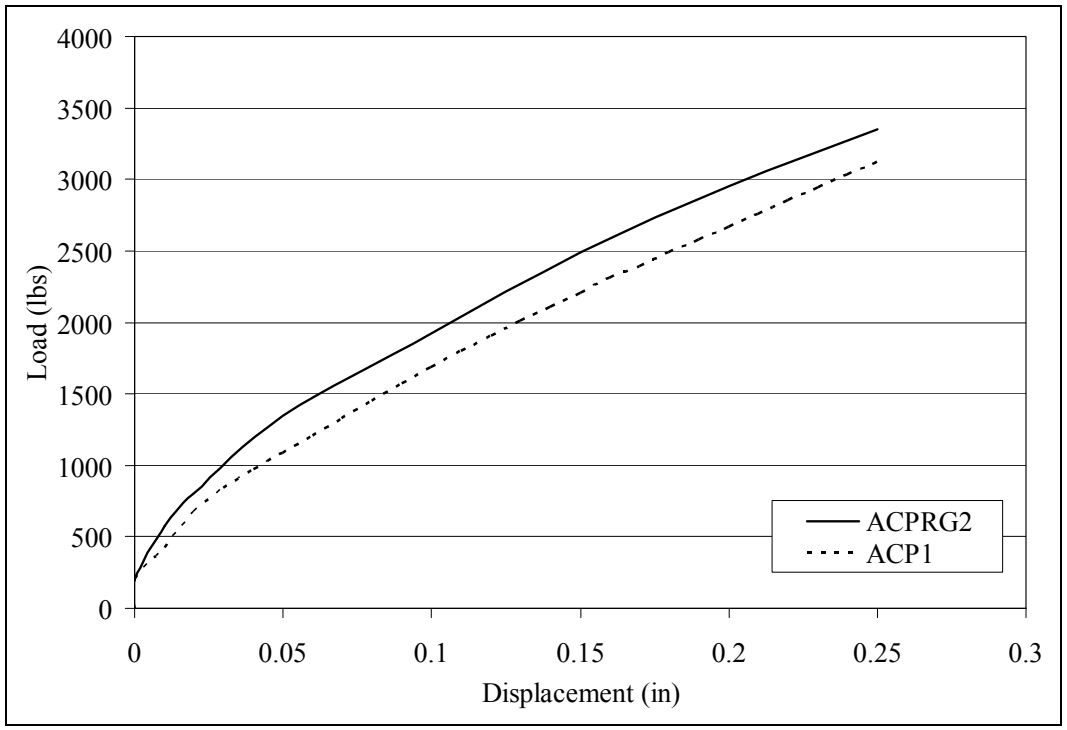

Figure 4.29 Axial load-deflection curve for ACPRG2 test

Table 4.12 shows the pile geometry for ACPRG2 with no defects observed upon excavation. The four pile lengths ranged from 16″-18″. All piles had COV values between 20% and 29% over the entire pile length. Considering only the intermediate pile diameters, however, all COV values were less than 6.5%. With the top diameters less than 4″ and intermediate pile diameter COV values less than 10%, the piles were considered to be of acceptable quality.

Table 4.12 Pile length and diameters at various depths for ACPRG2

Pile label		SW (0)	NW (1)	NE (2)	SE (3)
Overall length		18	16	16	16.5
	0	3.141	2.950	3.686	3.215
	2	2.107	2.098	2.111	2.139
	4	2.092	2.204	2.303	2.151
	6	2.093	2.252	2.161	2.144
Depth (in)	8	2.127	2.140	2.295	2.202
	10	2.118	2.150	2.151	2.231
	12	2.118	2.164	2.131	2.536
	14	2.120	2.189	2.213	2.355
	16	2.135	1.239	1.153	1.291
	18	0.780	X	X	X
Average*		2.083	2.154	2.245	2.251
STDEV*		0.560	0.431	0.644	0.498
COV*		26.904	20.017	28.713	22.099
Average**		2.114	2.171	2.195	2.251
STDEV**		0.015	0.050	0.078	0.147
COV**		0.732	2.292	3.539	6.519

*Statistics include diameters at all depths

**Statistics without the top and bottom pile diameters

Table 4.13 shows the geometry of the grouted piers for ACPRG2. The target 18″ installation depth was reached for all 4 piers, while the grouted portion ranged from 12″-16″. Pier W and E had sections of grout near the top that fell apart during excavation. The COV values for the 4 piers ranged from 3%-25%. The grout length was acceptable for 3 of the 4 piers, with a grout length of only 12″ for pier S due to a detached helix. Only pier N had a COV value greater than 20%. Consequently, only piers W and E were considered to be successfully installed.

Table 4.13 Pier length and diameters at various depths for ACPRG2

Pier label		W	N	E	S
Overall length		18	18	18	18
	0	1.992	2.516	2.100	2.217
	1	1.992	2.615	2.100	2.407
	2	1.992	2.207	2.100	2.298
	3	2.187	2.228	1.980	2.235
	4	2.303	2.130	1.934	2.222
	5	2.258	2.085	1.907	2.227
	6	2.255	2.088	2.084	2.171
	7	2.301	2.189	2.016	2.148
	8	2.253	2.269	2.017	2.139
Depth (in)	9	2.213	2.334	1.924	2.164
	10	2.202	2.359	2.046	2.185
	11	2.219	1.425	1.924	2.264
	12	2.256	1.350	1.251	1.891
	13	2.183	1.316	1.294	0.662
	14	2.201	1.326	1.436	0.729
	15	2.189	1.355	2.143	0.700
	16	2.278	1.334	2.299	0.695
	17	0.822	0.838	0.972	0.744
	18	P	P	0.693	P
Average*		2.219	1.948	1.890	2.197
STDEV*		0.075	0.475	0.311	0.117
COV*		3.365	24.376	16.436	5.313

Shaded values are assumed diameters as grout fell apart during excavation.
Horizontal lines in each column separate the above and below helix values
*Above bottom helix.

4.3 Lateral Load Tests

4.3.1 Cap Only (LC)

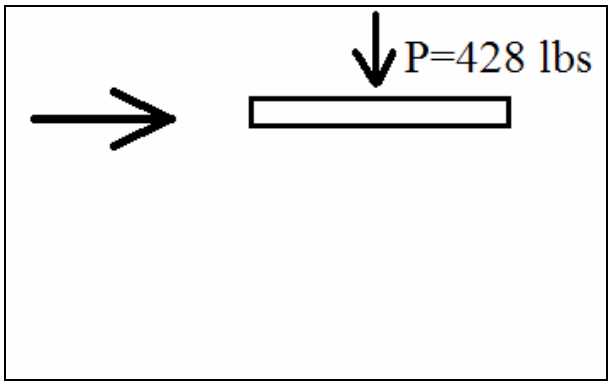

Figure 4.30 Schematic of LC test

Figure 4.31 Picture of LC test

The lateral cap only test was performed to determine the load deflection curve for the cap only. The resulting load deflection curve can be seen in Figure 4.32.

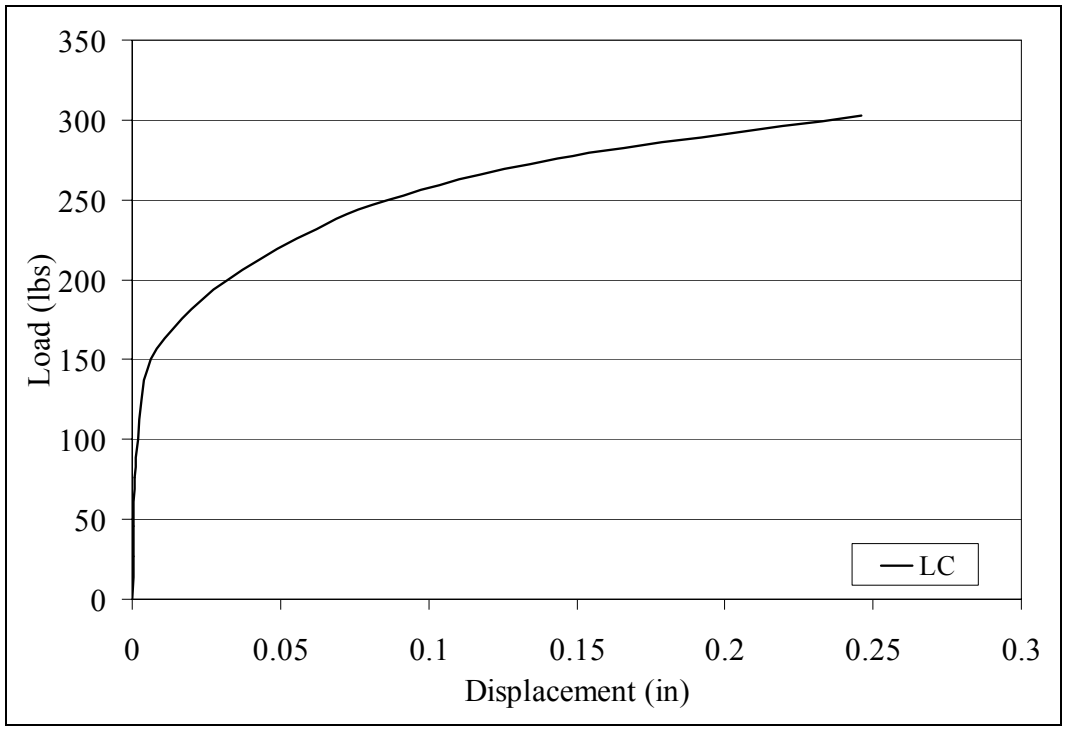

Figure 4.32 Lateral load-deflection curve for LC test

4.3.2 Cap and Piles (LCP)

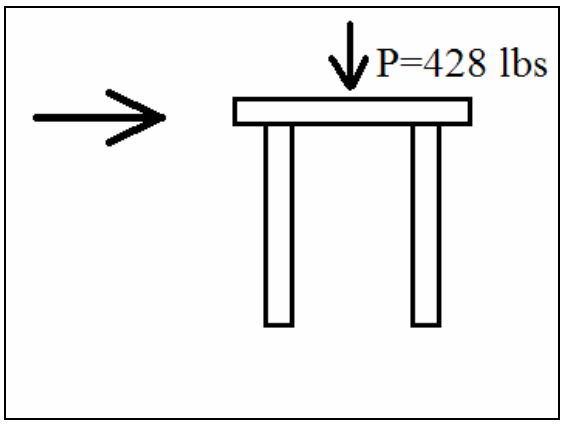

Figure 4.33 Schematic of LCP test

The lateral cap and piles test was performed to show how the addition of piles affected the lateral performance of the cap only load deflection curve.

4.3.2.1 LCP1

The initial LCP test load-deflection curve can be seen in Figure 4.34.

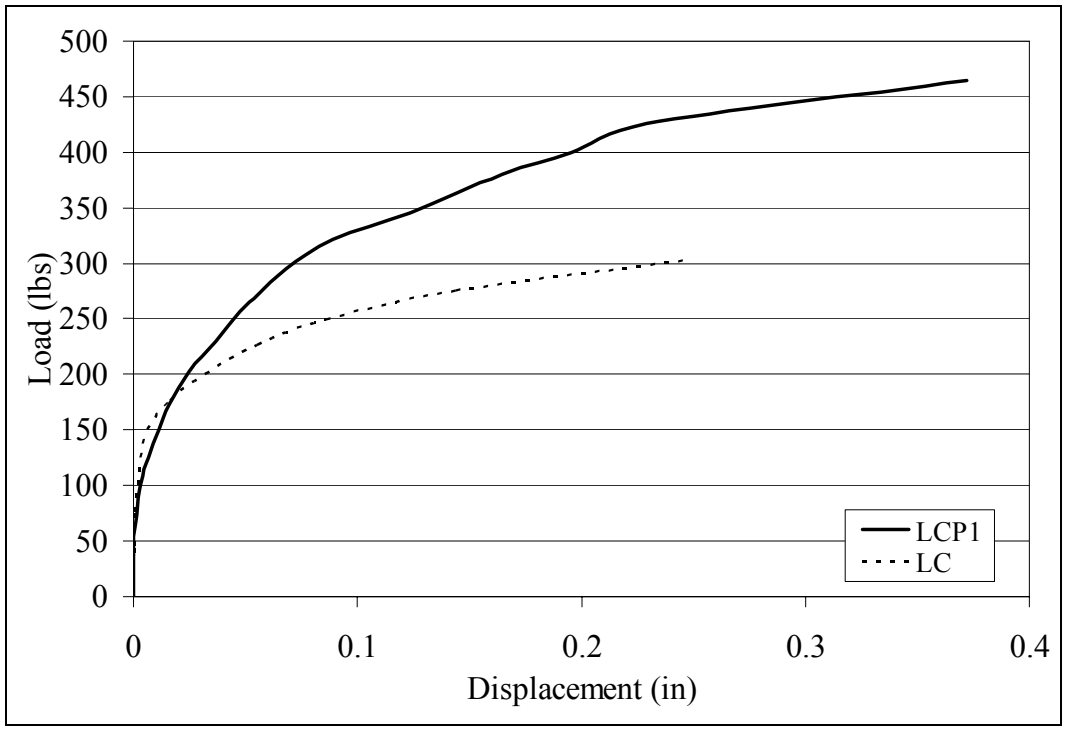

Figure 4.34 Lateral load-deflection curve for LCP1 test

Table 4.14 shows the pile geometry for LCP1 with no defects observed upon excavation. All four piles showed similar lengths, measuring between 15.5″ and 16.5″. All piles had COV values between 1% and 5% over the entire pile length. Considering only the intermediate pile diameters, however, all COV values were less than 4.5%. With the top diameters less than 4″ and intermediate pile diameter COV values less than 10%, the piles were considered to be of acceptable quality.

Table 4.14 Pile length and diameters at various depths for LCP1

Pile label		SW (0)	NW (1)	NE (2)	SE (3)
Overall length		15.5	16.5	15.5	16
Depth (in)	0	2.138	2.346	2.368	2.305
	2	2.071	2.280	2.187	2.221
	4	2.076	2.276	2.205	2.248
	6	2.103	2.181	2.165	2.368
	8	2.046	2.116	2.132	2.113
	10	2.068	2.121	2.098	2.120
	12	2.091	2.098	2.088	2.186
	14	2.104	2.133	1.996	2.094
	16	X	2.076	X	2.014
	18	X	X	X	X
Average*		2.087	2.180	2.155	2.185
STDEV*		0.028	0.096	0.109	0.112
COV*		1.349	4.419	5.041	5.115
Average**		2.076	2.172	2.146	2.193
STDEV**		0.020	0.077	0.048	0.096
COV**		0.952	3.542	2.224	4.401

*Statistics include diameters at all depths

**Statistics without the top and bottom pile diameters

4.3.2.2 LCP2

A second LCP test was performed to help show the repeatability of the LCP1 load-deflection curve. A comparison of the LCP1 and LCP2 load deflection curves can be seen in Figure 4.35.

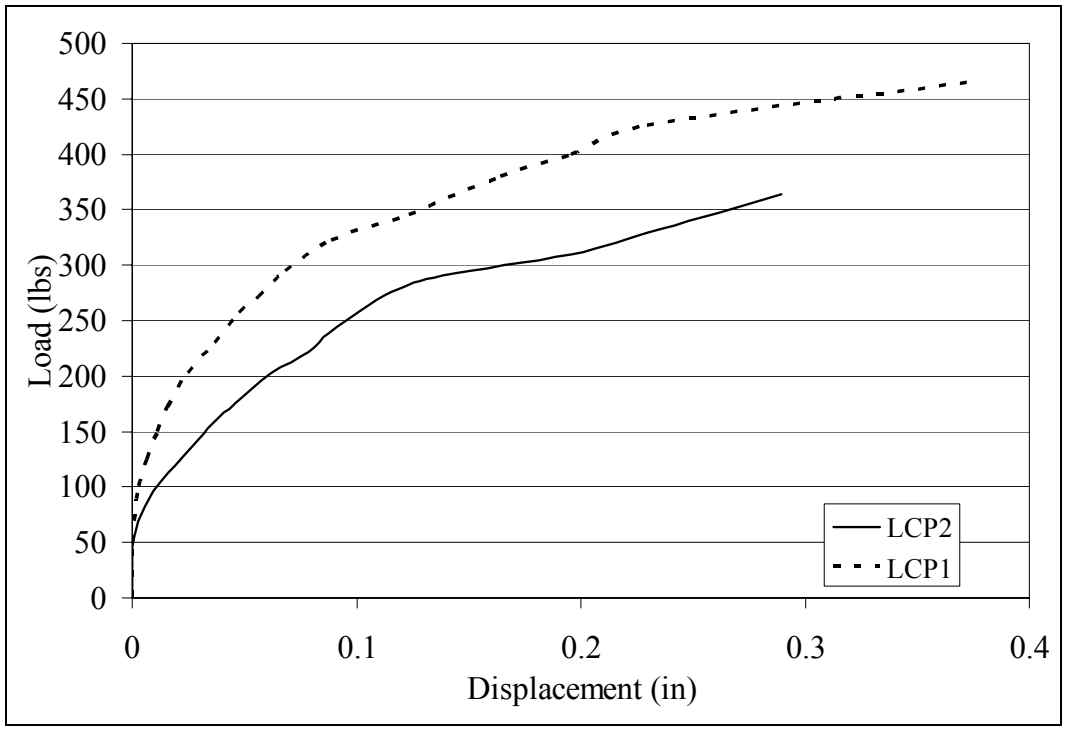

Figure 4.35 Lateral load-deflection curve for LCP2 test

Table 4.15 shows the pile geometry for LCP2 with defects observed in NW(1) upon excavation. The section of exposed cage contained no concrete and was considered to drastically alter the piles performance. All four piles showed similar lengths, measuring between 16″ and 17″. All piles had COV values between 2% and 17% over the entire pile length. Considering only the intermediate pile diameters, however, 3 of the 4 piles had COV values smaller than 3%, and NW(1) at approximately 10%. With the top diameters less than 4″ and intermediate pile diameter COV values less than 10%, 3 of the 4 piles were considered to be of acceptable quality, and pile NW(1) was considered to be of poor quality.

Table 4.15 Pile length and diameters at various depths for LCP2

Pile label		SW (0)	NW (1)	NE (2)	SE (3)
Overall length		17	17	16	17
Depth (in)	0	2.094	2.630	2.903	2.719
	2	2.126	2.309	2.291	2.043
	4	2.078	2.262	2.178	2.096
	6	2.103	2.389	2.255	2.126
	8	2.140	2.080	2.299	2.162
	10	2.132	1.741	2.142	2.137
	12	2.120	2.245	2.166	2.143
	14	2.129	2.252	2.175	2.146
	16	2.036	1.808	1.451	1.729
	18	X	X	X	X
Average*		2.106	2.190	2.206	2.144
STDEV*		0.033	0.278	0.368	0.254
COV*		1.571	12.708	16.658	11.838
Average**		2.118	2.182	2.215	2.122
STDEV**		0.021	0.216	0.065	0.040
COV**		0.996	9.892	2.915	1.901

*Statistics include diameters at all depths

**Statistics without the top and bottom pile diameters

4.3.3 Cap and Piers (LCR)

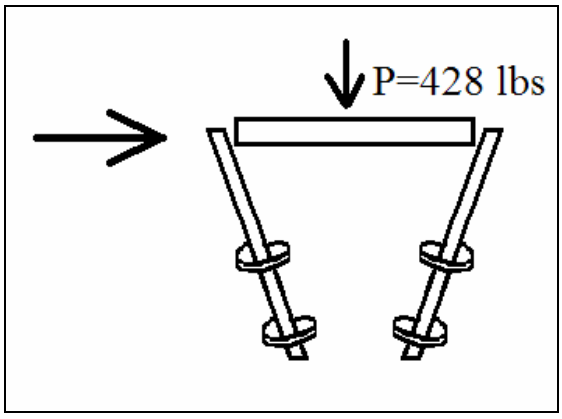

Figure 4.36 Schematic of LCR test

Figure 4.37 Picture of LCR test

The lateral cap and piers test was performed to determine how the addition of helical piers would affect the cap only load deflection curve. A comparison of the LC and LCR test load-deflection curves can be seen in Figure 4.38.

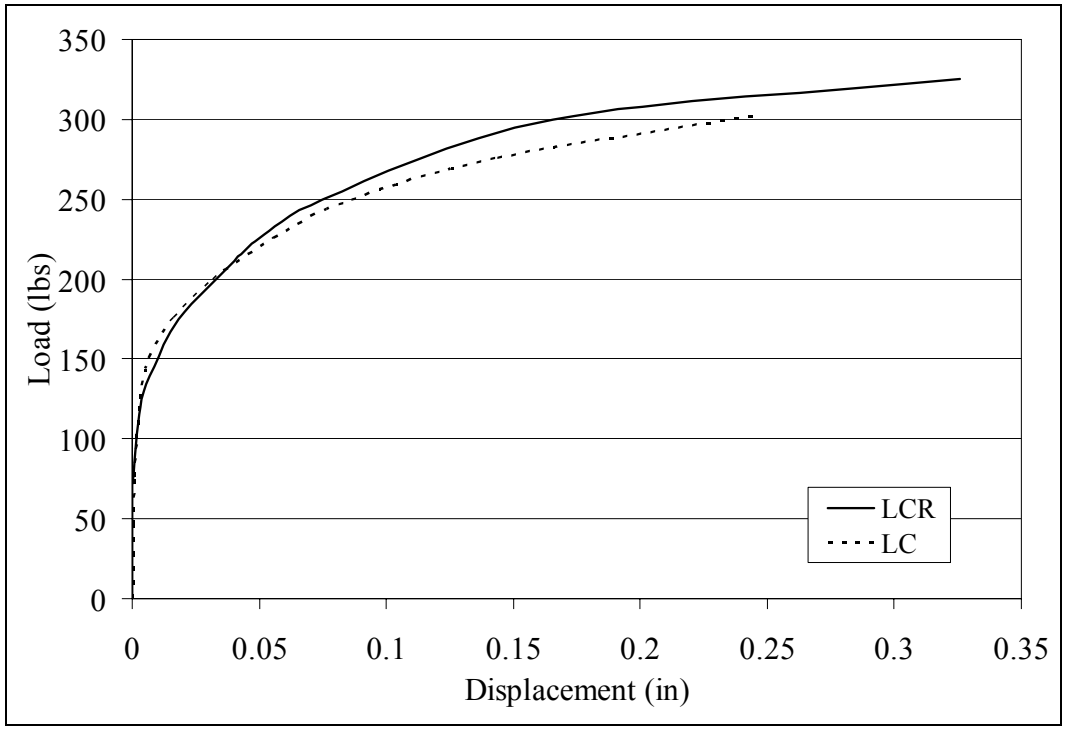

Figure 4.38 Lateral load-deflection curve for LCR test

4.3.4 Cap and Grout (LCG)

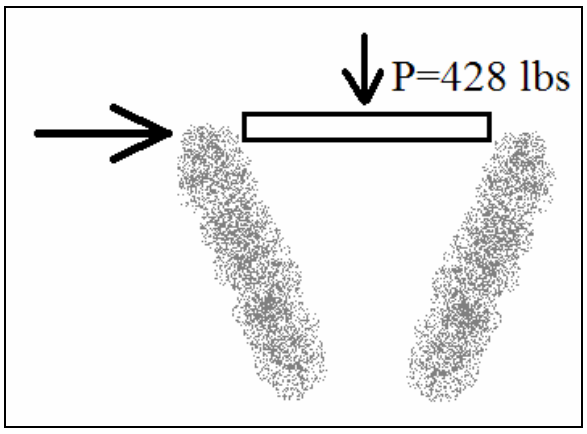

Figure 4.39 Schematic of LCG test

Figure 4.40 Picture of LCG test

The lateral cap and grout test was performed to show how the addition of the grouted columns would affect the cap only load displacement curve. A comparison of the LC and LCG test load-deflection curves can be seen in Figure 4.41.

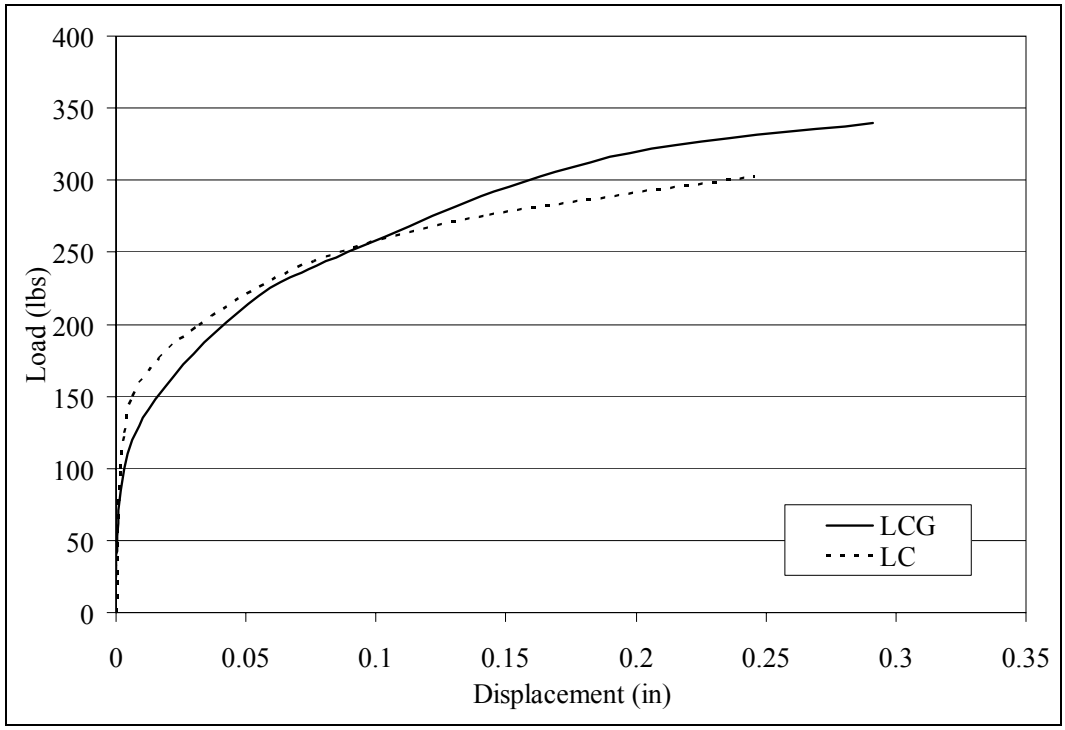

Figure 4.41 Lateral load-deflection curve for LCG test

Table 4.16 shows the geometry of the grouted piers for LCG. The target 18″ installation depth was reached for 3 of the 4 piers, with pier E being installed to 5″, while the grouted portion ranged from 5″-16″. While installing pier E, the grouting apparatus became clogged at 5″ and the remaining length was not installed. None of the piers had sections of grout that fell apart during excavation. The COV values for the 4 piers ranged from 17%-27%. Only pier N and S were considered to be successfully installed, as the grout length of E was less than 14″ and the COV of W was greater than 20%.

Table 4.16 Pier length and diameters at various depths for LCG

Pier label		W	N	E	S
Overall length		18	18	5	18
	0	0.960	1.277	1.211	1.823
	1	1.028	2.250	2.072	2.418
	2	1.008	1.905	1.570	2.864
	3	1.043	1.078	1.830	2.633
	4	1.827	2.025	1.817	2.633
	5	1.975	2.103	1.596	1.977
	6	2.163	2.222	X	2.222
	7	2.134	2.219	X	3.750
	8	2.134	2.315	X	2.167
Depth (in)	9	2.030	2.184	X	2.173
	10	2.070	2.209	X	2.207
	11	2.104	2.260	X	2.224
	12	2.140	2.430	X	2.216
	13	2.234	2.503	X	2.195
	14	2.285	2.558	X	2.190
	15	2.270	2.552	X	2.196
	16	2.380	2.572	X	2.191
	17	0.847	0.821	X	0.791
	18	0.613	0.638	X	0.644
Average*		1.869	2.156	1.682	2.357
STDEV*		0.507	0.416	0.295	0.436
COV*		27.142	19.270	17.514	18.487

Shaded values are assumed diameters as grout fell apart during excavation.
Horizontal lines in each column separate the above and below helix values
*Above bottom helix.

4.3.5 Cap, Piles, and Piers (LCPR)

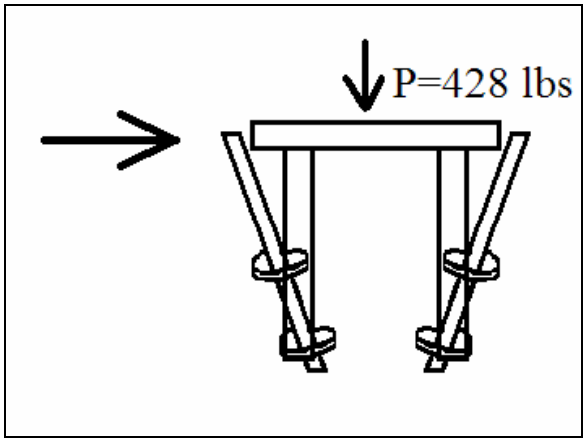

Figure 4.42 Schematic of LCPR test

Figure 4.43 Picture of LCPR test

The lateral cap, piles and piers test was performed to show how the addition of helical piers would affect the cap and pile load deflection curve. A comparison of the LCP1 and LCPR test load-deflection curves can be seen in Figure 4.44.

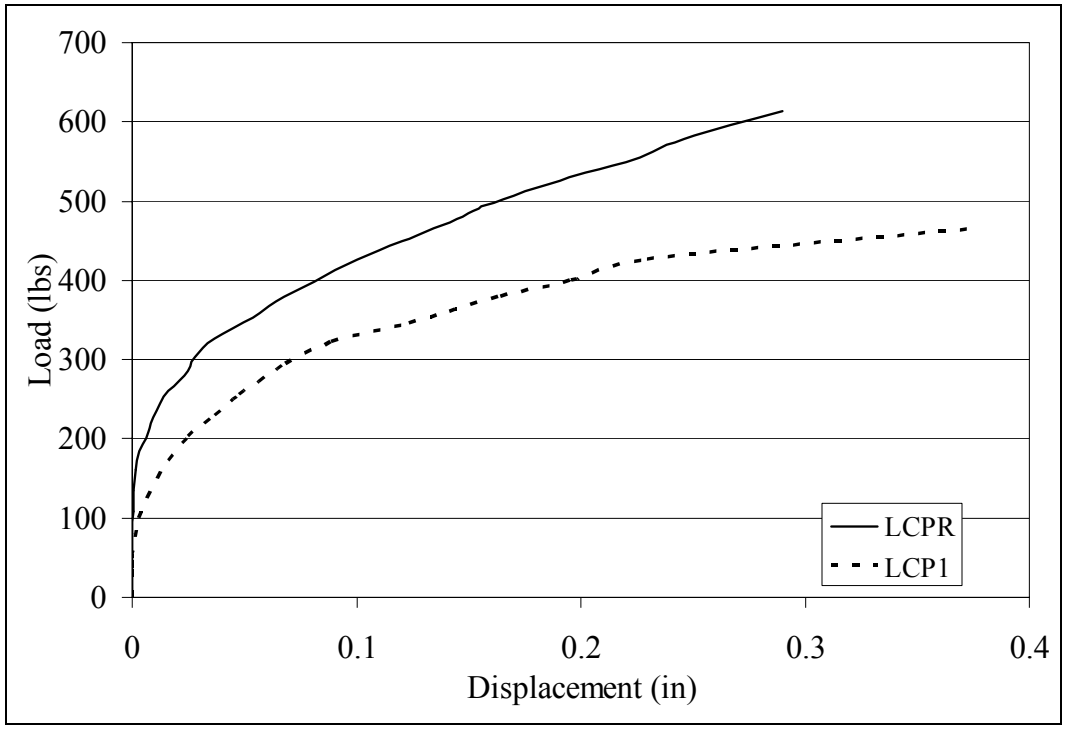

Figure 4.44 Lateral load-deflection curve for LCPR test

Table 4.17 shows the pile geometry for LCPR with no defects observed upon excavation. All four piles showed similar lengths, measuring between 18″ and 18.5″. All piles had COV values of approximately 15% over the entire pile length. Considering only the intermediate pile diameters, however, all COV values ranged from 3%-8%. With the top diameters less than 4″ and intermediate pile diameter COV values less than 10%, the piles were considered to be of acceptable quality.

Table 4.17 Pile length and diameters at various depths for LCPR

Pile label		SW (0)	NW (1)	NE (2)	SE (3)
Overall length		18.5	18	18	18
	0	2.477	3.112	2.674	2.993
	2	2.129	2.158	2.120	2.141
	4	2.199	2.382	2.097	2.140
	6	2.098	2.363	2.101	2.201
Depth (in)	8	2.117	2.340	2.214	2.344
	10	2.310	2.358	2.521	2.289
	12	2.328	2.386	2.355	2.339
	14	2.361	2.391	2.444	2.399
	16	2.471	2.476	2.223	2.265
	18	1.331	1.649	1.441	1.535
Average*		2.182	2.361	2.219	2.264
STDEV*		0.330	0.354	0.335	0.354
COV*		15.120	14.993	15.105	15.631
Average**		2.251	2.356	2.259	2.265
STDEV**		0.136	0.090	0.163	0.097
COV**		6.027	3.822	7.211	4.266

*Statistics include diameters at all depths

**Statistics without the top and bottom pile diameters

4.3.6 Cap, Piles, and Grout (LCPG)

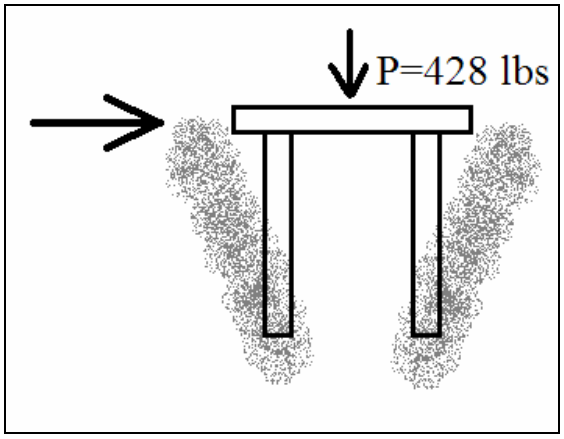

Figure 4.45 Schematic of LCPG test

Figure 4.46 Picture of LCPG test

The lateral cap, piles, and grout test was performed to show how the addition of grouted columns would affect the cap and pile load deflection curve.

4.3.6.1 LCPG1

A comparison of the LCP1 and LCPG1 load-deflection curves can be seen in Figure 4.47.

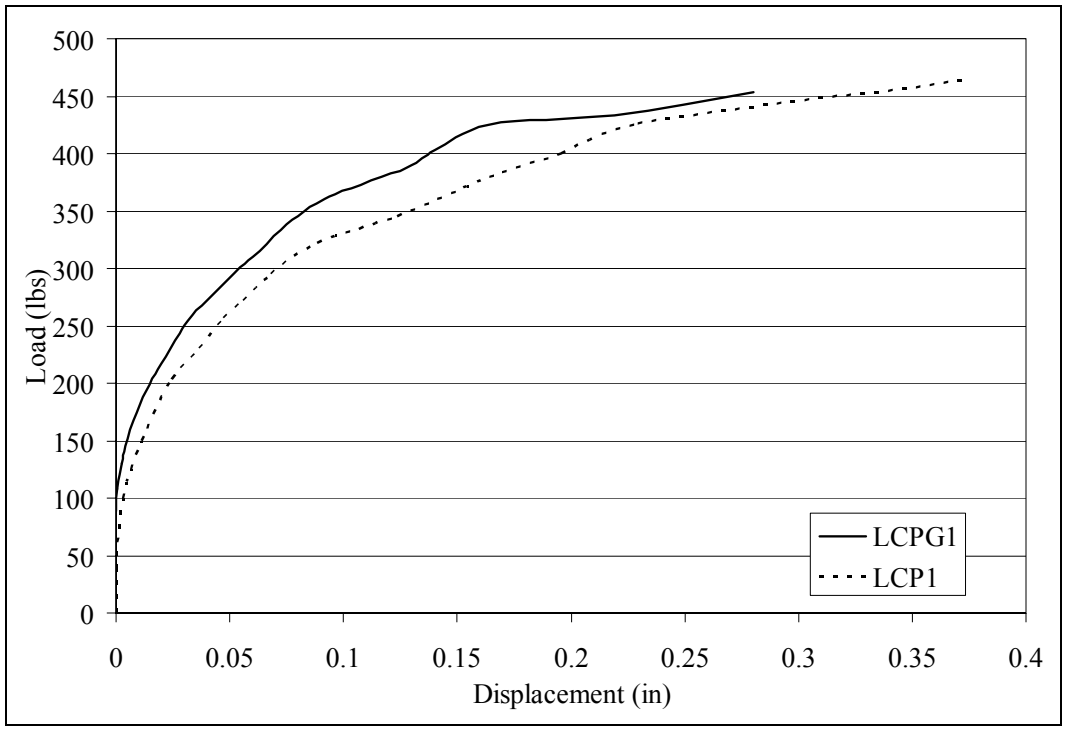

Figure 4.47 Lateral load-deflection curve for LCPG1 test

Table 4.18 shows the pile geometry for LCPG1 with extreme cage exposure observed in NE(2) and SE(3) upon excavation. The four pile lengths ranged from 15″ to 18.5″. All piles had COV values between 6% and 8% over the entire pile length. All intermediate pile diameter COV values ranged from 0.5% - 8.5%. With the top diameters less than 4″ and intermediate pile diameter COV values less than 10%, the piles were statistically considered to be of acceptable quality, however, the extreme cage exposure and wide range of pile lengths makes the piles of poor quality.

Table 4.18 Pile length and diameters at various depths for LCPG1

Pile label		SW (0)	NW (1)	NE (2)	SE (3)
Overall length		18	18.5	17.5	15
	0	2.032	2.105	2.133	2.097
	2	2.047	2.103	2.014	2.010
	4	2.070	2.101	1.728	1.969
	6	2.066	2.070	1.801	1.627
Depth (in)	8	2.067	2.062	1.803	1.860
	10	2.058	2.068	1.961	2.059
	12	2.055	2.045	2.013	2.044
	14	2.065	2.070	2.076	1.791
	16	2.072	2.093	1.720	X
	18	1.654	1.596	X	X
Average*		2.018	2.031	1.916	1.932
STDEV*		0.129	0.154	0.155	0.161
COV*		6.372	7.591	8.109	8.330
Average**		2.062	2.076	1.914	1.928
STDEV**		0.009	0.020	0.134	0.164
COV**		0.415	0.983	7.006	8.494

*Statistics include diameters at all depths

**Statistics without the top and bottom pile diameters

Table 4.19 shows the geometry of the grouted piers for LCPG1. The target 18″ installation depth was reached for 2 of the 4 piers, with pier N being installed to 5″ and pier E being installed to 3″. Both N and E incurred clogs in the grouting apparatus, resulting in grout lengths substantially short of the target 16″. None of the piers had sections fall apart during excavation. The COV values for the 4 piers ranged from 6%-18%. Only pier W and S were considered to be successfully installed, as both reached the target depth and had COV values less than 20%.

Table 4.19 Pier length and diameters at various depths for LCPG1

Pier label		W	N	E	S
Overall length		18	5	2	17
	0	1.894	2.881	2.090	2.224
	1	2.000	2.803	1.928	2.635
	2	2.094	2.268	1.834	1.573
	3	2.209	2.304	X	1.865
	4	2.254	1.972	X	2.113
	5	2.370	1.874	X	2.094
	6	2.371	X	X	2.390
	7	2.291	X	X	2.274
	8	2.145	X	X	2.348
Depth (in)	9	2.056	X	X	2.237
	10	1.939	X	X	2.228
	11	2.124	X	X	2.266
	12	2.072	X	X	2.191
	13	2.391	X	X	2.139
	14	2.475	X	X	2.226
	15	2.521	X	X	2.198
	16	2.453	X	X	2.110
	17	0.862	X	X	1.742
	18	0.640	X	X	X
Average*		2.215	2.350	1.950	2.158
STDEV*		0.194	0.416	0.129	0.239
COV*		8.764	17.707	6.637	11.094

Shaded values are assumed diameters as grout fell apart during excavation.
Horizontal lines in each column separate the above and below helix values
*Above bottom helix.

4.3.6.2 LCPG2

Due to the poor construction and installation of LCPG1, a second LCPG test was performed. A comparison of LCP1 and LCPG2 load-deflection curves can be seen in Figure 4.48.

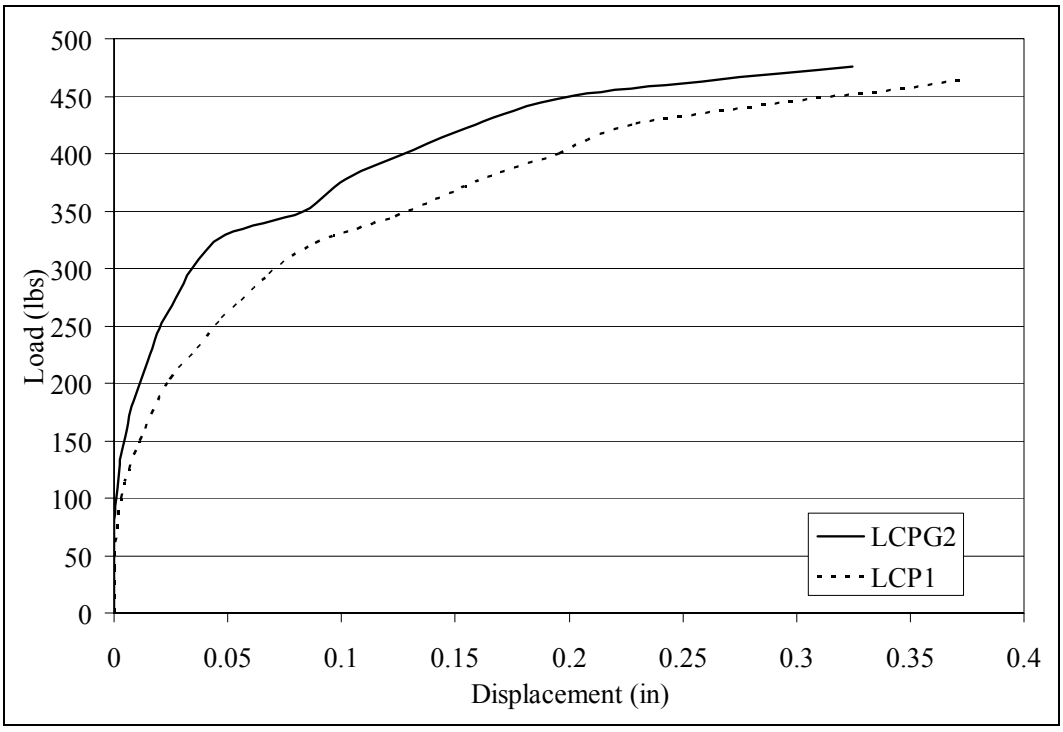

Figure 4.48 Lateral load-deflection curve for LCPG2 test

Table 4.20 shows the pile geometry for LCPG2 with minor cage exposure observed in SW(0) and NE(2) upon excavation. All four piles showed similar lengths, measuring between 16.5″ and 18″. All piles had COV values between 15% and 20% over the entire pile length. Considering only the intermediate pile diameters, however, all COV values were less than 1.5%. With the top diameters less than 4″ and intermediate pile diameter COV values less than 10%, the piles were considered to be of acceptable quality.

Table 4.20 Pile length and diameters at various depths for LCPG2

Pile label		SW (0)	NW (1)	NE (2)	SE (3)
Overall length		17.5	16.5	18	18
	0	2.116	2.039	2.598	2.628
	2	2.098	2.059	2.059	2.087
	4	2.093	2.064	2.061	2.072
	6	2.037	2.073	2.059	2.014
Depth (in)	8	2.065	2.070	2.023	2.048
	10	2.056	2.067	1.999	2.077
	12	2.081	2.064	2.056	2.063
	14	2.104	2.109	2.060	2.065
	16	0.993	1.168	2.090	2.069
	18	X	X	1.001	1.037
Average*		1.960	1.968	2.000	2.016
STDEV*		0.364	0.301	0.392	0.388
COV*		18.557	15.279	19.586	19.243
Average**		2.076	2.072	2.051	2.062
STDEV**		0.025	0.017	0.028	0.023
COV**		1.183	0.806	1.350	1.092

*Statistics include diameters at all depths

**Statistics without the top and bottom pile diameters

Table 4.21 shows the geometry of the grouted piers for LCPG2. The target 18″ installation depth and 16″ grouted length was reached for all 4 piers. Only piers W and E had sections that fell apart during excavation. The COV values for the 4 piers ranged from 7%-17%. All the piers were considered to be successfully installed as both the grout length and COV values were acceptable.

Table 4.21 Pier length and diameters at various depths for LCPG2

Pier label		W	N	E	S
Overall length		18	18	18	18
	0	1.852	1.589	2.214	2.342
	1	1.852	1.357	2.214	2.443
	2	1.852	1.418	2.214	1.946
	3	1.852	1.764	2.214	1.425
	4	1.852	2.068	2.214	1.971
	5	1.852	2.093	2.237	2.083
	6	1.908	2.084	2.145	2.095
	7	1.967	2.056	2.080	2.314
	8	1.990	2.043	2.063	2.049
Depth (in)	9	2.083	2.038	1.838	1.864
	10	2.300	2.042	1.838	1.826
	11	2.385	2.070	1.951	1.842
	12	2.476	2.378	1.867	1.942
	13	2.507	2.441	1.953	2.282
	14	2.533	2.433	1.932	2.374
	15	2.633	2.460	1.956	2.507
	16	2.490	2.431	1.924	2.479
	17	0.731	0.838	0.820	0.801
	18	0.609	0.646	0.623	0.614
Average*		2.140	2.045	2.050	2.105
STDEV*		0.302	0.344	0.150	0.292
COV*		14.120	16.841	7.327	13.853

Shaded values are assumed diameters as grout fell apart during excavation.
Horizontal lines in each column separate the above and below helix values
*Above bottom helix.

4.3.7 Cap, Piers, and Grout (LCRG)

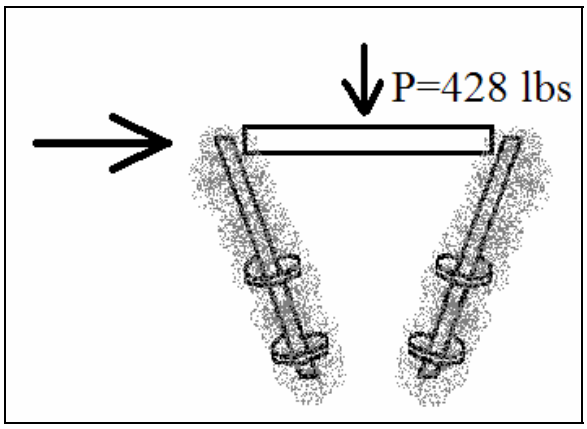

Figure 4.49 Schematic of LCRG test

Figure 4.50 Picture of LCRG test

The lateral cap, piers and grout test was performed to show how the addition of grouted helical piers would affect the cap only load deflection curve. A comparison of the LC and LCRG load-deflection curves can be seen in Figure 4.51.

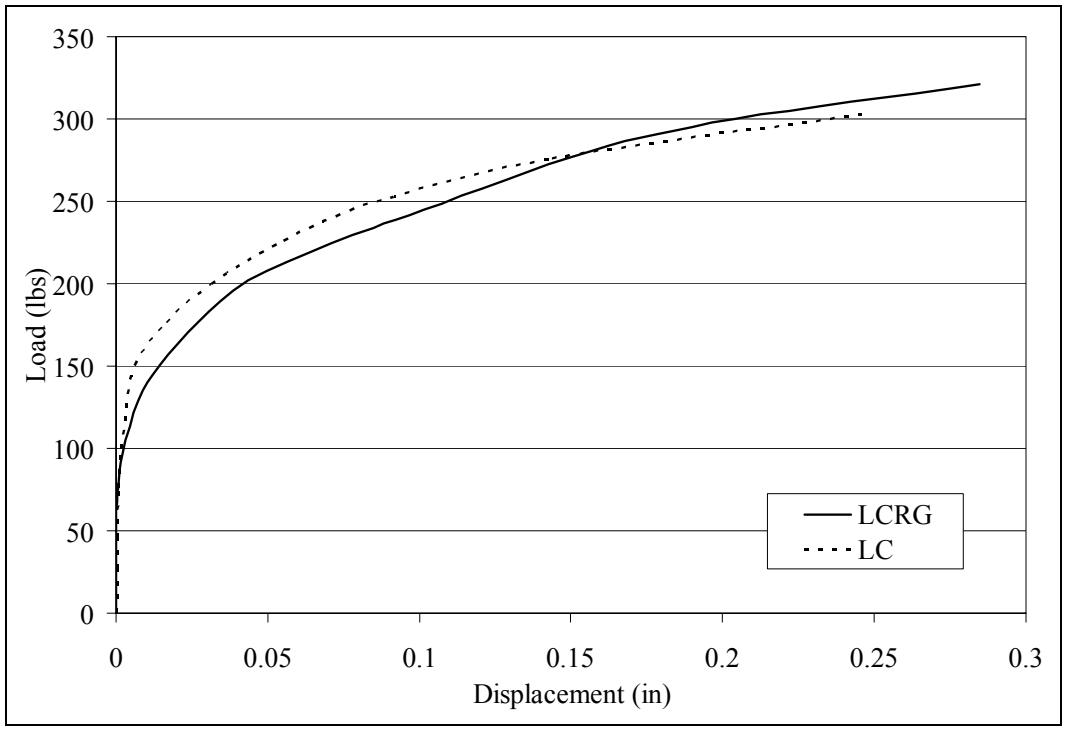

Figure 4.51 Lateral load-deflection curve for LCRG test

Table 4.22 shows the geometry of the grouted piers for LCRG. The target 18″ installation depth and 16″ grouted length was reached for all 4 piers. Only piers N and S had sections at the top that fell apart during excavation. The COV values for the 4 piers ranged from 2%-32%. Only pier E was not considered to be successfully installed as the COV value was greater than 20%.

Table 4.22 Pier length and diameters at various depths for LCRG

Pier label		W	N	E	S
Overall length		18	18	18	18
Depth (in)	0	2.029	2.178	2.199	2.122
	1	2.442	2.178	2.188	2.122
	2	2.306	2.234	2.279	2.122
	3	2.246	2.271	2.190	2.122
	4	2.254	2.189	2.133	2.122
	5	2.198	2.161	2.277	2.145
	6	2.191	2.186	2.383	2.154
	7	2.189	2.132	2.580	2.099
	8	2.127	2.150	2.753	1.999
	8.5	2.127	2.150	4.422	1.999
	9	2.156	2.168	2.494	1.969
	10	2.170	2.129	1.711	1.900
	11	2.177	2.163	2.172	2.033
	12	2.196	2.166	2.244	2.015
	13	2.193	2.175	1.513	2.158
	14	2.143	2.152	1.220	2.221
	15	2.183	2.183	1.353	2.338
	16	2.197	2.184	1.411	2.318
	17	0.960	0.837	0.711	0.803
	18	0.733	0.667	P	0.694
Average*		2.196	2.175	2.195	2.108
STDEV*		0.085	0.034	0.709	0.113
COV*		3.851	1.555	32.282	5.362

Shaded values are assumed diameters as grout fell apart during excavation.
Horizontal lines in each column separate the above and below helix values
*Above bottom helix.

4.3.8 Cap, Piles, Piers, and Grout (LCPRG)

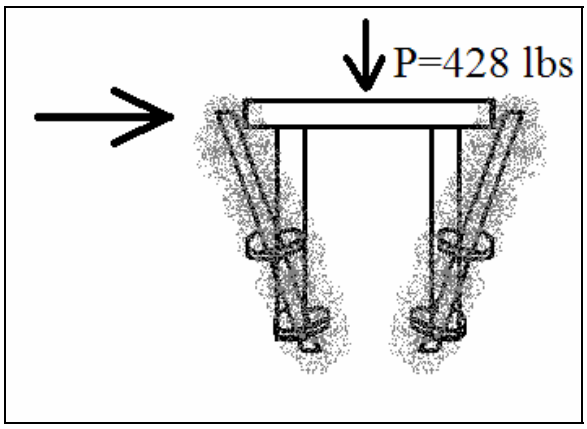

Figure 4.52 Schematic of LCPRG test

Figure 4.53 Picture of LCPRG test

The cap, piles, piers and grout test was performed to show how the addition of grouted helical piers affected the cap and piles lateral load deflection curve. A comparison of the LCP1 and LCPRG load-deflection curves can be seen in Figure 4.54.

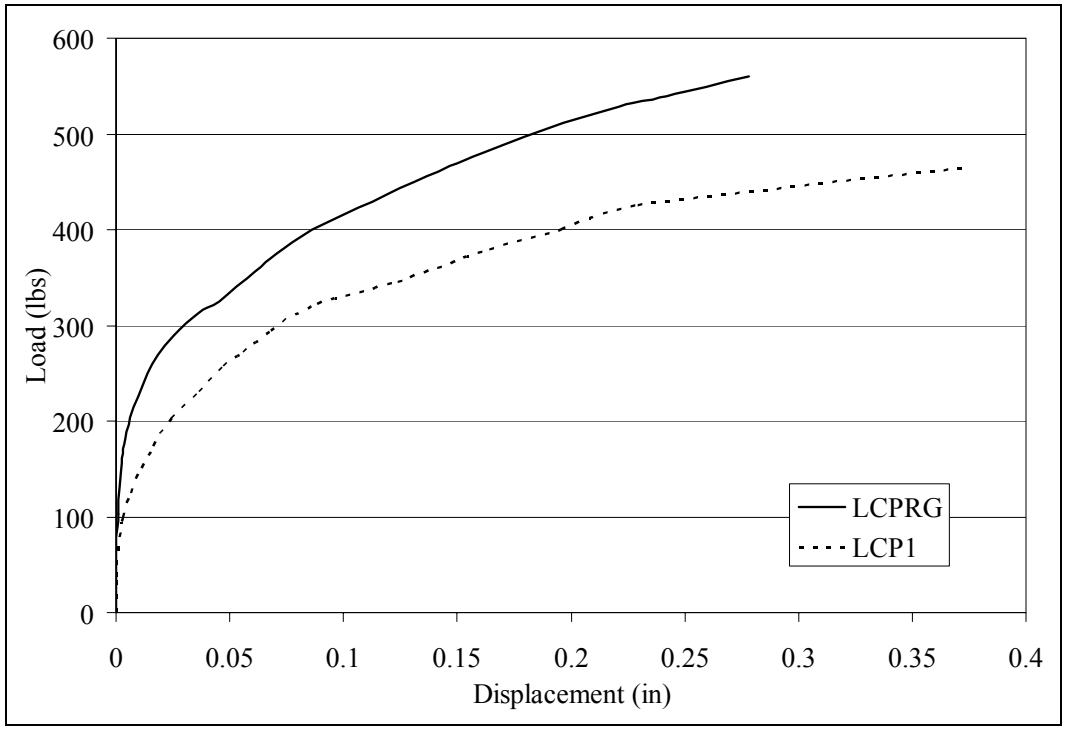

Figure 4.54 Lateral load-deflection curve for LCPRG test

Table 4.23 shows the pile geometry for LCPRG with no defects observed upon excavation. All four piles showed similar lengths, measuring between 18.5″ and 19″. All piles had COV values between 4% and 8% over the entire pile length. Considering only the intermediate pile diameters, however, all COV values were less than 4.5%. With the top diameters less than 4″ and intermediate pile diameter COV values less than 10%, the piles were considered to be of acceptable quality.

Table 4.23 Pile length and diameters at various depths for LCPRG

Pile label		SW (0)	NW (1)	NE (2)	SE (3)
Overall length		18.5	19	18.5	18.5
	0	2.413	2.161	2.254	2.274
	2	2.073	2.082	2.087	2.075
	4	2.070	2.083	2.076	2.064
	6	2.054	2.187	2.063	2.071
Depth (in)	8	2.084	2.108	2.060	2.073
	10	2.088	2.108	2.075	2.076
	12	2.083	2.259	2.079	2.058
	14	2.105	2.330	2.066	2.072
	16	2.129	2.277	2.080	2.083
	18	1.754	1.896	1.792	1.883
Average*		2.085	2.149	2.063	2.073
STDEV*		0.157	0.124	0.111	0.092
COV*		7.507	5.780	5.386	4.455
Average**		2.085	2.179	2.073	2.071
STDEV**		0.023	0.098	0.009	0.008
COV**		1.096	4.508	0.443	0.369

*Statistics include diameters at all depths

**Statistics without the top and bottom pile diameters

Table 4.24 shows the geometry of the grouted piers for LCPRG. The target 18″ installation depth was reached for all 4 piers and the grouted lengths ranged from 14″-16″. Pier W incurred a detached helix resulting in a grout length of 14″. No of the piers had sections that fell apart during excavation. The COV values for the 4 piers ranged from 6%-

19%. All the piers were considered to be successfully installed as both the grout length and COV values were acceptable.

Table 4.24 Pier length and diameters at various depths for LCPRG

Pier label		W	N	E	S
Overall length		18	18	18	18
	0	2.477	2.247	2.104	2.662
	1	2.477	2.247	2.104	2.662
	2	2.342	2.186	2.081	2.474
	3	2.218	2.049	2.014	2.361
	4	2.225	2.130	2.051	2.419
	5	2.091	1.992	2.003	2.516
	6	2.066	2.170	1.980	2.553
	7	1.961	1.954	1.962	2.399
	8	2.131	2.351	2.211	2.192
Depth (in)	9	2.293	2.119	2.067	2.086
	10	2.393	1.779	1.503	2.087
	11	2.369	2.128	1.404	2.049
	12	2.273	2.220	1.350	1.883
	13	2.220	2.172	1.508	2.003
	14	2.214	1.836	1.276	2.341
	15	0.845	2.079	1.513	2.080
	16	0.700	1.710	1.465	2.521
	17	0.557	0.559	0.741	0.794
	18	P	P	P	P
Average*		2.234	2.070	1.781	2.289
STDEV*		0.140	0.176	0.328	0.234
COV*		6.258	8.508	18.436	10.245

Shaded values are assumed diameters as grout fell apart during excavation.
Horizontal lines in each column separate the above and below helix values
*Above bottom helix.

4.4 Axial PILES load test

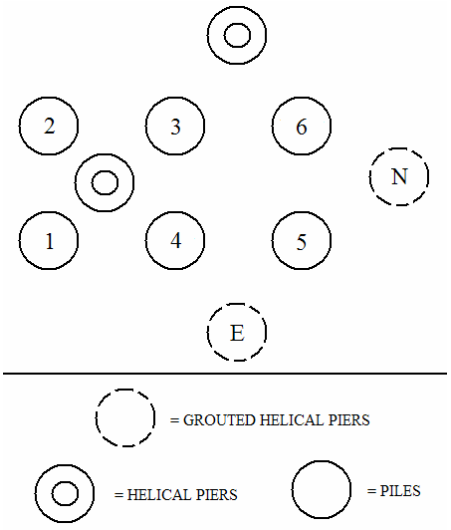

Figure 4.55 Schematic of PILES

Figure 4.56 Picture of PILES

The PILES tests were performed to determine the effect that the presence of the ungrouted and grouted helical pier had on individual piles. The resulting load-deflection curves for all the piles tests can be seen in Figure 4.57. Pile 3 was not included as the load instrumentation failed during testing.

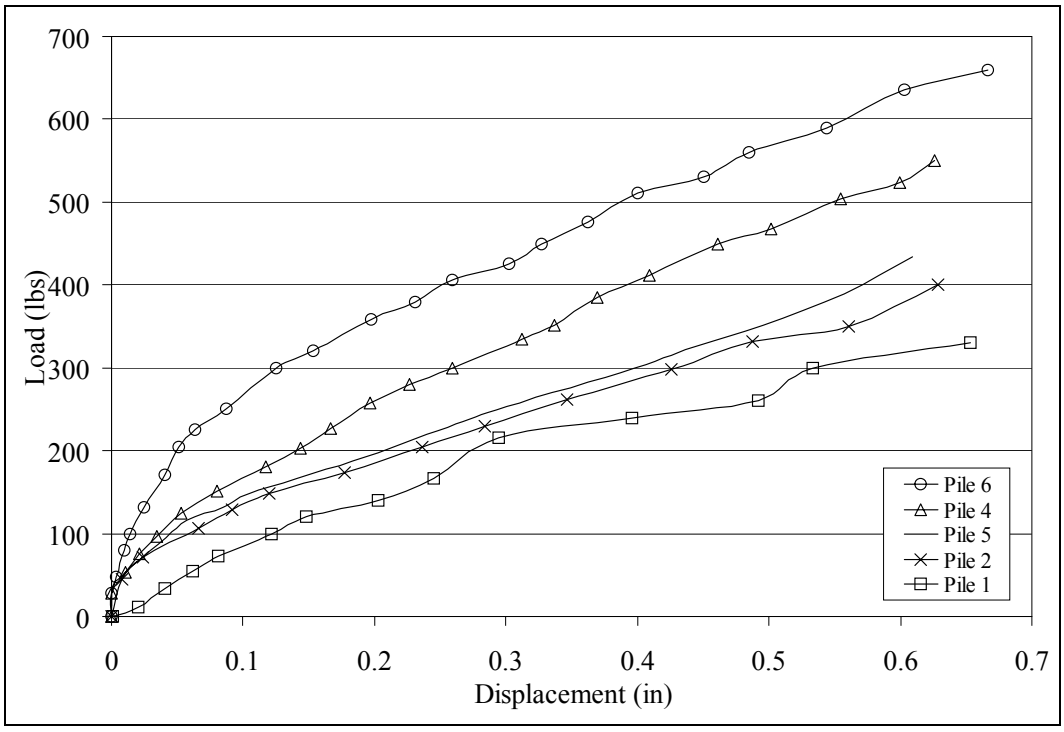

Figure 4.57 Load-deflection curve comparison for PILES test

Table 4.25 shows the pile geometry for the PILES test with minor cage exposure observed in P3 upon excavation. All six piles showed similar lengths, measuring between 16″ and 17″. All piles had COV values between 3% and 19% over the entire pile length. Considering only the intermediate pile diameters, however, all COV values were less than 8%. With the top diameters less than 4″ and intermediate pile diameter COV values less than 10%, the piles were considered to be of acceptable quality.

Table 4.25 Pile length and diameters at various depths for PILES

Pile label		1	2	3	4	5	6
Overall length		16	16	17	17	16	16
Depth (in)	0	2.073	2.157	2.281	2.415	2.358	2.408
	2	2.096	2.144	2.132	2.211	2.160	2.183
	4	2.061	2.094	2.086	2.227	2.181	2.080
	6	2.075	2.069	1.683	2.116	2.114	2.156
	8	2.100	2.072	2.072	2.090	2.087	2.077
	10	2.059	2.072	2.075	2.061	2.089	2.055
	12	2.074	2.067	2.069	2.071	2.074	2.059
	14	2.051	2.074	2.081	2.074	2.060	2.070
	16	1.605	1.897	1.068	1.908	1.244	1.118
	18	X	X	X	X	X	X
Average*		2.021	2.072	1.949	2.130	2.041	2.023
STDEV*		0.157	0.074	0.366	0.141	0.312	0.357
COV*		7.766	3.558	18.787	6.629	15.306	17.670
Average**		2.074	2.084	2.028	2.121	2.109	2.097
STDEV**		0.019	0.028	0.154	0.069	0.045	0.051
COV**		0.896	1.332	7.588	3.252	2.144	2.426

*Statistics include diameters at all depths

**Statistics without the top and bottom pile diameters

Table 4.26 shows the geometry of the grouted piers for the PILES test. Pier E reached the 18″ installation depth, while pier N was only installed to 16″. Both piers had an acceptable grout length, with 16″ for pier E and 14″ for pier N. Pier E had a large middle section of grout fall apart during excavation. The COV values for the 2 piers were approximately 17% for pier E and 21% for pier N. Only pier E was successfully installed as it met both the grout length and COV criteria.

Table 4.26 Pier length and diameters at various depths for PILES

Pier label		N	E
Overall length		16	18
	0	2.784	2.883
	1	2.440	2.341
	2	2.333	2.341
	3	2.253	2.341
	4	2.185	2.341
	5	2.158	2.341
	6	2.167	2.341
	7	2.005	2.341
	8	1.954	2.341
Depth (in)	9	2.019	1.987
	10	1.141	2.073
	11	1.084	1.475
	12	2.221	2.102
	13	2.334	2.163
	14	2.353	2.358
	15	0.869	2.450
	16	0.657	2.502
	17	X	0.849
	18	X	0.671
Average*		2.095	2.233
STDEV*		0.447	0.373
COV*		21.343	16.699

Shaded values are assumed diameters as grout fell apart during excavation.
Horizontal lines in each column separate the above and below helix values
*Above bottom helix.

4.5 Telltale data

Telltales were installed in all piles for all axially loaded cap and pile foundations. The initial two rounds proved unsuccessful due to inconsistent implementation and inadequate instrumentation. A successful method was developed for rounds 3 and 4, however, it was not consistently implemented. Consequently, only a few successful test results were produced. Figure 4.58 illustrates the telltale data obtained for a non-

defective pile, with the pile top displacement measured from the corner of the pile cap where the pile was located, and the pile base displacement measured from the top of the telltale. The difference is simply the pile top displacement minus the pile base displacement, showing the amount of compression in the pile at various loads.

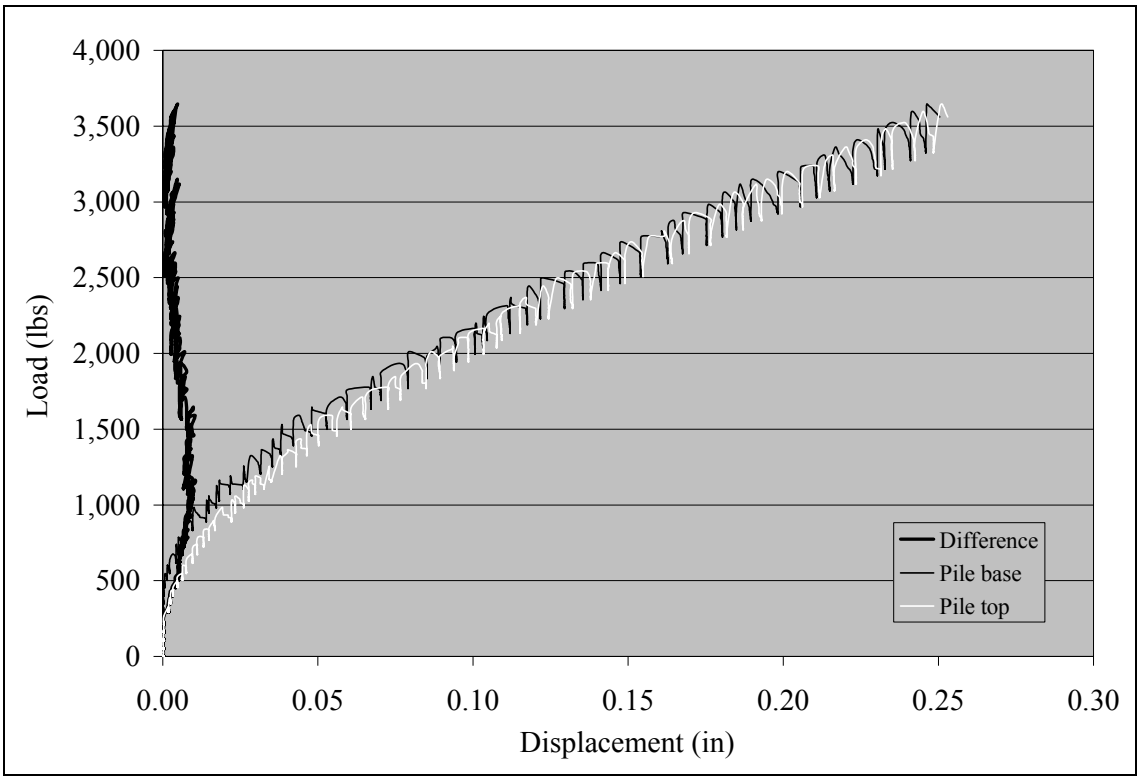

Figure 4.58 Telltale data for a non-defective pile

The pile top was shown to move more than the pile base over the initial 1,500 lbs, indicating compression in the pile. As the load increased beyond 1,500 lbs, the difference in displacements began to decrease. This decrease implies that the pile lost some of its compression. This loss of compression was believed to have occurred from an upward movement of the pile occurring from a bending of the pile cap.

Figure 4.59 illustrates the telltale data for a defective pile, where a large section of cage exposure occurred.

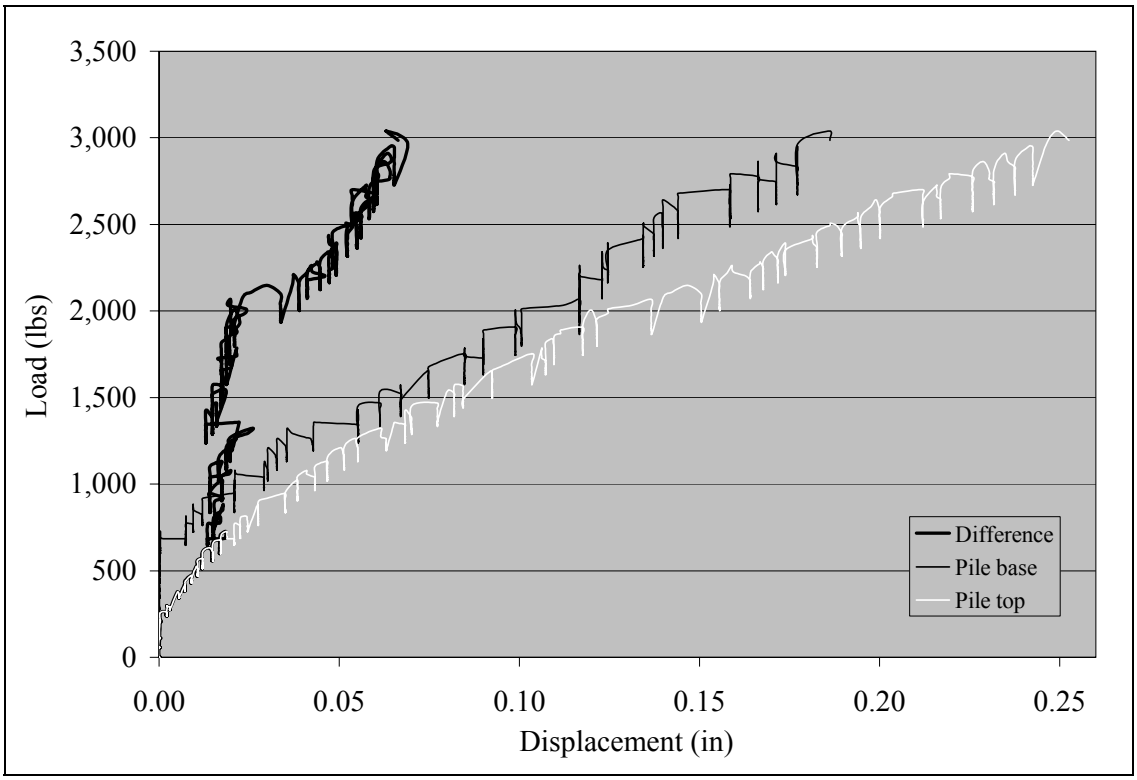

Figure 4.59 Telltale data for a defective pile

The difference between the load-deflection curves is initially small, however, once the pile begins to take a significant amount of load (approximately 2,000 lbs) there is a clear change in behavior. As the pile develops side friction, the section of exposed cage is unable to resist the compression forces and the pile undergoes a larger compression than that experienced by the non-defective pile.

4.6 Material property scaling

In order to verify that the target range for the modulus of elasticity was achieved, compression tests were performed both before and after the foundations were load tested. The desired range for the modulus of the concrete at the time of testing was 390,000 – 503,000 psi and for the grout was 100,000 – 125,000 psi. Pre-test cylinders were formed

from concrete or grout left over after completion of foundation or grout installation. The post-test cylinders were obtained by cutting down the excavated piles into 4″ tall cylinders after the foundation load tests were performed. Three of these cylinders were taken from a pile on each foundation and compression tests were performed on them. Table 4.27 shows that most of the pre-test concrete cylinders tested lower than the target range at an average of 311,000 psi. Table 4.28 shows that the pos-test concrete cylinders tested at an average of 316,000 psi, very similar to the pre-test values. The pre-test modulus for the grout cylinders proved to be slightly lower than the target range. Post-test modulus was not determined for the grout mix as the piers were not sufficiently strong to allow cutting.

Table 4.27 Pre-test strength and stiffness

Label	σ	E	Label	σ	E
	Concrete		LCPR	1,372	250,324
AC	1,350	267,734	LCPRG	1,347	347,804
ACP2	1,612	321,940	LCRG	1,482	358,316
ACP3	1,082	190,923	Average	1,400	311,651
ACP4	1,536	364,160	STDEV	227	88,140
ACPG	n/a	194,632	COV	16	28
ACPR	776	400,240		Grout	
ACPRG1	1,617	421,423	GACPRG2	527	84,585
ACPRG2	1,567	366,591	GACPRG1	530	84,933
ACRG	1,696	426,850	GACRG	497	78,751
P1	1,407	236,309	GLCPG	684	150,365
LCG	1,501	304,669	GLCRG	476	77,445
LCP1	1,254	222,845	PG1	492	94,925
LCP2	1,385	365,287	Average	534	95,167
LCPG1	1,587	458,040	STDEV	76	27,739
LCPG2	1,586	468,969	COV	14	29

σ =strength (psi), E=modulus of elasticity (psi)

Table 4.28 Post-test strength and stiffness

Label	σ	E
ACP2	1,612	321,940
ACP3	1,082	190,923
ACPG	n/a	194,632
ACPR	1,527	400,240
LCP2	1,385	365,287
LCPG	1,587	458,040
LCPR	1,372	250,324
LCPRG	1,347	347,804
Average	1,416	316,149
STDEV	182	96,685
COV	13	31

σ =strength (psi), E=modulus of elasticity (psi)

4.7 Summary

The preceding sections illustrate the test results for all axial and lateral tests, and evaluate the installation quality of each pile and pier. Foundations ACP4, LCP2, and LCPG1 were all determined to have poorly installed piles, while all grouted foundations had at least one pier that did not meet the installation criteria, except for LCPG2 and LCPRG, which both had all 4 piers successfully installed. The telltale data was shown to be successfully obtained, while the pre- and post-test compression tests showed good correlation, despite being below the target range.

5 COMPARATIVE ANALYSIS

5.1 Introduction

5.1.1 Organization

The following chapter is a comparative analysis of the test results presented in Chapter 4. Sections 5.2 and 5.3 illustrate the axial and lateral test comparisons, respectively, while section 5.4 shows the pile test results comparison.

5.1.2 Purpose

As previously stated, similitude must exist for several installation characteristics, including pile geometry, pier geometry and subsurface density, to justify the comparison of the tested foundations. Chapter 4 illustrated the pile and pier geometry of each individual pile and pier for each foundation, and, while this data is sufficient to illustrate the installation repeatability, it does not provide a means of comparing each foundation as a whole. The beginning of both section 5.2 and 5.3 compare the cumulative pile and pier lengths and diameters, as well as the subsurface density at each foundation location, resulting in a means of comparing the foundations as a whole.

5.1.3 Data Analysis Structure

The tables on pile and pier length simply show the sum of the lengths of the four piles or four piers (cumulative) and the average pile or pier length. The pier length is considered the section of a grouted pier above the bottom helix, thus, if a helix broke off and moved during installation, only the grouted length above the helix is considered. An ideal pier is installed to a depth of 18″, with 16″ of grout above the bottom helix.

The tables concerning the pile and pier diameters give values based on the combined diameters of the four piles or piers for each test with which they apply. By combining the

diameters of all piles or piers, an average pier/pile diameter can be determined for the entire foundation and is referred to as the cumulative pile/pier average diameter. This diameter is then compared to and expressed as a percent of difference from the target diameter of 2.1″ for the piles and 2.25″ for the grouted piers and columns. It should be noted that while installing the piles, the removal of the casing caused the target diameter to change from 2.25″ to 2.1″.

Chapter 4 stated that several of the piers were not considered successfully installed on an individual basis. When the COV for the entire foundation is considered, however, the low COV values of the successfully installed piers reduce the significance of the high COV values of individual piers and an intermediate COV value becomes representative of the foundation performance as a whole. Therefore, a cumulative COV value is evaluated for each of the foundations concerning grouted modifications.

Lastly, the soil density is compared at various depths in 1′ intervals from 0.5′ to 5.5′ depths. The 0.5′ and 1.5′ depths are the most relevant density measurements, because they are in direct contact with the foundations, 6″ below the pile cap and at the base of the 1.5′ long piles.

5.2 Axial Tests

5.2.1 Installation characteristic comparison

Tables 5.1-5.6 describe the installation characteristics for each of the axially loaded foundations. Table 5.1 illustrates the cumulative and average pile length comparison for the axial tests. The statistical analysis of all foundations with respect to pile length indicates only ACP3 lies considerably more than one standard deviation from the

average. Without the pile length of ACP3, the COV reduces to 3.5%, indicating that the remaining foundations are sufficient for direct comparison based on pile lengths.

Table 5.1 Cumulative pile length comparison for axial tests

Label	SW (0)	NW (1)	NE (2)	SE (3)	Average	Cumulative*
ACP1	16.5	16.5	17.0	16.5	16.6	66.5
ACP2	16.5	16.5	16.5	16.0	16.4	65.5
ACP3	18.0	19.5	18.5	18.0	18.5	74.0
ACP4	18.5	18.0	18.0	18.0	18.1	72.5
ACPR	17.0	17.0	17.0	17.5	17.1	68.5
ACPG	16.5	17.0	17.5	17.0	17.0	68.0
ACPRG1	16.5	17.0	18.0	18.0	17.4	69.5
ACPRG2	18.0	16.0	16.0	16.5	16.6	66.5

*Average=68.9, Std. Dev.=3.0, Coeff. Var.=4.4

Table 5.2 illustrates the cumulative average pile diameter and percent difference from the target 2.1″ diameter. Most of the foundations show less than a 2% difference, with only ACPRG2 being larger at 4%, but still a small value. With such a small percent difference for each of the foundations, all foundations are considered to be sufficient for direct comparison based on cumulative average pile diameter.

Table 5.2 Cumulative pile diameter comparison for axial tests

Label	SW (0)	NW (1)	NE (2)	SE (3)	Average*	% Diff**
ACP1	2.098	2.115	2.104	2.148	2.116	0.78
ACP2	2.055	2.139	2.096	2.257	2.137	1.75
ACP3	2.220	2.151	2.124	2.072	2.142	1.99
ACP4	2.063	2.078	2.109	2.197	2.112	0.56
ACPR	2.044	2.097	2.133	2.084	2.089	-0.50
ACPG	2.090	2.081	2.106	1.985	2.065	-1.65
ACPRG1	2.136	2.018	2.132	2.180	2.117	0.79
ACPRG2	2.083	2.154	2.245	2.251	2.183	3.96

*Average = 2.120, Std. Dev. = 0.04, Coeff. Var. = 1.7

**% Diff. is the percent the average diameters are from the target 2.1 inch diameter

Table 5.3 shows the average and cumulative length of grouted piers and columns above the bottom helix. Cap only tests ACG and ACRG both show very low cumulative grouted pier lengths. For cap only foundations, the grouted piers are considered to pass through the stress bulb beneath the cap, with the upper portion of the piers interacting with the higher stress areas. The upper portion of the piers in ACG and ACRG were considered to have provided sufficient ground modification to closely represent the presence of a fully grouted pier. Therefore, the cap only tests were felt to be considered sufficient for direct comparison to the other foundations.

The cap and piles tests showed good correlation to the target cumulative grout length, and are sufficient for direct comparison to the other foundations.

Table 5.3 Cumulative grout length for axial tests

Label	W	N	E	S	Avg.	Cumulative*
ACG	12.0	10.0	13.0	15.0	12.5	50.0
ACPG	15.0	14.0	16.0	15.0	15.0	60.0
ACRG	10.0	14.0	16.0	14.0	13.5	54.0
ACPRG1	16.0	16.0	16.0	16.0	16.0	64.0
ACPRG2	16.0	16.0	16.0	12.0	15.0	60.0

*Average=57.6, Std. Dev.=5.5, Coef. Var.=9.6

Table 5.4 shows the cumulative average pier diameter for the grouted pier and grouted columns. When compared to the target 2.25″ pier diameter, only ACRG shows a significant deviation. Most of the piers for ACRG have a tapered shape, whereas the piers of the other foundations do not. Thus, the smaller diameters toward the base of the piers lower the overall average diameter. For a cap only foundation, this lower diameter at a greater depth is not considered as significant as if it were for a cap and pile foundation, as the larger diameter portion of the pier is influencing the areas of higher soil stress beneath the cap only foundation.

Table 5.4 Cumulative pier diameter comparison for axial tests

Label	W	N	E	S	Average*	% Diff**
ACG	2.055	2.127	1.943	2.171	2.074	-7.8
ACRG	1.329	1.731	2.082	1.702	1.711	-24.0
ACPG	2.461	1.839	2.187	2.180	2.167	-3.7
ACPRG1	1.708	2.225	1.827	1.943	1.926	-14.4
ACPRG2	2.219	1.948	1.890	2.197	2.064	-8.3

*Average = 1.988, Std. Dev. = 0.177, Coef. Var. = 8.9

**% Diff. is the percent the average diameters are from the target 2.25 inch diameter

Table 5.5 shows the cumulative coefficient of variation for all the axial tests, with COV values ranging from 10%-20%. With all the COV values within 10% of each other, and the average values close to the target diameter, the pier diameters are of sufficient consistency to allow for direct comparison between the axially loaded foundations.

Table 5.5 Cumulative pier coefficient of variations for axial tests

Label	W	N	E	S	Cumulative*
ACG	9.214	3.353	11.239	13.468	10.682
ACRG	14.909	22.278	8.268	21.736	15.099
ACPG	6.803	23.252	5.694	5.521	20.993
ACPRG1	13.751	6.603	12.383	21.755	17.374
ACPRG2	3.365	24.376	16.436	5.313	16.110

*Average = 16.1, Std. Dev. = 3.74, Coef. Var. = 23.3

Table 5.6 shows the density at six depths for each of the foundations. As only the top two measurements were felt to have considerable influence on the performance of the foundations, only those are analyzed here. ACP2 and ACP3 lie outside one standard deviation at the 1.5′ depth, while ACPRG1 and ACPRG2 lie outside one standard deviation for the 0.5′ and 1.5′ depth.

Table 5.6 Subsurface relative density comparison for axial tests

Label	Depth (ft)					
	0.5	1.5	2.5	3.5	4.5	5.5
AC	64.8	54.0	66.1	59.7	62.0	62.7
ACR	61.2	54.2	61.2	61.6	58.0	58.0
ACG	63.9	59.0	58.2	65.7	26.6	54.9
ACRG	58.8	65.0	65.5	66.5	57.6	55.1
ACP1	62.7	64.4	66.1	64.2	65.7	64.2
ACP2	59.2	41.1	61.8	60.1	50.7	61.0
ACP3	56.3	47.7	65.5	61.4	48.7	61.0
ACP4	61.8	62.0	55.1	62.4	59.0	61.2
ACPR	62.9	58.6	62.9	61.6	51.6	53.4
ACPG	47.3	53.8	52.2	54.4	36.0	59.7
ACPRG1	68.3	68.3	70.5	63.3	69.2	65.2
ACPRG2	69.6	67.4	62.4	59.9	59.7	59.3
Average	61.1	58.7	62.0	62.0	52.5	59.5
Std. Dev.	6.3	8.9	5.5	3.5	13.1	3.9
Coeff. Var.	10.4	15.1	8.9	5.6	24.9	6.6

5.2.2 Cap and Piles

Several ACP tests were performed to determine the repeatability of the ACP load-deflection curve (Figure 5.1).

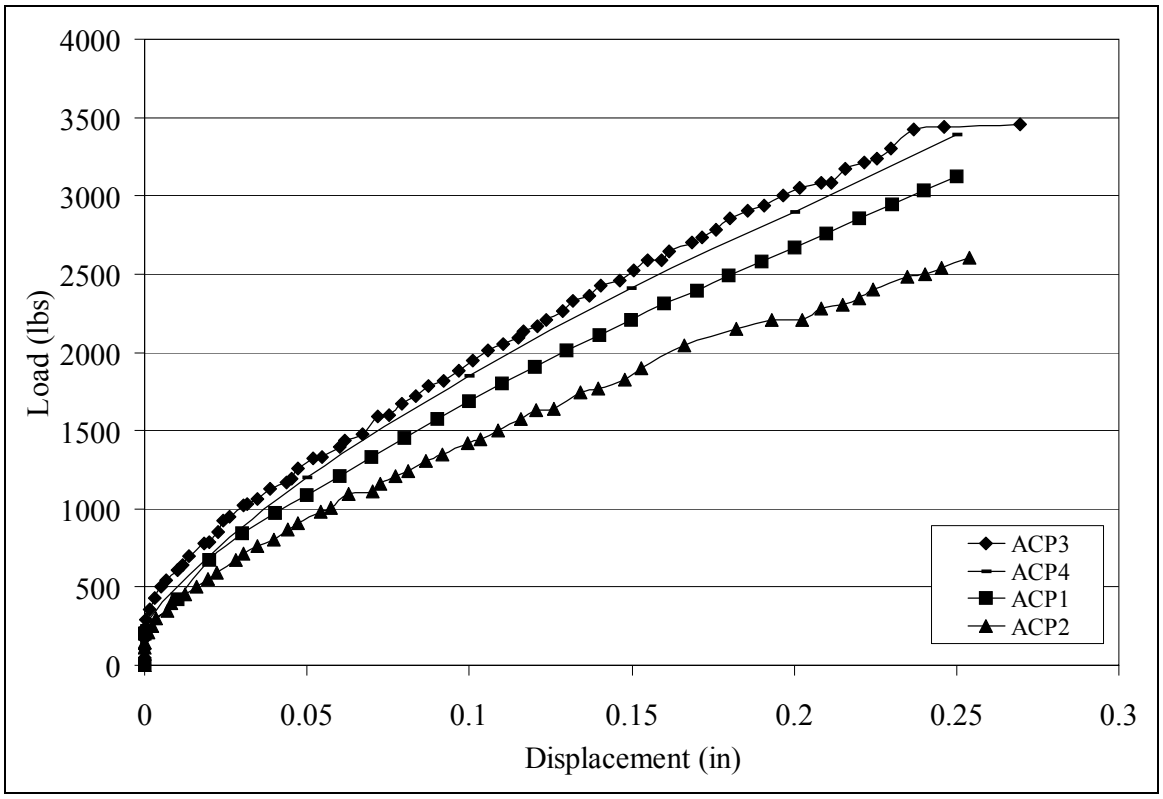

Figure 5.1 Comparison of ACP load-deflection curves

As previously discussed in Section 4.2.2, ACP3 and ACP4 experienced installation errors and are not considered comparable to the other two ACP tests. When inspecting the installation characteristics for the remaining two tests (ACP1 and ACP2), the only notable variation is the soil density at the base of the piles, 64% for ACP1 to 41% for ACP2. This difference is believed to have caused ACP2 to perform significantly lower than ACP1, and causes ACP2 to not be fully comparable to ACP1. As a result, ACP1 was selected as having the most reliable load-deflection curve and was, thus, used as the representative ACP curve.

5.2.3 ACPRG tests

The load-deflection curves for both ACPRG tests can be seen in Figure 5.2.

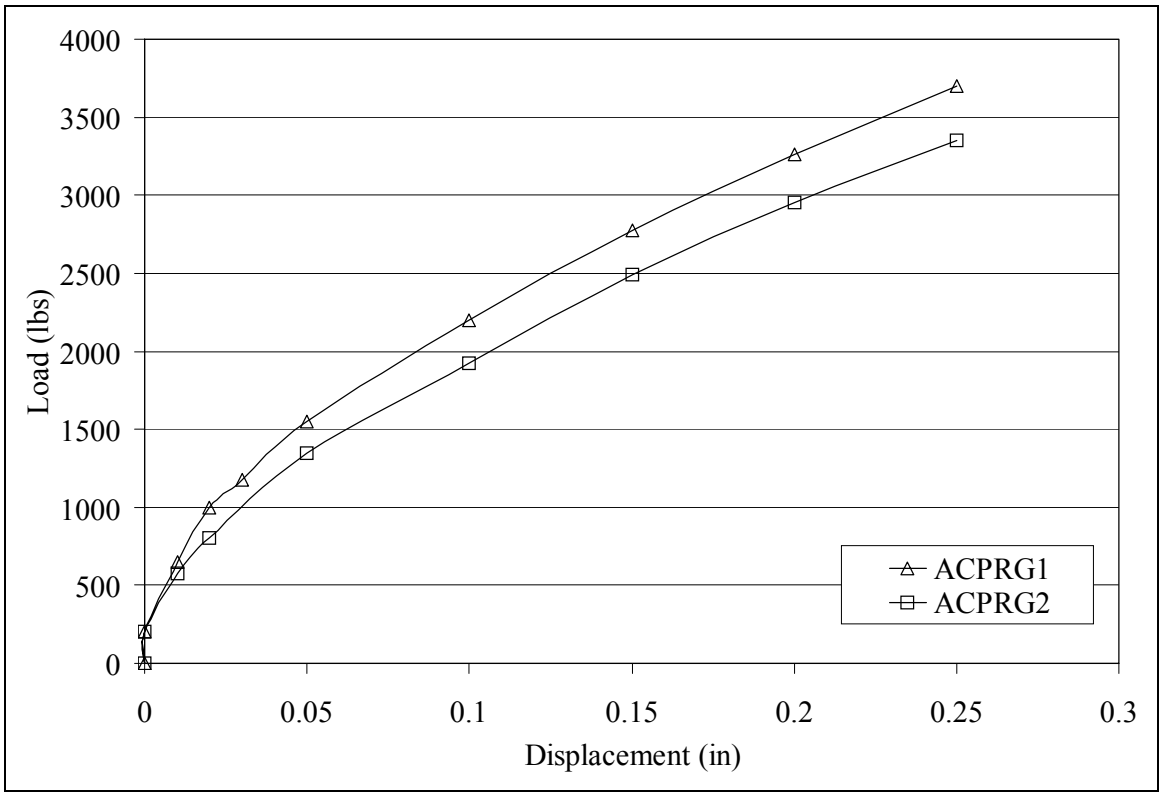

Figure 5.2 Comparison of ACPRG load-deflection curves

Upon excavation of the foundations, the necking in ACPRG1 was not as severe as initially believed. Table 5.8 shows consistent installation characteristics between the two tests, resulting in the average of the two tests to be the representative load-deflection curve for ACPRG.

Table 5.7 Comparison of ACPRG tests

Description	ACPRG1	ACPRG2	AVG. ACPRG
Cumulative pile data			
Average diameer	2.117	2.183	2.150
Coefficient of variation	21.5	23.9	22.7
Length	69.5	66.5	68.0
Cumulative pier data			
Average diameter	1.926	2.064	1.995
Coefficient of variation	17.3	16.1	16.7
Length	64.0	60.0	62.0
Density data			
Subsurface density at 0.5 ft	68.3	69.6	69.0
Subsurface density at 1.5 ft	68.3	67.4	67.9

Due to the similarity between the installation characteristics of ACPRG1 and ACPRG2, it is proposed that the repeatability of the foundations can be determined from them. Table 5.9 shows the comparison of load for various displacements, the resulting average load, and the percent difference from the average. The resulting repeatability is approximately ±8%, and will be taken as such for all foundations.

Table 5.8 Load (lbs) at various displacements for the ACPRG axial tests

Test	Displacement (inches)									
	0*	0.01	0.02	0.03	0.04	0.05	0.1	0.15	0.2	0.25
ACPRG1	200	650	1000	1180	1385	1550	2200	2775	3260	3700
ACPRG2	200	575	800	1005	1190	1350	1925	2490	2950	3350
AVG	200	613	900	1093	1288	1450	2063	2633	3105	3525
% Diff.	0	7	13	9	8	7	7	6	5	5

*All tests began at 0 load and 0 displacement. This is the load just prior to any displacement

5.2.4 All axial tests

Figure 5.3 graphically compares all axial test load deflection curves, and Table 5.10 shows a quantitative comparison of loads at various displacements for all the axial tests. All tests were begun at zero load and zero displacement. The load for zero displacement in Table 5.10 represents the load at which displacement was first observed.

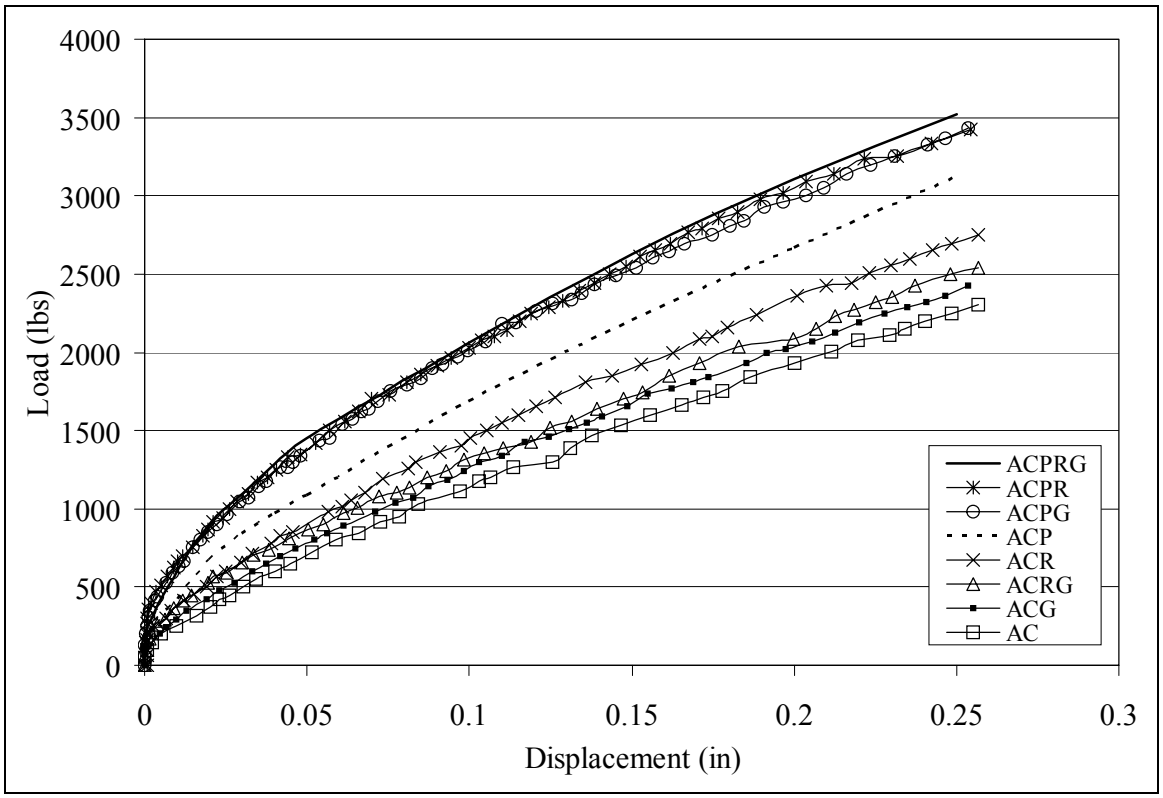

Figure 5.3 All axial tests load-deflection comparison

Table 5.9 Axial test loads at various displacements (lbs)

Test	Displacement (inches)									
	0*	0.01	0.02	0.03	0.04	0.05	0.1	0.15	0.2	0.25
AC	100	250	360	490	600	705	1145	1560	1935	2260
ACG	100	300	430	560	680	780	1260	1670	2035	2390
ACRG	140	390	540	660	765	865	1325	1720	2090	2515
ACR	140	380	525	660	790	905	1450	1895	2360	2710
ACP	200	420	670	840	970	1090	1685	2210	2670	3120
ACPR	140	650	860	1070	1230	1375	2030	2575	3055	3400
ACPG	170	625	855	1050	1230	1370	2025	2530	2980	3400
ACPRG	200	613	900	1093	1288	1450	2063	2633	3105	3525

*All tests began at 0 load and 0 displacement. This is the load just prior to any displacement

Prior to testing, it was assumed that the load-deflection curves would perform from worst to best was as follows: AC, ACR, ACG, ACRG, ACP, ACPR, ACPG, and ACPRG, (Table 5.11) which placed the cap with the lowest performance, followed by the

other cap only foundations, then the cap and piles foundation with the best performers being the treated pile foundations. The basis for this assumption was that the cap only foundations would all test with a lower performance than any of the cap and pile foundations.

Table 5.10 Assumed and tested axial test performance

Test label	Tested ranking	Assumed ranking	Actual load (lbs) at 0.1" displacement	Actual load (lbs) at 0.25" displacement
ACPRG	1	1	2,063	3,525
ACPR	2	3	2,030	3,400
ACPG	3	2	2,025	3,400
ACP	4	4	1,685	3,120
ACR	5	7	1,450	2,710
ACRG	6	5	1,325	2,515
ACG	7	6	1,260	2,390
AC	8	8	1,145	2,260

For the cap only foundation, the settlement of the cap is determined by the effective stress increase in the soil beneath the cap, commonly represented as a stress bulb (Coduto, 2001). The cap only test was assumed to have a lower performance than the cap only tests where modifications were made, as the helical pier, grouted column, or grouted helical pier foundations were assumed to cross into the stress bulb, thereby causing a redistribution of the stress to the installed elements. As the soil would undergo a smaller effective stress increase, the settlement performance would improve. Of the three intervention schemes, the stress redistribution was assumed to be least affected by the helical piers, which have the smallest cross-section. Subsequently, the larger cross-section of the grouted column and grouted helical pier cause a larger interaction with the stress bulb, leading to a larger performance improvement. Since the grouted column and grouted helical pier were of the same geometry, with the only difference being an

increased bending strength for the grouted, helical pier due to the presence of the helical pier, it was assumed that their performance would be similar, with a slightly increased performance for the grouted, helical pier.

With the addition of piles to the cap, the load-deflection performance of the cap was assumed to significantly increase and perform greater than all of the cap only foundations. When a load is applied to a piled footing, some of the load is transferred to the soil beneath the pile cap, with the remainder being transferred to the piles, first along the shaft into the soil and then to the end of the pile. Long (1993) proposed that once the maximum load of the piles had been reached, the soil in contact with the pile cap absorbs the additional load. Therefore, the initial increased stresses in the soil occur along the shaft of the piles. The addition of modification elements between the existing piles was assumed to interact with these soil stress areas and transfer some of the stress to the installed foundation elements, causing arching, but in this case in a more effective manner than the cap only foundations because of the closer proximity of the intervention to the high stress areas.

After testing, the order of performance from worst to best was as follows: AC, ACG, ACRG, ACR, ACP, ACPG, ACPR and ACPRG (Table 5.11). As assumed, all of the cap only foundations performed worse than all of the cap and pile foundations, and the AC and ACP test had the lowest performance of the cap only foundations and cap and piles foundations, respectively. The tests generally performed in the order expected, with the exception of those with only the helical piers, as the ACR test performed considerably higher than the other cap only tests, and the ACPR test performed slightly better than the

ACPG test. It should be noted that the ACPRG test may have performed slightly higher than the ACPG and ACPR tests due to the slightly denser soil conditions.

From the test results, the assumptions concerning the influence of the ungrouted helical piers were insufficient to explain the recorded performance. Some additional mechanism must exist that allows the ungrouted helical piers to increase the pile foundation performance to the same as the grouted helical piers, or for the grouted modifications to negatively impact the performance of the helical pier.

The consistently superior performance of the foundation and foundation elements in the presence of helical piers over the grouted helical piers was felt to occur because of the soil in which it was tested. Typical field installations of grouted, helical piers are performed in non-uniform soils with a non-zero water content, such that as the pier is installed, the helix carved path is able to remain open such that the grout can fill it. In the lab testing, the dry sand did not allow the helix carved path to stay open, rather, the grout was mixed with the sand possibly loosening the soil around the piles. This looser soil configuration would result in a decreased soil-pile interface friction angle and, ultimately, a decrease in pile capacity.

To quantify the improvement of each foundation, Table 5.11 shows the percent improvement of each foundation as compared to the cap only foundation.

Table 5.11 Percent of load improvement over AC at various displacements

Test	Displacement (inches)									
	0*	0.01	0.02	0.03	0.04	0.05	0.1	0.15	0.2	0.25
ACG	0	20	19	14	13	11	10	7	5	6
ACRG	40	56	50	35	28	23	16	10	8	11
ACR	40	52	46	35	32	28	27	21	22	20
ACP	100	68	86	71	62	55	47	42	38	38
ACPG	70	150	138	114	105	94	77	62	54	50
ACPR	40	160	139	118	105	95	77	65	58	50
ACPRG	100	145	150	123	115	106	80	69	60	56

*All tests began at 0 load and 0 displacement. This is the load just prior to any displacement

Table 5.11 shows that large improvements are realized at low displacements, with decreasing level of improvement as the load increases. The trend is most clearly seen in Figure 5.4.

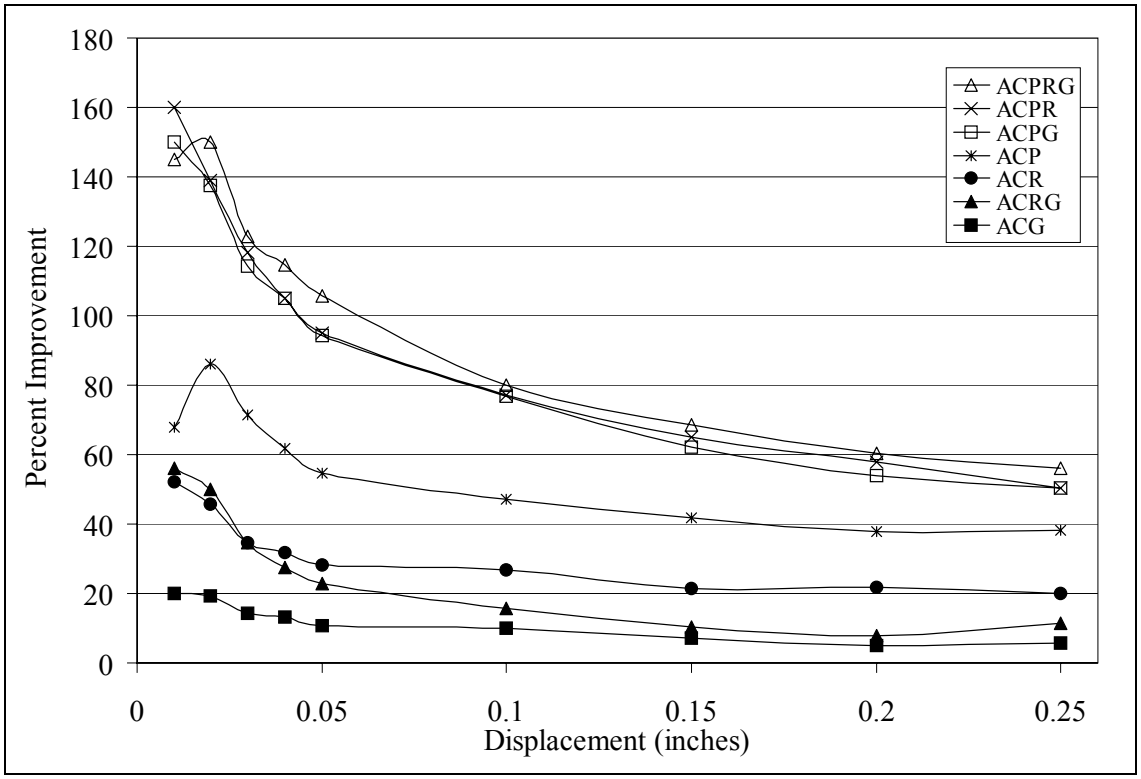

Figure 5.4 Percent improvement of axial load for increasing displacements

5.3 Lateral Tests

5.3.1 Installation characteristics comparison

Similar to the axial tests, Tables 5.12-5.15 compare the installation characteristics for the laterally loaded tests. Table 5.12 illustrates the cumulative and average pile length comparison for the lateral tests. LCP1 lies greater than one standard deviation below the group average and LCPRG lies greater than one standard deviation above the group average. Without these two tests, the COV reduces to 3.3%, indicating that the remaining foundations are sufficient for direct comparison based on pile lengths. LCP1 and LCPRG were still used in direct comparison to the other foundations, however, their different pile lengths should be considered when making definitive assessments regarding relative performance capacity.

Table 5.12 Cumulative pile length comparison for lateral tests

Label	SW (0)	NW (1)	NE (2)	SE (3)	Average	Cumulative*
LCP1	15.5	16.5	15.5	16.0	15.9	63.5
LCP2	17.0	17.0	16.0	17.0	16.8	67.0
LCPR	18.5	18.0	18.0	18.0	18.1	72.5
LCPG1	18.0	18.5	17.5	15.0	17.3	69.0
LCPG2	17.5	16.5	18.0	18.0	17.5	70.0
LCPRG	18.5	19.0	18.5	18.5	18.6	74.5

*Average=69.4, Std. Dev.=3.9, Coeff. Var.=5.6

Table 5.13 illustrates the average cumulative pile diameter and percent difference from the target 2.1″ diameter. The COV for these values is 5%, indicating that, while not as consistent as the axial foundations, the lateral foundations were considered to be sufficient for direct comparison based on cumulative average pile diameter.

Table 5.13 Cumulative pile diameter comparison for lateral tests

Label	SW (0)	NW (1)	NE (2)	SE (3)	Average*	% Diff**
LCP1	2.087	2.180	2.155	2.185	2.152	2.47
LCP2	2.106	2.190	2.206	2.144	2.162	2.95
LCPR	2.182	2.361	2.219	2.264	2.257	7.45
LCPG1	2.018	2.031	1.916	1.932	1.974	-5.98
LCPG2	1.960	1.968	2.000	2.016	1.986	-5.43
LCPRG	2.085	2.149	2.063	2.073	2.092	-0.36

*Average = 2.104, Std. Dev. = 0.11, Coeff. Var. = 5

**% Diff. is the percent the average diameters are from the target 2.1 inch diameter

Table 5.14 shows the average and cumulative length of grouted piers and columns above the bottom helix. The LCG and LCPG1 tests show poor correlation to the other foundations, as they have substantially less grouted pier length in the ground. The remaining foundations have sufficient grouted pier length to be considered comparable to the other foundations.

Table 5.14 Cumulative pier length comparison for lateral tests

Label	W	N	E	S	Avg.	Cumulative*
LCG	16.0	16.0	5.0	16.0	13.3	53.0
LCPG1	16.0	5.0	2.0	17.0	10.0	40.0
LCPG2	16.0	16.0	16.0	16.0	16.0	64.0
LCRG	16.0	16.0	16.0	16.0	16.0	64.0
LCPRG	13.0	15.0	15.0	15.0	14.5	58.0

*Average = 55.8, Std. Dev.=10, Coef. Var.=17.8

Table 5.15 presents the cumulative pier diameter for the grouted pier and grouted columns. When compared to the target 2.25″ pier diameter, none of the tests showed significant difference from the target diameter.

Table 5.15 Cumulative pier diameter comparison for lateral tests

Label	W	N	E	S	Average*	% Diff**
LCG	1.869	2.156	1.682	2.357	2.016	-10.4
LCRG	2.196	2.175	2.195	2.108	2.169	-3.6
LCPG1	2.215	2.350	1.950	2.158	2.168	-3.6
LCPG2	2.140	2.045	2.050	2.105	2.085	-7.3
LCPRG	2.234	2.070	1.781	2.289	2.093	-7.0

*Average = 2.106, Std. Dev. = 0.064, Coef. Var. = 3.0

**% Diff. is the percent the average diameters are from the target 2.25 inch diameter

As described in section 5.2, the COV for the entire foundation can be used for foundation comparison. Table 5.16 shows the cumulative coefficient of variation for the all lateral tests, with COV values ranging from 11%-17%, with the exception of LCG at 24%. Only the piers for LCG had an average and COV value to not be considered comparable to the other foundations.

Table 5.16 Cumulative pier coefficient of variations for lateral tests

Label	W	N	E	S	Cumulative*
LCG	27.142	19.270	17.514	18.487	23.564
LCRG	3.851	1.555	32.282	5.362	16.409
LCPG1	8.764	17.707	6.637	11.094	11.706
LCPG2	14.120	16.841	7.327	13.853	13.782
LCPRG	6.258	8.508	18.436	10.245	14.534

*Average = 16.0, Std. Dev. = 4.6, Coef. Var. = 28.5

Table 5.17 presents the density at six depths for each of the foundations. As explained in the axial section, only the top two measurements are analyzed here. The average and standard deviation for the density at 0.5′ depth is 60.5% and 7.3%, and at a depth of 1.5′ are 58.9% and 6.3%. Only LCPG2 lies considerably outside one standard deviation at the 0.5′ depth, LC, LCP2, and LCPR all were outside one standard deviation for the 1.5′ depth.

Table 5.17 Subsurface relative density comparison for lateral tests

Label	Depth (ft)					
	0.5	1.5	2.5	3.5	4.5	5.5
LC	63.7	50.3	56.9	61.4	67.4	53.8
LCP1	60.3	54.7	61.0	68.0	66.3	61.2
LCP2	61.6	68.7	67.4	63.3	64.6	60.7
LCR	63.7	53.8	55.3	59.0	57.8	54.2
LCG	53.8	54.9	53.0	54.2	65.9	54.9
LCPR	63.9	66.7	63.7	66.5	62.6	65.9
LCRG	67.8	59.3	55.9	60.7	64.4	63.7
LCPG1	62.4	62.2	59.3	53.8	59.9	61.2
LCPG2	42.5	64.8	49.9	61.0	53.4	55.1
LCPRG	65.2	53.8	57.4	59.5	63.7	54.4
Average	60.5	58.9	58.0	60.7	62.6	58.5
Std. Dev.	7.3	6.3	5.1	4.6	4.4	4.5
Coeff. Var.	12.1	10.8	8.8	7.5	7.0	7.7

5.3.2 Cap and Piles

Two lateral cap and piles tests were performed, with the resulting load-deflection curves seen in Figure 5.5. LCP2 was shown to have performed significantly lower than LCP1, due largely in part to the construction errors previously described in section 4.3.2.2. Given the faulty installation of LCP2, only LCP1 was used for the representative LCP load-deflection curve for comparative analysis.

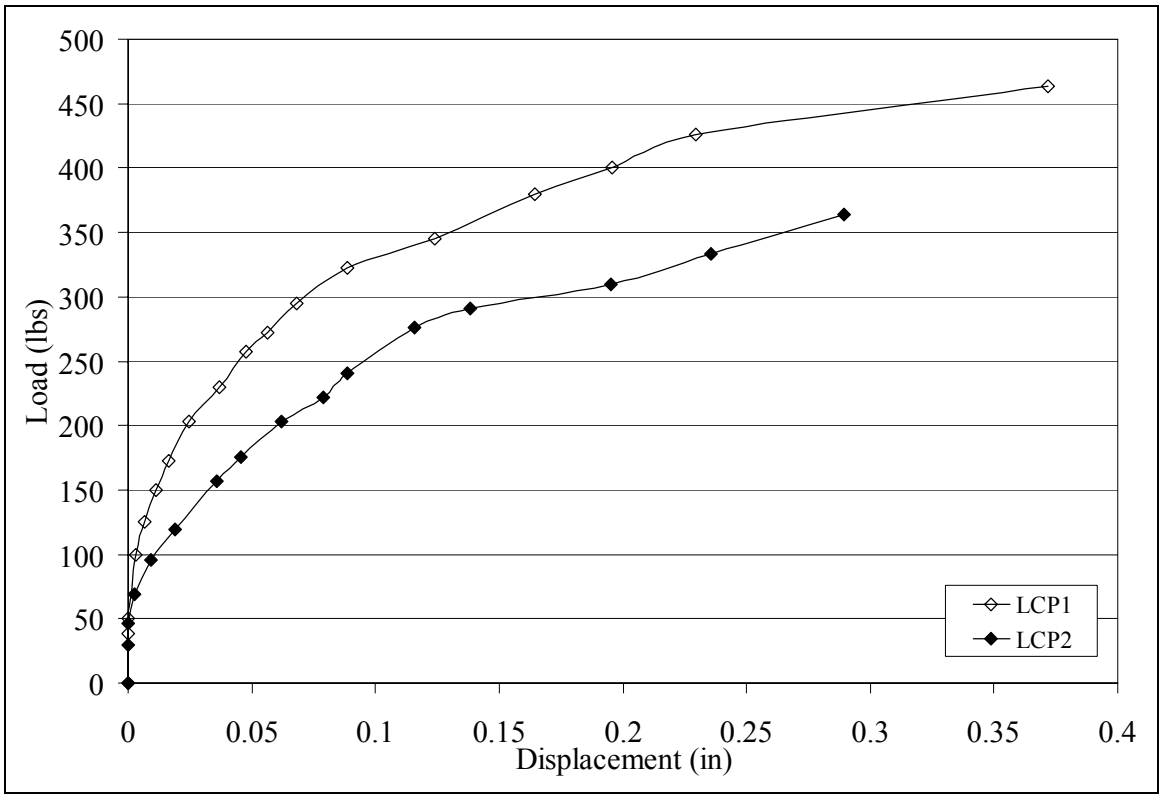

Figure 5.5 Load-deflection comparison for LCP tests

5.3.3 LCPG tests

Upon excavation of the initial LCPG test, it was found that only two of the four piers were successfully installed, with the other two having exposed cages. Consequently, a second LCPG arrangement (LCPG2) was tested, with the comparison of the results seen in Figure 5.6.

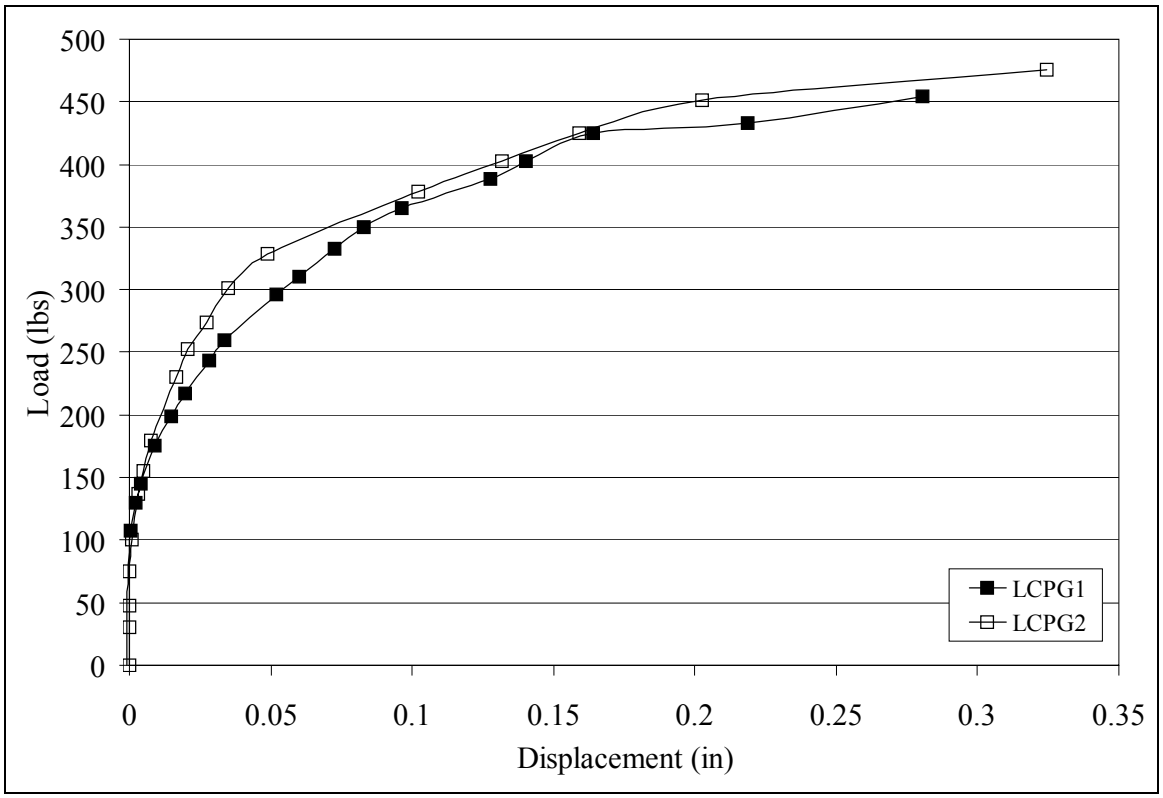

Figure 5.6 Load-deflection curve comparison for LCPG tests

LCPG2 was used as the representative LCPG test because of inconsistent installation of both the piles and piers for LCPG1 (Section 4.3.6.2), however, it should be noted that the low density at 0.5′ probably caused LCPG2 to have a lower load-deflection performance than would otherwise be expected.

5.3.4 All lateral tests

Figure 5.6 shows the graphical comparison of all the load deflection curves, and Table 5.18 shows a quantitative comparison of loads at various displacements for all the lateral tests. All tests were begun at zero load and zero displacement. The load for zero displacement in Table 5.18 represents the load at which displacement was first observed.

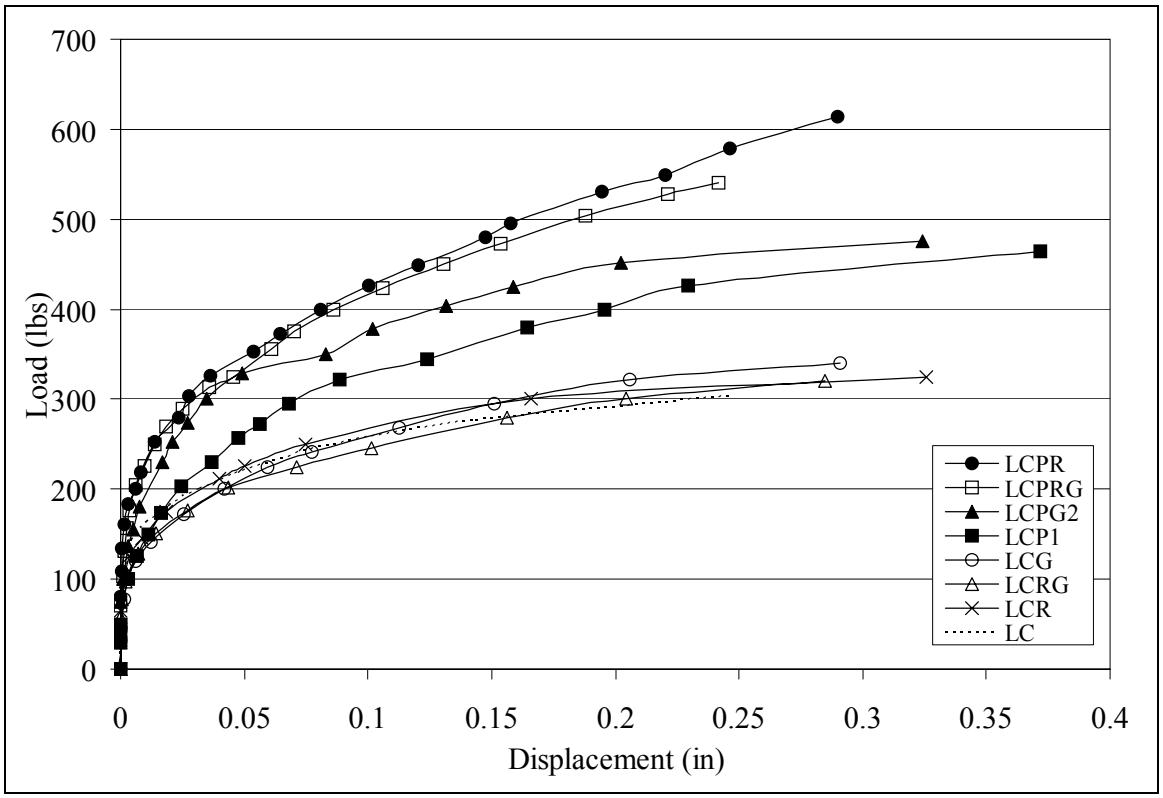

Figure 5.7 Load-deflection comparison for all lateral tests

Table 5.18 Lateral test loads at various displacements (lbs)

Test	Displacement (inches)									
	0*	0.01	0.02	0.03	0.04	0.05	0.1	0.15	0.2	0.25
LC	100	161	182	197	210	220	258	279	292	305
LCRG	90	140	163	183	198	209	245	275	299	313
LCR	90	150	178	195	211	225	267	295	308	317
LCG	70	135	160	180	198	213	259	295	320	333
LCP	70	143	187	215	239	262	330	368	404	432
LCPG	100	195	248	285	313	330	375	418	450	461
LCPRG	100	229	274	300	319	333	416	470	513	543
LCPR	130	231	270	310	332	347	427	485	533	582

*All tests began at 0 load and 0 displacement. This is the load just prior to any displacement

Prior to testing, it was assumed that the load-deflection curves would perform from worst to best as follows: LC, LCR, LCG, LCRG, LCP, LCPR, LCPG, and LCPRG, (Table 5.21) which placed the cap with the lowest performance, followed by the other cap only foundations, then the cap and piles foundation and the best performers being the

treated pile foundations. The basis for this assumption was that the cap only foundations would always perform lower than any of the cap and pile foundations.

Table 5.19 Assumed and tested lateral test performance

Test label	Tested ranking	Assumed ranking	Actual load (lbs) at 0.1" displacement	Actual load (lbs) at 0.25" displacement
LCPR	1	3	427	582
LCPRG	2	1	416	543
LCPG	3	2	375	461
LCP	4	4	330	432
LCG	5	6	259	333
LCR	6	7	267	317
LCRG	7	5	245	313
LC	8	8	258	305

For the cap only foundation, the displacement of the cap is determined soil-cap interaction. Initially it was assumed that there would be little difference between any of the cap only tests, however, the question arose as to whether or not grout installation would alter the surface soil conditions and, thus, change the soil-cap interaction. Subsequently, it was assumed that the helical pier would not alter the soil-cap interface and the grouted column and grouted helical pier would alter the interface to a similar extent if any.

With the addition of piles to the cap, the load-deflection performance of the cap was assumed to increase significantly. With additional elements between the existing piles, it was assumed that the modification elements would alter the soil matrix, resulting in a decreased amount of displacement under a similar load. Since the grouted column and grouted helical pier would leave a more rigid element between the piles and would alter the existing soil conditions, it was felt that the grouted modifications would improve

the load-deflection performance more significantly than just the helical pier due to an increased arching capacity.

After testing, the order of performance, from worst to best, was as follows: LC, LCRG, LCR, LCG, LCP, LCPG, LCPRG and LCPR (Table 5.21). All the cap only foundations performed worse than the cap and pile foundations, as expected, and all the cap only tests performed in a similar manner, confirming that the addition of elements had little to no effect on the cap only performance. The LCG test was previously stated to not be comparable to the other lateral tests because essentially only 3 of the 4 piers were installed, however, due to the similar testing of the lateral cap tests, the addition of a 4th pier would not have altered the load-deflection performance and is, thus, comparable to the other foundations. Of the cap and pile foundations, only the foundation modified with the ungrouted helical piers performed higher than assumed resulting in the best load-deflection performance of all the lateral tests. To quantify the improvement of each foundation, Table 5.22 shows the percent improvement of each foundation as compared to the cap only foundation.

Table 5.20 Percentage improvement at various displacements

Test	Displacement (inches)									
	0*	0.01	0.02	0.03	0.04	0.05	0.1	0.15	0.2	0.25
LCR	-10	-7	-2	-1	0	2	3	6	5	4
LCG	-30	-16	-12	-9	-6	-3	0	6	10	9
LCRG	-10	-13	-10	-7	-6	-5	-5	-1	2	3
LCP	-30	-11	3	9	14	19	28	32	38	42
LCPG	0	21	36	45	49	50	45	50	54	51
LCPRG	0	42	51	52	52	51	61	68	76	78
LCPR	30	43	48	57	58	58	66	74	83	91

*All tests began at 0 load and 0 displacement. This is the load just prior to any displacement

Table 5.22 shows that the percentage of load improvement increases with increasing displacements. This trend is more clearly illustrated in Figure 5.8.

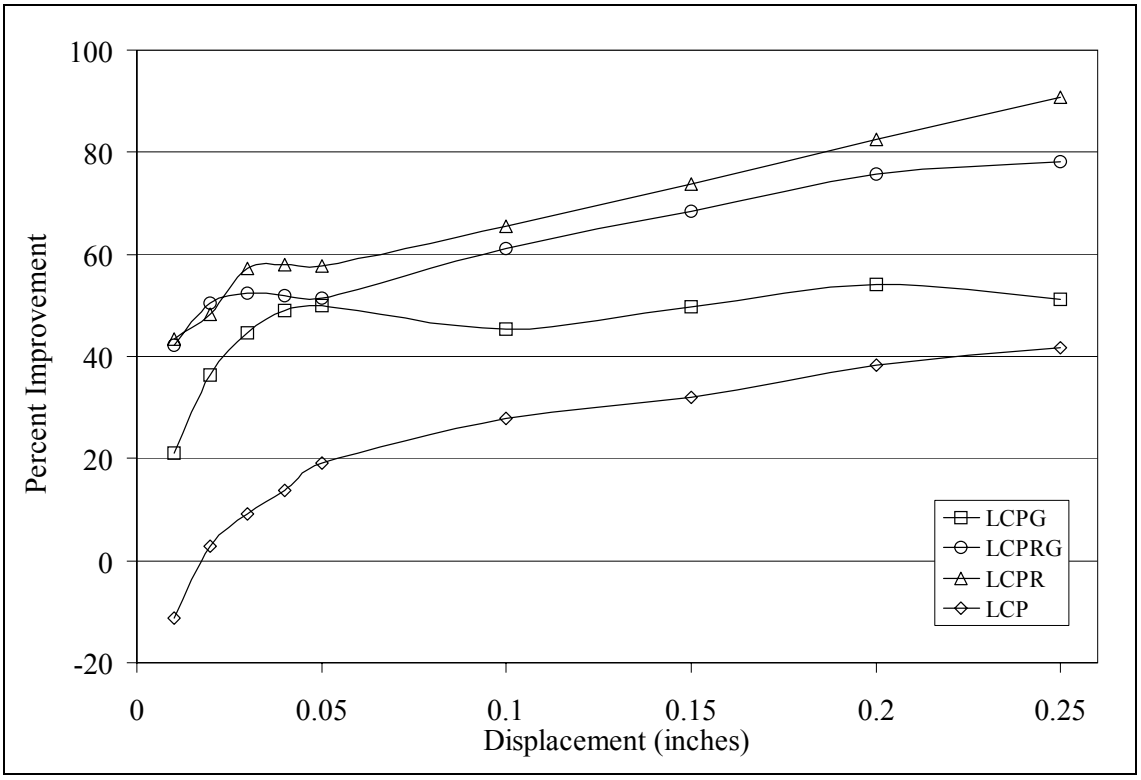

Figure 5.8 Percent improvement of lateral load for increasing displacement

5.4 PILES tests

The load-deflection curves for the six individual piles can be seen in Figure 5.7. Piles 1 and 2 were tested without any adjacent improvement, while piles 4 and 6 were both tested with an adjacent grouted and ungrouted helical pier. Pile 5 was tested adjacent to two grouted helical piers. Unfortunately, pile 3, which was adjacent to two ungrouted helical piers, had instrumentation malfunction and no data was obtained.

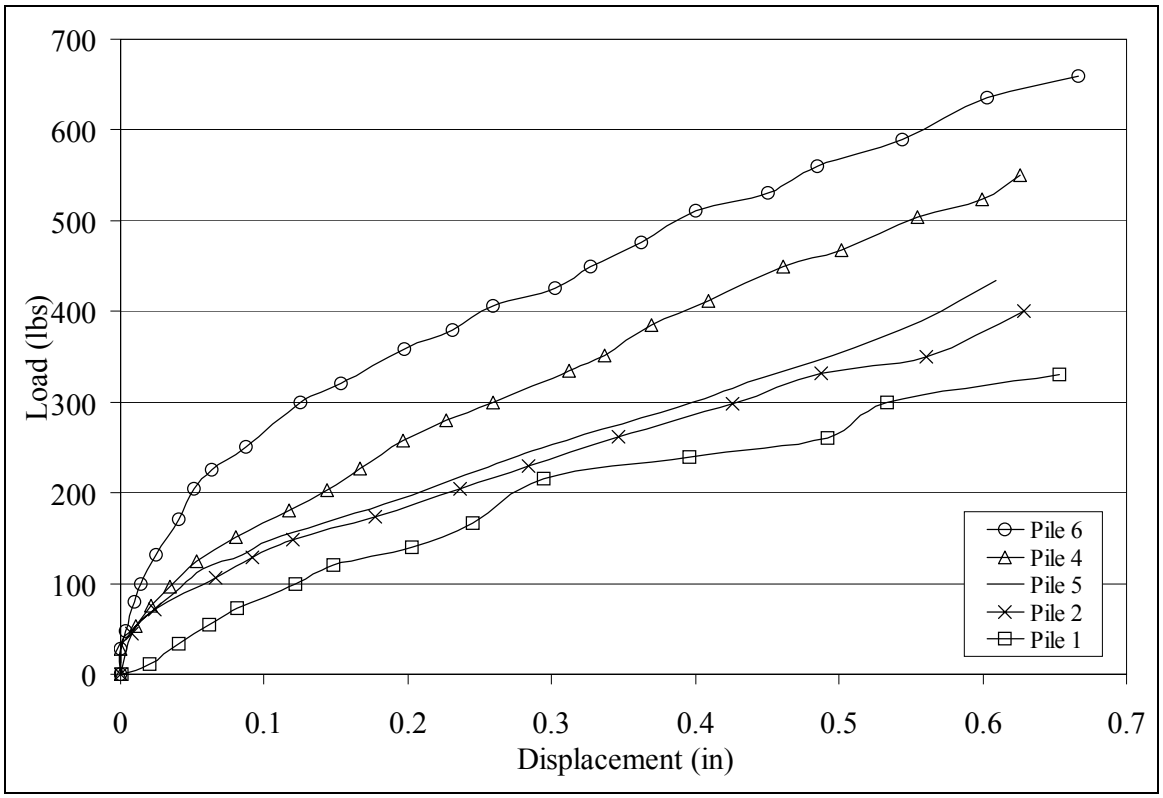

Figure 5.9 Load-deflection curves for the individual PILES tests

Table 5.21 Displacement comparison at different loads for PILES test

Test	Displacement (inches)									
	0*	0.01	0.02	0.03	0.04	0.05	0.1	0.15	0.2	0.25
P1	0	5	10	15	32	52	87	121	139	170
P2	0	52	68	77	85	93	136	162	187	212
P5	30	52	67	80	92	108	147	171	197	225
P4	30	52	73	90	106	122	167	208	262	295
P6	30	81	119	143	171	202	267	320	360	400

*All tests began at 0 load and 0 displacement. This is the load just prior to any displacement

The assumed performance of the piles, from worst to best, was as follows: 1, 2, 3, 4, 6 and 5. Tests 1 and 2 were assumed to test the lowest because no ground modification was performed in their vicinity prior to testing. As stated previously, it was assumed that the presence of the grouted helical pier would have a greater affect on the load-deflection performance than the ungrouted helical pier. Thus, pile 3, adjacent to two ungrouted

piers, was assumed to perform lower than piles 4 and 6, adjacent to one ungrouted pier and one grouted pier, which, in turn, was assumed to perform lower than pile 5, adjacent to two grouted helical piers. After testing the order of performance from worst to best was: 1,2,4,6, and 5 (Table 5.24).

Table 5.22 Assumed and tested performance for individual pile tests

Test label	Tested ranking	Assumed ranking	Load (lbs) at 0.1" displacement	Load (lbs) at 0.25" displacement
P6	1	3	267	400
P4	2	2	167	295
P5	3	1	147	225
P2	4	4	136	212
P1	5	5	87	170

The unmodified piles tested the lowest, as expected, however, P5 tested higher than P4 and P6, contrary to the initial prediction. The only difference between P5, P4, and P6 was that one of the two adjacent modification techniques for P4 and P6 was an ungrouted helical pier. Once again, the foundation element in the presence of an ungrouted helical pier performed greater than those installed in the proximity of the grouted helical piers.

Using the individual pile data, an analysis can be performed to determine how well the model data relates to the prototype. Using equation 2.2, the side friction for the prototype is calculated as: $f_s = K_{o*} \sigma'_{z*} \tan \varphi_{f,}$ where K_o is the coefficient of lateral earth pressure and is calculated as 1-sinφ', σ'_z is the vertical effective stress, and φ_f is the soil-foundation interface friction angle, where ratios of φ_f/φ' have been shown approximately equal to 1 for drilled shafts with temporary casings (Coduto, 2001). As the friction angle of the prototype is unknown, the side friction is calculated for a range of 15^o-35^o. With this range of a friction angle, and a vertical effective stress calculated using a soil density of 100 lb/ft^3 and a depth of 6′, a range for the side friction is 120-180 lb/ft^2. In order to

determine the total frictional force from the piles, the side friction is multiplied by the surface area. The surface area for a 12′ long, 1.4′ diameter pile is approximately 53 ft^2, leading to an approximate frictional force in the range of 6,300 – 9,500 lbs. At $^1/_8{}^{th}$ scale, this range reduces to 790 – 1,190 lbs. The untreated piles, P1 and P2, tested at 170 and 220 lbs, respectively, at the 1/4″ displacement, and approximately 260 and 360 lbs at 1/2″ displacement, considerable lower than the 790-1,190 lb range. Additional consideration must be placed on the fact that the load from the model also had additional capacity from end bearing, while the simple analysis presented above does not.

5.5 Summary

Each of the installation characteristics was analyzed and quantified to provide a determination of which foundations were directly comparable. Multiple tests and defective tests were analyzed and an appropriate load-deflection curve for each of the eight tests was determined and compared for both axial and lateral tests. The cap and pile foundations always performed higher than the cap only foundations, as expected. The ungrouted helical piers, however, often performed close to or greater than the grouted modifications for the axial, lateral and PILES tests, contrary to initial predictions. It was felt that the grout installation method may have reduced the soil-pile interface friction angle, thus, causing a decrease in the pile capacity. An analysis is also proved showing that the modeled piles have poor translation to the prototype.

6 DISCUSSION

6.1 Introduction

The following section provides a discussion as to the viability of superposition as the design paradigm for axially and laterally loaded composite foundations which implement grouted helical piers.

6.2 Axial tests

The percent improvements of each axially loaded foundation over the cap only foundation were shown in the previous chapter (Table 5.11). To evaluate the validity of superposition, the contribution from each individual component must equal the performance of the combination test involving those components. With this premise, the tested performance of ACPRG should equal the sum of the improvements (beyond the base performance of only the cap) from the following combination of tests: 1) ACP, ACR, and ACG, 2) ACPR and ACG, 3) ACRG and ACP and 4) ACPG and ACR. Table 6.1 shows the sum of the improvement of these tests and their relationship with the tested improvement of ACPRG values at various displacements. The sum of combinations 1 and 2 agree with the tested ACPRG within an average absolute percent difference of 6%, while those for combinations 3 and 4 tested at 19% and 24%, respectively.

Table 6.1 Evaluation of superposition for axial tests at various displacements

Disp.	ACPRG %	Combination 1:					Combination 2:			
(inches)	Improv.	ACP	ACR	ACG	Sum	%Diff	ACPR	ACG	Sum	%Diff
0.01	145	68	52	20	140	-3	160	20	180	24
0.02	150	86	46	19	151	1	139	19	158	6
0.03	123	71	35	14	120	-2	118	14	132	7
0.04	115	62	32	13	107	-7	105	13	118	3
0.05	106	55	28	11	94	-11	95	11	106	0
0.10	80	47	27	10	84	5	77	10	87	9
0.15	69	42	21	7	70	1	65	7	72	4
0.20	60	38	22	5	65	8	58	5	63	5
0.25	56	38	20	6	64	14	50	6	56	0
Absolute avg % Diff:						6				6
Disp.	ACPRG %	Combination 3:					Combination 4:			
(inches)	Improv.	ACRG	ACP	Sum	%Diff		ACPG	ACR	Sum	%Diff
0.01	145	56	68	124	-14		150	52	202	39
0.02	150	50	86	136	-9		138	46	183	22
0.03	123	35	71	106	-14		114	35	149	21
0.04	115	28	62	90	-22		105	32	137	19
0.05	106	23	55	78	-26		94	28	122	15
0.10	80	16	47	63	-21		77	27	104	30
0.15	69	10	42	52	-25		62	21	83	20
0.20	60	8	38	46	-23		54	22	76	27
0.25	56	11	38	49	-13		50	20	70	25
Absolute avg % Diff:					19					24

% Diff. = Percent difference of the sum to the tested ACPRG values

Superposition appears to be an adequate design paradigm when analyzing the results of the individual combination tests. When grouting is implemented in relation to the piles and piers, however, there appears to be some additional mechanisms that do not provide such a strong correlation. In the case of the grouting with piers there is a significant loss of capacity (19%), with respect to the individual components. Conversely, when the grouting is installed in the presence of the piles, but without the piers the enhanced capacity is a full 24% greater than the summation of the individual component. Therefore, while superposition shows potential as the design methodology

for composite foundations, further testing is warranted to determine how the grouting mechanism impacts the performance and whether this is a side-effect of the small-scale 1-g testing or a phenomenon that also appears in full-scale installations.

6.3 Lateral tests

Similar to the axial tests, the lateral component tests should sum to the level of performance exhibited by the composite foundation. Table 6.2 illustrates the sum of the component tests and their relationship with the tested LCPRG values at various displacements.

Table 6.2 Evaluation of superposition of combined foundations to LCPRG

Disp.	LCPRG %	Combination 1:					Combination 2:			
(inches)	Improv.	LCP	LCR	LCG	Sum	%Diff	LCPR	LCG	Sum	%Diff
0.01	42	-11	-7	-16	-34	-181	43	-16	27	-36
0.02	51	3	-2	-12	-11	-122	48	-12	36	-29
0.03	52	9	-1	-9	-1	-102	57	-9	48	-8
0.04	52	14	0	-6	8	-85	58	-6	52	0
0.05	51	19	2	-3	18	-65	58	-3	55	8
0.10	61	28	3	0	31	-49	66	0	66	8
0.15	68	32	6	6	44	-35	74	6	80	18
0.20	76	38	5	10	53	-30	83	10	93	22
0.25	78	42	4	9	55	-29	91	9	100	28
Absolute avg % Diff:						78				17
Disp.	LCPRG %	Combination 3:					Combination 4:			
(inches)	Improv.	LCRG	LCP	Sum	%Diff		LCPG	LCR	Sum	%Diff
0.01	42	-13	-11	-24	-157		21	-7	14	-67
0.02	51	-10	3	-7	-114		36	-2	34	-33
0.03	52	-7	9	2	-96		45	-1	44	-15
0.04	52	-6	14	8	-85		49	0	49	-6
0.05	51	-5	19	14	-73		50	2	52	2
0.10	61	-5	28	23	-62		45	3	48	-21
0.15	68	-1	32	31	-54		50	6	56	-18
0.20	76	2	38	40	-47		54	5	59	-22
0.25	78	3	42	45	-42		51	4	55	-29
Absolute avg % Diff:					82					23

% Diff. = Percent difference of the sum to the tested LCPRG values

The lateral cap only tests performed at nearly the same level, regardless of intervention method, showing that the modification elements had only a minimal effect on the performance of the cap only load-deflection curve. Since a cap only baseline is unrealistic given how important the piles are to changing the load-deflection response, it could be argued that the LCP arrangement would be a better baseline. In such a case, the improvement of the LCPRG test should equal the sum of the improvements of the LCPR and LCPG tests. Section 5.3.4 shows, however, that the LCPR test performed greater than the LCPRG test, indicating that there is no superposition relationship between the laterally tested foundations, when the intervention mechanisms are not connected to the cap itself.

6.4 Summary

The experimental program was based on the precept that the sum of individual component contributions should equal the total composite foundation. When examining the data set for both axially and laterally loaded tests, of the methodologies described in chapter 2 (superposition, combined effect, and chain theory) only a form of superposition appears to be an appropriate design methodology for axial, with none apparently appropriate for design under lateral loading. Of note, however, for the axial tests, some additional mechanism(s) appears to exist under certain grouting conditions that cause the grouted modifications to deviate from precise use of a superposition methodology. Further testing should be performed to determine unknown mechanisms, their validity at full-scale, and their impact on the foundation enhancement performance.

7 SUMMARY AND CONCLUSIONS

7.1 Summary

The reuse of in-situ, pile foundations often requires some form of capacity enhancement to accommodate additional loads. This capacity enhancement can arise from structural improvement, soil improvement, or a combination of both. Various ground improvement and ground reinforcement technologies can be implemented to achieve this improvement. The experimental program presented here was performed to evaluate whether superposition was an appropriate design methodology for the influence of one such technology (ie. grouted, helical piers) on the axial and lateral load-deflection performance of a piled foundation.

The experimental program required the execution of axial and lateral load tests on eight various foundation configurations. The potential expense of full-scale testing on pile groups informed the decision to conduct model-scale work as a pilot study. The research was conducted at a $^{1}/_{8}^{th}$ scale, under 1-g conditions and addressed issues of both geometric and material property scaling. Little previous research was found on small-scale model testing of cast-in-place foundations, with no research implementing ground modification or specifically addressing the material property scaling issue.

Both axial and lateral tests revealed that the foundations that received some sort of GIGR improvement showed a definite improvement, although some mechanism caused the improvement from the ungrouted helical piers to test as well as the grouted columns and grouted helical piers. The responsible mechanism was believed to arise during grout installation causing a reduction in the soil-structure interface friction angle, thereby resulting in a decreased foundation performance. This initial assessment showed that

superposition has strong potential as a design approach but that further testing including full-scale testing, and testing where the improvement is directly attached to the pile cap is needed.

7.2 Conclusions

The research presented here has resulted in the following experimental advancements and technological conclusions.

7.2.1 Experimental Advancements

-A material property scaling method was developed by introducing bentonite into cement, sand, and water mixes to reduce the concrete and grout modulus of elasticity to $^{1}/_{8}^{th}$ their full-scale equivalent.

-Small-scale construction methods were developed to install the cast-in-place foundations and implement the grouted, helical piers.

-A method for the creation and installation of telltales was developed.

7.2.2 Technological Assessment

-The presence of various ground modification elements causes an improvement in the load-deflection performance of a piled foundation, even when these elements are not directly connected to the existing foundation.

- While superposition shows potential as the design methodology for composite foundations, further testing is warranted to determine how the grouting mechanism impacts the performance and whether this is a side-effect of the small-scale 1-g testing or a phenomenon that also appears in full-scale installations.

-The laterally loaded behavior was indeterminate due to the importance of the addition of the piles to the pile cap. The component tests could not be compared to the

combination foundations as the piles provided a significant contribution to the load deflection response of the foundation, and further study should be conducted with the improvement elements attached to the pile cap to evaluate an appropriate design method.

7.2.3 Future Studies

-This research was performed in part as preliminary work to further testing as a joint venture between the University of California-Irvine and the University of California-Davis. The work conducted to date will be used to greatly enhance the centrifuge capabilities, as well as to further validate the conclusions of the 1-g testing conducted as part of this thesis.

8 REFERENCES

ACI (1999). American Concrete Institute: Building Code Requirements for Structural Concrete (318-99) and Commentary (318R-99), Farmington Hills, MI: ACI International.

ADSC (1999). ADSC Standards and Specifications.

Akinmusuru, J. O. (1980). Interaction of Piles and Cap in Piled Footings. Journal of Geotechnical Engineering Division. Vol. 106, GT11, 1263-1268.

Altaee, A. & Fellenius, B. H. (1994). Physical modeling in sand. Canadian Geotechnical Journal. No. 31, 420-431.

Breitsprecher, G. & Toth, P. S. (2003). Underpinning of a Pier by Mircrofine Cement Grouting and Compensation Grouting. In L. F. Johnson, D. A. Bruce, & M. J. Byle (Eds.), Grouting and Ground Treatment: Proceedings of the 3rd International Conference, Geotechnical Special Publication No. 120 (pp. 741-751). Reston, VA: ASCE.

Brusey, W. G. (2000). Post-Grouted Test Shafts at JFK International Airport. In N. D. Dennis Jr., R. Castelli & M. W. O'Neill (Eds.), New Technological and Design Developments in Deep Foundations Geotechnical Special Publication No. 100 (pp. 18-32). Reston, VA: ASCE.

Buch, A. (1999). Pure Metals Properties: A Scientific-Technical Handbook. Materials Park, Ohio: ASM International.

Carville, C. A., & Walton, R. W. (1995). Foundation Repair Using Helical Screw Anchors Foundation Upgrading and Repair For Infrastructure Improvement. Proceedings of the Symposium sponsored by the Deep Foundations Committee of the Geotechnical Engineering Division of the American Society of Civil Engineers in conjunction with the ASCE Convention in San Diego California. (pp 56-75) New York: ASCE.

Chapman, T., Marsh, B., & Foster, A. (2001). Foundations for the future. Proceedings of the Institute of Civil Engineers. *Civil* Engineering 144, Paper 12340, (pp. 36-41).

Chapman, T. J. P., Chow, F. C., & Skinner, H. (2002). Building on old foundations – sustainable construction for urban regeneration. CEWorld Conference, ASCE on-line conference.

Chellis, R. D. (1961). Pile Foundations. (2nd ed.). New York: McGraw-Hill Company, Inc.

Chow, F. C., Chapman, T. J. P., & St. John, H. D. (2002). Reuse of existing foundations: Planning for the future. Proceedings of the 2nd International Conference on Soil Structure Interaction in Urban Civil Engineering. Zurich

Coduto, D. P. (2001). Foundation Design: Principles and Practices (3rd ed.). Upper Saddle River, New Jersey: Prentice-Hall Inc.

Das, B. M. (1998). Principles of Geotechnical Engineering (4th ed.). Boston, Massachusetts: PWS Publishing Company.

Durgunoglu, H. T., Kulac H. F., Yilmaz, S., & Kocak, D. (2003). Case History for Soil Improvement of SETAT 2002 High Rise Residential by Jet Grouting in Istanbul. In L. F. Johnson, D. A. Bruce, & M. J. Byle (Eds.), Grouting and Ground Treatment: Proceedings of the 3rd International Conference, Geotechnical Special Publication No. 120 (pp. 377-388). Reston, VA: ASCE.

El-Kelesh, A. M., & Matsui, T. (2003). Effect of Soil and Grouting Parameters on the Effectiveness of Compaction Grouting. In L. F. Johnson, D. A. Bruce, & M. J. Byle (Eds.) Grouting and Ground Treatment: Proceedings of the 3rd International Conference, Geotechnical Special Publication No. 120 (pp. 1056-1070). Reston, VA: ASCE.

Fang, H. Y. (Ed.) (1991). Foundation Engineering Handbook. (2nd ed.). New York: Van Nostrand Reinhold.

Gorbunov-Possadov, M. & Serebrjanyi, R. V. (1961). Design of Structures on Elastic Foundations. Proceedings of the 5th International Conference on Soil Mechanics and Foundation Engineering. Vol. 1. (pp 643-648).

Hilsdorf, H.K., (1969). Investigation into the Failure Mechanism of Brick Masonry Products Designing. In F. B. Johnson (Ed.), Engineering and Construction with Masonry Products. Houston, TX: Gulf Publishing.

Jarred, D. J., & Haberfield, C. M. (1997). Tendon/Grout Interface Performance in Grouted Anchors, Ground Anchorages, and Anchored Structures. In J. S. Littlejohn (Ed.) Proceedings of the International Conference Organized by the Institute of Civil Engineers and held in London. London: Thomas Telford.

Kishida, H., and Meyerhof, G.G. (1965). Bearing capacity of pile groups under eccentric loads in sand. Proceedings of the sixth international conference on soil mechanics and foundation engineering, Toronto, vol. 2, pp. 270-274.

Ko, H. Y., Atkinson, R. H., Goble, G. G., & Ealy, C. D. (1984). Centrifugal Modeling of Pile Foundations. In J. R. Meyer (Ed.), Analysis and Design of Pile Foundations. (pp. 21-40). Reston, VA: ASCE.

Laefer, D. F. (2001). Prediction and Assessment of Ground Movement and Building Damage Induced by Adjacent Excavation. Unpublished doctoral dissertation. University of Illinois-Champaign, Illinois.

Langhaar, H. L. (1951). Dimensional Analysis and Theory of Models. New York: John Wily & Sons, Inc.

Lees, D., & Chuaqui, M. (2003). Soil Grouting: Means, Methods and Design. In L. F. Johnson, D. A. Bruce, & M. J. Byle (Eds.) Grouting and Ground Treatment: Proceedings of the 3rd International Conference, Geotechnical Special Publication No. 120 (pp. 1347-1359) Reston, VA: ASCE.

Littlechild, B. D., Plumbridge, G. D., Hill, S. J., & Lee, S. C. (2000). Shaft Grouting of Deep Foundations in Hong Kong. In N. D. Dennis Jr., R. Castelli & M. W. O'Neill (Eds.), New Technological and Design Developments in Deep Foundations Geotechnical Special Publication No. 100 (pp. 33-45). Reston, VA: ASCE.

Long, P. D. (1993). Footings with Settlement-Reducing Piles in Non-Cohesive Soil (Swedish Geotechnical Institute, Report No. 43). Linkoping, Sweden: SGI.

Martin, G. R. & Lamin, I. P. (2000). Earthquake Resistant Design of Foundations: Retrofit of Existing Foundations. GeoEng2000: An International Conference on Geotechnical and Geological Engineering, Vol 1. (1025-1047) Lancaster, PA: Technomic Publishing Inc.

Mayne, P. W., Kulhawy, F. H., & Trautmann, C. H. (1994). Laboratory Modeling of Laterally-Loaded Drilled Shafts in Clay. Journal of Geotechnical Engineering. Vol. 121, No. 12, pp. 827-835.

O'Neill, M. W. & Reese, L. C. (1999). Drilled Shafts: Construction Procedures and Design Methods. Dallas, TX: ADSC.

Pack, J. S. (2000). Design of Helical Piles for Heavily Loaded Structures. In N. D. Dennis Jr., R. Castelli & M. W. O'Neill (Eds.), New Technological and Design Developments in Deep Foundations Geotechnical Special Publication No. 100 (pp. 353-367). Reston, VA: ASCE.

Perko, H. A., & Rupiper, S. J. (2000). Helix Pier Engineering Handbook 2000. Ingal Precision Foundations, Inc.

Poulos, H. G., & Davis, E. H. (1980). Pile Foundation Analysis and Design. New York: John Wiley and Sons.

Rogers, W. (2002). Manual of: Screw Pile Foundations (5th ed.). Houston, Texas: Energy Structures Inc.

Schaap, L. H. J. & de Vos, J. (1985). The Sonic Pile Test Recorder and its Application. In G. Holm, H. Bredenberg, & C. J. Gravare (Eds.), Application of Stress Wave Theory on Piles: The 2nd International Conference. (pp. 79-84). Stockholm, Sweden: A. A. Balkema.

Schaefer, V. R. (Ed.). (1997). Ground Improvement, Ground Reinforcement, and Ground Treatment: Developments 1987-1997. Geotechnical Special Publication No. 69. Reston, VA: ASCE.

Shvets, V. B., Feklin, V. I., & Ginzburg, L. K. (1996). Reinforcement and Reconstruction of Foundations. Brookfield, VT: A. A. Balkema Publishers.

Tomlinson, M. J. (1994). Pile Design and Construction Practice (4th ed.). London: E & FN Spon.

Van der Stoel, A. E. C. (2003). Pile Foundation Improvement by Permeation Grouting. In L. F. Johnson, D. A. Bruce, & M. J. Byle (Eds.), Grouting and Ground Treatment: Proceddings of the 3rd International Conference, Geotechnical Special Publication No. 120 (pp. 728-739). Reston, VA: ASCE.

Vickars, R. A., & Clemence, S. P. (2000). Performance of Helical Piles with Grouted Shafts. In N. D. Dennis Jr., R. Castelli & M. W. O'Neill (Eds.), New Technological and Design Developments in Deep Foundations, Geotechnical Special Publication No. 100 (pp. 327-341). Reston, VA: ASCE.

Warner, J. (2003). Soil Strengthening by Grouting. In L. F. Johnson, D. A. Bruce, & M. J. Byle (Eds.), Grouting and Ground Treatment: Proceedings of the 3rd International Conference, Geotechnical Special Publication No. 120 (pp. 913-928). Reston, VA: ASCE.

Warner, J. (2004). Practical Handbook of Grouting: Soil, Rock, and Structures. Hoboken, New Jersey: John Wiley & Sons, Inc.

Welsh, J. P., & Burke, G. K. (1991) Jet Grouting – Uses for Soil Improvement. In F. G. Mclean, D. A. Campbell, & D. W. Harris (Eds.), Geotechnical Engineering Congress 1991, Geotechnical Special Publication No. 27, Vol. 1 (pp. 334-345). Reston, VA: ASCE.

Yan, L., & Byrne, P. M. (1989). Application of Hydraulic Gradient Similitude Method to Small-Scale Footing Tests on Sand. Canadian Geotechnical Journal. Vol. 26, No. 2, 246-259.

Zelikson, A. (1969). Geotechnical Models Using the Hydraulic Gradient Similarity Method. Geotechnique. Vol. 19, No. 4, 495-508.

Zhang, Y. Q., Li, D. X., & Zhao, X. M. (1985). Analysis and Processing of Reflected Waves from Piles. In G. Holm, H. Bredenberg, & C. J. Gravare (Eds.), Application of Stress Wave Theory on Piles: The 2nd International Conference. (pp. 79-84). Stockholm, Sweden: A. A. Balkema.

APPENDICES

Appendix A: Setup proof

A.1 Introduction

The following appendix contains the calculations to justify that the spacing of the foundations is sufficient to minimize the effects from the adjacent pit walls, rigid base, and other installed foundations.

A.2 Stress calculation at the rigid base

The rigid base must be at a sufficient depth to prevent the redistribution of stress and alteration of the settlement for both the cap only foundations and the cap and pile foundations. The cap only foundations consisted of an 11.25″ square foundation with approximately 6′ of sand between the cap and rigid base. The applied load is transferred to the soil along the soil-cap interface.

The cap and pile foundations have the same cap dimension in plan, and the bottom of the piles are approximately 4.5′ from the base of the pit. The load is ptransferred to the soil along the soil-cap interface, as well as along the sides and base of the piles. For simplicity, the effects of the load shall be conservatively analyzed as if it were a cap only foundation with 4.5′ between the cap and rigid base. This assumes that the load is perfectly transferred to the end bearing of the piles, with none lost in skin friction. Figure A.1 shows the values for the ratio of vertical effective stress to the applied stress (Gorbunov-Possadov, 1961).

Values of $\sigma_z(0,0,0)/q$

h/a	Circle radius =a	Rectangle (m = b/a)				Infinite strip m = ∞
		m = 1	m = 2	m = 3	m = 10	
0	1	1	1	1	1	1
0.25	1.009	1.009	1.009	1.009	1.009	1.009
0.5	1.064	1.053	1.033	1.033	1.033	1.033
0.75	1.072	1.082	1.059	1.059	1.059	1.059
1	0.965	1.027	1.039	1.026	1.025	1.025
1.5	0.684	0.762	0.912	0.911	0.902	0.902
2	0.473	0.541	0.717	0.769	0.761	0.761
2.5	0.335	0.395	0.593	0.651	0.636	0.636
3	0.249	0.298	0.474	0.549	0.560	0.560
4	0.148	0.186	0.314	0.392	0.439	0.439
5	0.098	0.125	0.222	0.287	0.359	0.359
7	0.051	0.065	0.113	0.170	0.262	0.262
10	0.025	0.032	0.064	0.098	0.181	0.185
20	0.006	0.008	0.016	0.024	0.068	0.086
50	0.001	0.001	0.003	0.005	0.014	0.037

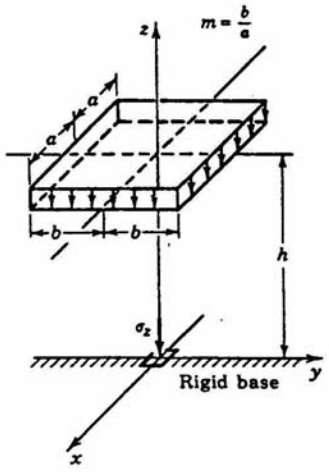

Figure A. 1 Values for the ratio of vertical effective stress to applied stress

Using Figure A.1:

Cap only:

$$a = b = \frac{11.25"}{2} = 5.625", \quad m = \frac{b}{a} = 1, \quad \text{h} = 72'', \quad \frac{h}{a} = \frac{72"}{5.625"} = 12.8$$

$$\rightarrow \quad \frac{\sigma}{q} \approx 0.02$$

Cap and piles:

$$a = b = \frac{11.25"}{2} = 5.625", \quad m = \frac{b}{a} = 1, \quad \text{h} = 54'', \quad \frac{h}{a} = \frac{54"}{5.625"} = 9.6$$

$$\rightarrow \quad \frac{\sigma}{q} \approx 0.025$$

The calculations above show that a maximum of 2.5% of the applied stress is felt at the rigid base, if the applied stress is taken to be at the base of the piles, and 2.0% if it is applied at the ground surface.

A.3 Calculation of radius of influence

The following calculations show that the lateral foundation spacing is sufficient to prevent influence from adjacent foundations. The figure below shows the horizontal influence from an axially loaded square footing (Coduto, 2001).

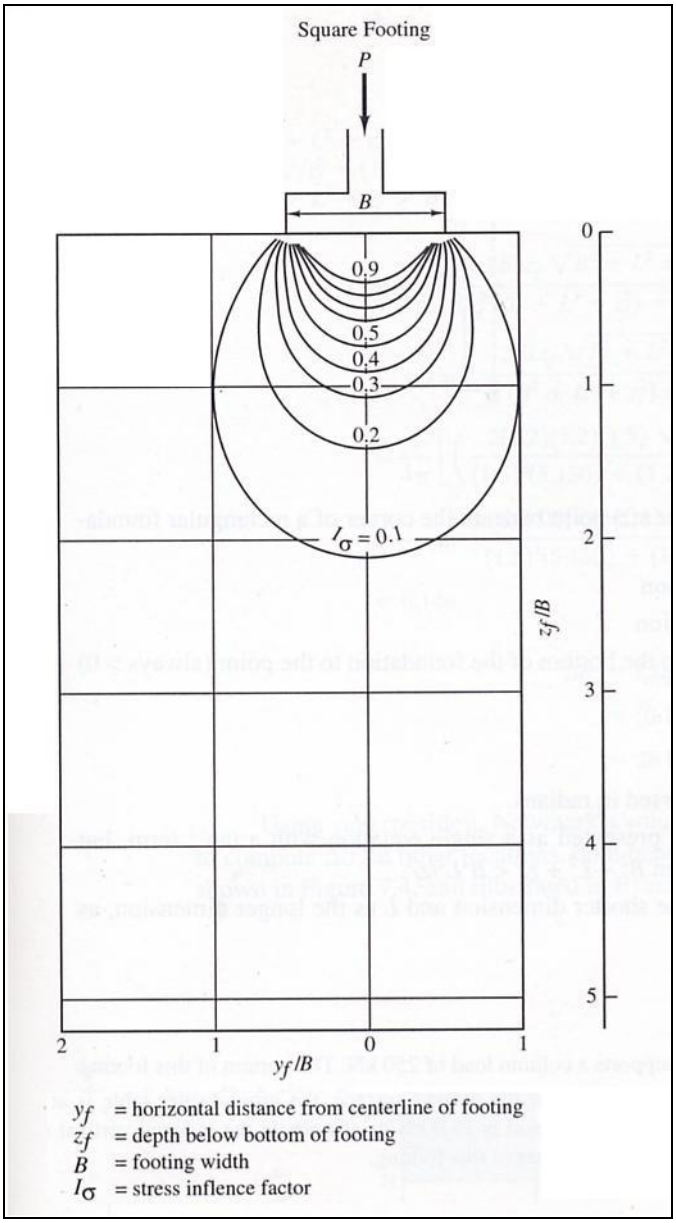

Figure A. 2 Vertical and horizontal influence from footing

The foundations were placed at a 3′ center-to-center spacing, giving an allowable distance of influence of 1.5′ from the center of each foundation. If the footing width, B, is 11.25″ and the influence at a distance of 18″ from the center of the footing, y_f, is desired, then $y_f/B = 18″/11.25″ = 1.6$. From the above figure, the influence factor is substantially less than 10%.

The influence from the lateral tests was not considered to be substantial as the tests were pushed in the direction of the axially loaded foundations and were always performed after the axial testing was completed.

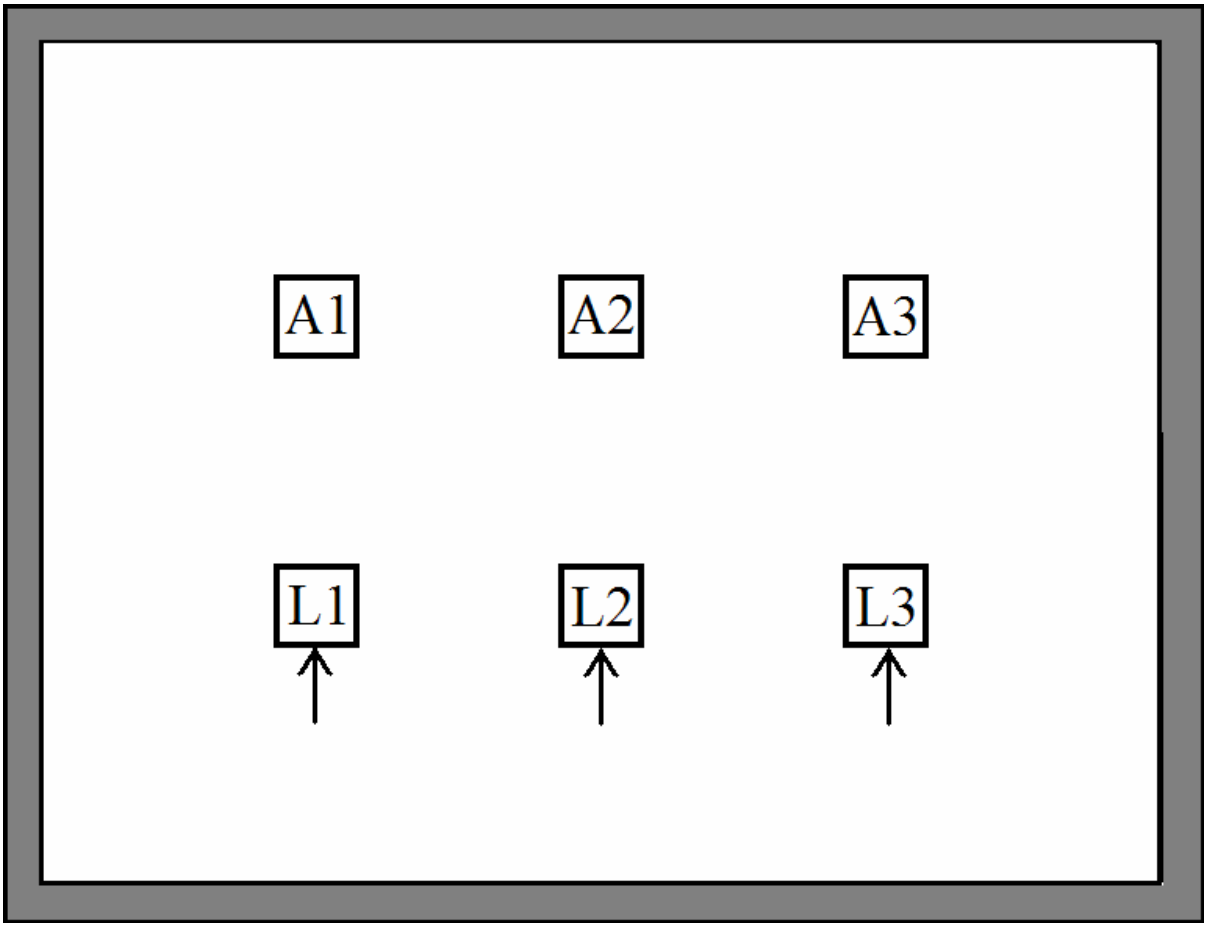

Figure A. 3 Direction of loading of lateral tests

A.4 Summary

The preceding calculations show that the spacing for each round of testing was sufficient to minimize any settlement influences from the pit walls, base and other installed foundations.

Appendix B: Equipment development

B.1 Introduction

The following appendix discusses the development and implementation of different equipment used for the installation and testing of the experimental foundations.

B.2 Sand setup

To obtain a repeatable soil profile, the sand was pluviated from a constant height and at a constant rate. To achieve this, a 12′ x 2.5′ x 2′ sand pluviation box was designed with a pegboard bottom, consisting of $^{1}/_{4}$″ holes spaced on a 1″ grid pattern. An external door was used to keep the sand from falling until it was moved into position, whereupon the door was released and the sand began pluviation (Figures B.1-B.4). The door was controlled using ropes and pulleys, such that to open the door a central rope loop was cut.

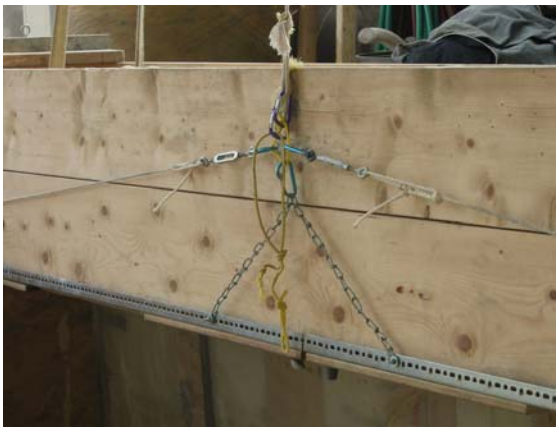

Figure B. 4 Box opening system

Figure B. 5 Box being positioned

Figure B. 6 Releasing the trap door

Figure B. 7 Beginning sand pluviation

B.3 Helical pier construction

The major issue with the grouted helical piers was developing a method that produced a consistently repeatable result. Ultimately, the final pier had to have a consistent geometry, angle of installation, and installation process so as to not cause different soil disturbance or otherwise alter the substrata conditions to allow for comparison between the various foundation configurations.

Thirty-two helical piers were constructed to complete the experimental program. The full-scale helical pier design was contributed by Precision Pier USA, Inc., and the modeled piers were constructed to $^{1}/_{8}^{th}$ the dimensions of their design (as discussed in section 3.4.1.2). The helixes were modeled using 2″ inch diameter fender washers with a 0.5″ center hole. The washers were cut and formed into a helical shape using a specially made press and mold (Figure B.5). The press consists of several bolts set to gradually decreasing heights, until a 0.375″ pitch was obtained (Figures B.6 and B.7). The washer was then placed into the wooden mold (Figure B.8) and the press was applied to bend the washer into a helical shape.

Figure B. 8 Helix press in mold

Figure B. 9 Helix press (plan view)

Figure B. 10 Helix press (side view)

Figure B. 11 Helix press mold

Once the helixes were pressed, the surfaces of both the washers and the round tube were scored to increase the effectiveness of the bonding adhesive, JB Weld. A completed helical pier is shown in Figure B.9.

Figure B. 12 Helices on assembled helical pier

B.4 Grouted pier installation

The installation of the grouted helical piers into the sand required both a consistent rate of installation and the simultaneous injection of the grout. The rate of installation of a helical pier depended on two variables: the pitch of the helices and the rotation rate of the pier. The construction of the helices was consistently achieved through the helix press previously described. However, in order to attach the helices to the shaft in a repeatable manner, a template was made of styrofoam and eight piers were simultaneously constructed (Figure B.10).

Figure B. 13 Mass production of helical piers

To achieve the consistent installation rate, a single speed motor (9 rpm) was mounted to a wooden frame to create a sliding jig (Figures B.11-B.12). The pier was attached to the motor using a coupler (Figure B.18), and the jig was then placed on an angled platform such that the pier could rotate itself into the ground (Figures B.13-B.14). The platform was angled at 79^{o} and was leveled before each pier was installed to ensure a consistent angle of installation.

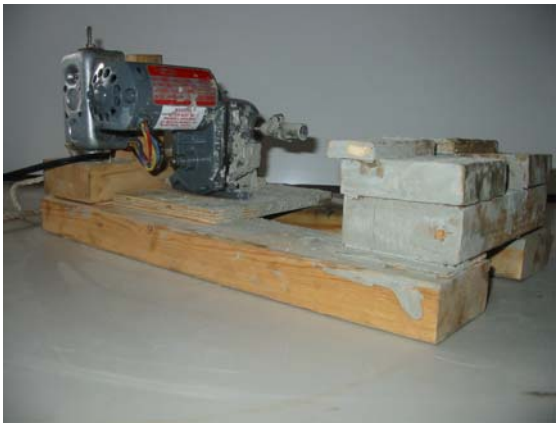

Figure B. 14 Motor mounted jig

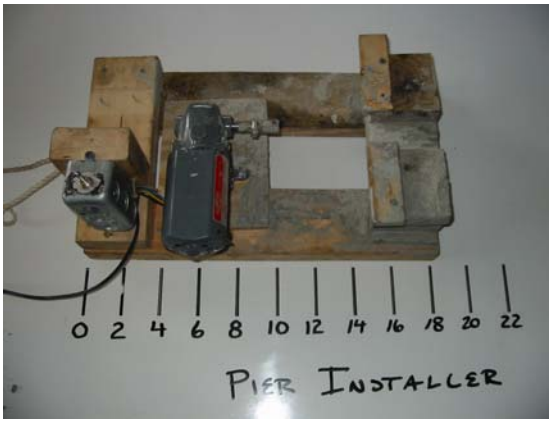

Figure B. 15 Motor mounted jig

Figure B. 16 Jig mounted on platform

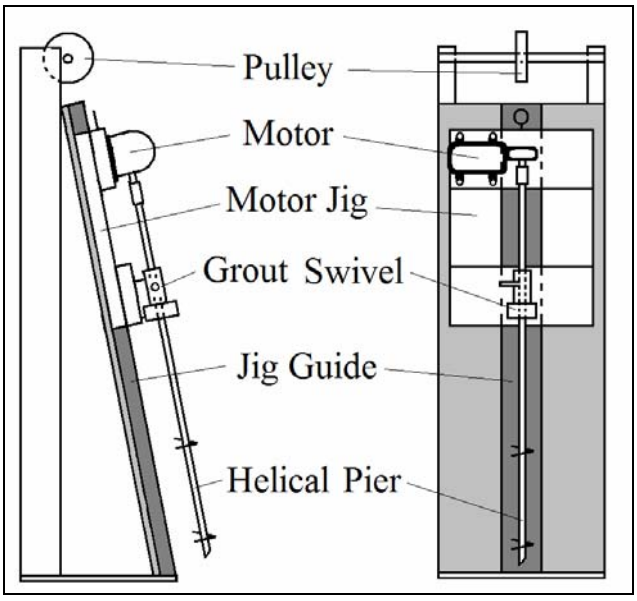

Figure B. 17 Jig and platform schematic

The grout was initially placed in a pressurized cylinder (Figures B.15 and B.16). The grout cylinder was a 2′ tall, 1′ diameter steel cylinder with a $^{5}/_{8}$″ grout exit nozzle 1″ from the bottom of the cylinder. The top of the cylinder has a pressure release valve and an air intake. Pressurized air was pumped through the intake to pressurize the grout, and was regulated by a gage and valve attached to the top of the cylinder (Figure B.17).

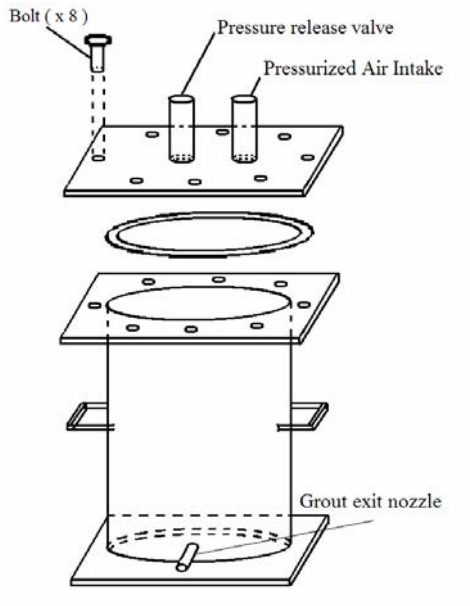

Figure B. 18 Pressurized grout cylinder cylinder

Figure B. 19 Pressurized grout

Figure B. 20 Pressure gage and valve

With the motor being attached to the end of the pier (Figure B.18), the grout has to be injected into the pier through a slot cut into the side of the pier (Figure B.19). To accomplish this, a grouting system was designed to allow for the simultaneous rotation of the pier and for the injection of the grout via a grout swivel.

Figure B. 21 Pier-motor coupler

Figure B. 22 Slot for grout injection

A grout swivel is a mechanism that allows for the helical pier to rotate while injecting grout (Figures B.20 and B.21). The pier was placed through the swivel and attached to the motor such that the pier's slot was aligned with the swivel's grout reservoir (Figure B.22). When the reservoir was full, the grout was then forced into the slot on the helical pier and out the base of the pier. The swivel was attached to the pier using a rubber hose and hose clamps (Figure B.23).

Figure B. 23 Grout swivel exploded view

Figure B. 24Grout swivel

Figure B. 25 Grout reservoir

Figure B. 26 Grout-pier attachment

Once the grout was in the pressurized cylinder and the helical pier and grout swivel were mounted on the motor jig, the cylinder was attached to the swivel via a grouting tube and the jig was placed on the angled platform (Figure B.24). The entire grouting system can be seen in Figures B.25 and B.26. When the helical pier was to be backed out for installation of the grouted columns, a weight equal to the weight of the jig was hung from a rope that passed over a pulley and attached to the back of the jig (Figure B.26).

Figure B. 27 Grout tube connected to grout swivel

Figure B. 28 Grouting system profile

Figure B. 29 Grouting system

B.5 Telltale setup

Telltales were setup in order record any pile shortening that may have occurred during axial compression. The final telltale design can be seen in Figure B.27, and consists of a $^{1}/_{16}$″ threaded bar, with a $^{1}/_{8}$″ diameter aluminum casing. Nuts and washer at the bottom acted as an anchor to ensure that the telltale was bonded to the concrete, and wetted cotton was used to prevent concrete from entering the casing. The top nuts held the L-bracket as a surface for the displacement gage, and the L-bracket has an indentation in it to keep the gage from sliding off the bracket (Figure B.28). When the piles were cast, the telltale was covered in grease and inserted down the center of the pile and steel cage. As the concrete cured, the telltale casing was rotated every 20 minutes to break any developing bond. Eventually the casing was removed, resulting in a functioning telltale.

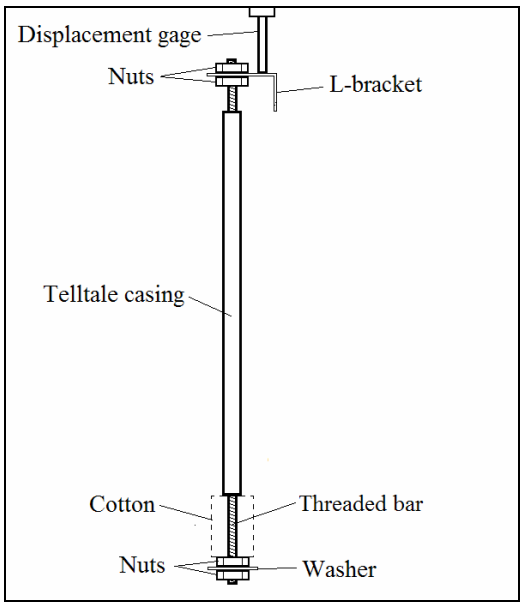

Figure B. 30 Schematic of telltale

Figure B. 31 Picture of installed telltale

B.6 Steel reinforcing cages

The modeled reinforcing cages (as described in chapter 3) were constructed by equally spacing six lead wires around the outside of a 1.25″ diameter PVC. The wires consisted of two $^{1}/_{16}$″ diameter lead wire strands twisted together and taped to the PVC. An individual wire was then wrapped around the outside of the wires such that there was a $^{3}/_{4}$″ spacing. The wire was temporarily taped in place, then every other longitudinal/lateral joint was sodered together (Figures B.29 and B.30). All the tape was then removed and the cage was slid off the PVC and placed in an installed casing prior to concreting of the pile.

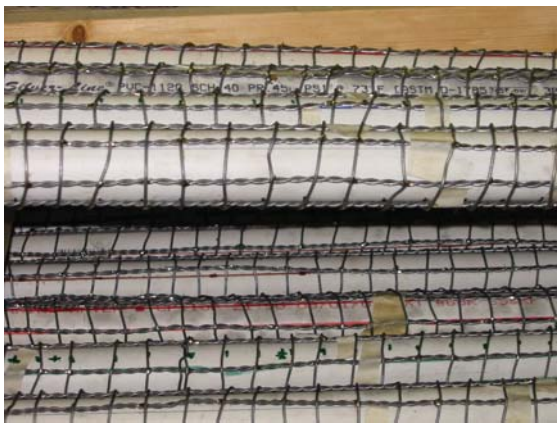

Figure B. 32 Closeup of reinforcing cages with temporary PVC insets

Figure B. 33 All reinforcing cages

B.7 Summary

The preceding has shown the methods developed to obtain consistent installation for each foundation. This consistency is a function of various installation characteristics, including sand density, pier construction and grout installation. Additionally, specific details on the installation procedure for the telltales and the lead reinforcing cage construction are shown.

Appendix C: Development of scaled grouting methods

C.1 Introduction

This appendix discusses the development of a modeled grouting installation process and observations from several grouting practices. The full scale installation practice is described in section 2.3.3.1.

C.2 Scale-model installation process

C.2.1 Grouting pressure selection

The grout used by the consulted contractor in full-scale application has been found to be sufficiently fluid to flow under gravity into the groves carved into the ground by the helices. The $^{1}/_{8}^{th}$ scale grout mix, however, was of such a viscosity that it had to be pressurized to achieve consistent grout flow. Practice piers were installed to determine a grouting procedure that would result in a pier that was visually consistent with the prototype.

Once the grouting equipment was setup (see Appendix B), the helical pier was positioned in the center of a side of the foundation and a few inches above the ground. The grout was pressurized until it extruded from the grout hole at the base of the pier and was allowed to flow from the pier until a small mound of grout had formed on the soil surface. The motor jig was then allowed to lower into the ground. The first 3″ of ground penetration tended to advance faster than the helix pitch due to the weight of the motor jig and the low bearing capacity of the surface soil, so a force was applied opposite to the installation direction such that a consistent $^{3}/_{8}$″ advancement per revolution could be maintained. Once the pier had penetrated 3″ into the sand, the pier was then allowed to pull itself freely into the ground for the remainder of its length.

As the grout extruded from the grout hole, the bottom helix passed through the grout and pulled it away from the shaft to the edge of the helix, spreading it such that the final pier generated a diameter approximately equal to the helix diameters, with ridges occurring at every helix pass (as shown in detail below).

Initial installations were attempted at a constant pressure, resulting in sporadic grout flow and a decreasing grouted pier diameter with depth. This decreasing diameter was the result of increasing confining pressure from the sand and caused a restriction in the grout flow.

Figure C. 1 Pier with constant pressure

To offset the soil's increasing confining pressure, increasing grouting pressures were used, 12 psi for the initial half of the installation and 18 psi for the second half. This method proved more effective, however, the grout pressure proved insufficient for the initial half, causing the top six inches to not mix substantially enough to create a solid column. As a result, the top of the pier was not well bonded to the pier and fell apart during excavation.

Figure C. 2 Pier from two pressures (12 psi and 18 psi)

When the pressure was too low, the ridges failed to extend to the edges of the helix (Figure C.3). Conversely, when the grout pressure was too high, the grout extended past the diameter of the helix and failed to form the ridges (Figure C.4). Eventually, a proper grouting pressure was found that produced a ridged pier at a diameter of the helix (Figure C.5).

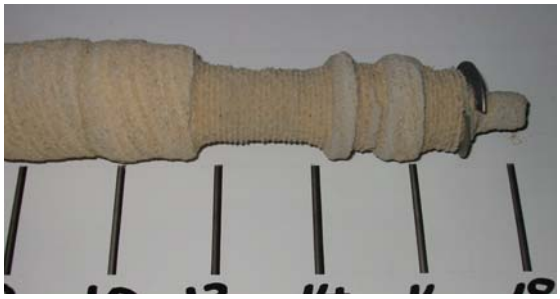

Figure C. 3 Insufficient grout pressure

Figure C. 4 Excessive grout pressure

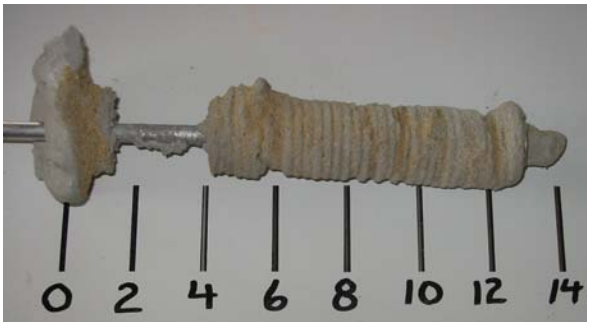

Figure C. 5 Good grout pressure

C.2.2 Grouted helical pier installation procedure

Once the appropriate grouting pressure was determined, the main challenge to consistent grouting was an inconsistent grout flow. Typically, the main cause of grout flow restriction was sand entering the grout hole or large particles in the grout getting clogged in the grout hole. When this clogging occurred, the pressure was increased to alleviate the clog. Once the clog was cleared, however, the increased pressure would cause the grout to flow indiscriminately beyond the helix diameter. Figure C.6 shows a pier that was believed to be clogged within the first several inches, had its pressure increased until regular grout flow was resumed, and then had its pressure decreased to the pre-specified level as the pier was advanced. While the increased pressure unclogged the hole, the grout became uncontrollable, then when the pressure was decreased the hole became clogged again prior to advancement. This second clog occurred because when the pressure increased, the grout in the system became compressed. When the pressure was decreased, the grout expanded and reverted back into the grout cylinder, whereupon the sand then clogged the pier. From this it was learned that the pressure should never be decreased once the pier was being advanced.

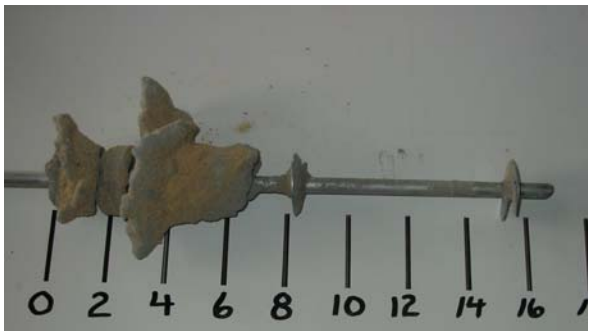

Figure C. 6 Erratic pier diameter

The implemented pressure criteria was to begin with an initial pressure of 18 psi and increase the pressure 1 psi for every inch of installation. Additionally, the grout flow

was monitored through the grout tube to identify the onset and ultimate clearing of any blockage. If the grout appeared to slow down, the pressure was increased more than the 1psi per inch until the flow returned to the desired rate.

Additionally, it was observed that the bottom helix occasionally detached from the pier. The bond between the steel washers and aluminum rod had a limited capacity that was sometimes exceeded by the installation torque, causing the bond to break. Typically, when this occurred the grout maintained an approximate diameter of the shaft below where the helix detached (Figure C.7).

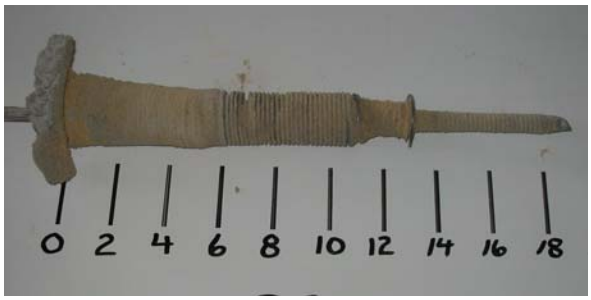

Figure C. 7 Pier with displaced helix

C.2.3 Grouted column installation pressure

Pressures were also needed to be determined when the helical pier was to be backed out and only a grouted column was to be installed. Once the pier reached the desired depth (as described in C.2.2) the pier rotation was reversed and a force was applied to assist in the pier removal. The pressure was reduced to a constant 18 psi for the removal of the entire pier length. It was found that the pressure could be reduced for removal as the wet grout kept the sand from clogging the grout hole. Also, as the pier was backed out, the ridges formed from the installation were disturbed, as has been found to be typical in the real world installation, as the helices do not follow the same path as when installed (Figures C.8 and C.9).

Figure C. 8 Grouted column

Figure C. 9 Grouted column

C.3 Summary

Even with a good grouting pressure technique, the appropriate installation pressure to produce a ridged pier as desired is directly related to the soil density and grout properties. If the viscosity of the grout is higher, the same pressures will not generate the same flow, and if the soil density varies, the grout will be flow more in the less dense areas, and vice versa.

Therefore, the grouting process chosen was the one that produced the most consistent results in the practice grouting, which was an initial installation pressure of 18 psi and increasing the pressure 1 psi for every 1″ of advancement. While removing the pier, the pressure was reduced to a constant 18 psi for the entire length of removal to fill the void left by the pier shaft. The soil density anomalies were overcome by monitoring the grout flow through the grout tube, and when the grout appeared to slow down the pressure was increased.

Appendix D: Manual and electronic load-deflection comparison

D.1 Introduction

The following appendix shows the comparison between the electronically recorded load deflection curve data and the manually recorded load deflection curve data. The axial curves are based on the average of the four corner displacement measurements while the lateral are based on the average of two corner displacement measurements. Data was not included in the averages for any displacement measurements where electronic failure or gage malfunction was observed. Good correlation is observed in 18 of 22 tests, with the exceptions of ACP1, ACP4, ACPRG1 and ACPRG2. For these four tests, an average displacement curve between the manual and electronic data is used.

D.2 Axial cap (AC)

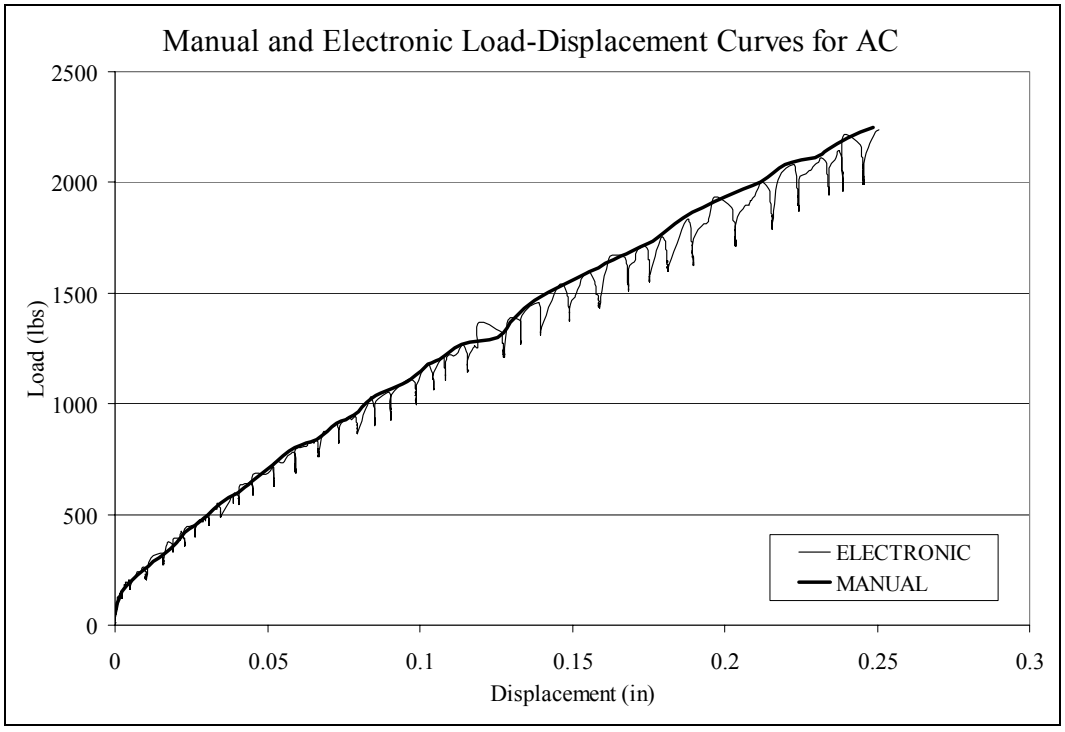

D.3 Axial cap and piles (ACP)

D.3.1 ACP 1

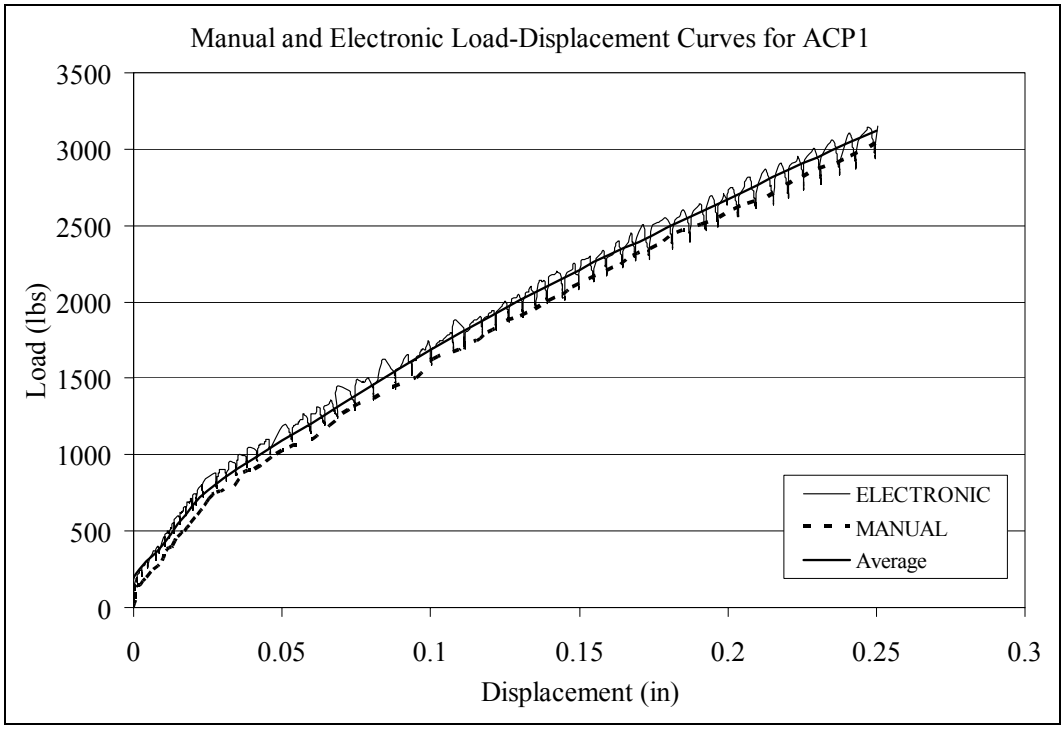

D.3.2 ACP2

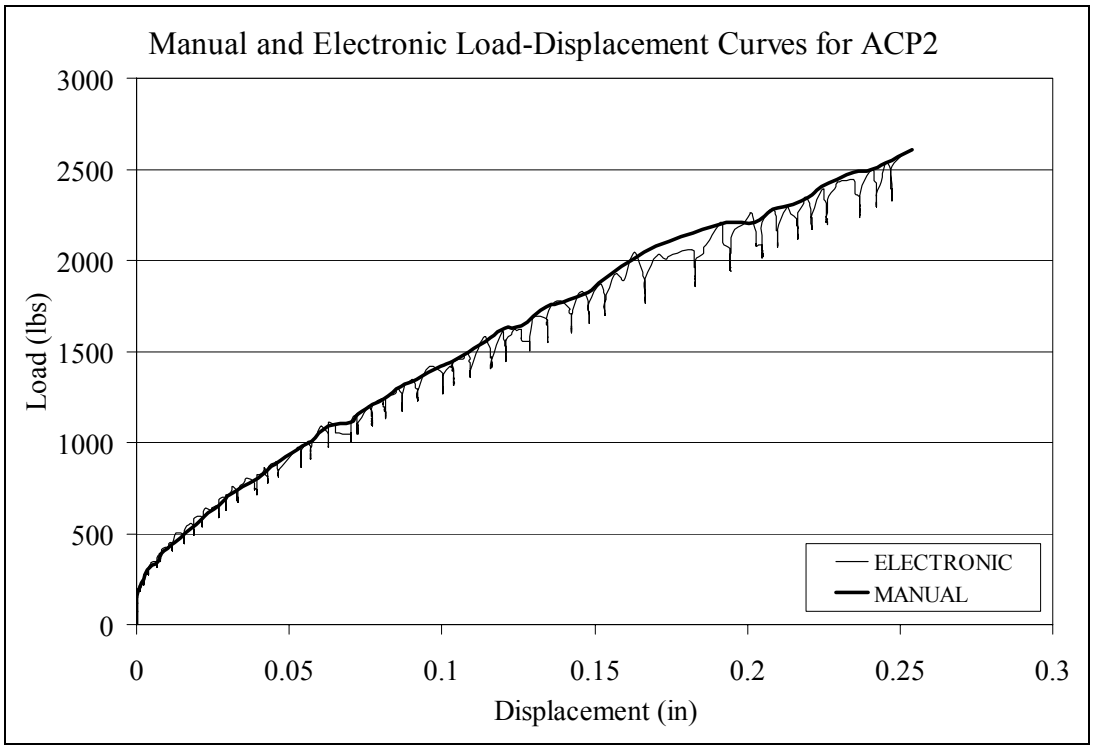

D.3.3 ACP3

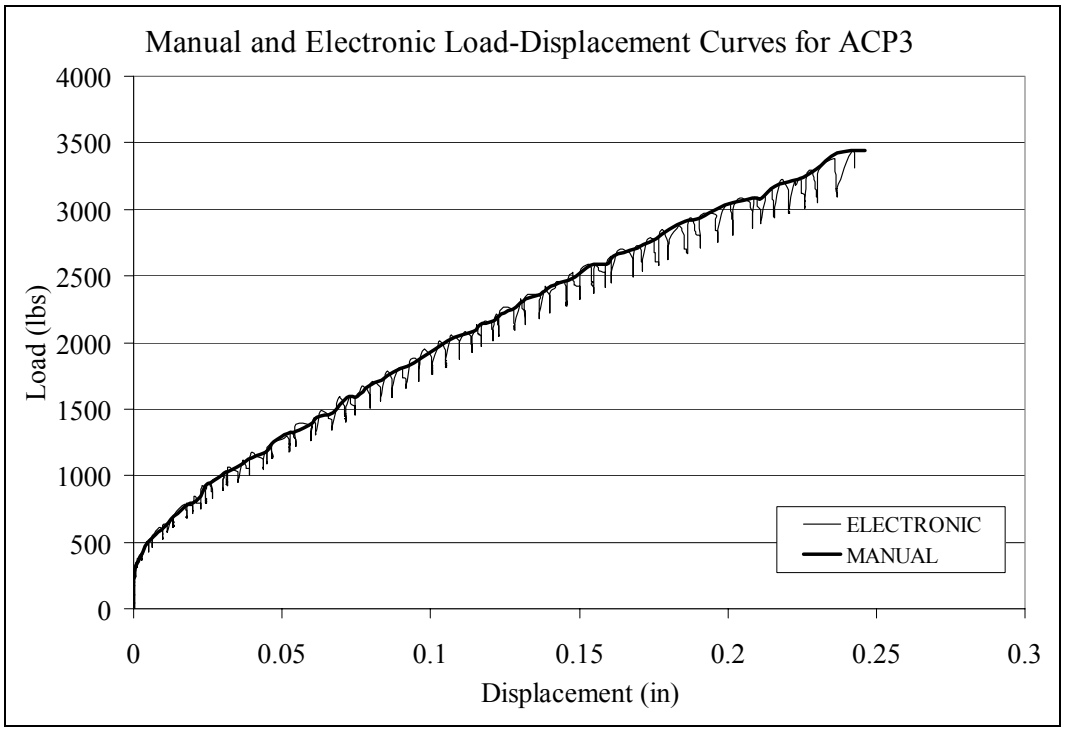

D.3.4 ACP4

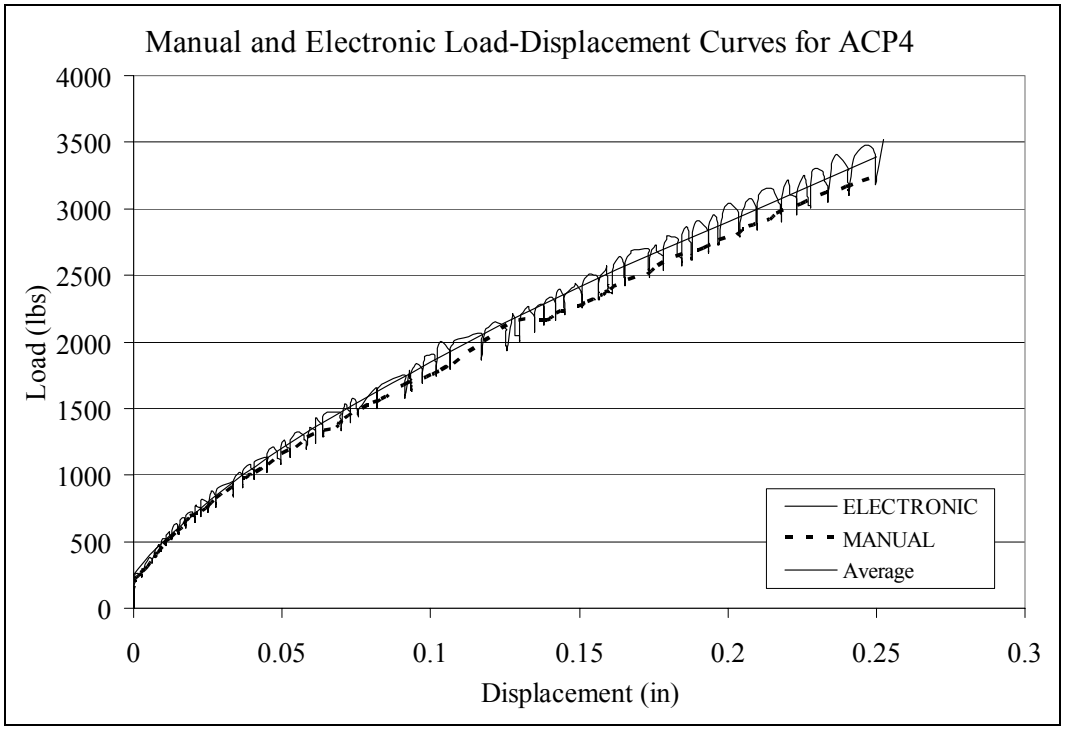

D.4 Axial cap and piers (ACR)

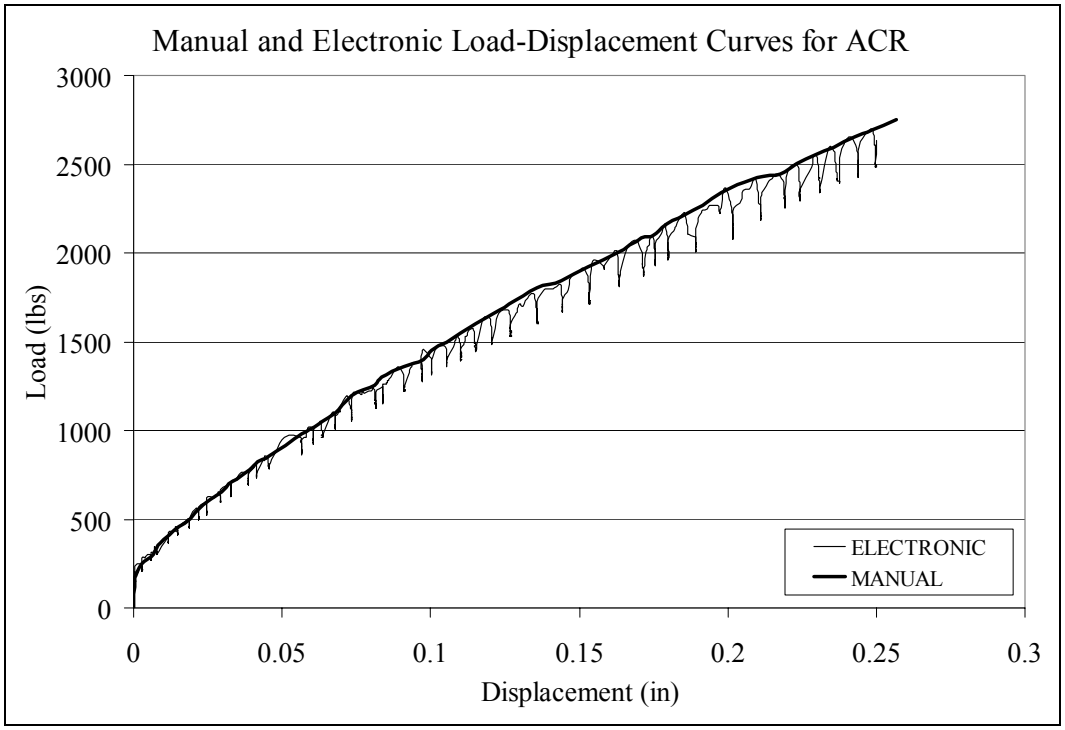

D.5 Axial cap and grout (ACG)

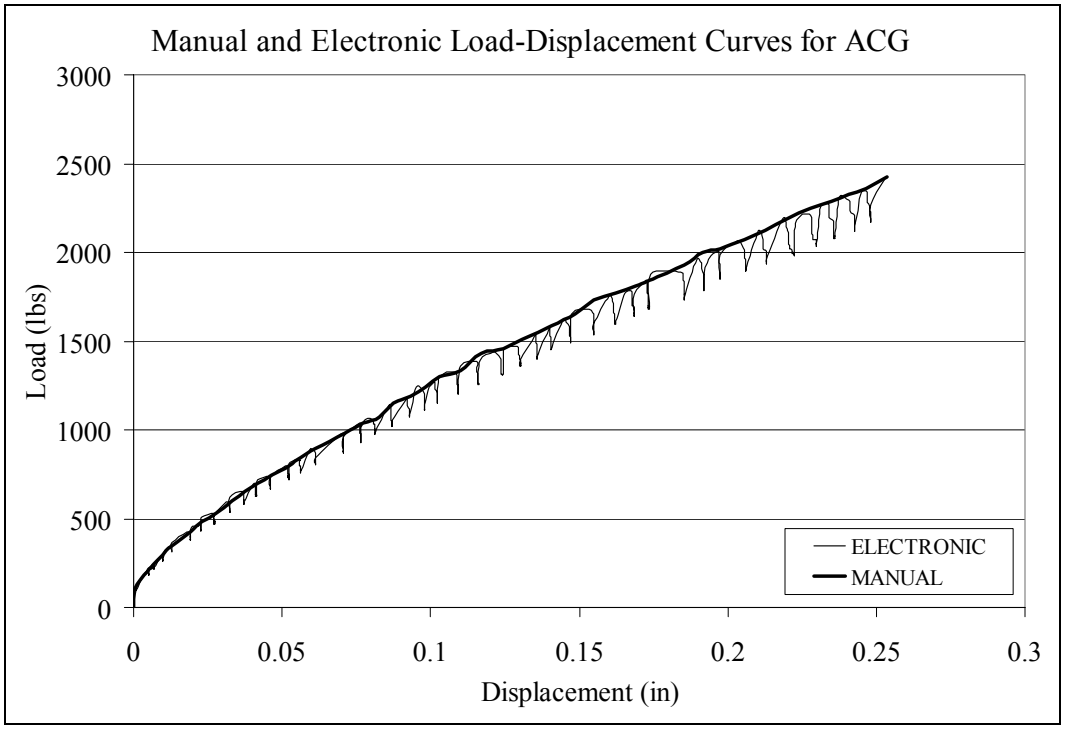

D.6 Cap, Piles, and Piers (ACPR)

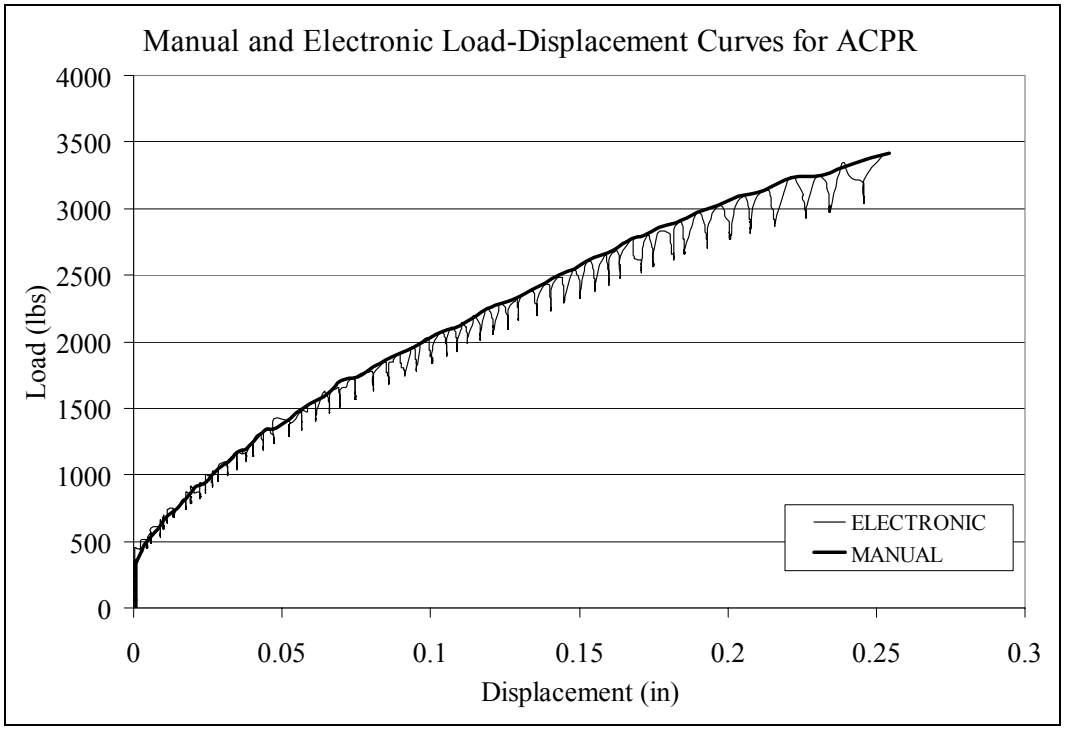

D.7 Cap, Piles, and Grout (ACPG)

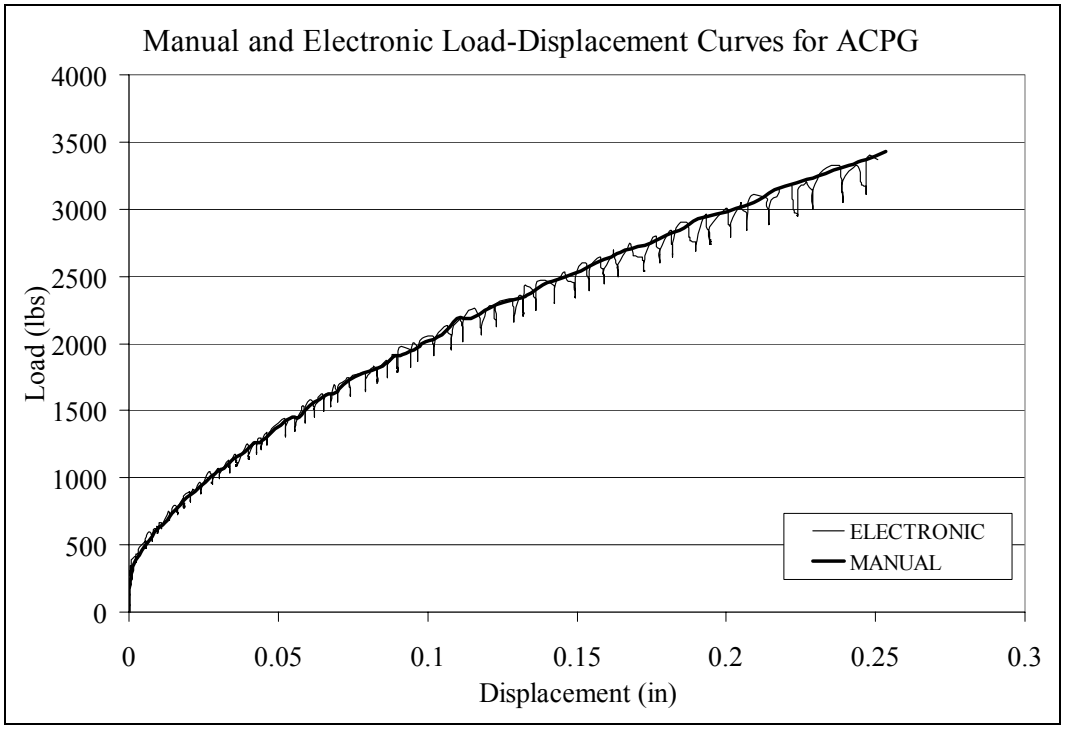

D.8 Cap, Piers, and Grout (ACRG)

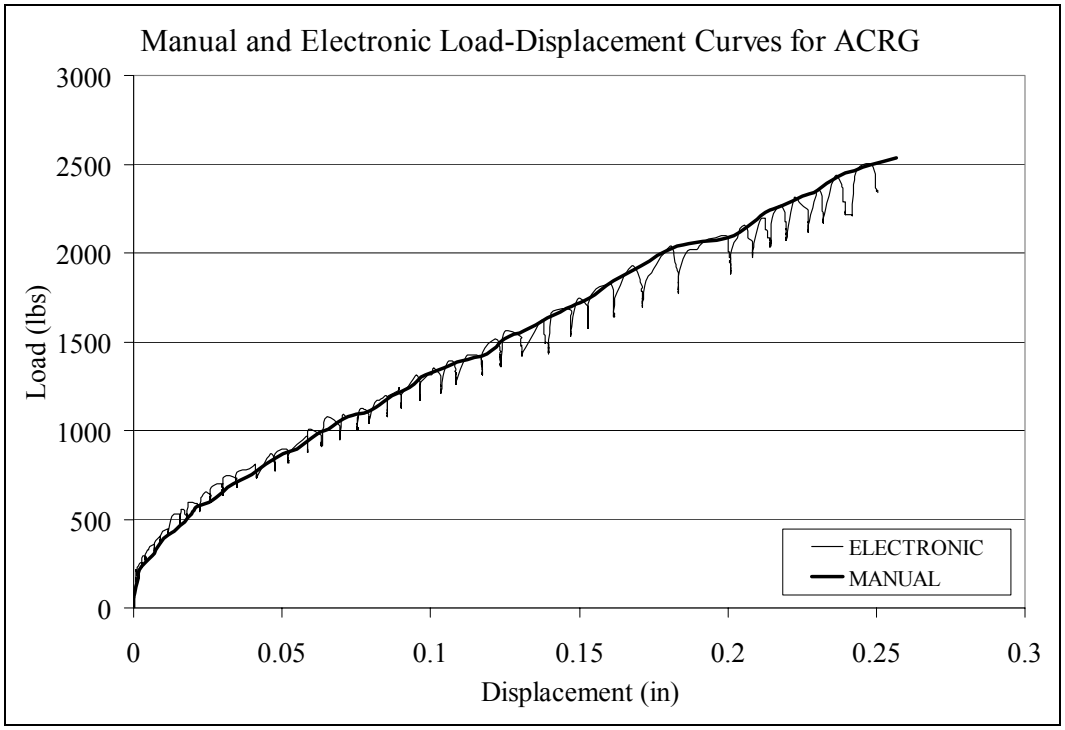

D.9 Cap, Piles, Piers, and Grout (ACPRG)

D.9.1 ACPRG1

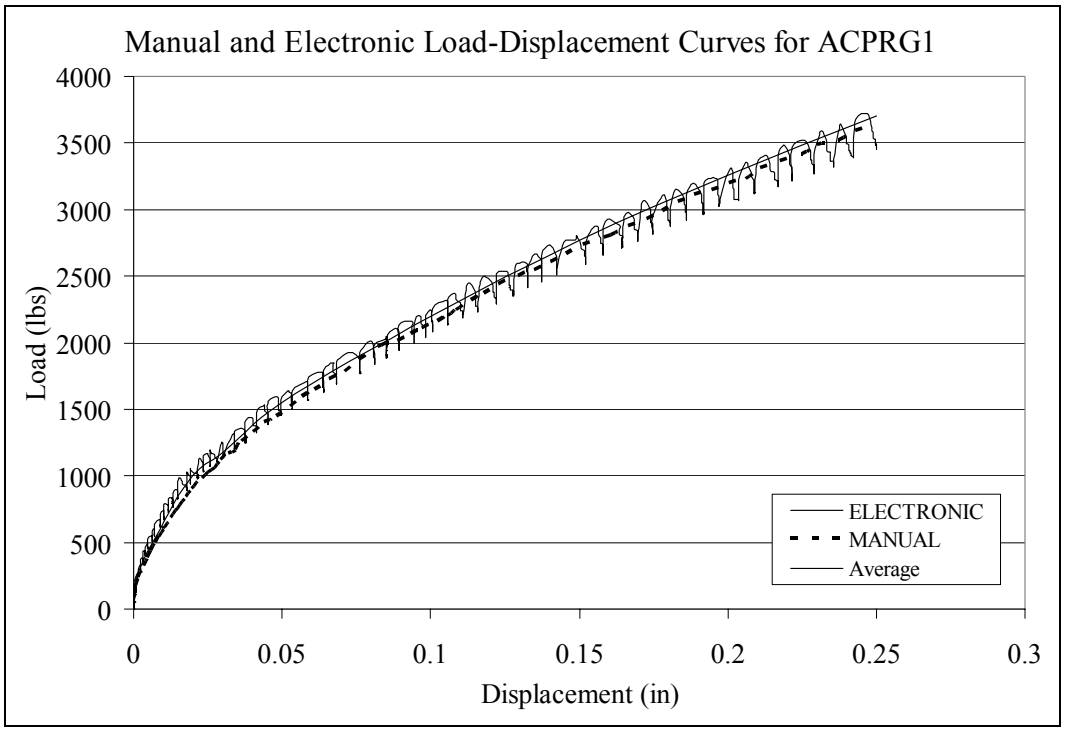

D.9.2 ACPRG2

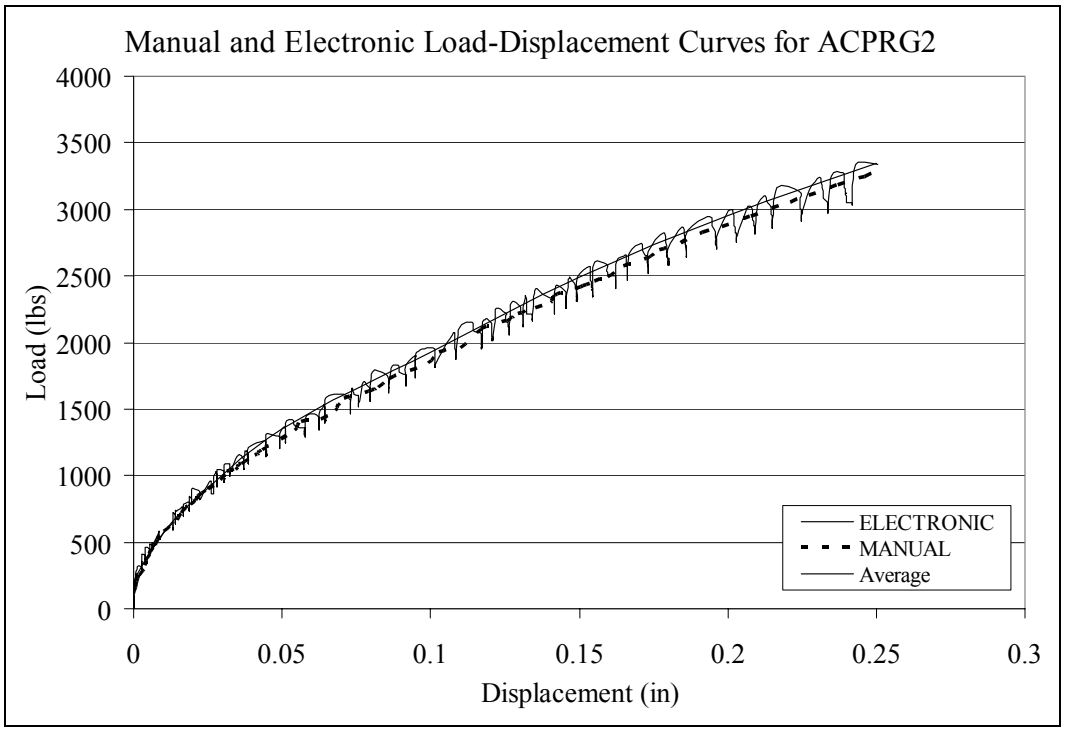

D.10 Cap Only (LC)

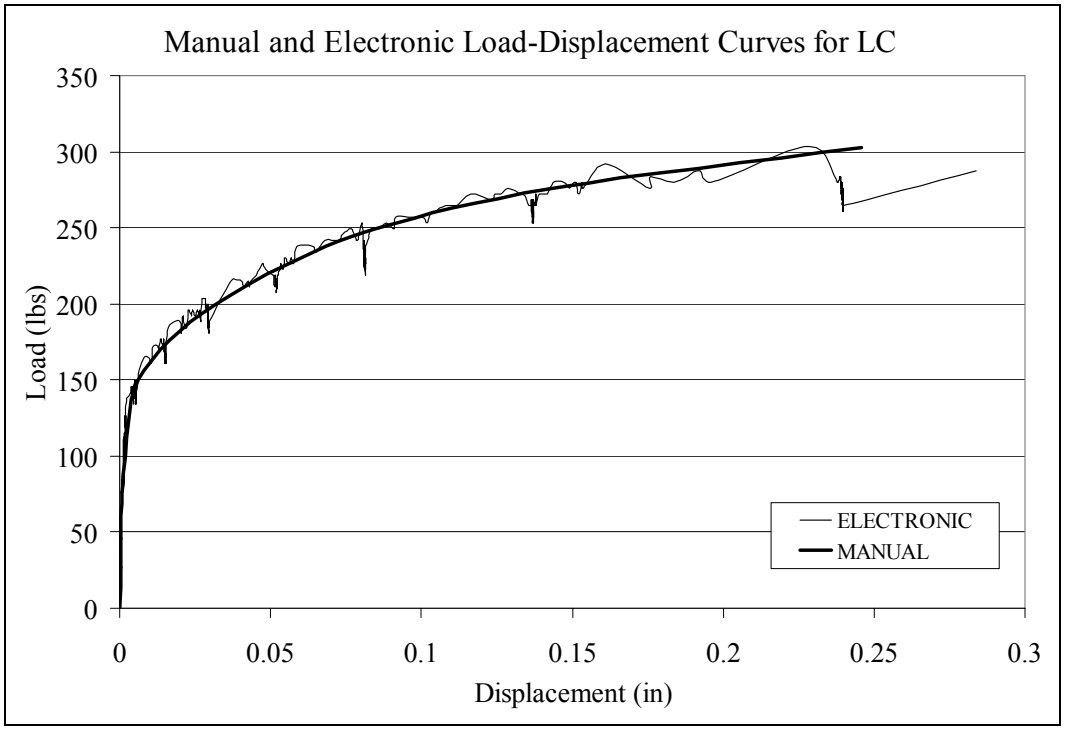

D.11 Cap and Piles (LCP)

D.11.1 LCP1

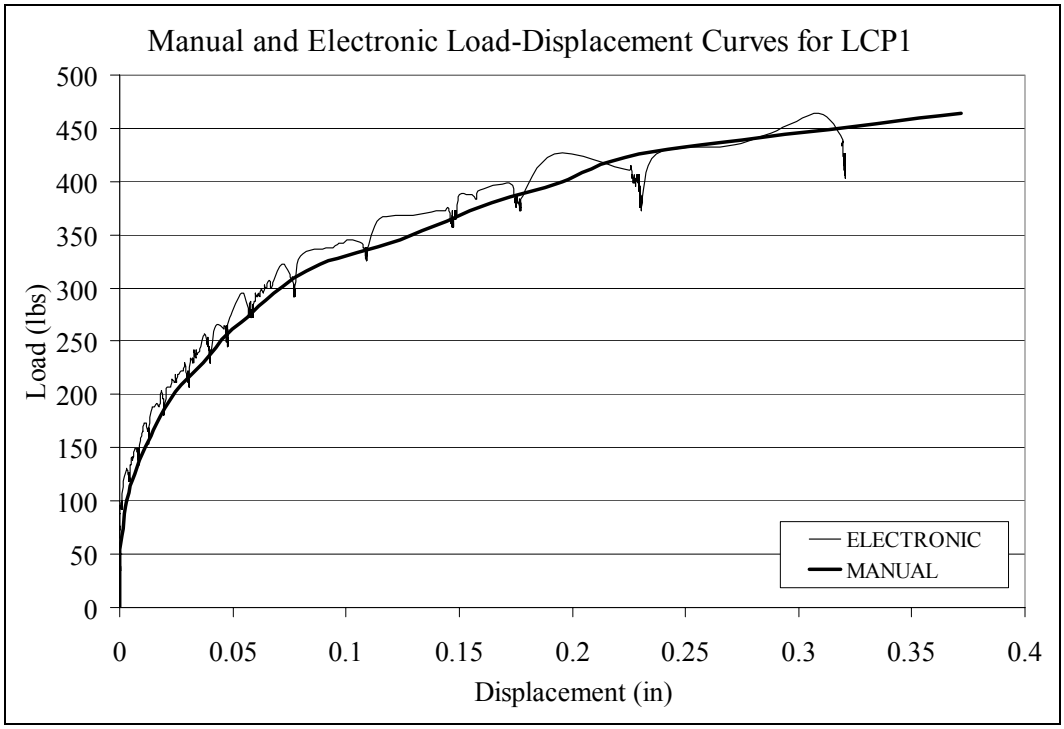

D.11.2 LCP2

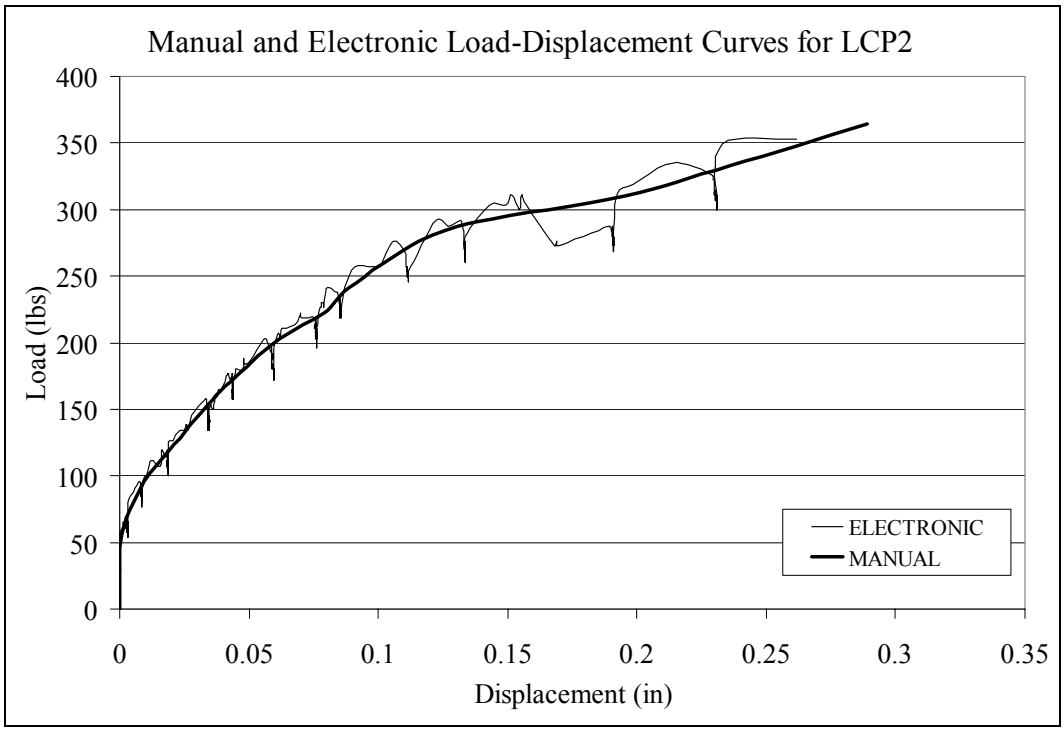

D.12 Cap and Piers (LCR)

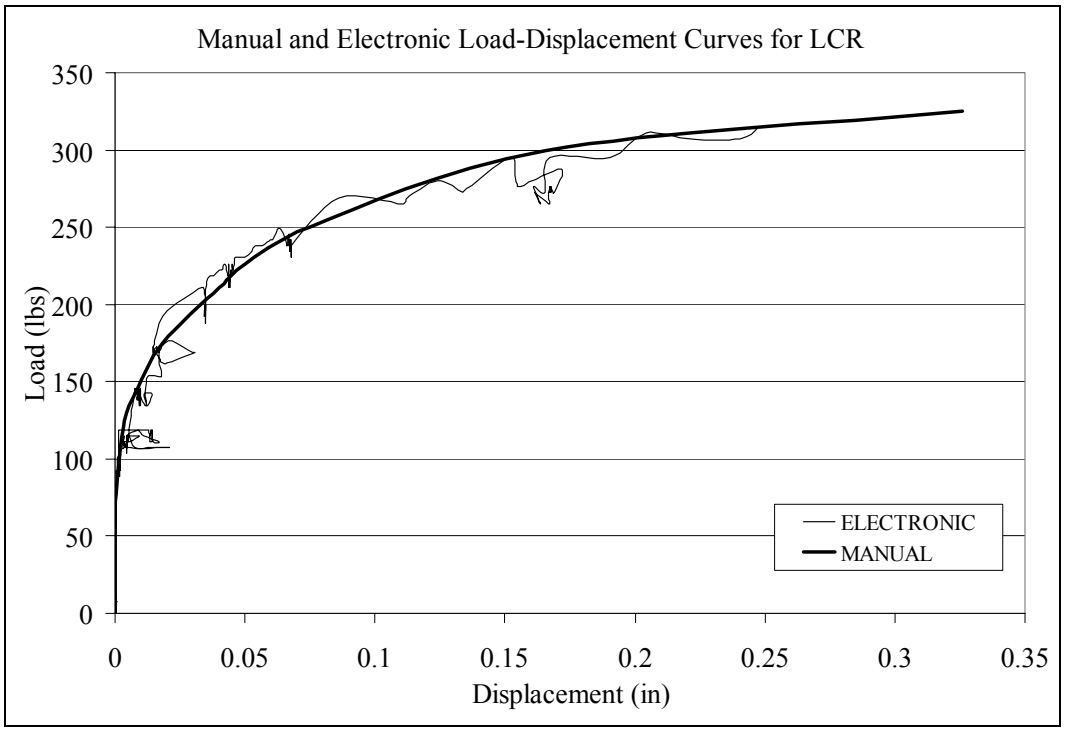

D.13 Cap and Grout (LCG)

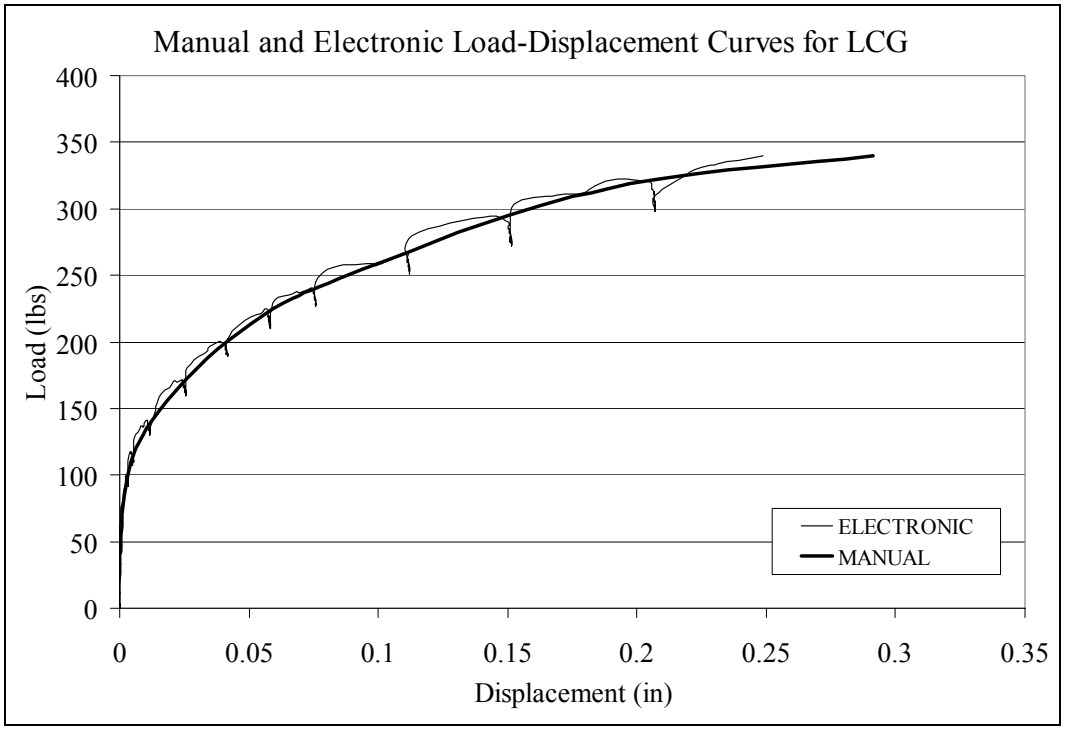

D.14 Cap, Piles, and Piers (LCPR)

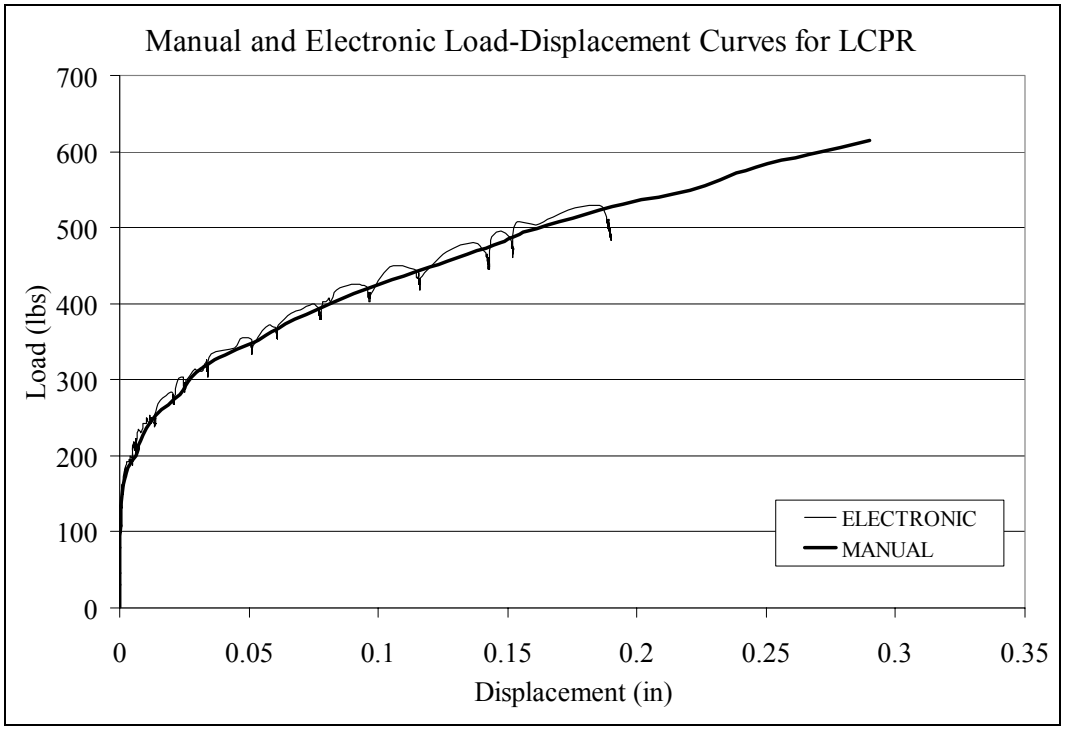

D.15 Cap, Piles, and Grout (LCPG)

D.15.1 LCPG1

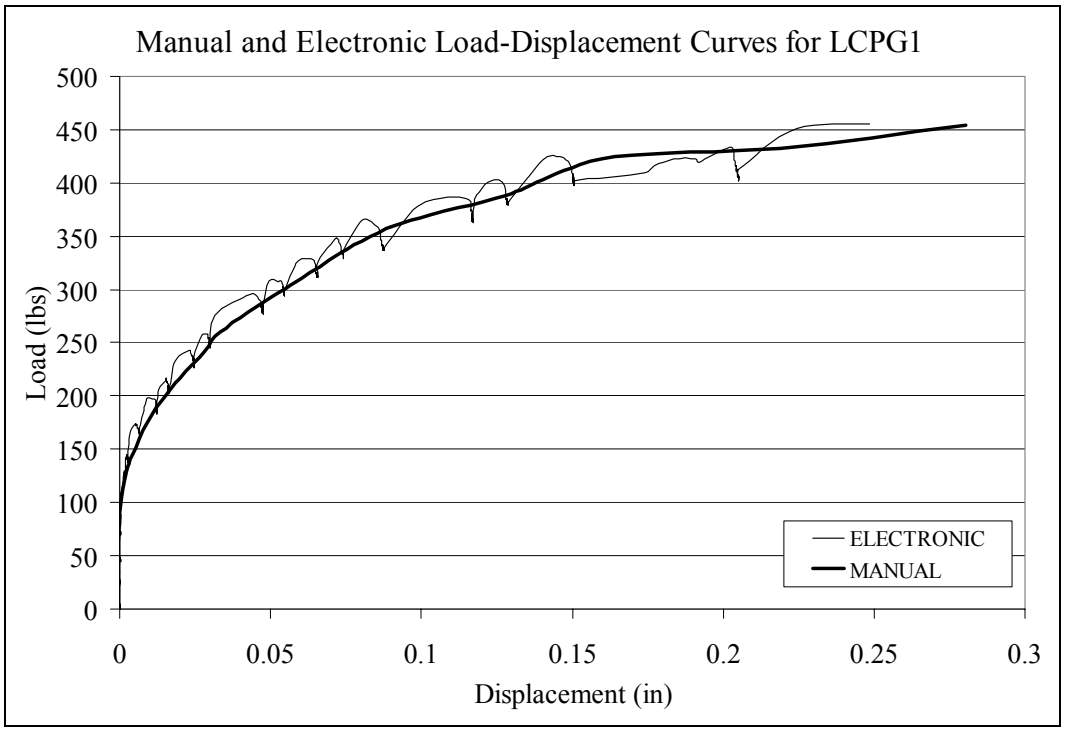

D.15.2 LCPG2

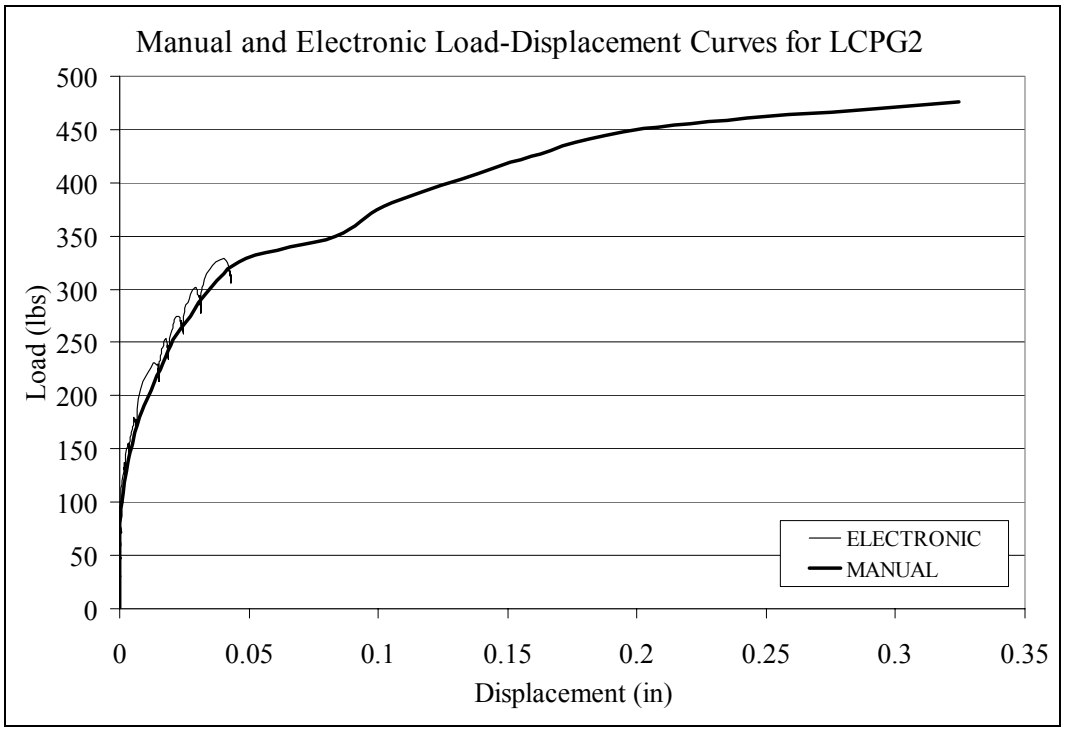

D.16 Cap, Piers, and Grout (LCRG)

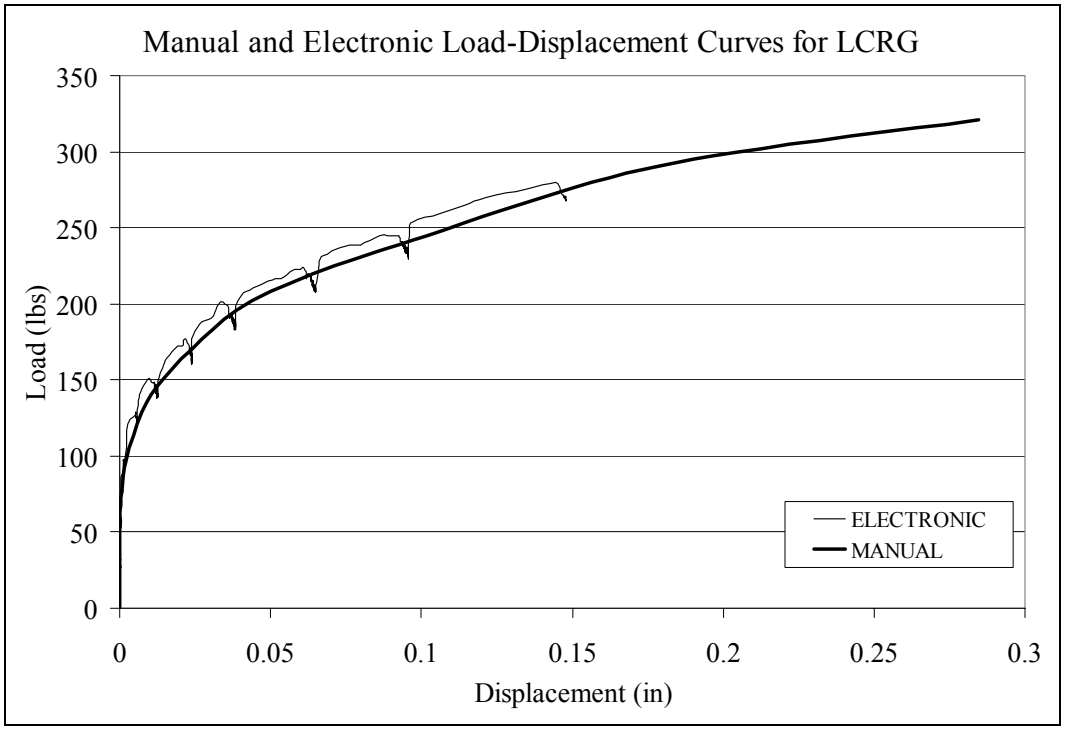

D.17 Cap, Piles, Piers, and Grout (LCPRG)

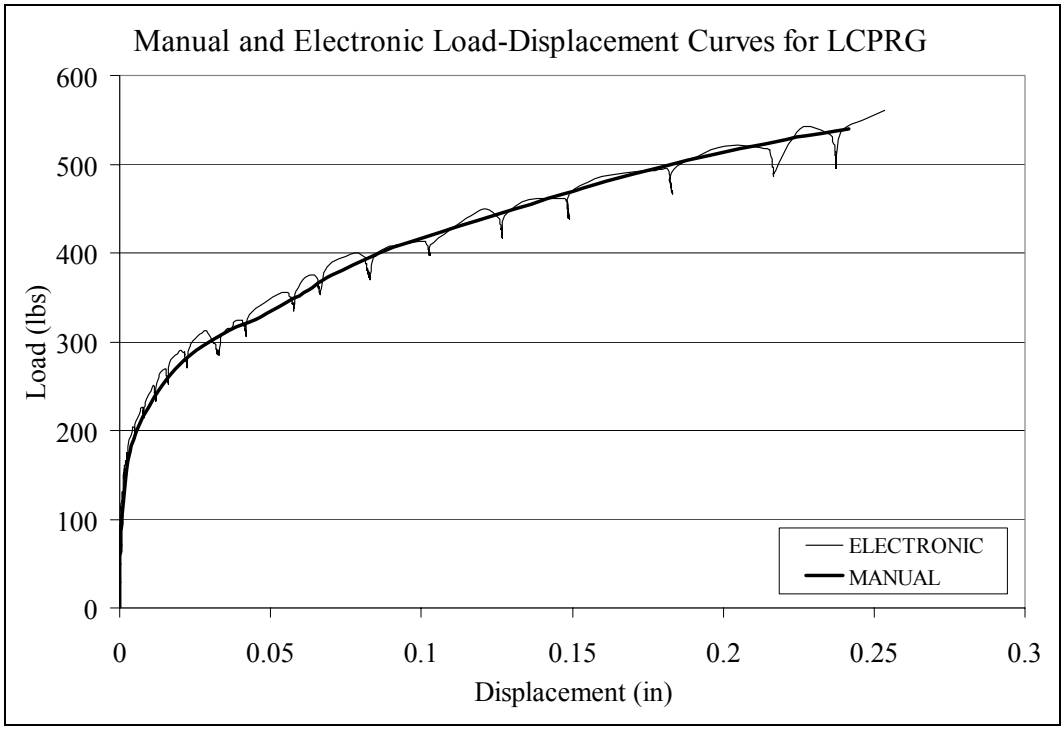

D.18 PILES

D.18.1 Pile 1

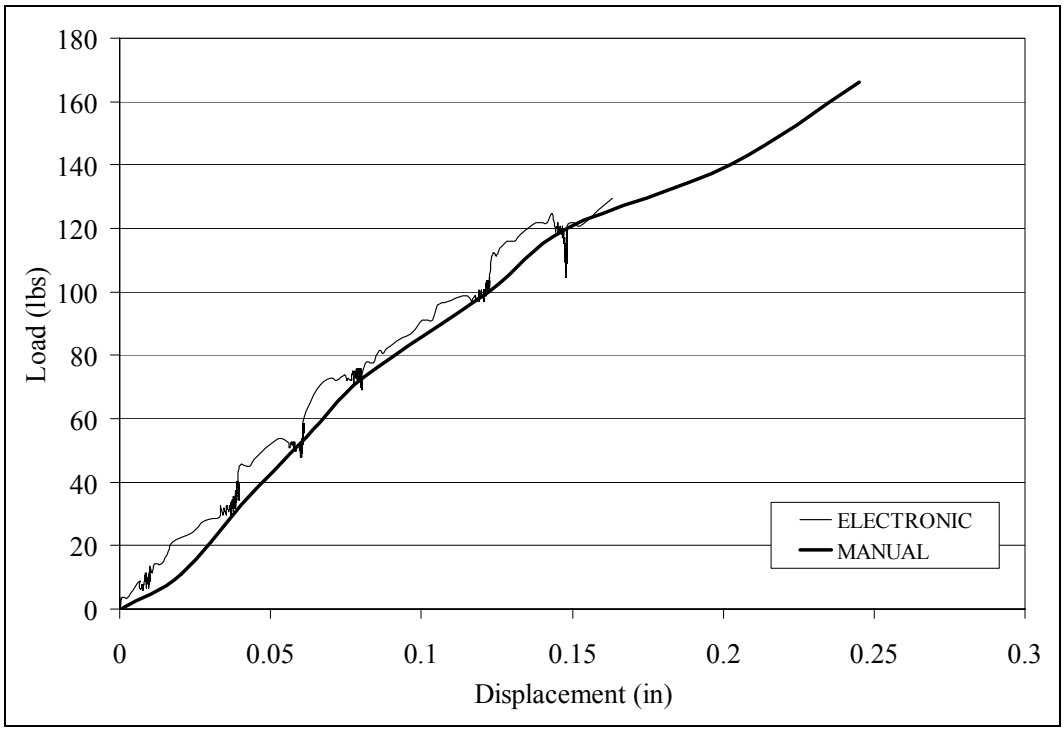

D.18.2 Pile 2

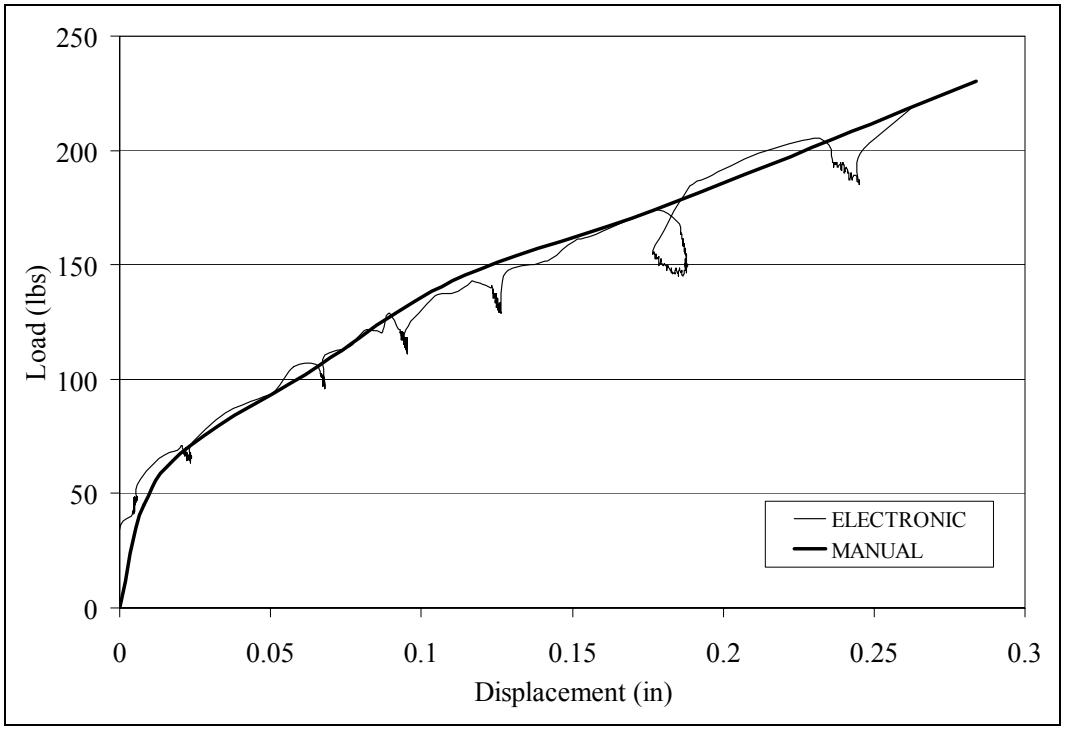

D.18.3 Pile 4

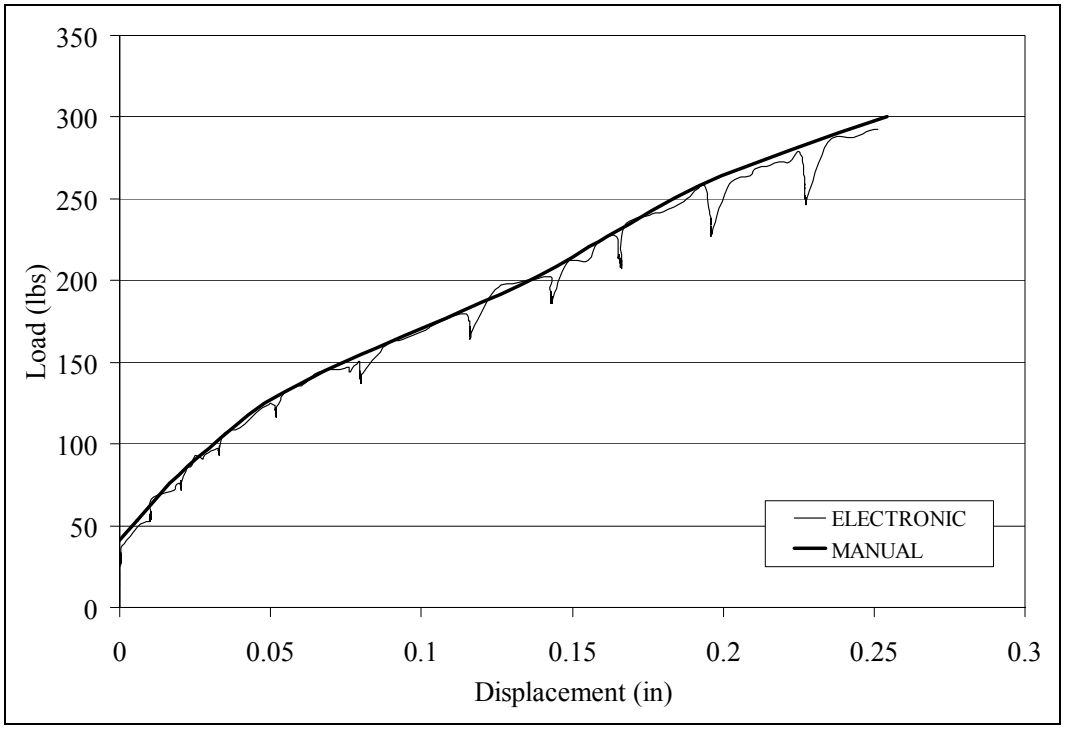

D.18.4 Pile 5

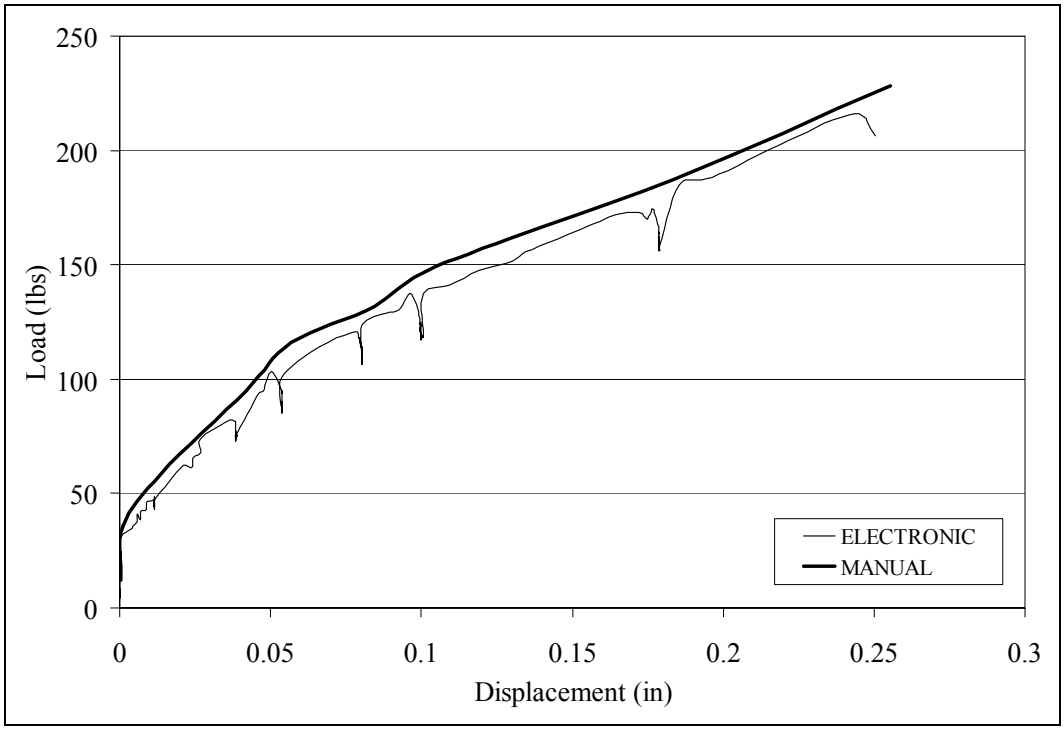

D.18.5 Pile 6

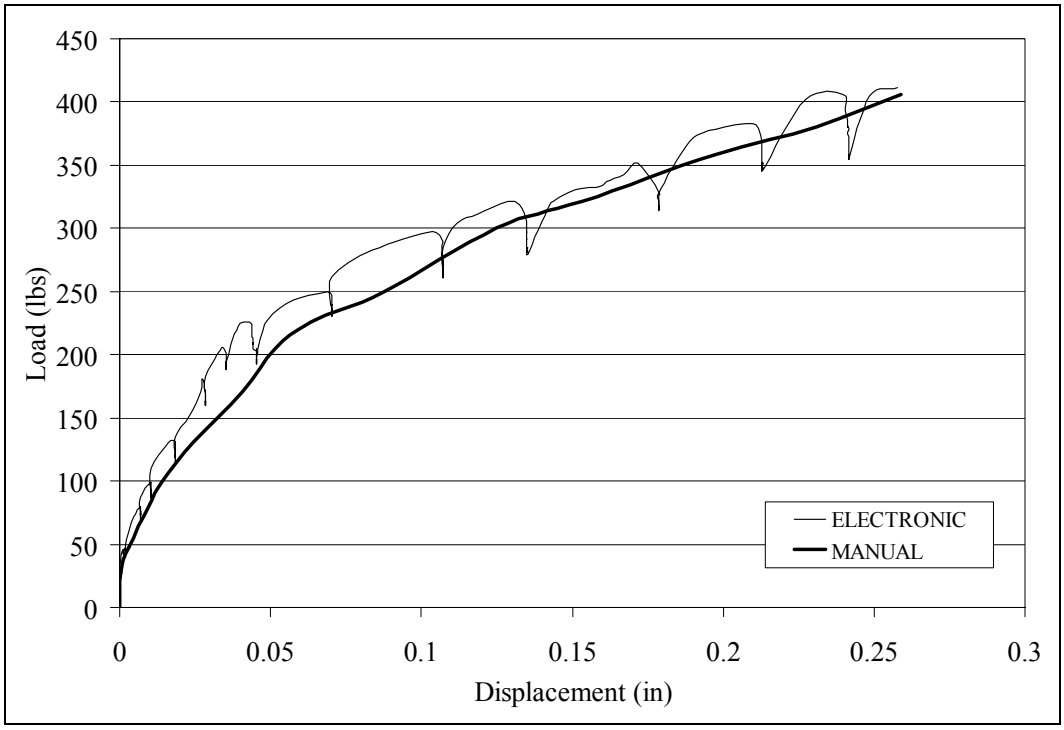

Appendix E: Pictures of grouted piers and grouted columns

E.1 Introduction

This appendix depicts all the grouted piers and grouted columns installed during testing. Some pictures show incomplete piers or piers that had sections break apart during excavation. For more detailed descriptions of these piers, please see Chapter 4. The scale in each picture is in inches. For pile pictures, see Appendix F. The labeling represents the pier location as shown in the figure below:

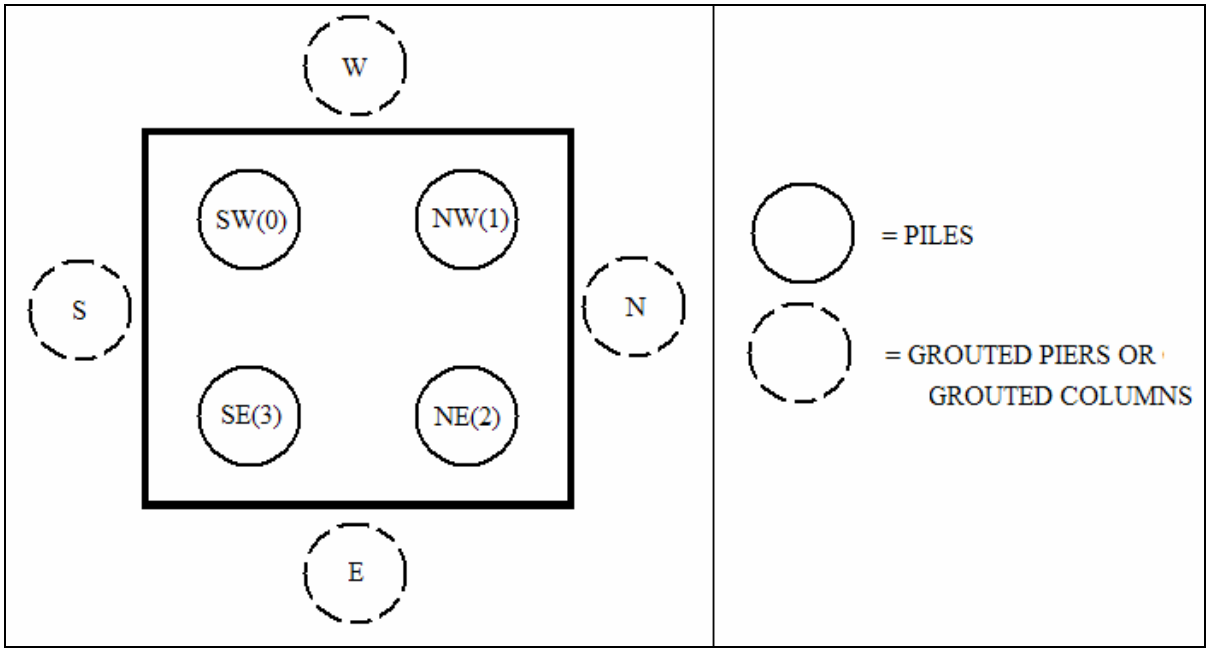

E.2 AXIAL TESTS

E.2.1 Cap and grout (ACG)

The top of the pier is to the left in each picture, while the bottom is to the right.

East (E)

North (N)

South (S)

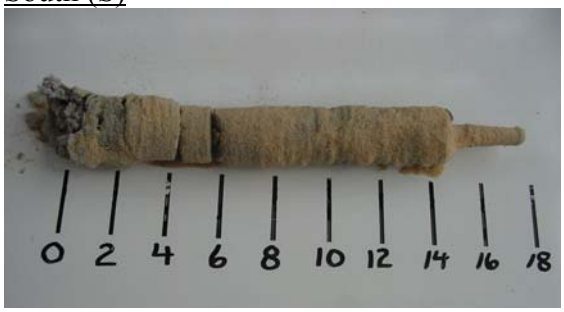

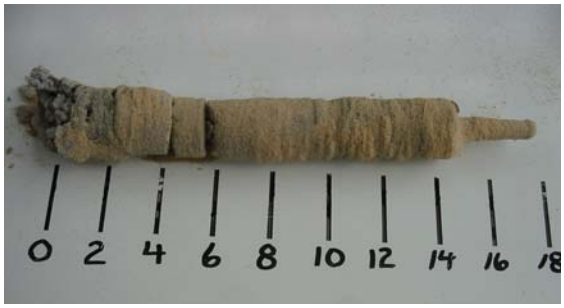

West (W)

E.2.2 Cap, Piles, and Grout (ACPG)

The top of the pier is to the left in each picture, while the bottom is to the right.

East (E)

North (N)

South (S)

West (W)

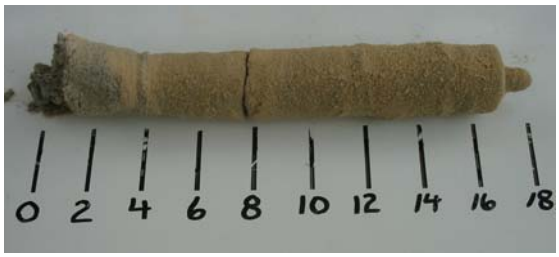

E.2.3 Cap, Piers, and Grout (ACRG)

The top of the pier is to the left in each picture, while the bottom is to the right.

East (E)

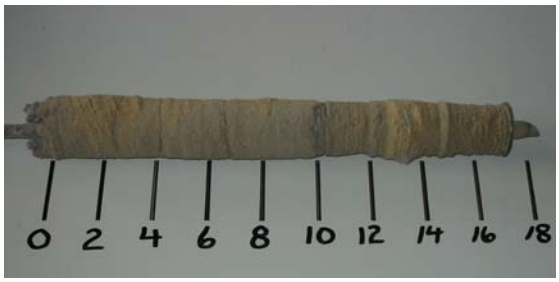

North (N)

South (S)

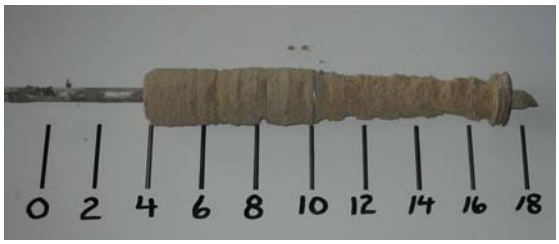

West (W)

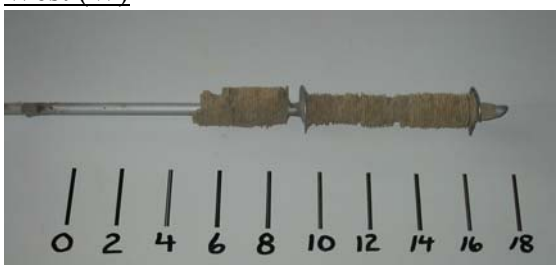

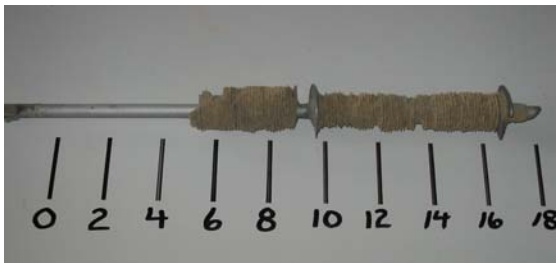

E.2.4 Cap, Piles, Piers, and Grout (ACPRG)

The top of the pier is to the right in each picture, while the bottom is to the left.

E.2.4.1 ACPRG1

East (E)

North (N)

South (S)

West (W)

E.2.4.2 ACPRG2

The top of the pier is to the right in each picture, while the bottom is to the left.

East (E)


North (N)


South (S)


West (W)


E.3 LATERAL TESTS

E.3.1 Cap and Grout (LCG)

The top of the pier is to the left in each picture, while the bottom is to the right.

East (E)

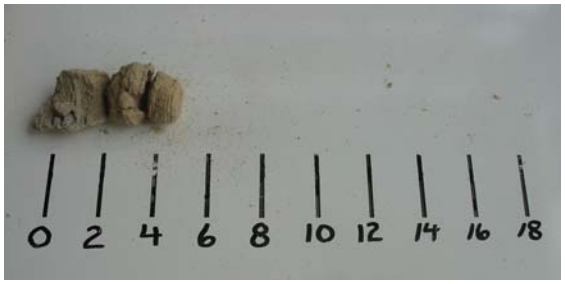

North (N)

South (S)

West (W)

E.3.2 Cap, Piles, and Grout (LCPG)

The top of the pier is to the left in each picture, while the bottom is to the right.

E.3.2.1 LCPG1

East (E)

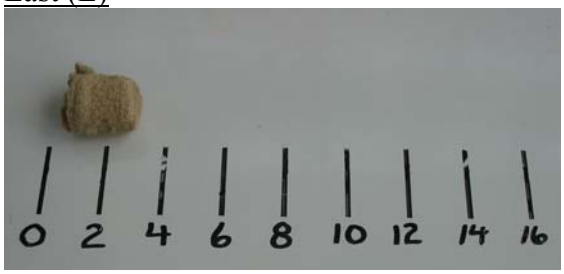

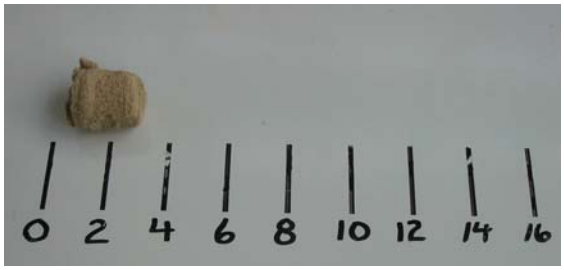

North (N)

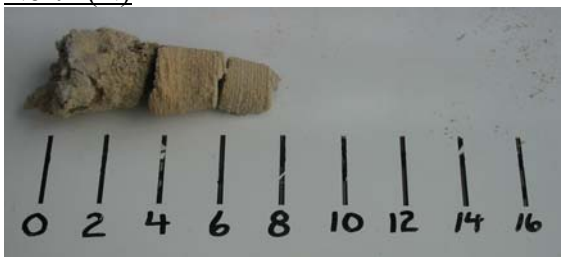

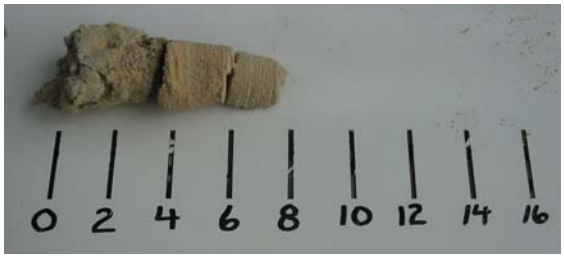

South (S)

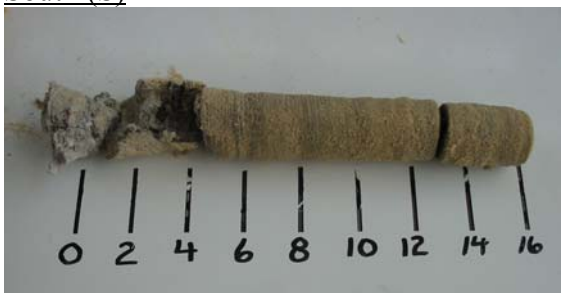

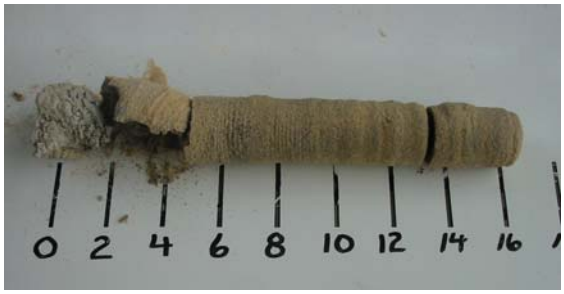

West (W)

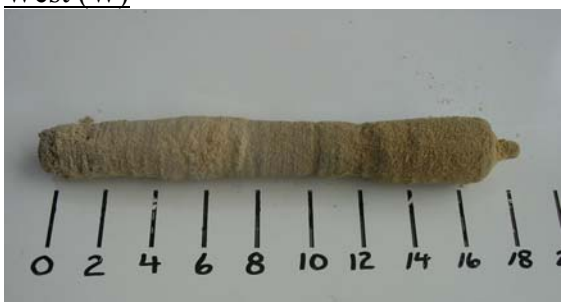

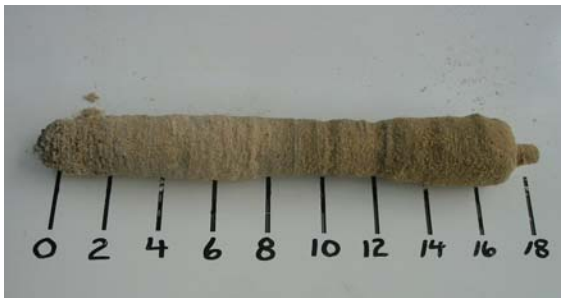

E.3.2.2LCPG2

The top of the pier is to the right in each picture, while the bottom is to the left.

East (E)


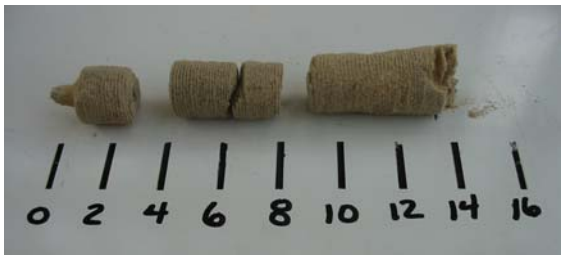

North (N)

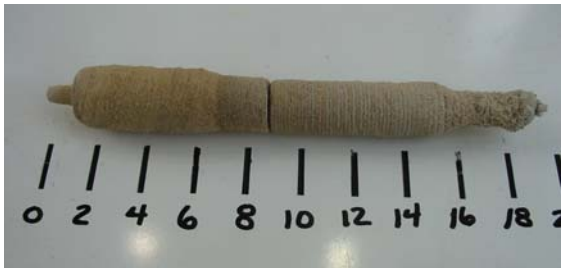
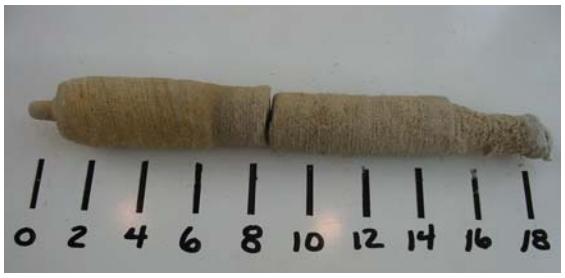

South (S)


West (W)

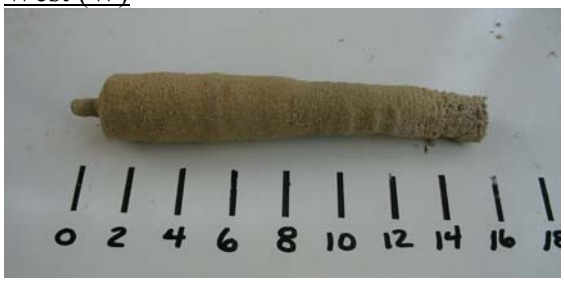
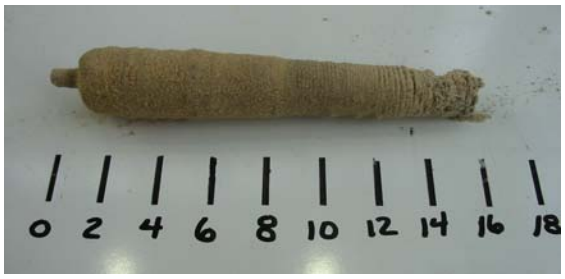

E.3.3 Cap, Piers, and Grout (LCRG)

The top of the pier is to the right in each picture, while the bottom is to the left.

East (E)


North (N)

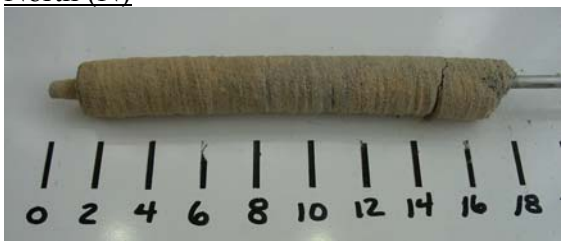
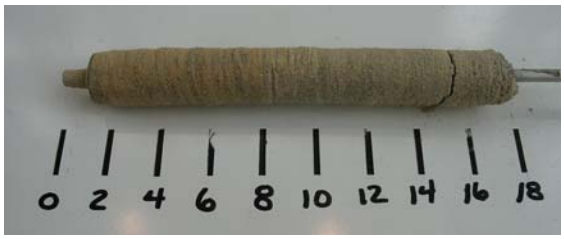

South (S)


West (W)


E.3.4 Cap, Piles, Piers, and Grout (LCPRG)

The top of the pier is to the left in each picture, while the bottom is to the right.

East (E)

North (N)

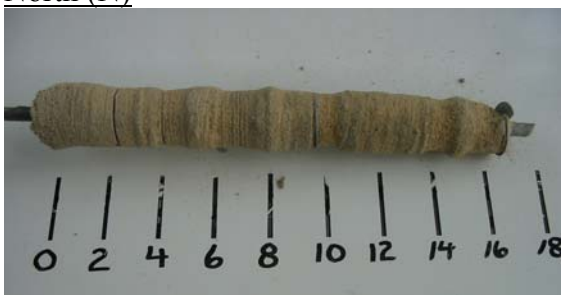

South (S)

West (W)

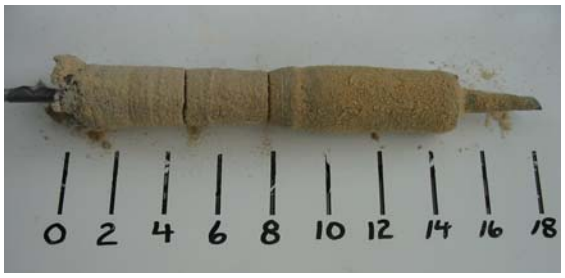

E.4 PILES

The top of the pier is to the right in each picture, while the bottom is to the left.

North (N)

East (E)

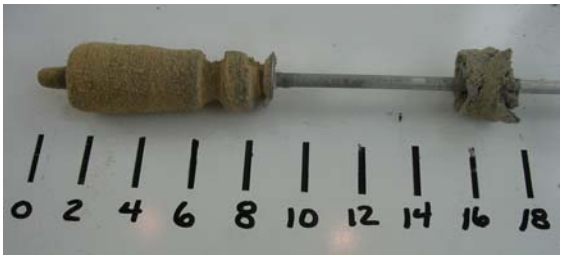

Appendix F: Pictures of piles

F.1 Introduction

The following appendix shows pictures of the piles constructed for this experimentation. Discussion for each is provided in Chapter 4 and is not provided here. No pictures are available for tests performed in Round 2 (ACPR, LCPR, ACP2, LCP2).

F.2 Axial cap and piles (ACP)

F.2.1 ACP 1

F.2.2 ACP3

F.2.3 ACP4

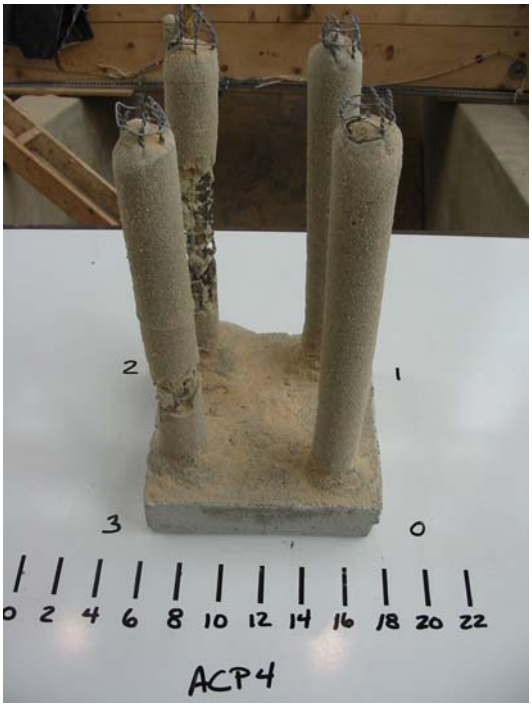

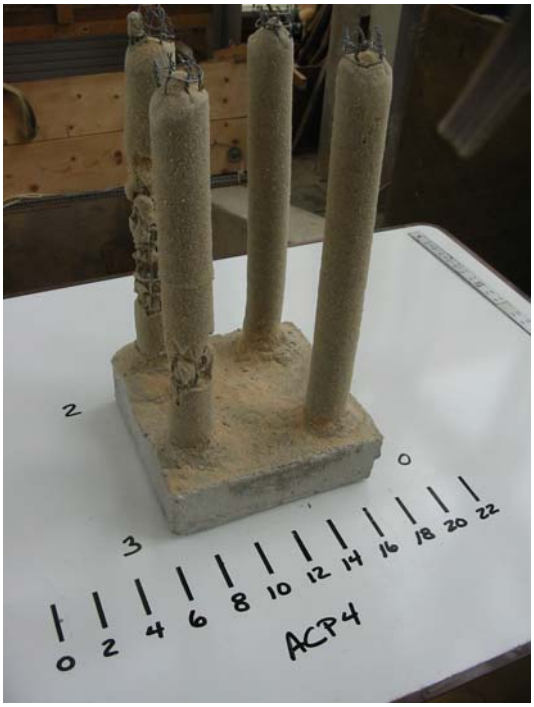

F.3 Cap, Piles, and Grout (ACPG)

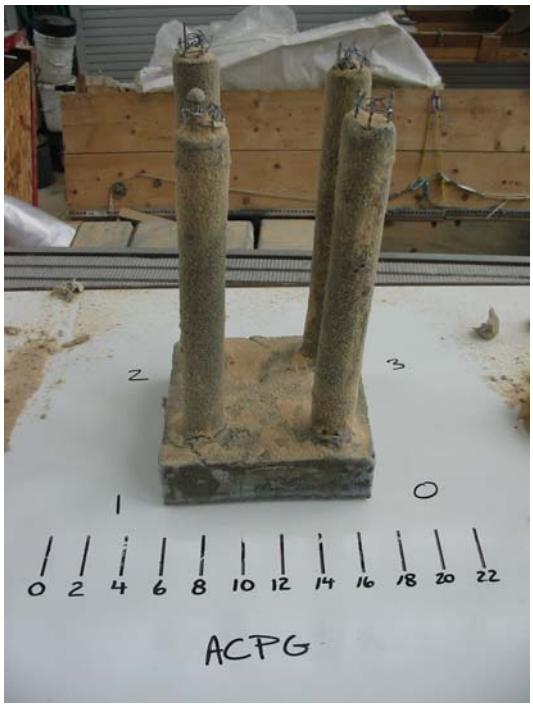

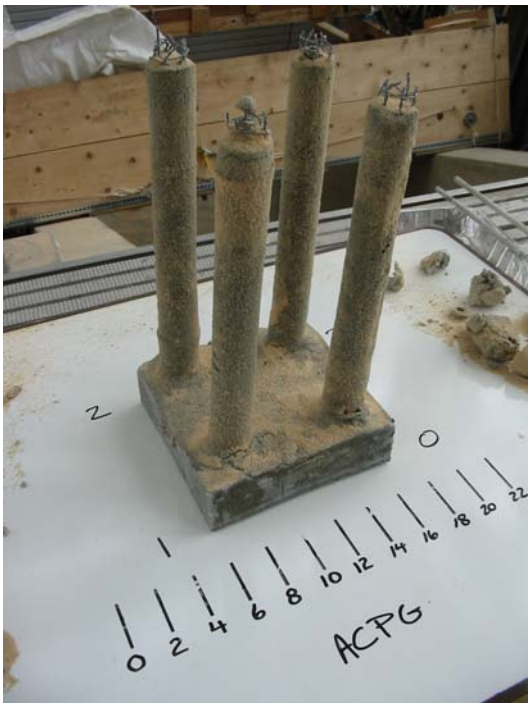

F.4 Cap, Piles, Piers, and Grout (ACPRG)

F.4.1 ACPRG1

F.4.2 ACPRG2

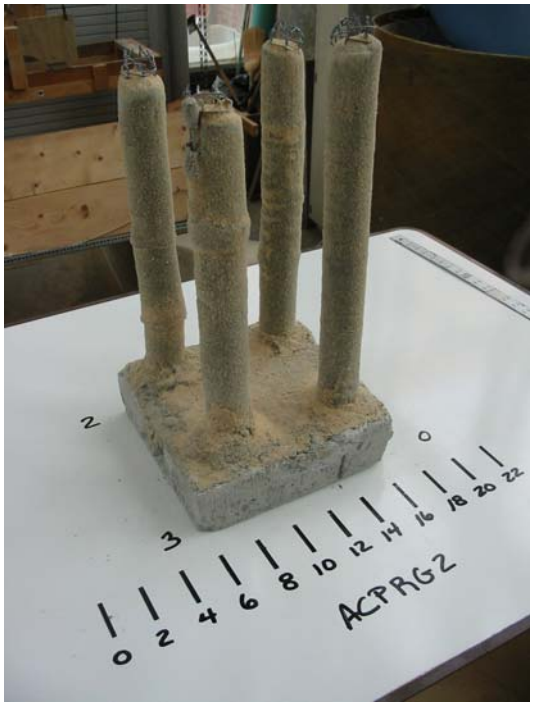

F.5 Cap and Piles (LCP)

F.5.1 LCP1

F.6 Cap, Piles, and Grout (LCPG)

F.6.1 LCPG1

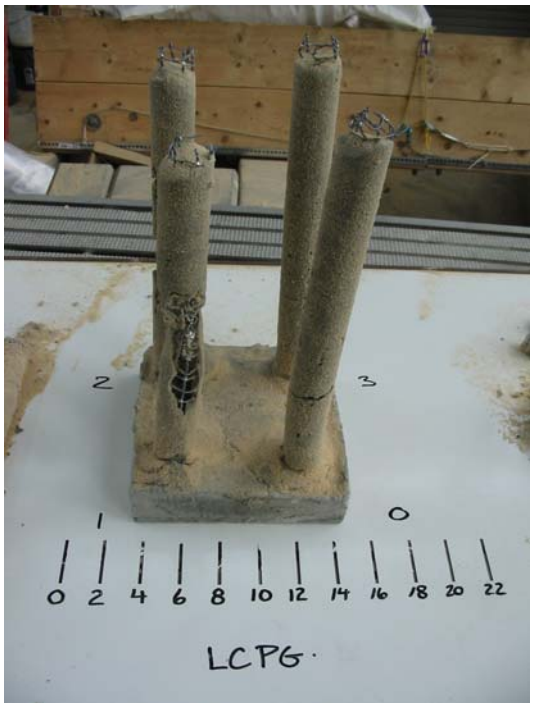

F.6.2 LCPG2

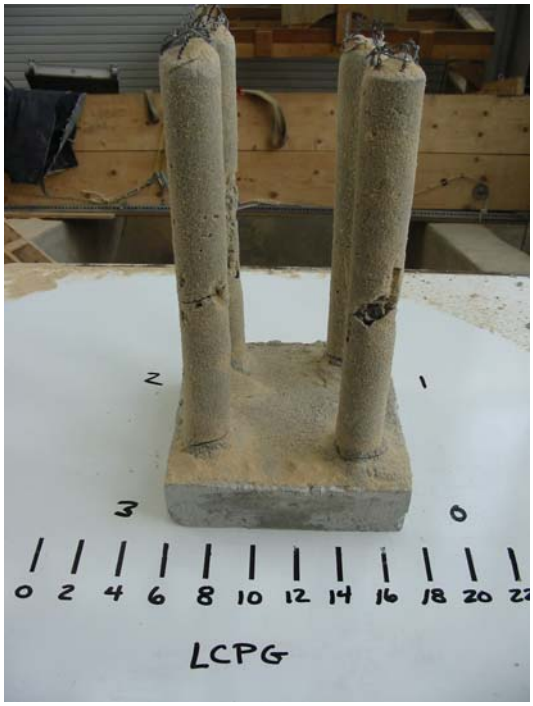

F.7 Cap, Piles, Piers, and Grout (LCPRG)

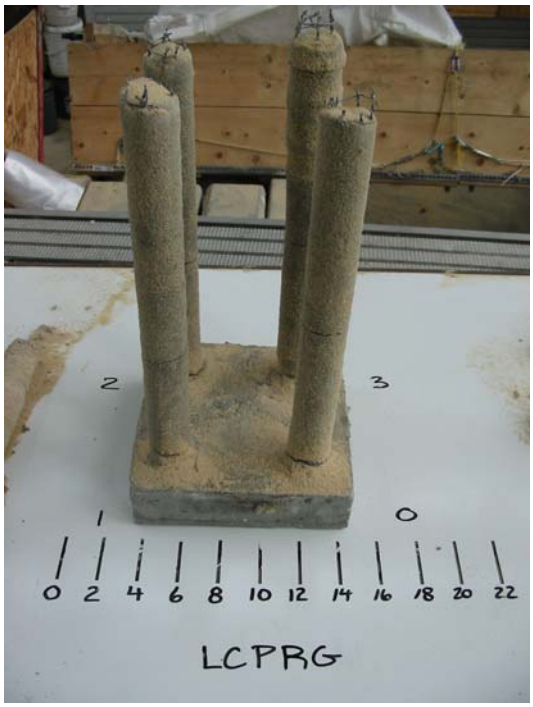

F.8 PILES tests

F.8.1 PILES pile 1

F.8.2 PILES pile 2

F.8.3 PILES pile 3

F.8.4 PILES pile 4

F.8.5 PILES pile 5

F.8.6 PILES pile 6

Appendix G: Density data for each location

G.1 Introduction

The following appendix shows the density readings taken at each testing location and the relative density data equivalent for each test. The target density was 100 lb/ft^3, or 60% relative density, ±5%. The relative density graphs illustrate the scatter for each location at six different depths and provide boundary lines at 55% and 65% relative density to better gage the accuracy of the actual density to the target density. The most influential depths on the foundation displacement are 0.5′ and 1.5′, as they are in direct contact with the foundations.

G.2 Axial cap (AC)

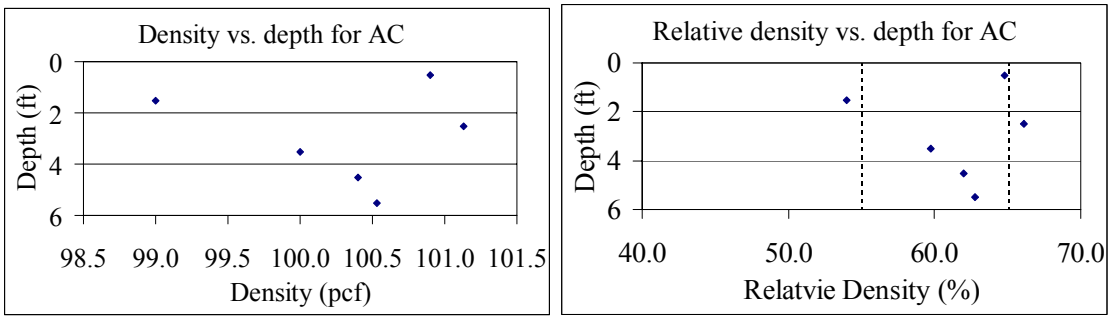

G.3 Axial cap and piles (ACP)

G.3.1 ACP 1

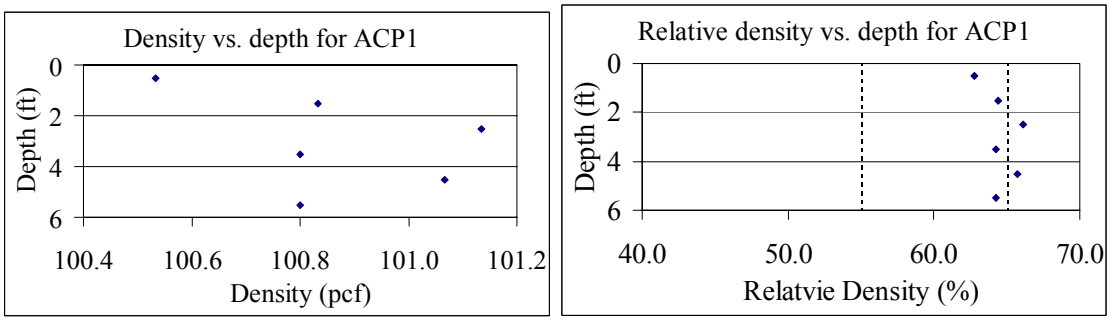

G.3.2 ACP2

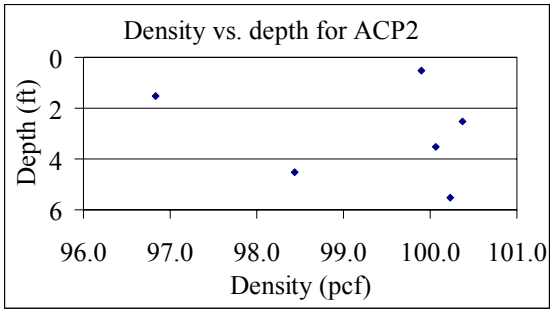

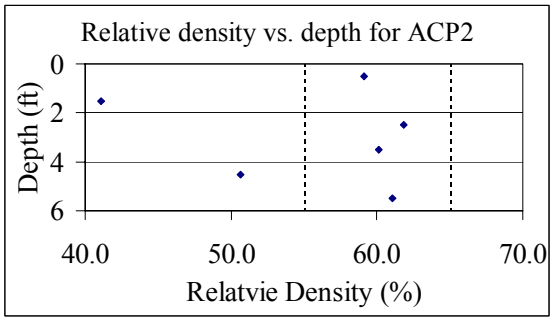

G.3.3 ACP3

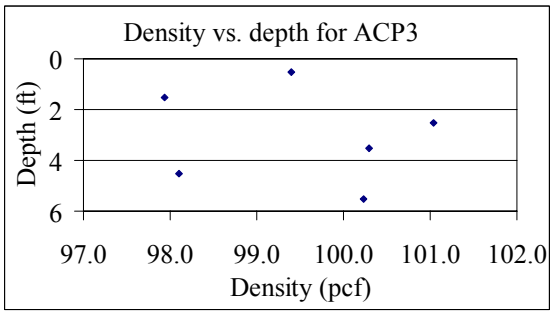

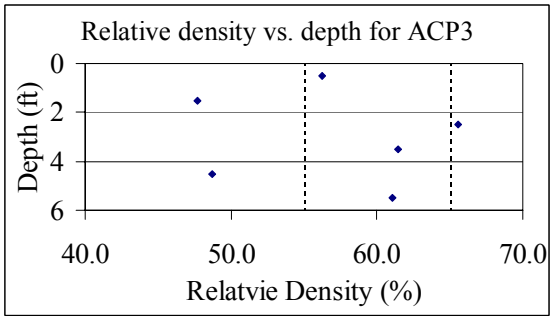

G.3.4 ACP4

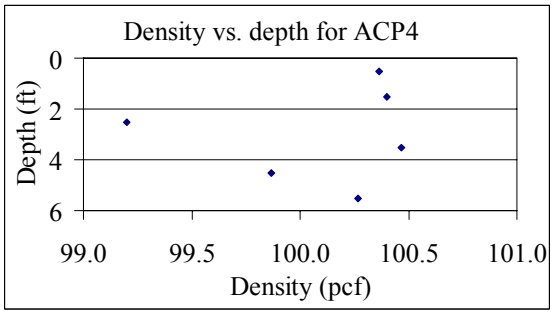

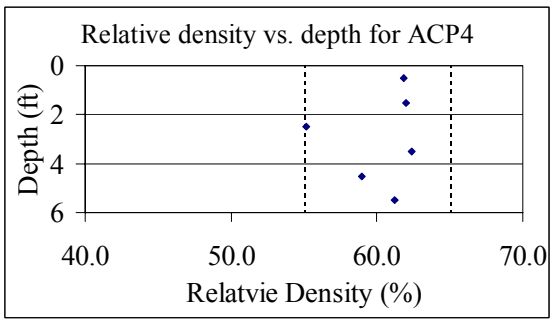

G.4 Axial cap and piers (ACR)

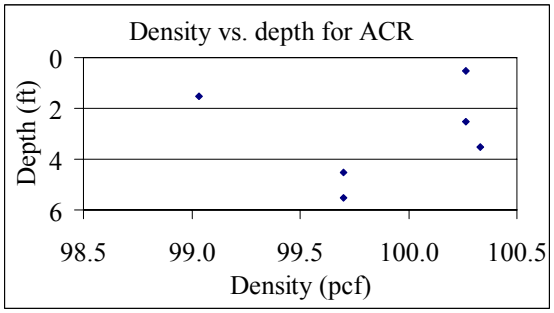

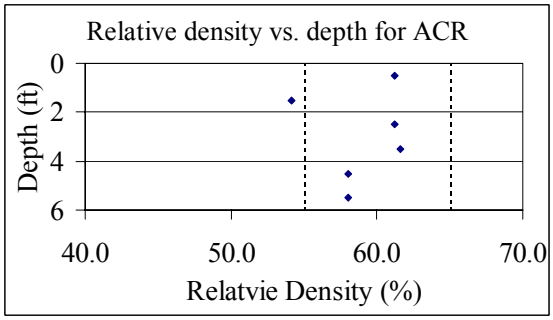

G.5 Axial cap and grout (ACG)

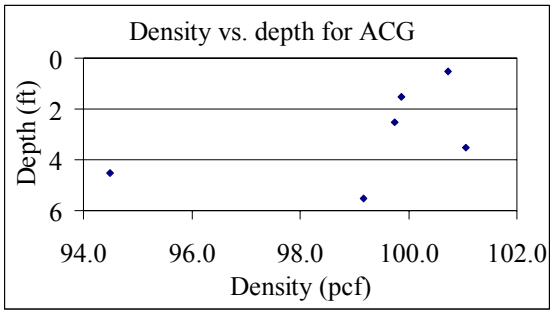

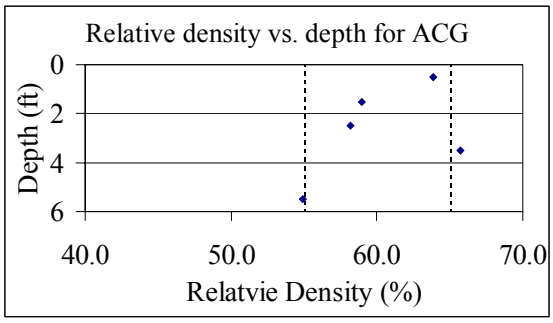

G.6 Cap, Piles, and Piers (ACPR)

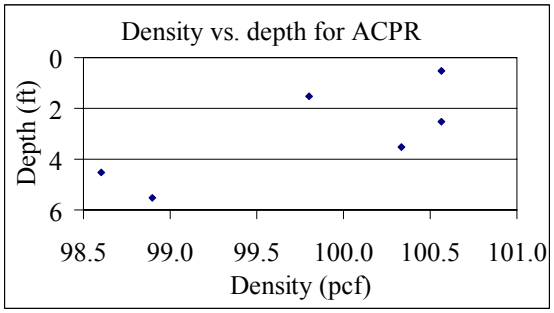

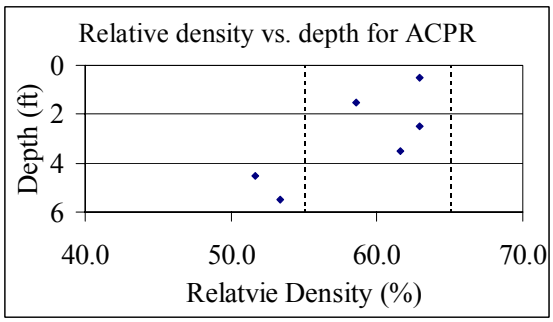

G.7 Cap, Piles, and Grout (ACPG)

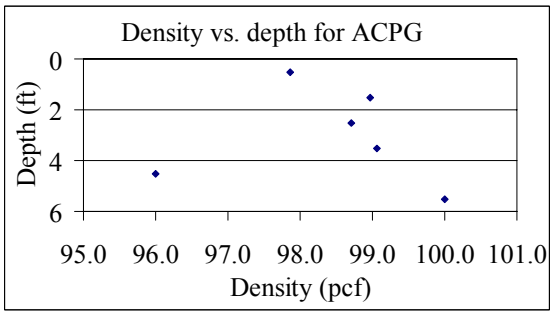

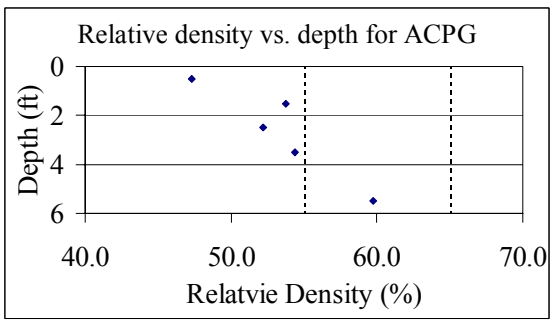

G.8 Cap, Piers, and Grout (ACRG)

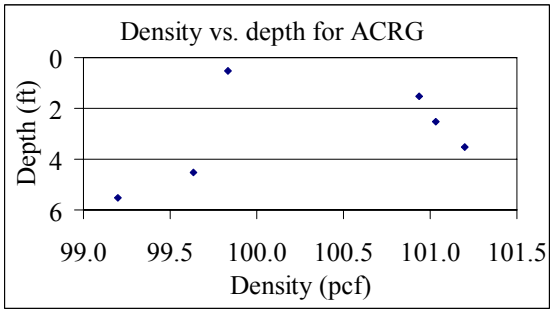

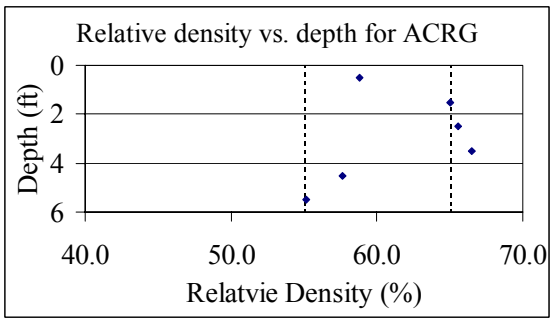

G.9 Cap, Piles, Piers, and Grout (ACPRG)

G.9.1 ACPRG1

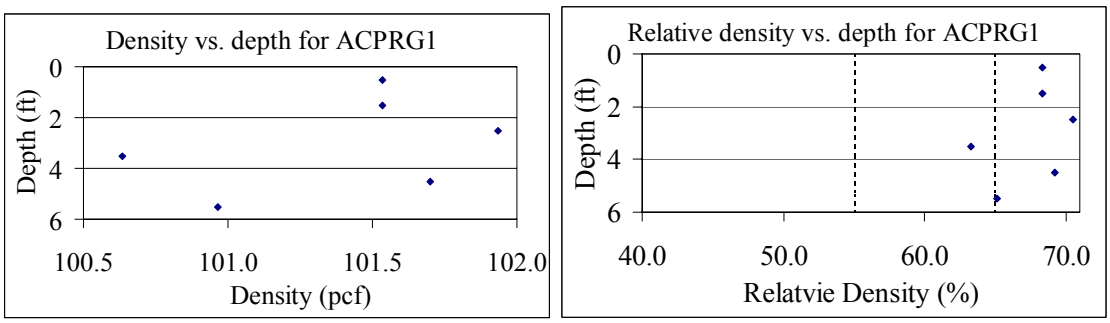

G.9.2 ACPRG2

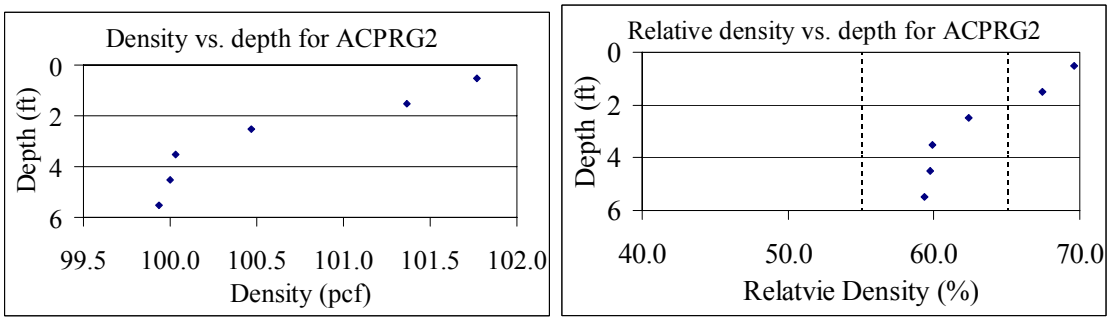

G.10 Cap Only (LC)

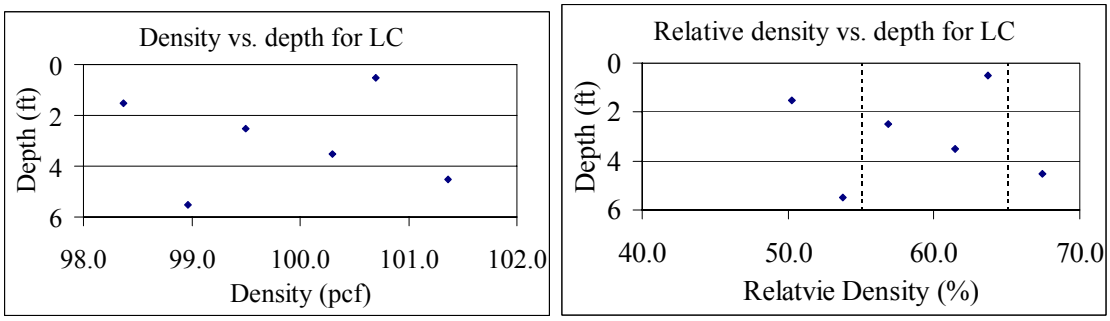

G.11 Cap and Piles (LCP)

G.11.1 LCP1

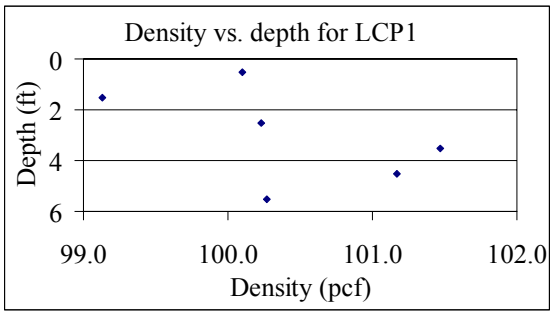

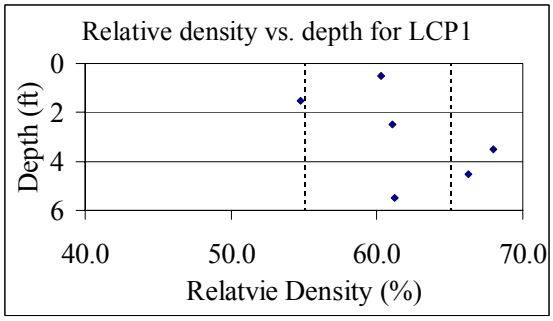

G.11.2 LCP2

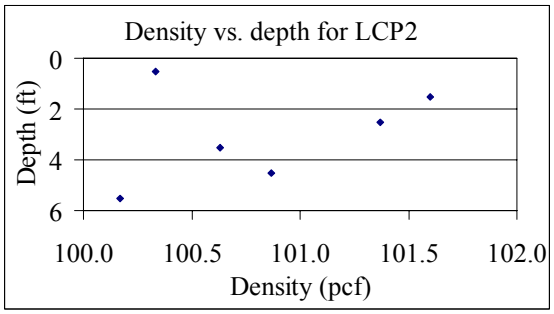

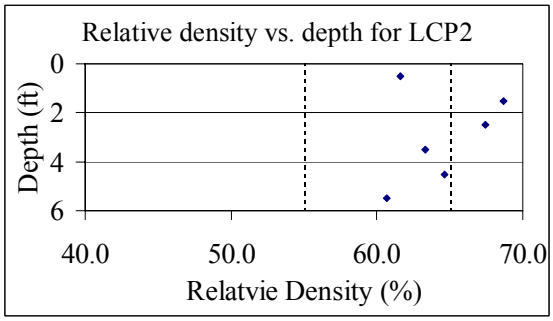

G.12 Cap and Piers (LCR)

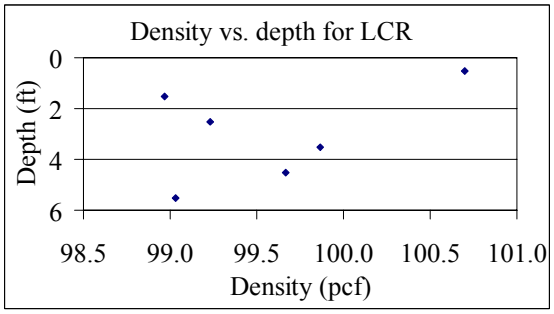

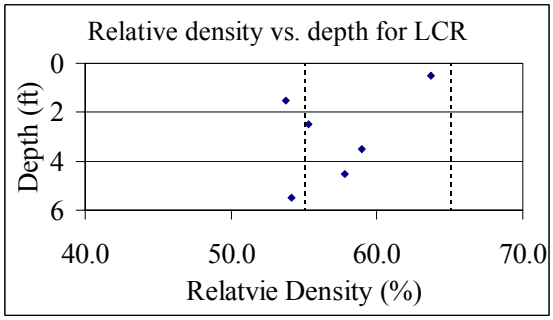

G.13 Cap and Grout (LCG)

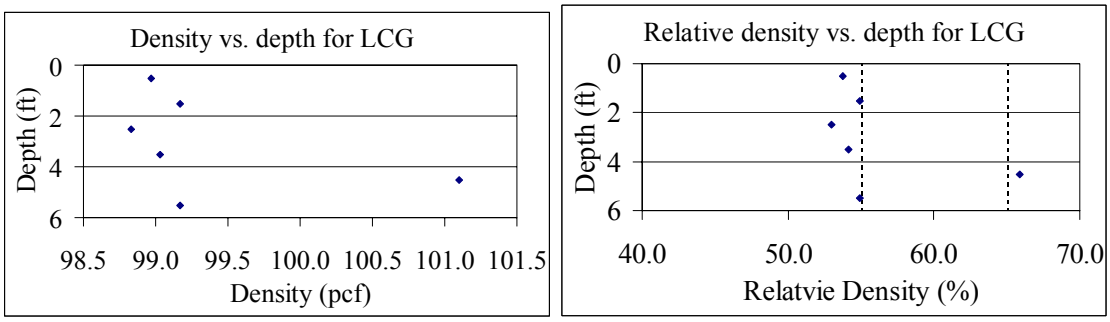

G.14 Cap, Piles, and Piers (LCPR)

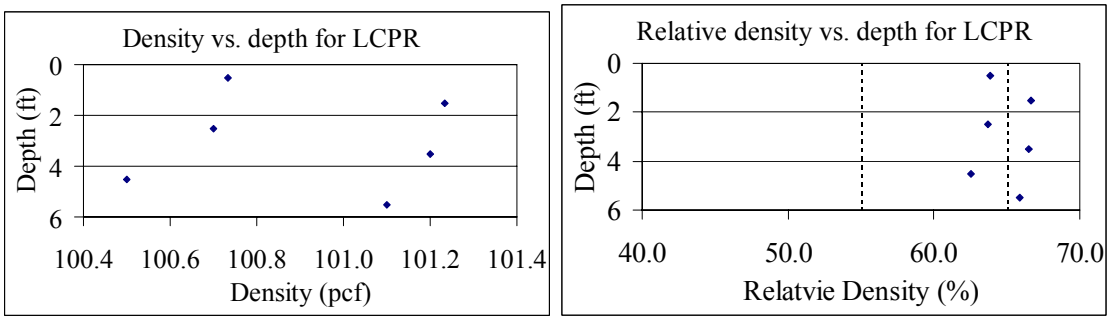

G.15 Cap, Piles, and Grout (LCPG)

G.15.1 LCPG1

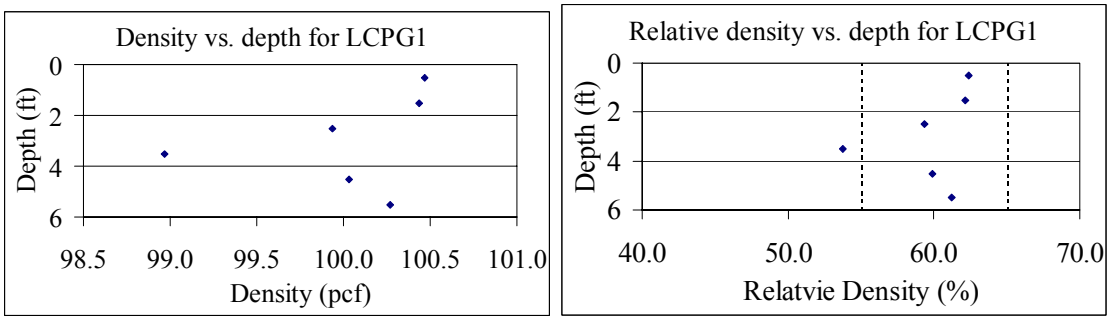

G.15.2 LCPG2

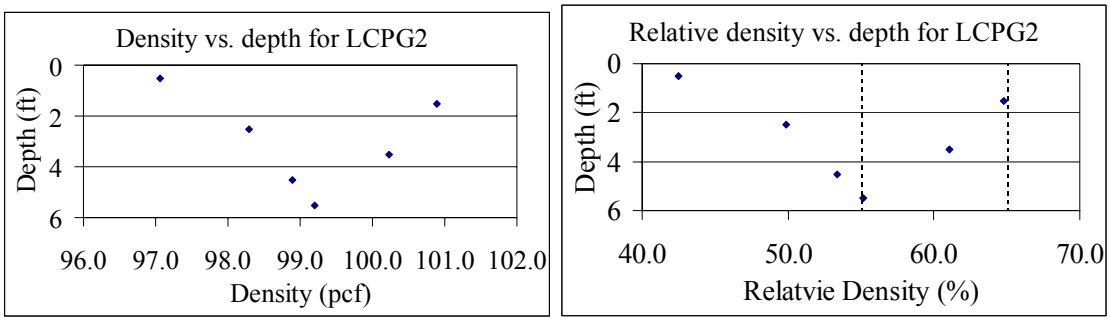

G.16 Cap, Piers, and Grout (LCRG)

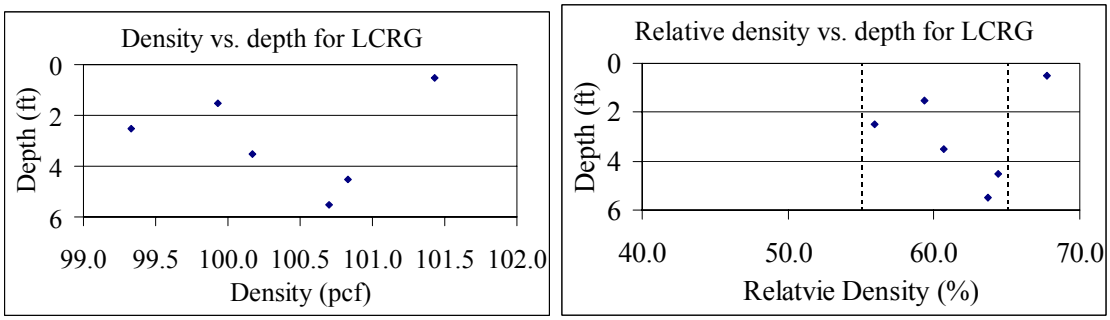

G.17 Cap, Piles, Piers, and Grout (LCPRG)

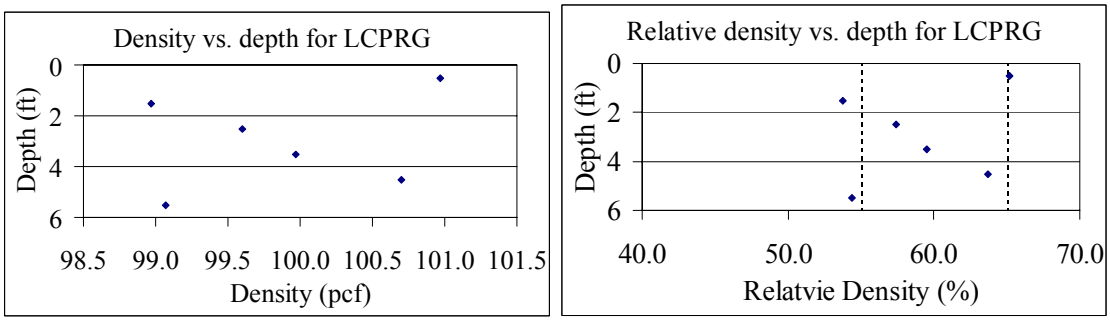

G.18 PILES

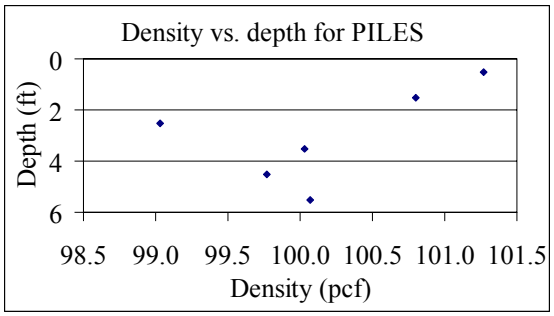
Density vs. depth for PILES
Depth (ft)
0
2
4
6
98.5
99.0
99.5
100.0
100.5
101.0
101.5
Density (pcf)

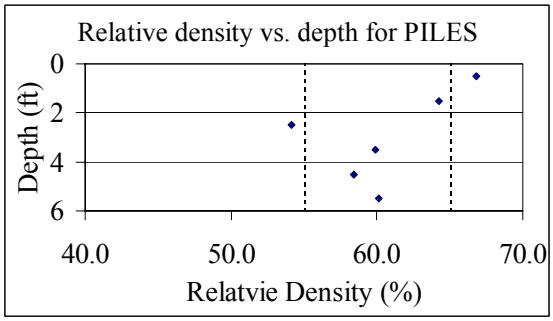
Relative density vs. depth for PILES
Depth (ft)
0
2
4
6
40.0
50.0
60.0
70.0
Relatvie Density (%)